MOLECULAR MECHANISMS OF PATIENT-DERIVED KEAP1 SUPERBINDER MUTANTS

Erica Won Cloer

A dissertation submitted to the faculty at the University of North Carolina at Chapel Hill in partial fulfillment of the requirements for the degree of Doctor of Philosophy in the Department of Cell Biology & Physiology in the University of North Carolina at Chapel Hill

Chapel Hill
2017

Approved by:

Michael Ben Major

D. Neil Hayes

Doug Cyr

Mohanish Deshmukh

Mike Emanuele

ABSTRACT

Erica Won Cloer: Molecular Mechanisms of Patient-Derived KEAP1 Superbinder Mutants
(Under the direction of Michael Ben Major)

In 30% of lung cancers, mutations in KEAP1 or NRF2 result in constitutive NRF2 activity. This promotes tumor progression, resistance to radio- and chemotherapy, and predicts poor patient outcome. Over 700 somatic mutations in the KEAP1 tumor suppressor gene have been identified in cancer, yet the mechanism and functional consequences of these mutations are unknown. This dissertation focuses on determining the phenotype and molecular profiles of patient-derived KEAP1 mutations. The objectives were to assign function for patient-derived KEAP1 mutations and to investigate the molecular mechanism(s) and phenotypes of functional classes of KEAP1 mutations.

Through biochemical characterization of 18 KEAP1 mutations identified in lung squamous cell carcinoma, we defined a novel class of KEAP1 ‘superbinder’ mutants. These superbinder mutants had increased association with the transcription factor NRF2, yet could not fully suppress NRF2-dependent transcription of cytoprotective genes. Cell-based and *in vitro* studies determined that superbinder mutants ubiquitylated NRF2 but were impaired for NRF2 proteasomal degradation. Molecular biology techniques were employed to understand the mechanism and phenotypic consequences of the KEAP1 superbinder mutants. Through these studies, five core characteristics were attributed to the superbinder mutant class. First, superbinder residues are highly conserved and are among the most frequently mutated residues across a variety of cancer types. Second, KEAP1 superbinders increase NRF2 association but are not altered in their association with other KEAP1 substrates proteasomal

chaperones, or ubiquitin receptors. Third, KEAP1 superbinders may impact KEAP1 tertiary structure thus stabilizing its interaction with the NRF2 degron. Fourth, KEAP1 superbinders sequester a pool of NRF2 in p62-dependent spherical clusters that are cleared by the cell. Furthermore, these clusters are comprised of a KEAP1 core surrounded by the autophagy adapter p62, phosphorylated p62 (pS351), polyubiqutin, and occasionally NRF2. Fifth, superbinders confer resistance to the DNA-damaging agent bleomycin in lung cancer cell lines stably overexpressing KEAP1 superbinder mutants. These studies expand our mechanistic understanding of KEAP1 superbinder mutants and provide insight into the dynamics and subcellular compartmentalization of the KEAP1-NRF2 complex.

ACKNOWLEDGEMENTS

To my committee members, each one of you has graciously given so much of your time to mentor and guide me through this challenging project. Thank you for all of the scientific input and discussion as well as for always having an open door for questions and advice.

To all of the members of the Major lab, thank you for your feedback and expertise in developing the ideas and experiments for this project. A special thanks to Priscila for all of the beautiful imaging data; to Dennis for countless hours of scientific debate, computational support, and never-ending patience; and to Emily, words cannot express my gratitude for your emotional support and excellent editorial skills.

To my family and friends, I could not have completed this journey without all of your love and support. A special thanks to my husband, Chris, for being my greatest advocate, supporter, and dearest friend.

PREFACE

Chapter 2 of this dissertation was previously published. Permission to include a modified version of the manuscript and accompanying figures was provided by the American Association for Cancer Research:

> Hast BE, Cloer EW, Goldfarb D, Li H, Siesser PF, Yan F, Walter V, Zheng N, Hayes DN, and Major MB. 2014. Cancer-derived mutations in KEAP1 impair NRF2 degradation but not ubiquitination. *Cancer Research* **74** 808:817.

TABLE OF CONTENTS

LIST OF TABLES

LIST OF FIGURES

LIST OF ABBREVIATIONS AND SYMBOLS

2SC	*S*-(2)-succinyl cysteine
4-HNE	4-Hydroxynonenal
15d-PGJ_2	15-Deoxy-delta-12,14-prostaglandin J2
A	Alanine
ABCC2	ABC transporter C family member 2
ACS	American Cancer Society
AD	Alzheimer's disease
AEM1	ARE expression modulator 1
AIM	Antioxidant inflammation modulator
ALS	Amyotrophic lateral sclerosis
AP	Affinity purification
ARE	Antioxidant response element
ATCC	American Type Culture Collection
ATG5	Autophagy related protein 5
ATG7	Autophagy related protein 7
ATRA	All-trans retinoic acid
BaP	Benzo[a]pyrene
BCL2	B-cell CLL/lymphoma 2
BCL2L1	B-cell lymphoma-extra large protein (BcL-xL)
BTB	Broad-complex, tramtrack, and bric-à-brac
BRAF	Serine/Threonine-protein kinase B-raf
BSA	Bovine serum albumin
BTRC	Beta-Transducin Repeat Containing E3 Ubiquitin Protein Ligase (BTrCP)
bZIP	Basic leucine zipper
C	Cysteine

CBP	CREB-binding protein
Cd^{2+}	Cadmium cation
CDDO	2-cyano-3,12-dioxooleana-1,9-dien-28-oic acid
CDDO-Im	1-(2-cyano-3,12-dioxooleana-1,9-dien-28-oyl) imidazole
CDDO-me	Bardoxolone methyl
CHD6	Chromodomain-helicase-DNA-binding protein 6
CHX	Cycloheximide
CKO	Conditional knockout
CNA	Copy number alteration
CNC	Cap‘n’collar
CNT	Control
CO	Carbon monoxide
CO_2	Carbon dioxide
COPD	Chronic obstructive pulmonary disease
COSMIC	Catalogue of somatic mutations in cancer
CP	Clobetasol proprionate
CpG	5’-cytosine-phosphate-guanine-3’
CQ	Chloroquine
CREB	coactivator cAMP-responsive element-binding
CRISPR	Clustered regularly interspaced short palindromic repeats
CRL	Cullin-RING ubiquitin ligase
CYP	Cytochrome P450 monooxygenase
CUL1	Cullin-1
CUL3	Cullin-3
D	Aspartic acid
DAPI	4’,6-diamidino-2-phenylindole

DBeQ	N^2, N^4-dibenzylquinazoline-2,4-diamine
DEF	Dimethylfumarate
DEG	Differentially expressed gene
DEM	Diethylmaleate
Dex-Mes	Dexamethasone 21-mesylate
DGR	Double glycine repeat
DMD	Discrete molecular dynamics
DME	Drug metabolizing enzyme
DMEM	Dulbecco's Modified Eagle Media
DMF	Dimethylformamide
DPP3	Dipeptidyl peptidase 3
DTT	Dithiothreitol
E	Glutamic acid
E-FRET	FRET efficiency
Eey1	Eeyarestatin-1
EDTA	Ethylenediaminetetraacetic acid
EGFR	Epidermal growth factor receptor
EGTA	Ethylene Glycol Tetraacetic Acid
EM	Electron microscopy
EpRE	Electrophile responsive element
FASP	Filter aided sample preparation
FBS	Fetal bovine serum
FDR	False discovery rate
FH	Fumarate hydratase, mitochondrial
FITC	Fluorescein
FLAG	Epitope tag DYKDDDDK

FLIM	Fluorescence lifetime imaging microscopy
FRAP	Fluorescence recovery after photobleaching
FRET	Förster resonance energy transfer
G	Guanine
G6PD	Glucose-6-phosphate 1-dehydrogenase
GBE1	1,4-alpha-glucan-branching enzyme
GCLC	Glutamate-cysteine ligase,catalytic subunit
GCLM	Glutamate-cysteine ligase modifier subunit
GEMM	Genetically engineered mouse model
GEO	Gene Expression Omnibus
GFP	Green fluorescent protein
GO	Gene ontology
GOF	Gain-of-function
GPX2	Glutathione peroxidase 2
GSEA	Gene Set Enrichment Analysis
GSH	Glutathione (reduced form)
GSK3B	Glycogen synthase kinase 3 beta
GSSG	Glutathione (oxidized form)
GST	Glutathione S-transferase
H_2O_2	Hydrogen peroxide
HA	Hemagglutinin
HCl	Hydrocholoric acid
HD	Huntington’s Disease
HEK	Human embryonic kidney
HMOX1	Heme oxygenase 1
HNSCC	Head and neck squamous cell carcinoma

HPLC	High-performance liquid chromatography
hr	Hour
HTS	High throughput screening
iASSP	Inhibitor of apoptosis-stimulating protein of p53
IDH1	Isocitrate dehydrogenase 1
IF	Immunofluorescence
IKBKB	Inhibitor of nuclear factor kappa-B kinase subunit beta
IL1B	Interleukin-1 beta
IL6	Interleukin-6
IP	Immunoprecipitation
ITC	Isothermal titration calorimetry
IVR	Intervening region
K	Lysine
KCl	Potassium chloride
K_D	Dissociation constant
K5	Keratin 5
KDE	Kernel density estimation
KEAP1	Kelch-like ECH-associated protein 1
KH_2PO_4	Potassium phosphate monobasic
KIR	KEAP1-interacting region
KRAS	GTPase KRas
LAMP2	Lysosome-associated membrane glycoprotein 2
LC	Liquid chromatography
LC3	Microtubule-associated protein 1A/1B light chain 3
LFQ	Label free quantification
LIMMA	Linear models for microarray data

LIR	LC3-interacting region
LOF	Loss-of-function
LUAD	Lung adenocarcinoma
LUSC	Lung squamous cell carcinoma
M	Molar
mCh	mCherry fluorescent protein
MCM3	Minichromosome maintenance complex component 3
$MgCl_2$	Magnesium chloride
Min	minute
MEF	Mouse embryonic fibroblast
MLN4924	NAE inhibitor
MS	Mass spectrometry
MYC	Myelocytomatosis viral oncogene
NaCl	Sodium chloride
Na_2HPO_4	Sodium phosphate dibasic
NAE	NEDD8-activating enzyme
$NaHCO_3$	Sodium bicarbonate
NBR1	Neighbor of BRCA1 gene 1
NDI	Nephrogenic diabetes insipidus
Neh	NRF2-ECH homology domain
NEKO	Nrf2-deficient in esophagus and Keap1-null
NEM	N-ethylmaleimide
NES	Nuclear export signal
NFE2L1	Nuclear factor erythroid 2-related factor 1 (gene)
NFE2L2	Nuclear factor erythroid 2-related factor 2 (gene)
NFKB1	Nuclear factor-kappa-B subunit 1

NFT	Neurofibrillary tangles
nl	nanoliter
NGS	Next-generation sequencing
NLS	Nuclear localization signals
NMR	Nuclear magnetic resonance
NO	Nitric oxide
NOX	NADPH oxidase enzyme
NPM1	Nucleophosmin
NQO1	NAD(P)H:quinone oxidoreductase 1
NRF1	Nuclear factor erythroid 2-related factor 1 (protein)
NRF2	Nuclear factor erythroid 2-related factor 2 (protein)
$NRF2^{FAMS}$	NRF2 Functionally Annotated Mutant Signature
NRMGS	NRF2-Regulated Metabolic Gene Signature
NSCLC	Non small cell lung carcinoma
•O2-	Superoxide anion
OA-NO_2	Nitro-oleic acid
•OH-	Hydroxyl radical
ONOO-	Peroxynitrite
OS	Overall survival
p	phosphorylation
p21/CDKN1A	Cyclin-dependent kinase inhibitor 1
p62/SQSTM1	Sequestosome 1
p97/VCP	Valosin containing protein
PALB2	Partner and localizer of BRCA2
PBS	Phosphate buffered saline
PCR	Polymerase chain reaction

PD	Parkinson’s disease
PE	Phosphatidylethanolamine
PGA_2	Prostaglandin A2
PGAM5	Phosphoglycerate mutase family member 5
PIK3CA	Phosphatidylinositol 4,5-bisphosphate 3-kinase catalytic subunit alpha Isoform
PIN	Protein Interaction Network
pKa	Acid dissociation constant
PKC	Protein kinase C
PLA	Proximity Ligation Assay
PMI	p62-mediated mitophagy inducer
PPP	Pentose phosphate pathway
PSMD2	26S proteasome non-ATPase regulatory subunit 2
PSMD4	26S proteasome non-ATPase regulatory subunit 2
PTEN	Phosphatidylinositol 3,4,5-trisphosphate 3-phosphatase and dual-specificity protein phosphatase
PTM	Post translational modification
qPCR	Quantitative polymerase chain reaction
R	Arginine
RAS	Rat sarcoma gene
REDOX	Oxidation reduction
RIPA	Radioimmunoprecipitation assay buffer
RLS	Reactive lipid species
RMSF	Root means square fluctuations
RNA	Ribonucleic acid
RNA-seq	RNA sequencing
RNS	Reactive nitrogen species

ROS	Reactive oxygen species
RRX	Rhodamine Red-X
RSEM	RNA-Seq by Expectation-Maximization
RT-PCR	Reverse transcription PCR
RTA 408	Omaveloxolone
RXRA	Retinoid X receptor alpha
S	Serine
SBP	Streptavidin binding peptide
SCLC	Small cell lung carcinoma
SCF	SKp, Cullin, F-box containing complex
SDM	Site-directed mutagenesis
SDS	Sodium dodecyl sulfate
SEM	Standard error the means
SFN	Sulforaphane
-SH	Thiol group
shRNA	Short hairpin RNA
siRNA	Small interfering RNA
SLK	STE20-like serine/threonine protein kinase
sMAF	small Musculoaponeurotic fibrosarcoma protooncogene
SNP	Single nucleotide polymorphism
SPR	Surface plasmon resonance
SQCC	Squamous cell carcinoma
STK11	Serine/threnonine protein kinase 11
STR	Short tandem repeat
T	Thymidine
TALDO1	Transaldolase

TAP	Tandem affinity purification
tBHQ	tert-Butylhydroquinone
TCA cycle	Tricarboxylic acid cycle
TCGA	The Cancer Genome Atlas
TP53	Cellular tumor antigen p53 (gene)
TXNRD1	Thioredoxin reductase 1
Ub	Ubiquitin
UBA	Ubiquitin-binding associated domain
UPLC	Ultra performance liquid chromatography
UPS	Ubiquitin proteasome system
V	Valine
VSV-g	Epitope tag YTDIEMNRLGK
W.blot	Western blot
WES	Whole-exome sequencing
WGS	Whole-genome sequencing
WT	Wild-type
WTX	Wilms tumor gene on the X chromosome protein
Y2H	Yeast two-hybrid screen
Zn^{2+}	Zinc cation
°	Degree
Å	Ångström
α	Alpha
β	Beta
Δ	Delta
µg	Microgram
µm	Micrometer

CHAPTER 1: INTRODUCTION

1.A. Lung cancer

Lung cancer is the leading cause of cancer-related mortalities worldwide and accounts for more than one million deaths each year (1-14). For 2017, the American Cancer Society (ACS) estimates that lung cancer will account for 14% of all newly diagnosed cancer cases (1, 4). Tobacco use is the single greatest risk factor associated with the development of lung cancer; 90% of all lung cancer cases in the United States can be attributed to smoking (4, 5). Environmental carcinogens are produced from cigarette smoke, radon, asbestos, or pollution (5, 13, 15). Exposure to these carcinogens results in DNA damage and increases the lifetime risk for the development of lung cancer (4-6, 8, 11, 15). Global health initiatives have raised awareness of the detrimental effects of smoking, thus contributing to declining rates in lung cancer incidence starting from the mid-1980s for men and from the mid-2000s for women (1, 5, 6, 8, 15). However, prognosis for lung cancer patients remains poor as diagnoses are often made when patients present with advanced stages of disease (1, 3, 4, 7, 14, 16-18). The five-year survival rate for patients diagnosed with stage IV disease is estimated to be 1% (1). Conventional treatment for lung cancer utilizes a combination of surgical intervention, radiation therapy (RT), and chemotherapy (8, 19).

1.A.1. Classification of lung cancer subtypes

There are two main histological subtypes of lung cancer: small cell lung carcinomas (SCLC) and non-small cell lung carcinomas (NSCLC) (3, 8). SLCLC comprises 10-15% of all lung cancer cases while 80-85% of cases are classified as NSCLC (1, 3, 4, 8, 14, 18). The

remaining 5% of lung cancer cases are classified as carcinoid or other (3). NSCLC can be further subclassified into three categories: lung adenocarcinomas (LUAD, 40% of all lung cancers), squamous cell carcinomas (LUSC, 25% of all lung cancers), and large cell carcinomas (abbreviation, 10% of all lung cancers) (1-4, 8, 18). LUAD tumors typically localize to the lung periphery, and 10-15% of patients diagnosed with LUAD have no history of smoking (1, 3, 4, 8, 18). In contrast, LUSC tumors generally localize to the center of the lung and are often associated with a history of smoking (3). LUSC tumors are thought to originate from squamous epithelial cells lining the lung airways (1, 3).

1.A.2. The mutational landscape of NSCLC

Acquired cellular mutations are known to cause cancer and are thought to occur over the lifetime of an individual (20, 21). The theory of how mutations accumulate begins with an initial 'gatekeeping' mutation that enables the first clonal expansion of a subpopulation of cells. Subsequent rounds of mutations and clonal expansions over time result in an aggressive and malignant tumor (20). It is estimated that for any given solid tumor, 33-66 genes will harbor mutations (20). Mutations within tumor suppressor genes often inactivate gene function, occur throughout the coding sequence, and are typically frameshift mutations or deletions (21-23). In contrast, mutations within oncogenes often activate gene function, occur at focally enriched regions within the coding sequence, and are primarily missense mutations impacting a single amino acid residue (21-23). The advent of next-generation sequencing (NGS) platforms has made large-scale genomic studies of patient tumors possible (20-23). These studies provide insight into the genetic mechanisms driving cancer by defining novel tumor suppressors and oncogenes as well as identifying passenger and driver mutations (22, 23).

Analysis of mutational frequency across 27 cancer types, demonstrated that lung cancers exhibit some of the highest levels of mutational frequency as compared to other types of cancer (23, 24). These elevated mutational rates can be attributed to cigarette smoke exposure which causes guanine (G) to thymidine (T) transversions often observed in LUAD and LUSC (25). Both LUAD and LUSC harbor significant alterations to common tumor suppressors namely: *TP53* (50% of LUAD cases; 80% of LUSC cases), serine/threonine protein kinase 11, (*STK11;* 15% of LUAD cases; 19% of LUSC cases), and Kelch-like ECH-associated protein (*KEAP1;* 12% of both LUAD and LUSC) (2, 3, 8, 16, 17, 25-28). Frequent alterations specifically associated with LUAD are activating mutations in the following oncogenes: *KRAS* (27% of LUAD cases), epidermal growth factor (*EGFR*; 17%), and phosphatidylinositol 4,5-bisphosphate 3-kinase catalytic subunit alpha isoform (*PIK3CA;* >10%) (3, 25, 26). In contrast, frequent oncogenic alterations specifically associated with LUSC are mutations in the nuclear factor erythroid 2-related factor 2 (*NFE2L2,* hereafter NRF2*;* 19%) and amplifications of *PIK3CA* (33%) and *EGFR* (30%) (2, 3, 8, 16, 17, 25-28).

The identification and characterization of these mutations can lead to earlier tumor detection and the development of targeted treatments (20, 21). Studies regarding the role of *EGFR* in lung cancer exemplify the integration of genomic data with molecular biology studies (7, 19, 29-33). The discovery of activating mutations in *EGFR* led to the development of EGFR-specific inhibitors (i.e. erlotinib and afatinib) and antibodies (i.e. cetuximab) for the targeted treatment of LUAD tumors; this has led to advances in therapeutic options for patients with EGFR-activated LUAD tumors (7, 31-33). Unfortunately, there are currently no clinically available targeted therapies for LUSC (7, 8, 12, 28, 29, 31, 34).

1.A.3. KEAP1-NFE2L2 mutations in NSCLC

In 2012, The Cancer Genome Atlas Consortium (TCGA) performed whole-exome sequencing (WES) and RNA-sequencing (RNA-seq) of tumors from patients diagnosed with LUAD (183 patients) and LUSC (178 patients) (2, 19). In addition to known tumor suppressors (i.e. *TP53*) and oncogenes (i.e. *KRAS*), both studies revealed significant and mutually exclusive alterations to the tumor suppressor *KEAP1* and to the oncogene *NFE2L2* (2, 19). Pathway alterations impacting KEAP1-NRF2 signaling were observed in 12% of LUAD cases studied (19). Subsequent studies investigating the co-occurrence of *KEAP1* and *NFE2L2* mutations in LUAD determined that 20% of LUAD tumors with mutant *KRAS* also harbor loss-of-function (LOF) mutations in *KEAP1* (35). Furthermore, 92% of LUAD *KEAP1* somatic missense mutations are predicted to abrogate KEAP1 protein function (30). Pathway alterations impacting KEAP1-NRF2 signaling were observed in 34% of all LUSC cases studied and in 62% of the LUSC classical subtype (2). Given the high percentage of *TP53* and *KEAP1* mutations in LUSC (80% and 30%, respectively), a significant number of tumors with *KEAP1* mutations may occur in the presence of *TP53* mutations (12).

1.B. KEAP1-NRF2 signaling

1.B.1. Understanding the stress response

Cells routinely encounter stress through a variety of insults such as chronic exposure to environmental pollutants and toxins (i.e. cigarette smoke or radon) or byproducts of metabolic processes (i.e. mitochondrial respiration) (36). These processes result in the accumulation of reactive intermediates capable of performing oxidation-reduction (redox) reactions (37-46). Uncontrolled redox reactions increase levels of oxidative stress and lead to the accumulation of reactive oxygen species (ROS) and reactive nitrogen species (RNS) within the cell. Common examples of ROS are hydrogen peroxide (H_2O_2), superoxide anion ($\bullet O2^-$), and hydroxyl radical ($\bullet$OH-) (40, 46-48). Common examples of RNS are nitric oxide

(NO) and peroxynitrite ($ONOO^-$) (40, 46, 48). Elevated levels of ROS and RNS result in DNA damage by oxidation (38, 39, 46, 49, 50); therefore, regulation of redox levels within the cell is critical for cellular homeostasis.

The KEAP1-NRF2 pathway is the primary intracellular defense against oxidative stress, and a delicate balance of NRF2 activity is required for homeostasis and effective disease prevention (44, 51-60). Low levels of NRF2 activity are associated with increased intracellular ROS (36, 54, 57). Inappropriately high levels of ROS and RNS can damage DNA and mitochondria, leading to aberrant apoptosis (54, 57, 61) Consequently, cells with low levels of NRF2 and elevated ROS are at risk for neurodegeneration, cardiovascular disease, and chronic inflammation (Figure 1.1) (54, 57, 58, 62-66). In contrast, high levels of NRF2 activity are associated with low basal levels of ROS, conferring a cellular growth advantage and enabling them to evade apoptosis (Figure 1.1) (52, 59, 64, 67). Therefore, mutations resulting in KEAP1 LOF or NRF2 gain-of-function (GOF) can contribute to cancer progression and the development of chemo-resistance (Fig. 1.2) (68).

1.B.2. Mechanism of KEAP1-NRF2 signaling

Under basal conditions, cytosolic KEAP1 functions as an adapter for the E3 ubiquitin ligase Cullin-3 (CUL3). KEAP1 is a homodimer that binds to two motifs in NRF2: a high affinity ETGE motif and a low affinity DLG motif. Binding via these two motifs is essential to sterically position seven key lysine residues located between the DLG and ETGE of NRF2 for ubiquitylation by the KEAP1-CUL3/RBX1 complex. Once ubiquitylated, NRF2 is delivered to the ubiquitin proteasome system (UPS) for degradation (Figure 1.2.A). NRF2 is dynamically regulated with a protein half-life of 15-20 minutes within most cell types, underscoring the essential role of KEAP1 in NRF2 regulation (69, 70).

Under conditions of oxidative stress or xenobiotic challenge, reactive cysteine residues within KEAP1 are modified leading to a conformational change in KEAP1 structure that prevents the degradation of NRF2 (54, 57, 59, 60, 69, 71-78). *De novo* synthesized NRF2 accumulates and translocates to the nucleus where it heterodimerizes with small musculoaponeurotic fibrosarcoma (sMAF) proteins, a family of basic region leucine zipper (bZIP) transcription factors comprised of three members: MAFF, MAFG, and MAFK (37, 79, 80). NRF2-sMAF heterodimers bind to antioxidant response elements (ARE)/electrophile responsive elements (EpRE) and drive the transcription of over 200 cytoprotective genes (Figure 1.2.A) (52, 81). The consensus sequence for ARE binding sites has been defined as TGACnnnGC (54, 82).

1.B.3. Functions of NRF2 target genes

NRF2 transcription regulates the expression of genes that govern 4 distinct processes within the cell: 1) antioxidant response, 2) drug detoxification, 3) cellular metabolism, and 4) inflammation (Figure 1.2.B) (54, 58, 83).

1.B.3.a. Antioxidant response

Genes involved in the antioxidant response are thought to be the primary function of NRF2-dependent transcription and result in the production of the ROS scavenger Y-glutamyl-cysteinyl glycine, more commonly referred to as glutathione (GSH). GSH is produced in an ATP-dependent two-step reaction that requires the NRF2 target genes glutamate-cysteine ligase catalytic subunit (*GCLC*) and glutamate-cysteine ligase modifier subunit (*GCLM*). The production of GSH generates reducing equivalents within the cell to counter rising levels of oxidants (54, 57, 58, 64, 83) (57). Other NRF2-transcriptionally regulated genes with antioxidant function include glutathione peroxidase 2 (*GPX2*) and thioredoxin reductase 1 (*TXNRD1*) (58, 83, 84).

1.B.3.b. Drug detoxification

Genes involved in cellular detoxification are important for the clearance of xenobiotic agents (i.e. drug efflux) from the cell (57, 58, 64, 83). Detoxification involves two classes of genes: 1) the receptor-mediated phase I cytochrome P450 monooxygenases (CYP) family and 2) the phase II conjugating enzymes (54). Phase I reactions prepare compounds for subsequent phase II reactions which utilize catalytic enzymes such as glutathione S-transferases (GSTs) to conjugate phase I products with GSH or other ligands for removal by the cell (54). Another well-known phase II detoxifying enzyme is NAD(P)H quinone dehydrogenase 1 (*NQO1*) (57, 64, 66, 83, 85-87).

1.B.3.c. Cellular Metabolism

NRF2 transcriptional targets also upregulate a host of genes involved in cellular metabolism, specifically genes that alter the utilization of glucose, glutamine, serine, and glycine (35, 88-91). Examples of these genes include glucose-6-phosphate 1-dehydrogenase (*G6PD*), 1,4,-alpha-glucan-branching enzyme (*GBE1*), isocitrate dehydrogenase 1 (*IDH1*), and transaldolase (*TALDO1*) (54, 57-59, 64, 66, 84).

1.B.3.c. Anti-inflammation

Nuclear NRF2 also regulates cellular inflammation by suppressing the transcription of genes involved in the production of pro-inflammatory cytokines interleukin-1 beta (IL1B) and interleukin-6 (IL6) (57, 82, 92-94). As such, NRF2 hyperactivation produces an anti-inflammatory response. A summary of the functions of NRF2 target genes is provided in Figure 1.2.B.

1.B.4. Outcomes of KEAP1 substrate ubiquitylation

In addition to NRF2, there are currently eight other validated KEAP1 substrates: nuclear factor erythroid-related factor 1 (NFE2L1; hereafter NRF1), mitochondrial phosphoglycerate mutase family member 5 (PGAM5), anti-apoptotic proteins B-cell CLL/lymphoma 2 (BCL2), B-cell lymphoma extra-large protein (BCL2L1), inhibitor of nuclear factor kappa-B kinase subunit beta (IKBKB), p62/sequestosome-1 (p62/SQSTM1; hereafter, p62), partner and localizer of BRCA2 (PALB2), and the mini-chromosome maintenance complex component 3 (MCM3) (44, 54, 57-60, 64, 69, 77, 94-102). KEAP1-dependent ubiquitylation of substrate proteins can result in 3 outcomes: 1) proteasomal degradation, 2) autophagic degradation, and 3) alterations to protein function (Figure 1.3).

The first potential outcome of KEAP1 substrate ubiquitylation is proteasomal degradation. The UPS is utilized by the cell for rapid turnover of short-lived proteins (i.e. NRF2) and requires a series of defined steps: 1) recognition of appropriately ubiquitylated substrates (commonly K48-specific polyubiquitin), 2) ATP-dependent substrate unfolding, 3) association with proteasomal ubiquitin receptors, and 4) removal of ubiquitin prior to proteolysis (103-107). KEAP1 substrates destined for proteasome-mediated degradation include: NRF2, NRF1, PGAM5, BCL2, BCL2L1, and IKBKB (Figure 1.3.A) (44, 54, 57-60, 64, 69, 77, 94-102).

A second potential outcome of KEAP1 substrate ubiquitylation is autophagic degradation. Autophagy is a bulk cellular recycling pathway for long-lived proteins (i.e. KEAP1) (108-114). The process of autophagy begins with the formation of an isolation membrane or phagophore around ubiquitylated proteins; these proteins are typically present as aggregates or inclusion bodies and localize to insoluble compartments within the cell (112-114). Next, ubiquitin cargo adapters such as p62 or next to BRCA1 (NBR1) recognize

and bind to polyubiquitin chains (usually K63-linked) within the aggregates and sequester the complex within the phagophore thus forming the autophagosome. The mature autophagosome is a double membraned structure indicated by phosphatidylethanolamine (PE) conjugated microtubule-associated protein 1A/B-light chain 3A (LC3) along the inner membrane (111-116). The autophagosome then fuses with lysosomes to form an autolysosome wherein contents are acidified and subsequently degraded (109, 110, 112-114, 117). KEAP1 substrates destined for autophagic degradation include KEAP1, p62, and IKBKB (Figure 1.3.B) (118-119). p62 binds to KEAP1 via a KEAP1-interacting region (KIR) containing the DPSTGE motif (96, 116, 119-122). Phosphorylation (p) of the serine residue within the KIR motif increases the affinity of p62 for KEAP1, potentially displacing the DLG motif of NRF2 (96). KEAP1 then ubiquitylates p62, a step required for correct tethering of p62 with LC3, and the KEAP1-p62 complex is degraded by autophagy (115, 116). IKBKB is unique in that it contains both DLG and ETGE motifs and can be degraded in a KEAP1-dependent manner through the proteasomal and autophagy pathways (Figure 1.3) (96, 116, 122).

The third potential outcome of KEAP1 substrate ubiquitylation is alterations to protein function for which there are two examples: PALB2 and MCM3 (Figure 1.3.C) (123-125). KEAP1-dependent ubiquitylation of PALB2 blocks the association of PALB2 and BRCA1 to suppress homologous recombination during the G1 phase of the cell cycle (124). In contrast to PALB2, the function of KEAP1-dependent MCM3 ubiquitylation has not yet been elucidated (125, 126).

The identification of additional KEAP1 substrates may support additional outcomes for proteins ubiquitylated by KEAP1. An examination of the KEAP1 protein interaction revealed enrichment for proteins containing ETGE or ESGE motifs (21/65 proteins studied);

however, whether all proteins encoding these motifs represent *bona fide* KEAP1 substrates remains to be determined (126, 127). A comprehensive table of proteins containing KEAP1 binding motifs is provided in Table S.1.1.

1.C. KEAP1-NRF2 complex formation and structure

1.C.1. NRF2 protein domains and structure

NRF2 is a cap'n'collar (CNC) basic leucine zipper (bZIP) transcription factor comprised of 605 amino acids (128, 129). NRF2 contains seven NRF2-ECH homology (Neh) domains, each with distinct functions and post-translational modifications. The Neh1 domain is responsible for NRF2 DNA binding as well as NRF2-sMAF dimerization (54, 130-136). NRF2-sMAF dimers are transcriptional activators that bind to *cis*-acting ARE elements in the promoters of genes (132). It is worth noting that NRF2-sMAF heterodimerization is required for sMAF activation as sMAF proteins lack transactivation domains; as such, sMAF homodimers are functional repressors (132). The CNC, bZIP, nuclear localization signals (NLS; ^{515}NLS^{518}), and nuclear export sequence (NES; ^{552}NES^{563}) are localized within the Neh1 domain (53, 137). The Neh2 domain is essential for KEAP1 cytosolic regulation of NRF2 and contains the two motifs required for KEAP1 association (the ^{29}DLG^{31} and ^{79}ETGE^{82} motifs) as well as the seven lysine (K) residues targeted by KEAP1-dependent ubiquitylation (K44, K50, K52, K53, K56, K64, and K68) (Fig. 1.4) (54, 57, 59, 60, 62, 66, 138-141). The Neh2 domain also contains a S40 residue that is phosphorylated by protein kinase C (PKC) (51, 142, 143). PKC phosphorylation at S40 results in KEAP1-NRF2 dissociation and nuclear localization of NRF2 (51, 142, 143). The Neh3 domain of NRF2 lies at the C-terminus of the protein and is proposed to function as a transactivation domain; Deletion of a ^{590}VFLVPK^{595} motif within the Neh3 domain suppresses NRF2 transcriptional activity (144). The Neh3 domain contains a ^{552}NES^{563} that is thought to be sterically blocked by NRF2-sMAF dimerization, thus retaining NRF2 in the nucleus (133). The Neh3 domain is

also responsible for the association of NRF2 with the chromodomain helicase DNA binding protein (CHD6) (144). The Neh4 and Neh5 domains of NRF2 are centrally located within the protein and function as transactivation domains. These two domains also bind to the transcriptional co-activator cAMP Responsive Element-Binding (CREB) binding protein (CBP) (145). Association of both Neh4 and Neh5 with CBP is required for maximal activation of NRF2 target genes; mutations disrupting CBP binding and inhibitors of CBP suppress NRF2-dependent transcriptional activity in cells (145). There are also putative nuclear export sequences (^{175}NES^{186} and ^{191}NES^{204}) localized within this region of the protein (59, 64, 84, 137). The Neh6 domain contains two beta-transducin repeat-containing E3 ubiquitin protein ligase (BTrCP; hereafter BTRC) degron motifs: ^{343}DSGIS^{347} and ^{382}DSAPGS^{384} (139-141). BTRC associates with the Skp1-Cullin 1 (CUL1) F-box containing complex (SCF) to form a ubiquitylation complex that targets proteins for proteasomal degradation within the nucleus of cells (139-141). Serine phosphorylation of the DSGIS motif by glycogen synthase kinase 3-beta (GSK3B) increases the affinity of the NRF2-Neh6-BTRC association and results in NRF2 degradation (139-141). BTRC regulation of NRF2 is primarily thought to occur in the nucleus of cells (139-141); in contrast, KEAP1 regulation is thought to occur in the cytosol of the cells (59, 139-141). The NRF2 Neh7 domain was defined in 2013 and binds to the retinoic X receptor alpha (RXRA); NRF2-RXRA association blocks NRF2 transcriptional activity (146). A schematic of the functional annotation of protein domains and motifs within NRF2 is provided in Figure 1.4.A.

1.C.2. KEAP1 protein domains and structure

KEAP1 was identified in 1999 via a yeast two hybrid (Y2H) screen utilizing NRF2 Neh2 as bait (147). KEAP1 is comprised of 624 amino acids and contains a broad complex, tramtrack, bric-à-brac (BTB) domain, an intervening region (IVR, also known as the BACK domain), and a C-terminal double glycine region (DGR) composed of six KELCH repeat

domains (52, 57, 59, 87). Each of these domains is essential to KEAP1 function. The BTB domain of KEAP1 is responsible for KEAP1 homodimerization and CUL3 association; both of which are required for NRF2 ubiquitylation (54, 57-59, 64, 66). Substitution of an alanine (A) residue at serine (S) 104 (S104A) of the BTB domain abolishes KEAP1 dimerization (148, 149). Similarly, cysteine (C) 151 (C151), located immediately after the BTB, is critical for KEAP1-CUL3 association as covalent modification of this residue blocks KEAP1-CUL3 interaction (74-76, 150-153). The next domain in KEAP1 is the IVR which serves two functions: 1) the stabilization of the CUL3 binding interface and 2) redox sensing via cysteine reactivity (84, 86, 87, 154). First, the BTB and IVR domains together form the true CUL3 binding interface (84, 86, 87, 154). The IVR contains a three-box (3-box) motif that bears homology to the F-box motif required for adapter binding with other members of the CULLIN family (i.e. SCF-CUL1) (84, 86, 154, 155). The ^{181}3-box^{212} is composed of two alpha helices that functionally extend the binding interface between KEAP1 and CUL3 from the BTB domain to the IVR thus stabilizing the KEAP1-CUL3 complex (86, 156). Second, the IVR domain of KEAP1 is heavily enriched for cysteine residues and functions as a sensor of oxidative stress (57, 59, 87, 157). It is worth discussing that KEAP1 is a cysteine-rich protein; in total, human KEAP1 contains 27 cysteines, whereas murine KEAP1 contains 25 cysteines (52, 57, 59, 87, 157). Cysteine reactivity is determined by the acid dissociation constant (pKa) of the thiol group (-SH) which in turn is dependent on the adjacent amino acid residues (158). Cysteines surrounded by basic residues have a thiol group with decreased pKa, rendering the cysteine more susceptible to an electrophilic attack; as such, these cysteines are highly reactive to oxidative stress (41, 158-160). The three most well-characterized cysteine residues in KEAP1 are C151, C273, and C288, two of which localize to the IVR domain (57, 66). Adjacent to the IVR is an unstructured linker which contains additional reactive cysteine residues, C297, and C299 (41, 159, 160). The DGR domain is responsible for NRF2 and other substrate binding as well as for association with the actin

cytoskeleton (57, 58, 64, 66, 84) The DGR is comprised of six KELCH repeats that together form a six-bladed propeller structure, the interior of which constitutes the NRF2 substrate binding pocket (52, 54, 57-59, 64, 66, 86, 94, 156, 161). KEAP1-NRF2 interactions are stabilized by a number of residues in the KELCH domain of KEAP1, most notably an arginine triad motif, R415, R478, and R483, that is responsible for electrostatic interactions with acidic residues in the NRF2 degrons (Figure 1.4.B) (52, 57-59, 64, 66, 86, 87, 156).

1.C.3. Survey of KEAP1-NRF2 structure studies

Though NRF2 and KEAP1 were discovered in the 1990s, the first crystal structure of the human KEAP1 KELCH was not resolved until 2004 (at 1.85 Å) followed by determination of the first crystal structure of the NRF2 Neh2 domain in 2006 (at 1.5 Å)(162-164). These two findings allowed for co-crystallization studies of the human KEAP1 KELCH domain with NRF2 which identified the DLG and ETGE motifs required for KEAP1-NRF2 association (58, 87, 162-169). The thermodynamic properties of the two motifs provided the basis for the proposed 'hinge and latch' mechanism of binding to be discussed in the following section. It was not until 2010 that electron microscopy studies revealed that dimeric KEAP1 forms a forked-stem-dimer or 'cherry-bob' structure providing further support for the hinge and latch mechanism. In June of 2014, the crystal structure of the BTB domain was determined (69, 86, 150, 154, 164, 170, 171). Thus far, neither the IVR nor the full-length crystal structure of KEAP1 structure has been determined. A timeline of structural studies of KEAP1-NRF2 complexes is provided in Figure 1.5.

1.D. Dynamics of KEAP1-NRF2 signaling

1.D.1. Stoichiometry of the KEAP1-NRF2 complex

The 2:1 stoichiometry of the KEAP1-NRF2 complex was originally determined in 2006 using nuclear magnetic resonance titration (NMR) and isothermal titration calorimetry

(ITC) of the KEAP1 KELCH and NRF2 Neh2 domains (167, 168). Differences in electrostatic potentials between the ETGE and DLG motifs formed the basis for the two-site binding model (also known as the 'hinge-and-latch' model) (87, 165, 168, 169). In this model, the high affinity ETGE binds first to one monomer of KEAP1 forming the 'hinge' of the system followed by subsequent binding of the DLG 'latch' (87, 165, 168, 169). The association of KEAP1-NRF2 ETGE occurs in a slow, entropy-driven reaction, forming a stable complex with a dissociation constant (Kd) of 100 μM (165). In contrast, association of the KEAP1-NRF2 DLG is both enthalpy- and entropy-driven and occurs as a rapid single-step reaction with a Kd of 1 μM. (58, 84, 165-169, 172). The differences in these affinities suggest that dimeric KEAP1 could associate with ETGE motifs in 2 molecules of NRF2 resulting in a stoichiometry of 2:2 for KEAP1: NRF2 (84). To determine if the 2:2 KEAP1: NRF2 stoichiometry occurs in cells, biochemical fraction of 5 different cell lines were performed, thus defining the "absolute amounts and status" of the CUL3: KEAP1: NRF2 complex to be 2:2:1 (84). Moreover, these stoichiometric studies concluded that cellular levels of CUL3 and KEAP1 protein remain constant even with NRF2 inducer treatment; in contrast, NRF2 protein levels were determined to be subject to dynamic changes and significant alterations in the presence of NRF2 inducers (84).

1.D.2. Conformational cycling of KEAP1

The prevailing model for KEAP1 dynamics was developed from live cell imaging of fluorescent constructs for murine Keap1 and Nrf2 (173). Termed the "cyclic sequential attachment and regeneration model of Keap1-mediated degradation of NRF2," this model posits that cytosolic KEAP1 fluctuates between two distinct cellular conformations: open and closed (173). Under basal conditions, homodimeric KEAP1 is readily available to scavenge newly synthesized molecules of NRF2 (173). First, NRF2 binds KEAP1 via the ETGE motif generating the 'open' form of the complex. Second, subsequent binding of the NRF2 DLG

motif results in the 'closed' formation of the complex in which NRF2 is ubiquitylated (173). Third, following ubiquitylation, NRF2 is delivered to the proteasome and removed from KEAP1 (173). Fourth, removal of ubiquitylated NRF2 'regenerates' free KEAP1 thus allowing cycling to proceed again (85). In the presence of NRF2 inducers, cycling is impaired resulting in accumulation of the closed complex. Because free KEAP1 is no longer available, *de novo* NRF2 is able to escape KEAP1 regulation resulting in elevated levels of NRF2 transcriptional activity (173).

1.E. KEAP1-NRF2 signaling in physiological systems

1.E.1. Phenotypes of Keap1 and Nfe2l2 mutant mice

In mice, global deletion of *Keap1* causes esophageal hyperkatosis and lethality at postnatal days 7-10 (57, 174, 175). The hyperproliferation of the upper gastrointestinal tract prevents swallowing, resulting in malnutrition and subsequent death shortly after pups are weaned (57, 175). The simultaneous deletion of *Nfe2l2*$^{-/-}$ and *Keap1*$^{-/-}$ rescues the aforementioned phenotype, suggesting that the hyperkeratosis is driven by elevated NRF2 transcriptional activity (57, 175). Furthermore, global deletion of *Nfe2l2*$^{-/-}$ in mice results in viable litters (176). The lack of an appreciable phenotype in *Nfe2l2*$^{-/-}$ mice is presumed to be due to compensation from *Nfe2l1* as *Nfe2l1*$^{-/-}$::*Nfe2l2*$^{-/-}$ double knockout (KO) mice are lethal (175). However, it should be noted that *Nfe2l2*$^{-/-}$ mice develop phenotypes when challenged with carcinogenic models of benzo(a)pyrene [B(a)P] as well as with models of chronic obstructive pulmonary disease (COPD) (177-180).

The development of KEAP1 conditional KO (CKO) mice has enabled a number of genetically engineered mouse models (GEMMs) for the investigation of KEAP1 function in cancer *in vivo* (See Table 1 for references). Thus far, there is no evidence to suggest that hyperactivation of NRF2 from KEAP1 deletion or mutation alone results in the spontaneous

development of tumors. A summary of phenotypes for *keap1* and *nfe2l2* mutant mice is provided in Table 1.

1.E.2. KEAP1-NRF2 dysregulation in disease

1.E.2.a. Neurodegenerative disorders

Neurodegenerative disorders are characterized by elevated levels of oxidative stress protein aggregates or inclusion bodies caused by defects in protein homeostasis. Because of the essential roles KEAP1-NRF2 signaling plays in both antioxidant response and proteostasis, appropriate KEAP1-NRF2 activity is critical for neuronal health and the prevention of neurodegenerative disease (44, 60, 65, 181, 182). Indeed, astrocyte-specific expression of NRF2 protects neuronal cells from apoptosis in three different murine models of neurodegenerative disease: 1) Amyotrophic lateral sclerosis (ALS), 2) Huntington's disease (HD), and 3) Parkinson's disease (PD) (170, 183, 184). Furthermore, the accumulation of Tau proteins and neurofibrillary tangles (NFT) and the formation of Lewy bodies are pathological features of Alzheimer's disease (AD) and Parkinson's disease (PD), respectively (60, 65, 182, 185, 186). Both NFTs and Lewy bodies collect along the actin cytoskeleton and colocalize with KEAP1 and p62 suggesting that KEAP1 may play a role in either the accumulation or degradation of these aggregates (61, 65, 97, 181, 183, 186, 187).

1.E.2.b. Inflammation

Oxidative stress and the upregulation of pro-inflammatory cytokines such as IL-6 and IL-1B are characteristic of chronic obstructive pulmonary disease (COPD) caused by smoking (57, 180, 188). As discussed in section 1.B.3, NRF2 transcriptional activity results in the downregulation of both IL-6 and IL1-B suggesting that NRF2 has an anti-inflammatory effect. Indeed, *Nfe2l2*$^{-/-}$ mice exhibit increased inflammation when challenged with two models of pulmonary inflammation: 1) elastase-induced emphysema and 2) cigarette

smoke-induced emphysema (178, 179). Lung-specific deletion of *keap1* was shown to be protective against cigarette smoke-induced emphysema suggesting that NRF2 transcriptional activity is anti-inflammatory (177).

1.F. KEAP1-NRF2 signaling in the development and progression of cancer

1.F.1. Mechanisms of NRF2 activation in cancer

NRF2 activation can occur in cancer via 3 mechanisms: 1) genetic alterations to *NFE2L2, CUL3,* or *KEAP1*, 2) expression of NRF2-competitive binding proteins that impair NRF2 ubiquitylation, and 3) endogenous post-translational modifications that functionally inactivate KEAP1. First, alterations to *NFE2L2, CUL3,* and *KEAP1* are well-established to occur at the genomic level; these alterations result in enhanced NRF2 expression and transcriptional activity (51, 55, 56, 59, 64, 66, 70, 94, 138, 141, 189-198). *NFE2L2* is located on chromosome 2q31.2. Several mechanisms by which genetic modification of *NFE2L2* can increase NRF2 transcriptional activity are copy number amplifications, oncogene-induced transcription of NRF2 ($cMYC^{ERT2}$, $BRAF^{V619E}$, and $KRAS^{G12D}$), and GOF somatic mutations in the DLG or ETGE motifs required for KEAP1 association (Figure 1.6A) (2, 19, 26, 30, 70, 94, 195, 197, 199, 200). *CUL3* is located on chromosome 2q36.2 and is functionally inactivated by homozygous deletion or by LOF mutations, resulting in loss of KEAP1-dependent NRF2 ubiquitylation and subsequent NRF2 stabilization (Figure 1.6B) (2, 19); mutations impacting CUL3 occur in 7% of TCGA-LUSC cases studied (2). *KEAP1* is located on chromosome 19p13.2 and can be functionally inactivated by homozygous deletion, methylation of CpG islands within its promoter region, or by KEAP1 LOF mutations (Figure 1.6C) (2, 70, 190, 198). Both *KEAP1* and *CUL3* LOF result in increased NRF2 transcriptional activity (70, 94, 195, 197, 199, 200).

Second, several groups have identified NRF2 competitive binding proteins that

displace the DLG of NRF2 resulting in impaired NRF2 ubiquitylation; the expression of these competitive binders in both *in vitro* and *in vivo* models of cancer contribute to NRF2 hyperactivity and confer protection from DNA damaging agents in a NRF2-dependent manner (123, 124, 127, 201-204). These competitive binding partners include ETGE-containing proteins: DPP3, PALB2, and WTX; DPSTGE-containing protein p62; a DLT-containing protein iASSP; and p21 *Cip1/WAF1* (p21), which contains a ^{154}KRR motif analogous to the arginine triad motif of KEAP1 (Figure 1.6D) (127, 201-204).

Third, post-translational modifications (PTMs) to KEAP1 that are functionally inactivating can occur endogenously in cancer cells deficient for the tumor suppressor fumarate hydratase (FH) (205, 206). The loss of FH results in the formation of *S*-(2-succinyl) adducts (2SC) on C151 and C288; these adducts are thought to increase NRF2 transcriptional activity by modifying KEAP1 structure (Figure 1.6E) (56, 94, 205).

1.F.2. NRF2 transcriptional target genes in cancer

A primary focus of the KEAP1-NRF2 field in cancer is to identify a biomarker for NRF2 activity. Towards this goal, several groups have examined cell-line based microarray datasets as well as publicly available patient tumor data (i.e. TCGA and cBioPortal) to develop a NRF2 gene signature for use as a biomarker. The first NRF2 gene signature was identified in 2008 by the Biswal group and is composed of 15 genes validated by RT-PCR profiling of NRF2 shRNA A549 and H460 lung cancer cell lines (207). More recently, two patient-derived signatures of NRF2 activity have been defined: NRF2^{ACT} and NRF2-regulated metabolic gene signature (NRMGS) (90, 208, 209). NRF2^{ACT} is a 28-gene derived from the TCGA-LUSC dataset of 104 patients binned into mutant *KEAP1/NFE2L2/CUL3* or WT (209). Unfortunately, NRF2^{ACT} exhibited no significant prognostic or predictive value (209). The NRMGS was identified using gene expression analyses from A549 cells stably

overexpressing mKeap1-pEGFP and A549-derived Nrf2-knockdown cell line, siNrf2-C7 (90, 208). Gene ontology (GO) analyses on the overlap of genes downregulated in both KEAP1 overexpressing and siNrf2-C7 identified metabolic genes as being significant, and comparison of significantly downregulated genes with TCGA-LUAD data identified a 12 gene signature (90). NRMGS was determined to be prognostic in studies examining eight lung cancer cohorts.

1.F.3. Small molecule compounds targeting KEAP1-NRF2

1.F.3.a. NRF2 inducers

NRF2 inducers are thought to have therapeutic applications in the prevention of cancer as well as for the treatment of neurodegenerative disorders and chronic inflammation (52, 53, 57, 59, 60, 62, 65, 67, 180-182, 188). NRF2 small molecule inducers inactivate KEAP1 function either through cysteine-modification of KEAP1 or through dissociation of the KEAP1-NRF2 complex resulting in NRF2 stabilization and transcriptional activity (57, 83, 210). As such, these inducers can be categorized roughly into five classes based on cysteine reactivity as determined by site-directed mutagenesis (SDM) and *in vivo* experiments with mice transgenic for KEAP1 cysteine mutants (57, 75, 83, 135). Class I inducers are KEAP1 C151-dependent and include compounds 1-[2-cyano-3,12-dioxooleana-1,9(11)-dien-28-oyl]imidazole (CDDO-Im), bardoxolone (CDDO-Me), diethylmaleate (DEM), dimethylfumarate (DMF), nitric oxide (NO), sulforaphane (SFN), and *tert*-butyl hydroquinone (tBHQ) (57, 83). Class II inducers are specific to the C288 residue in the IVR of KEAP1 and include 15-deoxy-$\Delta^{12,14}$-prostaglandin J_2(15d-PGJ_2) (57, 83). Class III molecules require KEAP1 C151, C273, and C288 and include (OA-NO_2)(4-HNE), (OA-NO_2) (57, 64, 83). Class IV compounds activate NRF2 through other cysteine residues in KEAP1 and do not require C151, C273, C288; these class IV compounds include cadmium cation (Cd^{2+}), dexamethasone 21-mesylate (Dex-Mes), H_2O_2, prostaglandin A2 (PGA_2), and zinc

cation (Zn^{2+}) (52, 57, 83). The primary mechanism of Class V NRF2 inducers is the disruption of the KEAP1-NRF2 interaction (57, 64, 83). Examples of Class V NRF2 inducers include ML334, tetrahydroisoquinolin-2-carbonyl]cyclohexane-1-carboxylic acid [compound (*S*,*R*,*S*)], the R1 competitive monobody, p62-mediated mitophagy inducer (PMI), and the antioxidant inflammation modulator (AIM), and omaveloxolone (RTA 408) (81, 83, 210-215). Although not assigned to a specific class, the NEDD8-activating enzyme inhibitor (NAE1; hereafter, MLN4924) and the CYP450 inhibitor oltipraz are also known to induce NRF2 activation (206, 216-221). To date, oltipraz is the only NRF2 inducer to be used in phase I and II clinical trials for the prevention of lung cancer in individuals who smoke (206, 218, 219, 222).

1.F.3.b. NRF2 inhibitors

Hyperactivation of NRF2 in the context of cancer is now appreciated as detrimental for survival (55, 58, 59, 64, 89, 92, 191, 192, 194, 223). As such, a current goal of the KEAP1-NRF2 field is the development of NRF2-specific inhibitors for the treatment of NRF2-active cancers (94, 224). NRF2 inhibitors function primarily through disruption of nuclear NRF2 transcriptional activity and are historically identified through the use of high throughput screening (HTS) using NRF2-ARE transcriptional activity to assay for function. Examples of these compounds include all-trans retinoic acid (ATRA), ARE expression modulator 1 (AEM1), brusatol, and clobetasol proprionate (CP) (51, 225-227).

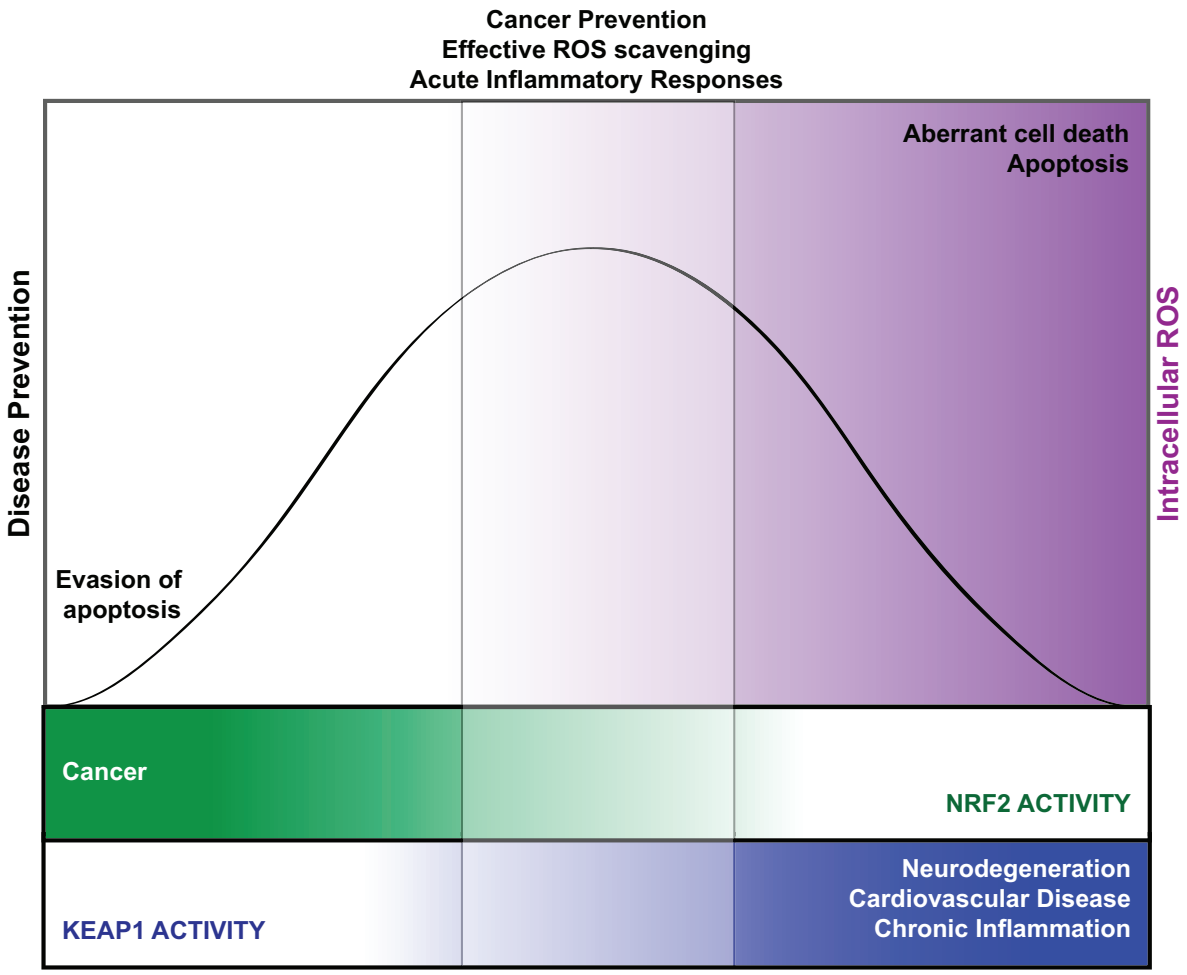

Figure 1.1. A balance of KEAP1-NRF2 activity is required for effective disease prevention.

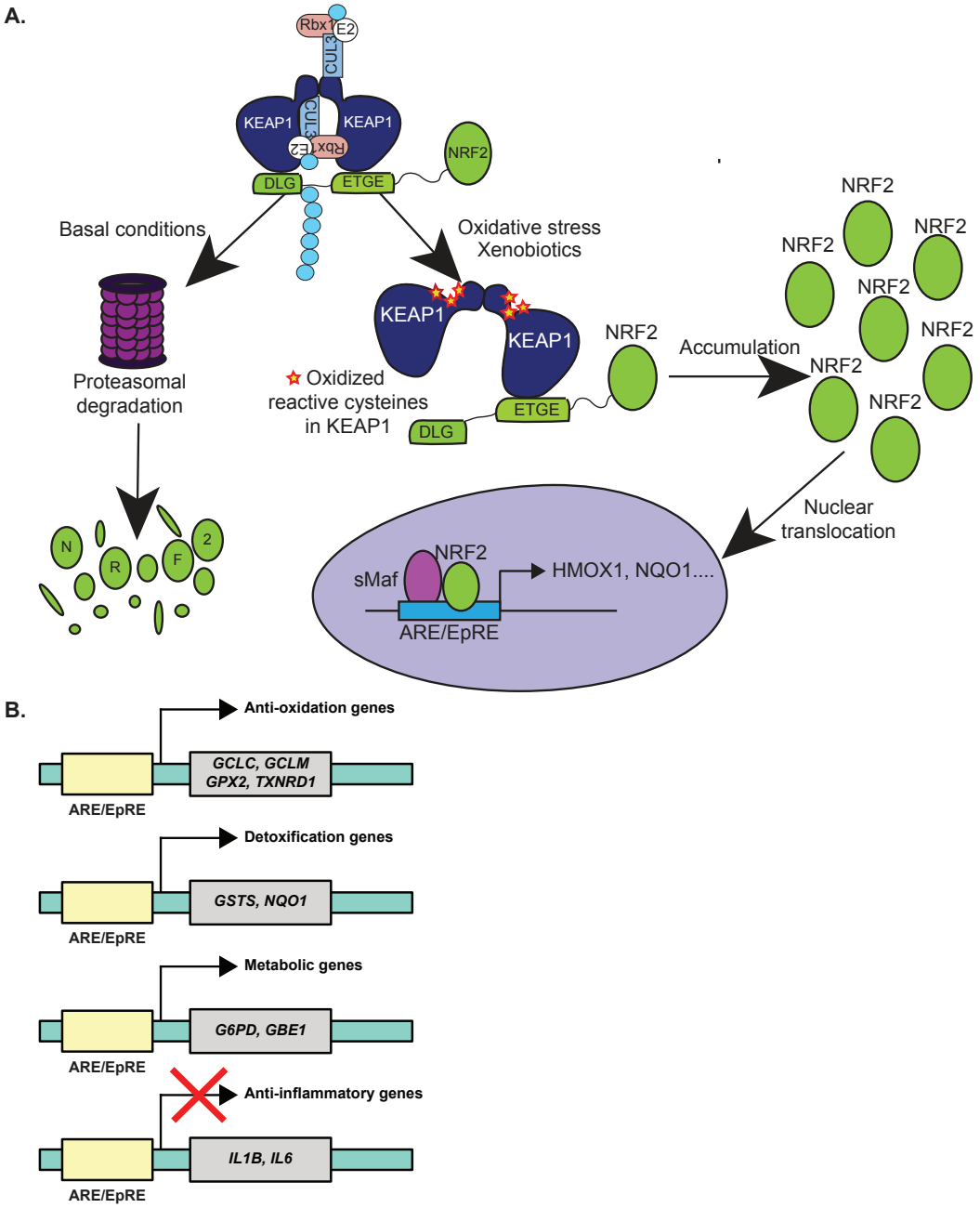

Figure 1.2. Overview of KEAP1-NRF2 signaling.
A. Cartoon illustration of the KEAP1-NRF2 pathway.
B. Function and examples of NRF2 target genes. Glutamate-cysteine ligase catalytic subunit (GCLC), glutamate-cysteine ligase modifier subunit (GCLM), glutathione peroxidase 2 (GPX2), thioredoxin reductase 1 (TXNRD1), glutathione S-transferases (GSTS), NAD(P)H quinone dehydrogenase 1 (NQO1), glucose-6-phosphate dehydrogenase (G6PD), 1,4,-alpha-glucan branching enzyme (GBE1), interleukin-1 beta (IL1B), and interleukin-6 (IL6).

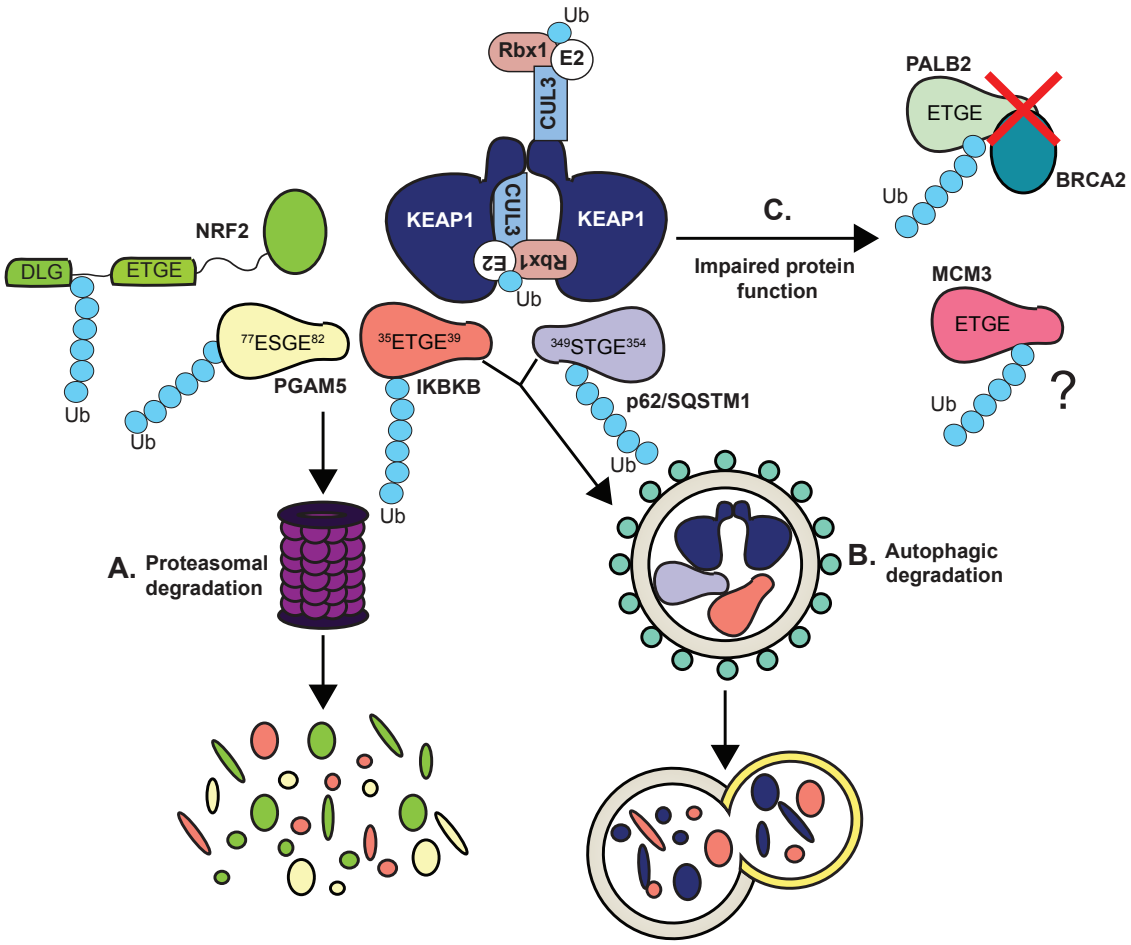

Figure 1.3. Outcomes of KEAP1 substrate ubiquitylation.
A. Proteasomal degradation (i.e. NRF2, PGAM5, and IKBKB).
B. Autophagic degradation (i.e. IKBKB and p62).
C. Impaired protein function (i.e. PALB2 and MCM3).

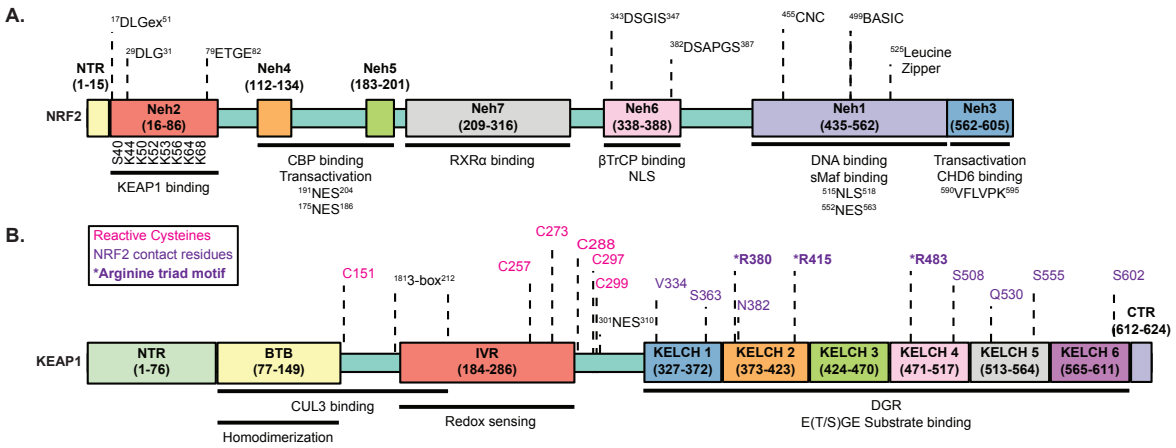

Figure 1.4 Overview of NRF2 and KEAP1 protein domains.
A. Functional annotation of protein domains and motifs within NRF2.
B. Functional annotation of protein domains and motifs within KEAP1.

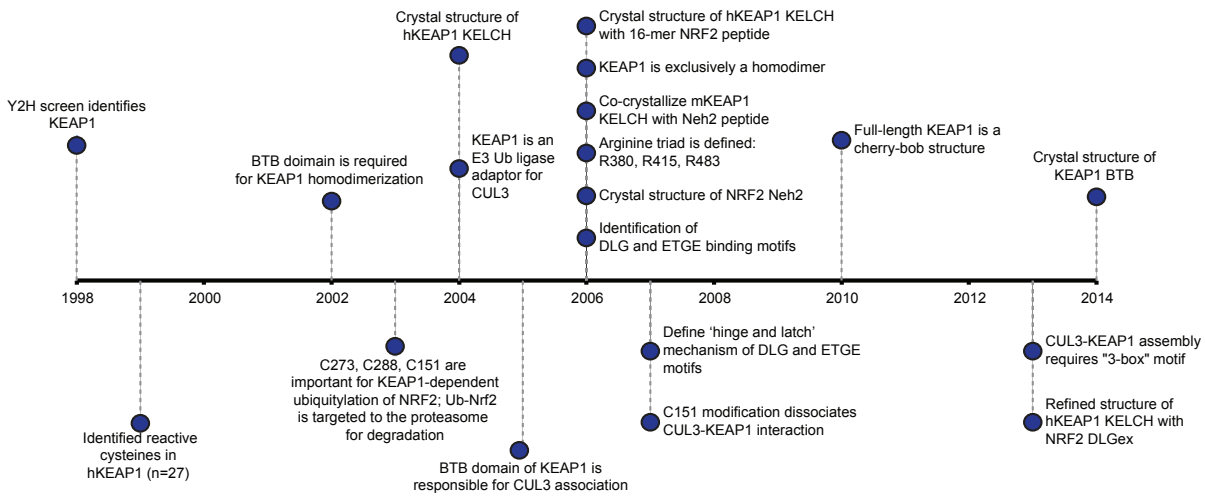

Figure 1.5.Timeline of KEAP1-NRF2 structural studies spanning 1998-2014.

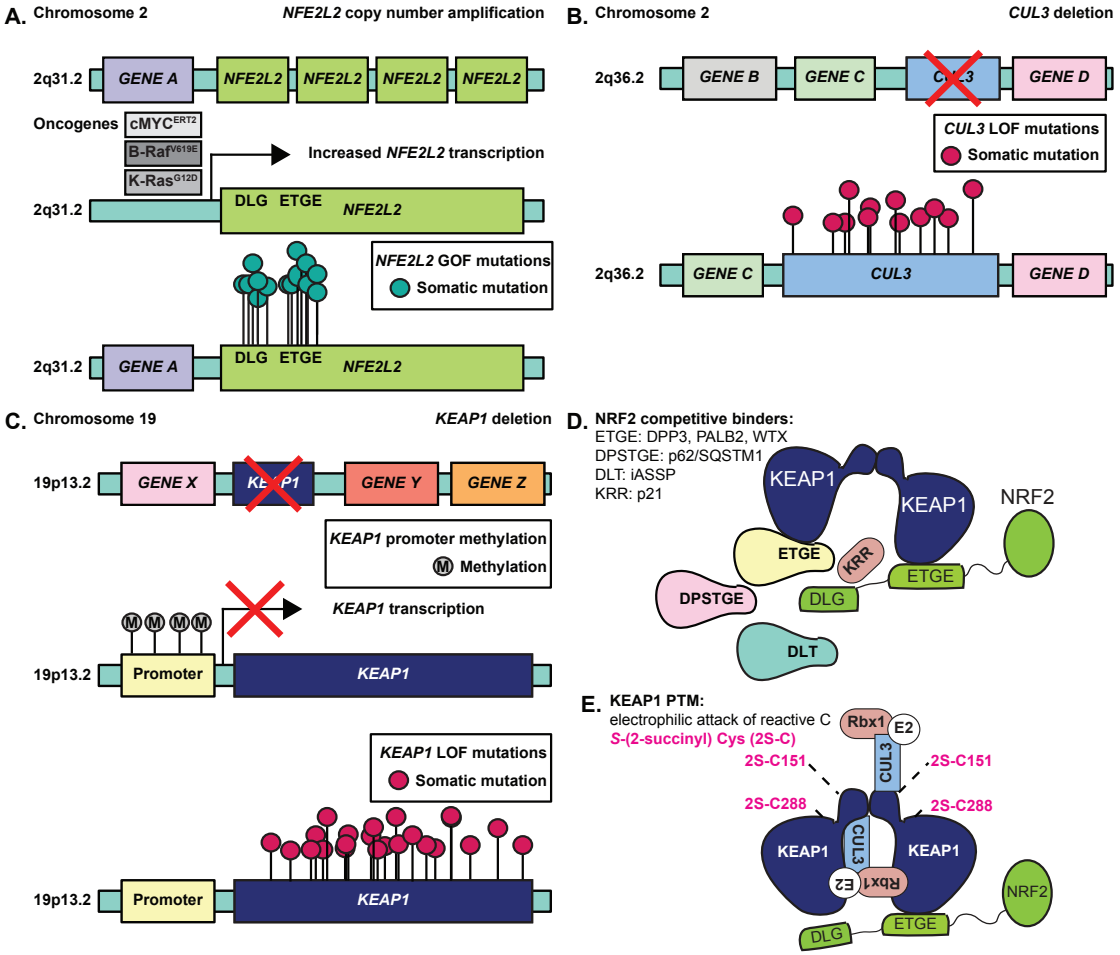

Figure 1.6. Mechanisms of NRF2 transcriptional activation.
A. *NFE2L2* is located on chromosome 2q31.2 and can be activated by copy number amplification, oncogene-induced increased transcription, or gain-of-function (GOF) mutations in the DLG or ETGE motifs required for KEAP1 association.
B. *CUL3* is located on chromosome 2q36.2 and can be functionally inactivated by homozygous deletion or by loss-of-function (LOF) mutations.
C. *KEAP1* is located on chromosome 19p13.2 and can be functionally inactivated by homozygous deletion, CpG island promoter methylation which blocks KEAP1 transcription, or by KEAP1 LOF mutations.
D. Overexpression of NRF2 competitive inhibitors impair NRF2 degradation. These proteins contain NRF2-competitive binding sites (ET(S)GE, DPSTGE, KRR, DLT) that can displace NRF2 from KEAP1 thus allowing for increased NRF2 transcriptional activity.
E. KEAP1 is a cysteine-rich molecule that is highly susceptible to electrophilic attack. Formation of S-(2-succinyl) 2SC adducts on cysteine molecules results in conformational inactivation of KEAP1and subsequent stabilization of NRF2.

Genotype	*Keap1*	*Nfe2l2*	Phenotype	Reference
nfe2l2$^{-/-}$	WT	KO	Survives Impaired stress response	Itoh et al 1997 *Biochem Biophys Res Commun*
keap1$^{-/-}$	KO	WT	Lethal at postnatal days 7-10 Hyperkeratosis of esophagus and forestomach Maximal NRF2 activation	Wakabayashi 2003 *Nature Genetics*
keap1$^{-/-}$*:: nfe2l2*$^{-/-}$	KO	KO	Survives Rescues *leap1*$^{-/-}$phenotype.	Wakabayashi 2003 *Nat Genetics*
nfe2l1$^{-/-}$*:: nfe2l2*$^{-/-}$	WT	KO	Lethal at E13.5 Impaired NRF2 stress response	Leung et al 2003 *JBC*
keap1$^{-/-}$*:: mafG*$^{-/-}$	KO	WT	Survives Rescues *keap1*$^{-/-}$phenotype.	Motohashi et al 2004 *PNAS*
mafF$^{-/-}$*::* *mafG*$^{-/-}$*::* *mafK*$^{-/-}$	WT	WT	Lethal at E13.5 Impaired NRF2 stress response	Motohashi et al 2004 *PNAS* Katsuoka et al 2005 *Mol Cell bio*
keap1$^{flox/flox}$*::* *Alb*-Cre (*keap1-Alb)*	CKO (hepatocyte-specific)	WT	Survives Slightly elevated NRF2 transcriptional activity (liver) Increased resistance to acetaminophen at toxic doses	Okawa et al 2006 *Biochem and Biophys Res Commun*
keap1$^{flox/-}$ *(keap1*-KD)	KD	WT	Survives Slightly elevated NRF2 transcriptional activity	Taguchi et al 2010 *Mol Cell Biol*
keap1$^{flox/flox}$*::K5*-Cre	CKO (squamous epithelium)	WT	Lethal Hyperkeratosis of esophagus and forestomach Maximal NRF2 activation only in esophagus and skin	Taguchi et al 2010 *Mol Cell Biol*
Pten::keap1-Alb	CKO (hepatocyte-specific)	WT	Lethal at 3 weeks Hyperactivate NRF2 metabolic target genes Hepatomegaly	Mitsuishi et al 2012 *Cancer Cell* Taguchi et al 2014 *Mol Cell Biol*
Pten:: *Keap1-Alb::* *Nfe2l2*$^{+/-}$	CKO	Het	Survives longer Polycistic fibrosis of liver at 6 months	Taguchi et al 2014 *Mol Cell Biol*
Keap1$^{flox/flox}$*::* *Pax8*-rtTA:: *TetO*-Cre (DOX administration to 4-week-old mice)	CKO (adult renal tubule-specific)	WT	Survives Resistant to renal ischemia-reperfusion injury	Noel et al 2016 *BMC Nephrol*
Keap1$^{flox/flox}$*::* *Trp53*$^{flox/flox}$*::* *R26*^{tdTomato}	CKO	WT	Necessitate euthanasia due to lung adenocarcinomas of *Trp53*$^{flox/flox}$*::R26*^{tdTomato} Mouse model of LUSC Increased tumor aggressiveness, metastasis, and resistance to radiotherapy	Jeong et al 2016 *Cancer Discovery*
Keap1$^{-/-}$*::* *Tg-Keap1*$^{C273W\&C288E}$	KO+OE KEAP1$^{C273W\&C288E}$	WT	Survives Still develop hyperkeratosis seen in *keap1*$^{-/-}$ phenotype.	Saito et al 2016 *Mol Cell Bio*
Keap1$^{-/-}$*::* *Nfe2l2*$^{flox/flox}$*::* *K5*-Cre (NEKO)	KO	WT	Survives (poor survival) Growth retardation Hydronephrosis (NDI) Maximal NRF2 activation (excluding esophagus and skin)	Suzuki et al 2017 *Nat Commun*
Keap1$^{flox/flox}$*::* *Pax8*-rtTA:: *TetO*-Cre (maternal DOX administration during pregnancy)	KO (embryonic renal tubule-specific)	WT	Survives Hydronephrosis (NDI) Maximal NRF2 activation in renal tubules	Suzuki et al 2017 *Nat Commun*
Kras$^{LSL-G12D/+}$*::* *Tp53*$^{flox/flox}$ with *sgKeap1* (CRISPR-Cas9 using pSECC lentiviral vectors)	KO	WT	Lethal at postnatal day 40 Mouse model of LUAD Increased tumor burden and aggressiveness	Romero et al 2017 *Nature medicine*
Keap1$^{flox/flox}$ *Kras*$^{LSL-G12D/+}$*::* *Pdx-1*-Cre (KC) (KC::Keap1)	CKO	WT	Lethal at postnatal day 40 Mouse model of pancreatic cancer Atrophy of pancreatic parenchyma *nfe2l2* heterozygous or homozygous cross rescues	Hamada et al 2017 *Journal of American Physiology*
Keap1$^{flox/flox}$ *Kras*$^{LSL-G12D/+}$*::* *p53*$^{LSL-R172H/+}$*::* *Pdx-1*-Cre (KPC) (KPC::Keap1)	CKO	WT	Mouse model of pancreatic cancer Atrophy of pancreatic parenchyma Cross with *nfe2l2*$^{+/-}$ or *nfe2l2*$^{-/-}$ rescues	Hamada et al 2017 *Journal of American Physiology*

Table 1. Phenotypes of *Keap1* and *Nfe2l2* mutant mice.

REFERENCES

1. **American Cancer Society.** About non-small cell lung cancer.

2. **Cancer Genome Atlas Research N.** 2012. Comprehensive genomic characterization of squamous cell lung cancers. Nature **489:**519-525.

3. **Herbst RS, Heymach JV, Lippman SM.** 2008. Lung cancer. N Engl J Med **359:**1367-1380.

4. **Institute NC.** 2017. General information about non-small cel llung cancer (NSCLC).

5. **Alberg AJ, Brock MV, Ford JG, Samet JM, Spivack SD.** 2013. Epidemiology of lung cancer: Diagnosis and management of lung cancer, 3rd ed: American College of Chest Physicians evidence-based clinical practice guidelines. Chest **143:**e1S-e29S.

6. **Alberg AJ, Ford JG, Samet JM, American College of Chest P.** 2007. Epidemiology of lung cancer: ACCP evidence-based clinical practice guidelines (2nd edition). Chest **132:**29S-55S.

7. **Chan BA, Hughes BG.** 2015. Targeted therapy for non-small cell lung cancer: current standards and the promise of the future. Transl Lung Cancer Res **4:**36-54.

8. **Latimer KM, Mott TF.** 2015. Lung cancer: diagnosis, treatment principles, and screening. Am Fam Physician **91:**250-256.

9. **Abazeed ME, Adams DJ, Hurov KE, Tamayo P, Creighton CJ, Sonkin D, Giacomelli AO, Du C, Fries DF, Wong KK, Mesirov JP, Loeffler JS, Schreiber SL, Hammerman PS, Meyerson M.** 2013. Integrative radiogenomic profiling of squamous cell lung cancer. Cancer Res **73:**6289-6298.

10. **Botling J, Edlund K, Lohr M, Hellwig B, Holmberg L, Lambe M, Berglund A, Ekman S, Bergqvist M, Ponten F, Konig A, Fernandes O, Karlsson M, Helenius G, Karlsson C, Rahnenfuhrer J, Hengstler JG, Micke P.** 2013. Biomarker discovery in non-small cell lung cancer: integrating gene expression profiling, meta-analysis, and tissue microarray validation. Clin Cancer Res **19:**194-204.

11. **Jemal A, Thun MJ, Ries LA, Howe HL, Weir HK, Center MM, Ward E, Wu XC, Eheman C, Anderson R, Ajani UA, Kohler B, Edwards BK.** 2008. Annual report to the nation on the status of cancer, 1975-2005, featuring trends in lung cancer, tobacco use, and tobacco control. J Natl Cancer Inst **100:**1672-1694.

12. **Jeong Y, Hoang NT, Lovejoy A, Stehr H, Newman AM, Gentles AJ, Kong W, Truong D, Martin S, Chaudhuri A, Heiser D, Zhou L, Say C, Carter JN, Hiniker SM, Loo BW, Jr., West RB, Beachy P, Alizadeh AA, Diehn M.** 2017. Role of KEAP1/NRF2 and TP53 Mutations in Lung Squamous Cell Carcinoma Development and Radiation Resistance. Cancer Discov **7:**86-101.

13. **Pfeifer GP, Denissenko MF, Olivier M, Tretyakova N, Hecht SS, Hainaut P.** 2002. Tobacco smoke carcinogens, DNA damage and p53 mutations in smoking-associated cancers. Oncogene **21:**7435-7451.

14. **Tsui DW, Berger MF.** 2016. Profiling Non-Small Cell Lung Cancer: From Tumor to Blood. Clin Cancer Res **22:**790-792.

15. **Asomaning K, Miller DP, Liu G, Wain JC, Lynch TJ, Su L, Christiani DC.** 2008. Second hand smoke, age of exposure and lung cancer risk. Lung Cancer **61:**13-20.

16. **Pietanza MC, Ladanyi M.** 2012. Bringing the genomic landscape of small-cell lung cancer into focus. Nat Genet **44:**1074-1075.

17. **Pietanza MC, Rudin CM.** 2012. Novel therapeutic approaches for small cell lung cancer: the future has arrived. Curr Probl Cancer **36:**156-173.

18. **Reck M, Rabe KF.** 2017. Precision Diagnosis and Treatment for Advanced Non-Small-Cell Lung Cancer. N Engl J Med **377:**849-861.

19. **Imielinski M, Berger AH, Hammerman PS, Hernandez B, Pugh TJ, Hodis E, Cho J, Suh J, Capelletti M, Sivachenko A, Sougnez C, Auclair D, Lawrence MS, Stojanov P, Cibulskis K, Choi K, de Waal L, Sharifnia T, Brooks A, Greulich H, Banerji S, Zander T, Seidel D, Leenders F, Ansen S, Ludwig C, Engel-Riedel W, Stoelben E, Wolf J, Goparju C, Thompson K, Winckler W, Kwiatkowski D, Johnson BE, Janne PA, Miller VA, Pao W, Travis WD, Pass HI, Gabriel SB, Lander ES, Thomas RK, Garraway LA, Getz G, Meyerson M.** 2012. Mapping the hallmarks of lung adenocarcinoma with massively parallel sequencing. Cell **150:**1107-1120.

20. **Vogelstein B, Papadopoulos N, Velculescu VE, Zhou S, Diaz LA, Jr., Kinzler KW.** 2013. Cancer genome landscapes. Science **339:**1546-1558.

21. **Stratton MR, Campbell PJ, Futreal PA.** 2009. The cancer genome. Nature **458:**719-724.

22. **Pon JR, Marra MA.** 2015. Driver and passenger mutations in cancer. Annu Rev Pathol **10:**25-50.

23. **Watson IR, Takahashi K, Futreal PA, Chin L.** 2013. Emerging patterns of somatic mutations in cancer. Nat Rev Genet **14:**703-718.

24. **Lawrence MS, Stojanov P, Polak P, Kryukov GV, Cibulskis K, Sivachenko A, Carter SL, Stewart C, Mermel CH, Roberts SA, Kiezun A, Hammerman PS, McKenna A, Drier Y, Zou L, Ramos AH, Pugh TJ, Stransky N, Helman E, Kim J, Sougnez C, Ambrogio L, Nickerson E, Shefler E, Cortes ML, Auclair D, Saksena G, Voet D, Noble M, DiCara D, Lin P, Lichtenstein L, Heiman DI, Fennell T, Imielinski M, Hernandez B, Hodis E, Baca S, Dulak AM, Lohr J, Landau DA, Wu CJ, Melendez-Zajgla J, Hidalgo-Miranda A, Koren A, McCarroll SA, Mora J, Crompton B, Onofrio R, Parkin M, et al.** 2013. Mutational heterogeneity in cancer and the search for new cancer-associated genes. Nature **499:**214-218.

25. **Kandoth C, McLellan MD, Vandin F, Ye K, Niu B, Lu C, Xie M, Zhang Q, McMichael JF, Wyczalkowski MA, Leiserson MDM, Miller CA, Welch JS, Walter MJ, Wendl MC, Ley TJ, Wilson RK, Raphael BJ, Ding L.** 2013. Mutational landscape and significance across 12 major cancer types. Nature **502:**333-339.

26. **Campbell JD, Alexandrov A, Kim J, Wala J, Berger AH, Pedamallu CS, Shukla SA, Guo G, Brooks AN, Murray BA, Imielinski M, Hu X, Ling S, Akbani R, Rosenberg M, Cibulskis C, Ramachandran A, Collisson EA, Kwiatkowski DJ, Lawrence MS, Weinstein JN, Verhaak RG, Wu CJ, Hammerman PS, Cherniack AD, Getz G, Cancer Genome Atlas Research N, Artyomov MN, Schreiber R, Govindan R, Meyerson M.** 2016. Distinct patterns of somatic genome alterations in lung adenocarcinomas and squamous cell carcinomas. Nat Genet **48:**607-616.

27. **Chaft JE, Arcila ME, Paik PK, Lau C, Riely GJ, Pietanza MC, Zakowski MF, Rusch V, Sima CS, Ladanyi M, Kris MG.** 2012. Coexistence of PIK3CA and other oncogene mutations in lung adenocarcinoma-rationale for comprehensive mutation profiling. Mol Cancer Ther **11:**485-491.

28. **Liao RG, Watanabe H, Meyerson M, Hammerman PS.** 2012. Targeted therapy for squamous cell lung cancer. Lung Cancer Manag **1:**293-300.

29. **Amann J, Kalyankrishna S, Massion PP, Ohm JE, Girard L, Shigematsu H, Peyton M, Juroske D, Huang Y, Stuart Salmon J, Kim YH, Pollack JR, Yanagisawa K, Gazdar A, Minna JD, Kurie JM, Carbone DP.** 2005. Aberrant epidermal growth factor receptor signaling and enhanced sensitivity to EGFR inhibitors in lung cancer. Cancer Res **65:**226-235.

30. **Berger AH, Brooks AN, Wu X, Shrestha Y, Chouinard C, Piccioni F, Bagul M, Kamburov A, Imielinski M, Hogstrom L, Zhu C, Yang X, Pantel S, Sakai R, Watson J, Kaplan N, Campbell JD, Singh S, Root DE, Narayan R, Natoli T, Lahr DL, Tirosh I, Tamayo P, Getz G, Wong B, Doench J, Subramanian A, Golub TR, Meyerson M, Boehm JS.** 2016. High-throughput Phenotyping of Lung Cancer Somatic Mutations. Cancer Cell **30:**214-228.

31. **Chmielecki J, Pietanza MC, Aftab D, Shen R, Zhao Z, Chen X, Hutchinson K, Viale A, Kris MG, Stout T, Miller V, Rizvi N, Pao W.** 2012. EGFR-mutant lung adenocarcinomas treated first-line with the novel EGFR inhibitor, XL647, can subsequently retain moderate sensitivity to erlotinib. J Thorac Oncol **7:**434-442.

32. **Huo L, Li CW, Huang TH, Lam YC, Xia W, Tu C, Chang WC, Hsu JL, Lee DF, Nie L, Yamaguchi H, Wang Y, Lang J, Li LY, Chen CH, Mishra L, Hung MC.** 2014. Activation of Keap1/Nrf2 signaling pathway by nuclear epidermal growth factor receptor in cancer cells. Am J Transl Res **6:**649-663.

33. **Rosell R, Moran T, Queralt C, Porta R, Cardenal F, Camps C, Majem M, Lopez-Vivanco G, Isla D, Provencio M, Insa A, Massuti B, Gonzalez-Larriba JL, Paz-Ares L, Bover I, Garcia-Campelo R, Moreno MA, Catot S, Rolfo C, Reguart N, Palmero R, Sanchez JM, Bastus R, Mayo C, Bertran-Alamillo J, Molina MA, Sanchez JJ, Taron M, Spanish Lung Cancer G.** 2009. Screening for epidermal growth factor receptor mutations in lung cancer. N Engl J Med **361:**958-967.

34. **Yamadori T, Ishii Y, Homma S, Morishima Y, Kurishima K, Itoh K, Yamamoto M, Minami Y, Noguchi M, Hizawa N.** 2012. Molecular mechanisms for the regulation of Nrf2-mediated cell proliferation in non-small-cell lung cancers. Oncogene **31:**4768-4777.

35. **Romero R, Sayin VI, Davidson SM, Bauer MR, Singh SX, LeBoeuf SE, Karakousi TR, Ellis DC, Bhutkar A, Sanchez-Rivera FJ, Subbaraj L, Martinez B, Bronson RT, Prigge JR, Schmidt EE, Thomas CJ, Goparaju C, Davies A, Dolgalev I, Heguy A, Allaj V, Poirier JT, Moreira AL, Rudin CM, Pass HI, Vander Heiden MG, Jacks T, Papagiannakopoulos T.** 2017. Keap1 loss promotes Kras-driven lung cancer and results in dependence on glutaminolysis. Nat Med doi:10.1038/nm.4407.

36. **Boutten A, Goven D, Artaud-Macari E, Bonay M.** 2011. [Protective role of Nrf2 in the lungs against oxidative airway diseases]. Med Sci (Paris) **27:**966-972.

37. **Rushmore TH, Morton MR, Pickett CB.** 1991. The antioxidant responsive element. Activation by oxidative stress and identification of the DNA consensus sequence required for functional activity. J Biol Chem **266:**11632-11639.

38. **Buttke TM, Sandstrom PA.** 1994. Oxidative stress as a mediator of apoptosis. Immunol Today **15:**7-10.

39. **Fleury C, Mignotte B, Vayssiere JL.** 2002. Mitochondrial reactive oxygen species in cell death signaling. Biochimie **84:**131-141.

40. **Turrens JF.** 2003. Mitochondrial formation of reactive oxygen species. J Physiol **552:**335-344.

41. **Wakabayashi N, Dinkova-Kostova AT, Holtzclaw WD, Kang MI, Kobayashi A, Yamamoto M, Kensler TW, Talalay P.** 2004. Protection against electrophile and oxidant stress by induction of the phase 2 response: fate of cysteines of the Keap1 sensor modified by inducers. Proc Natl Acad Sci U S A **101:**2040-2045.

42. **Park EY, Kim SG.** 2005. NO signaling in ARE-mediated gene expression. Methods Enzymol **396:**341-349.

43. **Itoh K.** 2006. [Protective mechanism against oxidative stress by Keap1/Nrf2 pathway]. Seikagaku **78:**79-92.

44. **Zhang DD.** 2006. Mechanistic studies of the Nrf2-Keap1 signaling pathway. Drug Metab Rev **38:**769-789.

45. **Kobayashi M, Li L, Iwamoto N, Nakajima-Takagi Y, Kaneko H, Nakayama Y, Eguchi M, Wada Y, Kumagai Y, Yamamoto M.** 2009. The antioxidant defense system Keap1-Nrf2 comprises a multiple sensing mechanism for responding to a wide range of chemical compounds. Mol Cell Biol **29:**493-502.

46. **Hancock JT.** 2009. The role of redox mechanisms in cell signalling. Mol Biotechnol **43:**162-166.

47. **Motohashi H, Yamamoto M.** 2004. Nrf2-Keap1 defines a physiologically important stress response mechanism. Trends Mol Med **10:**549-557.

48. **Yu BP.** 1994. Cellular defenses against damage from reactive oxygen species. Physiol Rev **74:**139-162.

49. **Nguyen T, Yang CS, Pickett CB.** 2004. The pathways and molecular mechanisms regulating Nrf2 activation in response to chemical stress. Free Radic Biol Med **37:**433-441.

50. **Orino K, Lehman L, Tsuji Y, Ayaki H, Torti SV, Torti FM.** 2001. Ferritin and the response to oxidative stress. Biochem J **357:**241-247.

51. **Bryan HK, Olayanju A, Goldring CE, Park BK.** 2013. The Nrf2 cell defence pathway: Keap1-dependent and -independent mechanisms of regulation. Biochem Pharmacol **85:**705-717.

52. **Dinkova-Kostova AT, Kostov RV, Canning P.** 2017. Keap1, the cysteine-based mammalian intracellular sensor for electrophiles and oxidants. Arch Biochem Biophys **617:**84-93.

53. **Giudice A, Arra C, Turco MC.** 2010. Review of molecular mechanisms involved in the activation of the Nrf2-ARE signaling pathway by chemopreventive agents. Methods Mol Biol **647:**37-74.

54. **Itoh K, Mimura J, Yamamoto M.** 2010. Discovery of the negative regulator of Nrf2, Keap1: a historical overview. Antioxid Redox Signal **13:**1665-1678.

55. **Kansanen E, Kuosmanen SM, Leinonen H, Levonen AL.** 2013. The Keap1-Nrf2 pathway: Mechanisms of activation and dysregulation in cancer. Redox Biol **1:**45-49.

56. **Leinonen HM, Kansanen E, Polonen P, Heinaniemi M, Levonen AL.** 2014. Role of the Keap1-Nrf2 pathway in cancer. Adv Cancer Res **122:**281-320.

57. **Suzuki T, Yamamoto M.** 2017. Stress-sensing mechanisms and the physiological roles of the Keap1-Nrf2 system during cellular stress. J Biol Chem **292:**16817-16824.

58. **Taguchi K, Motohashi H, Yamamoto M.** 2011. Molecular mechanisms of the Keap1-Nrf2 pathway in stress response and cancer evolution. Genes Cells **16:**123-140.

59. **Taguchi K, Yamamoto M.** 2017. The KEAP1-NRF2 System in Cancer. Front Oncol **7:**85.

60. **Zhang DD.** 2010. The Nrf2-Keap1-ARE signaling pathway: The regulation and dual function of Nrf2 in cancer. Antioxid Redox Signal **13:**1623-1626.

61. **Sykiotis GP, Bohmann D.** 2010. Stress-activated cap'n'collar transcription factors in aging and human disease. Sci Signal **3:**re3.

62. **Ahmed SM, Luo L, Namani A, Wang XJ, Tang X.** 2017. Nrf2 signaling pathway: Pivotal roles in inflammation. Biochim Biophys Acta **1863:**585-597.

63. **Keleku-Lukwete N, Suzuki M, Yamamoto M.** 2017. An Overview of the Advantages of KEAP1-NRF2 System Activation During Inflammatory Disease Treatment. Antioxid Redox Signal doi:10.1089/ars.2017.7358.

64. **Suzuki M, Otsuki A, Keleku-Lukwete N, Yamamoto M.** 2016. Overview of redox regulation by Keap1–Nrf2 system in toxicology and cancer. Current Opinion in Toxicology **1:**29-36.

65. **Yamazaki H, Tanji K, Wakabayashi K, Matsuura S, Itoh K.** 2015. Role of the Keap1/Nrf2 pathway in neurodegenerative diseases. Pathol Int **65:**210-219.

66. **Baird L, Dinkova-Kostova AT.** 2011. The cytoprotective role of the Keap1-Nrf2 pathway. Arch Toxicol **85:**241-272.

67. **Pandey P, Singh AK, Singh M, Tewari M, Shukla HS, Gambhir IS.** 2017. The see-saw of Keap1-Nrf2 pathway in cancer. Crit Rev Oncol Hematol **116:**89-98.

68. **Kensler TW, Wakabayashi N, Biswal S.** 2007. Cell survival responses to environmental stresses via the Keap1-Nrf2-ARE pathway. Annu Rev Pharmacol Toxicol **47:**89-116.

69. **Kobayashi A, Kang MI, Okawa H, Ohtsuji M, Zenke Y, Chiba T, Igarashi K, Yamamoto M.** 2004. Oxidative stress sensor Keap1 functions as an adaptor for Cul3-based E3 ligase to regulate proteasomal degradation of Nrf2. Mol Cell Biol **24:**7130-7139.

70. **Hast BE, Cloer EW, Goldfarb D, Li H, Siesser PF, Yan F, Walter V, Zheng N, Hayes DN, Major MB.** 2014. Cancer-derived mutations in KEAP1 impair NRF2 degradation but not ubiquitination. Cancer Res **74:**808-817.

71. **Kobayashi A, Ohta T, Yamamoto M.** 2004. Unique function of the Nrf2-Keap1 pathway in the inducible expression of antioxidant and detoxifying enzymes. Methods Enzymol **378:**273-286.

72. **Kobayashi M, Yamamoto M.** 2005. Molecular mechanisms activating the Nrf2-Keap1 pathway of antioxidant gene regulation. Antioxid Redox Signal **7:**385-394.

73. **McMahon M, Itoh K, Yamamoto M, Hayes JD.** 2003. Keap1-dependent proteasomal degradation of transcription factor Nrf2 contributes to the negative regulation of antioxidant response element-driven gene expression. J Biol Chem **278:**21592-21600.

74. **Takaya K, Suzuki T, Motohashi H, Onodera K, Satomi S, Kensler TW, Yamamoto M.** 2012. Validation of the multiple sensor mechanism of the Keap1-Nrf2 system. Free Radic Biol Med **53:**817-827.

75. **Yamamoto T, Suzuki T, Kobayashi A, Wakabayashi J, Maher J, Motohashi H, Yamamoto M.** 2008. Physiological significance of reactive cysteine residues of Keap1 in determining Nrf2 activity. Mol Cell Biol **28:**2758-2770.

76. **Zhang DD, Hannink M.** 2003. Distinct cysteine residues in Keap1 are required for Keap1-dependent ubiquitination of Nrf2 and for stabilization of Nrf2 by chemopreventive agents and oxidative stress. Mol Cell Biol **23:**8137-8151.

77. **Zhang DD, Lo SC, Cross JV, Templeton DJ, Hannink M.** 2004. Keap1 is a redox-regulated substrate adaptor protein for a Cul3-dependent ubiquitin ligase complex. Mol Cell Biol **24:**10941-10953.

78. **Zhang DD, Lo SC, Sun Z, Habib GM, Lieberman MW, Hannink M.** 2005. Ubiquitination of Keap1, a BTB-Kelch substrate adaptor protein for Cul3, targets Keap1 for degradation by a proteasome-independent pathway. J Biol Chem **280:**30091-30099.

79. **Rushmore TH, Pickett CB.** 1991. Xenobiotic responsive elements controlling inducible expression by planar aromatic compounds and phenolic antioxidants. Methods Enzymol **206:**409-420.

80. **Rushmore TH, Kong AN.** 2002. Pharmacogenomics, regulation and signaling pathways of phase I and II drug metabolizing enzymes. Curr Drug Metab **3:**481-490.

81. **Georgakopoulos ND, Frison M, Alvarez MS, Bertrand H, Wells G, Campanella M.** 2017. Reversible Keap1 inhibitors are preferential pharmacological tools to modulate cellular mitophagy. Sci Rep **7:**10303.

82. **Kuosmanen SM, Viitala S, Laitinen T, Perakyla M, Polonen P, Kansanen E, Leinonen H, Raju S, Wienecke-Baldacchino A, Narvanen A, Poso A, Heinaniemi M, Heikkinen S, Levonen AL.** 2016. The Effects of Sequence Variation on Genome-wide NRF2 Binding--New Target Genes and Regulatory SNPs. Nucleic Acids Res **44:**1760-1775.

83. **Saito H.** 2013. Toxico-pharmacological perspective of the Nrf2-Keap1 defense system against oxidative stress in kidney diseases. Biochem Pharmacol **85:**865-872.

84. **Iso T, Suzuki T, Baird L, Yamamoto M.** 2016. Absolute Amounts and Status of the Nrf2-Keap1-Cul3 Complex within Cells. Mol Cell Biol **36:**3100-3112.

85. **Baird L, Dinkova-Kostova AT.** 2013. Diffusion dynamics of the Keap1-Cullin3 interaction in single live cells. Biochem Biophys Res Commun **433:**58-65.

86. **Canning P, Cooper CD, Krojer T, Murray JW, Pike AC, Chaikuad A, Keates T, Thangaratnarajah C, Hojzan V, Ayinampudi V, Marsden BD, Gileadi O, Knapp S, von Delft F, Bullock AN.** 2013. Structural basis for Cul3 protein assembly with the BTB-Kelch family of E3 ubiquitin ligases. J Biol Chem **288:**7803-7814.

87. **Canning P, Sorrell FJ, Bullock AN.** 2015. Structural basis of Keap1 interactions with Nrf2. Free Radic Biol Med **88:**101-107.

88. **Mitsuishi Y, Taguchi K, Kawatani Y, Shibata T, Nukiwa T, Aburatani H, Yamamoto M, Motohashi H.** 2012. Nrf2 redirects glucose and glutamine into anabolic pathways in metabolic reprogramming. Cancer Cell **22:**66-79.

89. **DeNicola GM, Chen PH, Mullarky E, Sudderth JA, Hu Z, Wu D, Tang H, Xie Y, Asara JM, Huffman KE, Wistuba, II, Minna JD, DeBerardinis RJ, Cantley LC.** 2015. NRF2 regulates serine biosynthesis in non-small cell lung cancer. Nat Genet **47:**1475-1481.

90. **Namani A, Cui QQ, Wu Y, Wang H, Wang XJ, Tang X.** 2017. NRF2-regulated metabolic gene signature as a prognostic biomarker in non-small cell lung cancer. Oncotarget **8:**69847-69862.

91. **Chen PH, Smith TJ, Wu J, Siesser PF, Bisnett BJ, Khan F, Hogue M, Soderblom E, Tang F, Marks JR, Major MB, Swarts BM, Boyce M, Chi JT.** 2017. Glycosylation of KEAP1 links nutrient sensing to redox stress signaling. EMBO J **36:**2233-2250.

92. **Choi B-h, Kwak M-K.** 2016. Shadows of NRF2 in cancer: Resistance to chemotherapy. Current Opinion in Toxicology **1:**20-28.

93. **Chorley BN, Campbell MR, Wang X, Karaca M, Sambandan D, Bangura F, Xue P, Pi J, Kleeberger SR, Bell DA.** 2012. Identification of novel NRF2-regulated genes by ChIP-Seq: influence on retinoid X receptor alpha. Nucleic Acids Res **40:**7416-7429.

94. **Jaramillo MC, Zhang DD.** 2013. The emerging role of the Nrf2-Keap1 signaling pathway in cancer. Genes Dev **27:**2179-2191.

95. **Cazanave SC, Wang X, Zhou H, Rahmani M, Grant S, Durrant DE, Klaassen CD, Yamamoto M, Sanyal AJ.** 2014. Degradation of Keap1 activates BH3-only proteins Bim and PUMA during hepatocyte lipoapoptosis. Cell Death Differ **21:**1303-1312.

96. **Ichimura Y, Waguri S, Sou YS, Kageyama S, Hasegawa J, Ishimura R, Saito T, Yang Y, Kouno T, Fukutomi T, Hoshii T, Hirao A, Takagi K, Mizushima T, Motohashi H, Lee MS, Yoshimori T, Tanaka K, Yamamoto M, Komatsu M.** 2013. Phosphorylation of p62 activates the Keap1-Nrf2 pathway during selective autophagy. Mol Cell **51:**618-631.

97. **Kageyama S, Sou YS, Uemura T, Kametaka S, Saito T, Ishimura R, Kouno T, Bedford L, Mayer RJ, Lee MS, Yamamoto M, Waguri S, Tanaka K, Komatsu M.** 2014. Proteasome dysfunction activates autophagy and the Keap1-Nrf2 pathway. J Biol Chem **289:**24944-24955.

98. **Lo SC, Hannink M.** 2006. PGAM5, a Bcl-XL-interacting protein, is a novel substrate for the redox-regulated Keap1-dependent ubiquitin ligase complex. J Biol Chem **281:**37893-37903.

99. **Lo SC, Hannink M.** 2008. PGAM5 tethers a ternary complex containing Keap1 and Nrf2 to mitochondria. Exp Cell Res **314:**1789-1803.

100. **Niture SK, Jaiswal AK.** 2011. Inhibitor of Nrf2 (INrf2 or Keap1) protein degrades Bcl-xL via phosphoglycerate mutase 5 and controls cellular apoptosis. J Biol Chem **286:**44542-44556.

101. **Niture SK, Jaiswal AK.** 2011. INrf2 (Keap1) targets Bcl-2 degradation and controls cellular apoptosis. Cell Death Differ **18:**439-451.

102. **Tian H, Zhang B, Di J, Jiang G, Chen F, Li H, Li L, Pei D, Zheng J.** 2012. Keap1: one stone kills three birds Nrf2, IKKbeta and Bcl-2/Bcl-xL. Cancer Lett **325:**26-34.

103. **Pickart CM, Cohen RE.** 2004. Proteasomes and their kin: proteases in the machine age. Nat Rev Mol Cell Biol **5:**177-187.

104. **Pickart CM, Fushman D.** 2004. Polyubiquitin chains: polymeric protein signals. Curr Opin Chem Biol **8:**610-616.

105. **Murata S, Yashiroda H, Tanaka K.** 2009. Molecular mechanisms of proteasome assembly. Nat Rev Mol Cell Biol **10:**104-115.

106. **Ciechanover A, Stanhill A.** 2014. The complexity of recognition of ubiquitinated substrates by the 26S proteasome. Biochim Biophys Acta **1843:**86-96.

107. **Livneh I, Cohen-Kaplan V, Cohen-Rosenzweig C, Avni N, Ciechanover A.** 2016. The life cycle of the 26S proteasome: from birth, through regulation and function, and onto its death. Cell Res **26:**869-885.

108. **Jin M, Klionsky DJ.** 2014. Regulation of autophagy: modulation of the size and number of autophagosomes. FEBS Lett **588:**2457-2463.

109. **Klionsky DJ, Baehrecke EH, Brumell JH, Chu CT, Codogno P, Cuervo AM, Debnath J, Deretic V, Elazar Z, Eskelinen EL, Finkbeiner S, Fueyo-Margareto J, Gewirtz D, Jaattela M, Kroemer G, Levine B, Melia TJ, Mizushima N, Rubinsztein DC, Simonsen A, Thorburn A, Thumm M, Tooze SA.** 2011. A comprehensive glossary of autophagy-related molecules and processes (2nd edition). Autophagy **7:**1273-1294.

110. **Yin Z, Pascual C, Klionsky DJ.** 2016. Autophagy: machinery and regulation. Microb Cell **3:**588-596.

111. **Jiang P, Mizushima N.** 2014. Autophagy and human diseases. Cell Res **24:**69-79.

112. **Mizushima N.** 2007. Autophagy: process and function. Genes Dev **21:**2861-2873.

113. **Mizushima N.** 2010. Autophagy. FEBS Lett **584:**1279.

114. **Mizushima N, Komatsu M.** 2011. Autophagy: renovation of cells and tissues. Cell **147:**728-741.

115. **Peng H, Yang J, Li G, You Q, Han W, Li T, Gao D, Xie X, Lee BH, Du J, Hou J, Zhang T, Rao H, Huang Y, Li Q, Zeng R, Hui L, Wang H, Xia Q, Zhang X, He Y, Komatsu M, Dikic I, Finley D, Hu R.** 2017. Ubiquitylation of p62/sequestosome1 activates its autophagy receptor function and controls selective autophagy upon ubiquitin stress. Cell Res **27:**657-674.

116. **Lee Y, Chou TF, Pittman SK, Keith AL, Razani B, Weihl CC.** 2017. Keap1/Cullin3 Modulates p62/SQSTM1 Activity via UBA Domain Ubiquitination. Cell Rep **20:**1994.

117. **Kirkin V, Lamark T, Sou YS, Bjorkoy G, Nunn JL, Bruun JA, Shvets E, McEwan DG, Clausen TH, Wild P, Bilusic I, Theurillat JP, Overvatn A, Ishii T, Elazar Z, Komatsu M, Dikic I, Johansen T.** 2009. A role for NBR1 in autophagosomal degradation of ubiquitinated substrates. Mol Cell **33:**505-516.

118. **Thu KL, Pikor LA, Chari R, Wilson IM, Macaulay CE, English JC, Tsao MS, Gazdar AF, Lam S, Lam WL, Lockwood WW.** 2011. Genetic disruption of KEAP1/CUL3 E3 ubiquitin ligase complex components is a key mechanism of NF-kappaB pathway activation in lung cancer. J Thorac Oncol **6:**1521-1529.

119. **Jain A, Lamark T, Sjottem E, Larsen KB, Awuh JA, Overvatn A, McMahon M, Hayes JD, Johansen T.** 2010. p62/SQSTM1 is a target gene for transcription factor NRF2 and creates a positive feedback loop by inducing antioxidant response element-driven gene transcription. J Biol Chem **285:**22576-22591.

120. **Katsuragi Y, Ichimura Y, Komatsu M.** 2016. Regulation of the Keap1–Nrf2 pathway by p62/SQSTM1. Current Opinion in Toxicology **1:**54-61.

121. **Taguchi K, Fujikawa N, Komatsu M, Ishii T, Unno M, Akaike T, Motohashi H, Yamamoto M.** 2012. Keap1 degradation by autophagy for the maintenance of redox homeostasis. Proc Natl Acad Sci U S A **109:**13561-13566.

122. **Komatsu M, Kurokawa H, Waguri S, Taguchi K, Kobayashi A, Ichimura Y, Sou YS, Ueno I, Sakamoto A, Tong KI, Kim M, Nishito Y, Iemura S, Natsume T, Ueno T, Kominami E, Motohashi H, Tanaka K, Yamamoto M.** 2010. The selective autophagy substrate p62 activates the stress responsive transcription factor Nrf2 through inactivation of Keap1. Nat Cell Biol **12:**213-223.

123. **Ma J, Cai H, Wu T, Sobhian B, Huo Y, Alcivar A, Mehta M, Cheung KL, Ganesan S, Kong AN, Zhang DD, Xia B.** 2012. PALB2 interacts with KEAP1 to promote NRF2 nuclear accumulation and function. Mol Cell Biol **32:**1506-1517.

124. **Orthwein A, Noordermeer SM, Wilson MD, Landry S, Enchev RI, Sherker A, Munro M, Pinder J, Salsman J, Dellaire G, Xia B, Peter M, Durocher D.** 2015. A mechanism for the suppression of homologous recombination in G1 cells. Nature **528:**422-426.

125. **Mulvaney KM, Matson JP, Siesser PF, Tamir TY, Goldfarb D, Jacobs TM, Cloer EW, Harrison JS, Vaziri C, Cook JG, Major MB.** 2016. Identification and Characterization of MCM3 as a Kelch-like ECH-associated Protein 1 (KEAP1) Substrate. J Biol Chem **291:**23719-23733.

126. **Tamir TY, Mulvaney KM, Major MB.** 2016. Dissecting the Keap1/Nrf2 pathway through proteomics. Current Opinion in Toxicology **1:**118-124.

127. **Hast BE, Goldfarb D, Mulvaney KM, Hast MA, Siesser PF, Yan F, Hayes DN, Major MB.** 2013. Proteomic analysis of ubiquitin ligase KEAP1 reveals associated proteins that inhibit NRF2 ubiquitination. Cancer Res **73:**2199-2210.

128. **Moi P, Chan K, Asunis I, Cao A, Kan YW.** 1994. Isolation of NF-E2-related factor 2 (Nrf2), a NF-E2-like basic leucine zipper transcriptional activator that binds to the tandem NF-E2/AP1 repeat of the beta-globin locus control region. Proc Natl Acad Sci U S A **91:**9926-9930.

129. **Higgins LG, Hayes JD.** 2011. The cap'n'collar transcription factor Nrf2 mediates both intrinsic resistance to environmental stressors and an adaptive response elicited by chemopreventive agents that determines susceptibility to electrophilic xenobiotics. Chem Biol Interact **192:**37-45.

130. **Toki T, Itoh J, Kitazawa J, Arai K, Hatakeyama K, Akasaka J, Igarashi K, Nomura N, Yokoyama M, Yamamoto M, Ito E.** 1997. Human small Maf proteins form heterodimers with CNC family transcription factors and recognize the NF-E2 motif. Oncogene **14:**1901-1910.

131. **Katsuoka F, Motohashi H, Engel JD, Yamamoto M.** 2005. Nrf2 transcriptionally activates the mafG gene through an antioxidant response element. J Biol Chem **280:**4483-4490.

132. **Katsuoka F, Yamamoto M.** 2016. Small Maf proteins (MafF, MafG, MafK): History, structure and function. Gene **586:**197-205.

133. **Li W, Yu S, Liu T, Kim JH, Blank V, Li H, Kong AN.** 2008. Heterodimerization with small Maf proteins enhances nuclear retention of Nrf2 via masking the NESzip motif. Biochim Biophys Acta **1783:**1847-1856.

134. **Motohashi H, Katsuoka F, Engel JD, Yamamoto M.** 2004. Small Maf proteins serve as transcriptional cofactors for keratinocyte differentiation in the Keap1-Nrf2 regulatory pathway. Proc Natl Acad Sci U S A **101:**6379-6384.

135. **Li L, Kobayashi M, Kaneko H, Nakajima-Takagi Y, Nakayama Y, Yamamoto M.** 2008. Molecular evolution of Keap1. Two Keap1 molecules with distinctive intervening region structures are conserved among fish. J Biol Chem **283:**3248-3255.

136. **Li W, Kong AN.** 2009. Molecular mechanisms of Nrf2-mediated antioxidant response. Mol Carcinog **48:**91-104.

137. **Li W, Yu SW, Kong AN.** 2006. Nrf2 possesses a redox-sensitive nuclear exporting signal in the Neh5 transactivation domain. J Biol Chem **281:**27251-27263.

138. **Lau A, Villeneuve NF, Sun Z, Wong PK, Zhang DD.** 2008. Dual roles of Nrf2 in cancer. Pharmacol Res **58:**262-270.

139. **Hayes JD, Chowdhry S, Dinkova-Kostova AT, Sutherland C.** 2015. Dual regulation of transcription factor Nrf2 by Keap1 and by the combined actions of beta-TrCP and GSK-3. Biochem Soc Trans **43:**611-620.

140. **Chowdhry S, Zhang Y, McMahon M, Sutherland C, Cuadrado A, Hayes JD.** 2013. Nrf2 is controlled by two distinct beta-TrCP recognition motifs in its Neh6 domain, one of which can be modulated by GSK-3 activity. Oncogene **32:**3765-3781.

141. **Hayes JD, McMahon M, Chowdhry S, Dinkova-Kostova AT.** 2010. Cancer chemoprevention mechanisms mediated through the Keap1-Nrf2 pathway. Antioxid Redox Signal **13:**1713-1748.

142. **Huang HC, Nguyen T, Pickett CB.** 2002. Phosphorylation of Nrf2 at Ser-40 by protein kinase C regulates antioxidant response element-mediated transcription. J Biol Chem **277:**42769-42774.

143. **Huang HC, Nguyen T, Pickett CB.** 2000. Regulation of the antioxidant response element by protein kinase C-mediated phosphorylation of NF-E2-related factor 2. Proc Natl Acad Sci U S A **97:**12475-12480.

144. **Nioi P, Nguyen T, Sherratt PJ, Pickett CB.** 2005. The carboxy-terminal Neh3 domain of Nrf2 is required for transcriptional activation. Mol Cell Biol **25:**10895-10906.

145. **Katoh Y, Itoh K, Yoshida E, Miyagishi M, Fukamizu A, Yamamoto M.** 2001. Two domains of Nrf2 cooperatively bind CBP, a CREB binding protein, and synergistically activate transcription. Genes Cells **6:**857-868.

146. **Wang H, Liu K, Geng M, Gao P, Wu X, Hai Y, Li Y, Li Y, Luo L, Hayes JD, Wang XJ, Tang X.** 2013. RXRalpha inhibits the NRF2-ARE signaling pathway through a direct interaction with the Neh7 domain of NRF2. Cancer Res **73:**3097-3108.

147. **Itoh K, Wakabayashi N, Katoh Y, Ishii T, Igarashi K, Engel JD, Yamamoto M.** 1999. Keap1 represses nuclear activation of antioxidant responsive elements by Nrf2 through binding to the amino-terminal Neh2 domain. Genes Dev **13:**76-86.

148. **Nguyen T, Sherratt PJ, Huang HC, Yang CS, Pickett CB.** 2003. Increased protein stability as a mechanism that enhances Nrf2-mediated transcriptional activation of the antioxidant response element. Degradation of Nrf2 by the 26 S proteasome. J Biol Chem **278:**4536-4541.

149. **Zipper LM, Mulcahy RT.** 2002. The Keap1 BTB/POZ dimerization function is required to sequester Nrf2 in cytoplasm. J Biol Chem **277:**36544-36552.

150. **Cleasby A, Yon J, Day PJ, Richardson C, Tickle IJ, Williams PA, Callahan JF, Carr R, Concha N, Kerns JK, Qi H, Sweitzer T, Ward P, Davies TG.** 2014. Structure of the BTB domain of Keap1 and its interaction with the triterpenoid antagonist CDDO. PLoS One **9:**e98896.

151. **Quinti L, Dayalan Naidu S, Trager U, Chen X, Kegel-Gleason K, Lleres D, Connolly C, Chopra V, Low C, Moniot S, Sapp E, Tousley AR, Vodicka P, Van Kanegan MJ, Kaltenbach LS, Crawford LA, Fuszard M, Higgins M, Miller JRC, Farmer RE, Potluri V, Samajdar S, Meisel L, Zhang N, Snyder A, Stein R, Hersch SM, Ellerby LM, Weerapana E, Schwarzschild MA, Steegborn C, Leavitt BR, Degterev A, Tabrizi SJ, Lo DC, DiFiglia M, Thompson LM, Dinkova-Kostova AT, Kazantsev AG.** 2017. KEAP1-modifying small molecule reveals muted NRF2 signaling responses in neural stem cells from Huntington's disease patients. Proc Natl Acad Sci U S A **114:**E4676-E4685.

152. **Rachakonda G, Xiong Y, Sekhar KR, Stamer SL, Liebler DC, Freeman ML.** 2008. Covalent modification at Cys151 dissociates the electrophile sensor Keap1 from the ubiquitin ligase CUL3. Chem Res Toxicol **21:**705-710.

153. **Eggler AL, Small E, Hannink M, Mesecar AD.** 2009. Cul3-mediated Nrf2 ubiquitination and antioxidant response element (ARE) activation are dependent on the partial molar volume at position 151 of Keap1. Biochem J **422:**171-180.

154. **Chauhan N, Chaunsali L, Deshmukh P, Padmanabhan B.** 2013. Analysis of dimerization of BTB-IVR domains of Keap1 and its interaction with Cul3, by molecular modeling. Bioinformation **9:**450-455.

155. **Tao S, Liu P, Luo G, Rojo de la Vega M, Chen H, Wu T, Tillotson J, Chapman E, Zhang DD.** 2017. p97 Negatively Regulates NRF2 by Extracting Ubiquitylated NRF2 from the KEAP1-CUL3 E3 Complex. Mol Cell Biol **37**.

156. **Canning P, Bullock AN.** 2014. New strategies to inhibit KEAP1 and the Cul3-based E3 ubiquitin ligases. Biochem Soc Trans **42:**103-107.

157. **Fuse Y, Kobayashi M.** 2017. Conservation of the Keap1-Nrf2 System: An Evolutionary Journey through Stressful Space and Time. Molecules **22**.

158. **Wall SB, Oh JY, Diers AR, Landar A.** 2012. Oxidative modification of proteins: an emerging mechanism of cell signaling. Front Physiol **3:**369.

159. **Eggler AL, Liu G, Pezzuto JM, van Breemen RB, Mesecar AD.** 2005. Modifying specific cysteines of the electrophile-sensing human Keap1 protein is insufficient to disrupt binding to the Nrf2 domain Neh2. Proc Natl Acad Sci U S A **102:**10070-10075.

160. **Dinkova-Kostova AT, Holtzclaw WD, Cole RN, Itoh K, Wakabayashi N, Katoh Y, Yamamoto M, Talalay P.** 2002. Direct evidence that sulfhydryl groups of Keap1 are the sensors regulating induction of phase 2 enzymes that protect against carcinogens and oxidants. Proc Natl Acad Sci U S A **99:**11908-11913.

161. **Itoh K, Tong KI, Yamamoto M.** 2004. Molecular mechanism activating Nrf2-Keap1 pathway in regulation of adaptive response to electrophiles. Free Radic Biol Med **36:**1208-1213.

162. **Li X, Zhang D, Hannink M, Beamer LJ.** 2004. Crystallization and initial crystallographic analysis of the Kelch domain from human Keap1. Acta Crystallogr D Biol Crystallogr **60:**2346-2348.

163. **Li X, Zhang D, Hannink M, Beamer LJ.** 2004. Crystal structure of the Kelch domain of human Keap1. J Biol Chem **279:**54750-54758.

164. **Lo SC, Li X, Henzl MT, Beamer LJ, Hannink M.** 2006. Structure of the Keap1:Nrf2 interface provides mechanistic insight into Nrf2 signaling. EMBO J **25:**3605-3617.

165. **Fukutomi T, Takagi K, Mizushima T, Ohuchi N, Yamamoto M.** 2014. Kinetic, thermodynamic, and structural characterizations of the association between Nrf2-DLGex degron and Keap1. Mol Cell Biol **34:**832-846.

166. **Ogura T, Tong KI, Mio K, Maruyama Y, Kurokawa H, Sato C, Yamamoto M.** 2010. Keap1 is a forked-stem dimer structure with two large spheres enclosing the intervening, double glycine repeat, and C-terminal domains. Proc Natl Acad Sci U S A **107:**2842-2847.

167. **Tong KI, Katoh Y, Kusunoki H, Itoh K, Tanaka T, Yamamoto M.** 2006. Keap1 recruits Neh2 through binding to ETGE and DLG motifs: characterization of the two-site molecular recognition model. Mol Cell Biol **26:**2887-2900.

168. **Tong KI, Kobayashi A, Katsuoka F, Yamamoto M.** 2006. Two-site substrate recognition model for the Keap1-Nrf2 system: a hinge and latch mechanism. Biol Chem **387:**1311-1320.

169. **Tong KI, Padmanabhan B, Kobayashi A, Shang C, Hirotsu Y, Yokoyama S, Yamamoto M.** 2007. Different electrostatic potentials define ETGE and DLG motifs as hinge and latch in oxidative stress response. Mol Cell Biol **27:**7511-7521.

170. **Albagli O, Dhordain P, Deweindt C, Lecocq G, Leprince D.** 1995. The BTB/POZ domain: a new protein-protein interaction motif common to DNA- and actin-binding proteins. Cell Growth Differ **6:**1193-1198.

171. **Furukawa M, Xiong Y.** 2005. BTB protein Keap1 targets antioxidant transcription factor Nrf2 for ubiquitination by the Cullin 3-Roc1 ligase. Mol Cell Biol **25:**162-171.

172. **McMahon M, Thomas N, Itoh K, Yamamoto M, Hayes JD.** 2006. Dimerization of substrate adaptors can facilitate cullin-mediated ubiquitylation of proteins by a "tethering" mechanism: a two-site interaction model for the Nrf2-Keap1 complex. J Biol Chem **281:**24756-24768.

173. **Baird L, Lleres D, Swift S, Dinkova-Kostova AT.** 2013. Regulatory flexibility in the Nrf2-mediated stress response is conferred by conformational cycling of the Keap1-Nrf2 protein complex. Proc Natl Acad Sci U S A **110:**15259-15264.

174. **Kwak MK, Wakabayashi N, Greenlaw JL, Yamamoto M, Kensler TW.** 2003. Antioxidants enhance mammalian proteasome expression through the Keap1-Nrf2 signaling pathway. Mol Cell Biol **23:**8786-8794.

175. **Wakabayashi N, Itoh K, Wakabayashi J, Motohashi H, Noda S, Takahashi S, Imakado S, Kotsuji T, Otsuka F, Roop DR, Harada T, Engel JD, Yamamoto M.** 2003. Keap1-null mutation leads to postnatal lethality due to constitutive Nrf2 activation. Nat Genet **35:**238-245.

176. **Itoh K, Chiba T, Takahashi S, Ishii T, Igarashi K, Katoh Y, Oyake T, Hayashi N, Satoh K, Hatayama I, Yamamoto M, Nabeshima Y.** 1997. An Nrf2/small Maf heterodimer mediates the induction of phase II detoxifying enzyme genes through antioxidant response elements. Biochem Biophys Res Commun **236:**313-322.

177. **Blake DJ, Singh A, Kombairaju P, Malhotra D, Mariani TJ, Tuder RM, Gabrielson E, Biswal S.** 2010. Deletion of Keap1 in the lung attenuates acute cigarette smoke-induced oxidative stress and inflammation. Am J Respir Cell Mol Biol **42:**524-536.

178. **Iizuka T, Ishii Y, Itoh K, Kiwamoto T, Kimura T, Matsuno Y, Morishima Y, Hegab AE, Homma S, Nomura A, Sakamoto T, Shimura M, Yoshida A, Yamamoto M, Sekizawa K.** 2005. Nrf2-deficient mice are highly susceptible to cigarette smoke-induced emphysema. Genes Cells **10:**1113-1125.

179. **Ishii Y, Itoh K, Morishima Y, Kimura T, Kiwamoto T, Iizuka T, Hegab AE, Hosoya T, Nomura A, Sakamoto T, Yamamoto M, Sekizawa K.** 2005. Transcription factor Nrf2 plays a pivotal role in protection against elastase-induced pulmonary inflammation and emphysema. J Immunol **175:**6968-6975.

180. **Boutten A, Goven D, Artaud-Macari E, Boczkowski J, Bonay M.** 2011. NRF2 targeting: a promising therapeutic strategy in chronic obstructive pulmonary disease. Trends Mol Med **17:**363-371.

181. **Johnson JA, Johnson DA, Kraft AD, Calkins MJ, Jakel RJ, Vargas MR, Chen PC.** 2008. The Nrf2-ARE pathway: an indicator and modulator of oxidative stress in neurodegeneration. Ann N Y Acad Sci **1147:**61-69.

182. **Yang Y, Jiang S, Yan J, Li Y, Xin Z, Lin Y, Qu Y.** 2015. An overview of the molecular mechanisms and novel roles of Nrf2 in neurodegenerative disorders. Cytokine Growth Factor Rev **26:**47-57.

183. **Vargas MR, Johnson DA, Sirkis DW, Messing A, Johnson JA.** 2008. Nrf2 activation in astrocytes protects against neurodegeneration in mouse models of familial amyotrophic lateral sclerosis. J Neurosci **28:**13574-13581.

184. **Calkins MJ, Jakel RJ, Johnson DA, Chan K, Kan YW, Johnson JA.** 2005. Protection from mitochondrial complex II inhibition in vitro and in vivo by Nrf2-mediated transcription. Proc Natl Acad Sci U S A **102:**244-249.

185. **Barnham KJ, Masters CL, Bush AI.** 2004. Neurodegenerative diseases and oxidative stress. Nat Rev Drug Discov **3:**205-214.

186. **Deshmukh P, Unni S, Krishnappa G, Padmanabhan B.** 2017. The Keap1-Nrf2 pathway: promising therapeutic target to counteract ROS-mediated damage in cancers and neurodegenerative diseases. Biophys Rev **9:**41-56.

187. **Tanji K, Maruyama A, Odagiri S, Mori F, Itoh K, Kakita A, Takahashi H, Wakabayashi K.** 2013. Keap1 is localized in neuronal and glial cytoplasmic inclusions in various neurodegenerative diseases. J Neuropathol Exp Neurol **72:**18-28.

188. **Houghton AM.** 2013. Mechanistic links between COPD and lung cancer. Nat Rev Cancer **13:**233-245.

189. **Goldstein LD, Lee J, Gnad F, Klijn C, Schaub A, Reeder J, Daemen A, Bakalarski CE, Holcomb T, Shames DS, Hartmaier RJ, Chmielecki J, Seshagiri S, Gentleman R, Stokoe D.** 2016. Recurrent Loss of NFE2L2 Exon 2 Is a Mechanism for Nrf2 Pathway Activation in Human Cancers. Cell Rep **16:**2605-2617.

190. **Hanada N, Takahata T, Zhou Q, Ye X, Sun R, Itoh J, Ishiguro A, Kijima H, Mimura J, Itoh K, Fukuda S, Saijo Y.** 2012. Methylation of the KEAP1 gene promoter region in human colorectal cancer. BMC Cancer **12:**66.

191. **Hayes JD, McMahon M.** 2009. NRF2 and KEAP1 mutations: permanent activation of an adaptive response in cancer. Trends Biochem Sci **34:**176-188.

192. **Homma S, Ishii Y, Morishima Y, Yamadori T, Matsuno Y, Haraguchi N, Kikuchi N, Satoh H, Sakamoto T, Hizawa N, Itoh K, Yamamoto M.** 2009. Nrf2 enhances cell proliferation and resistance to anticancer drugs in human lung cancer. Clin Cancer Res **15:**3423-3432.

193. **Huang Y, Li W, Su ZY, Kong AN.** 2015. The complexity of the Nrf2 pathway: beyond the antioxidant response. J Nutr Biochem **26:**1401-1413.

194. **Jiang T, Chen N, Zhao F, Wang XJ, Kong B, Zheng W, Zhang DD.** 2010. High levels of Nrf2 determine chemoresistance in type II endometrial cancer. Cancer Res **70:**5486-5496.

195. **Solis LM, Behrens C, Dong W, Suraokar M, Ozburn NC, Moran CA, Corvalan AH, Biswal S, Swisher SG, Bekele BN, Minna JD, Stewart DJ, Wistuba, II.** 2010. Nrf2 and Keap1 abnormalities in non-small cell lung carcinoma and association with clinicopathologic features. Clin Cancer Res **16:**3743-3753.

196. **Wang XJ, Sun Z, Villeneuve NF, Zhang S, Zhao F, Li Y, Chen W, Yi X, Zheng W, Wondrak GT, Wong PK, Zhang DD.** 2008. Nrf2 enhances resistance of cancer cells to chemotherapeutic drugs, the dark side of Nrf2. Carcinogenesis **29:**1235-1243.

197. **Singh A, Misra V, Thimmulappa RK, Lee H, Ames S, Hoque MO, Herman JG, Baylin SB, Sidransky D, Gabrielson E, Brock MV, Biswal S.** 2006. Dysfunctional KEAP1-NRF2 interaction in non-small-cell lung cancer. PLoS Med **3:**e420.

198. **Martinez VD, Vucic EA, Thu KL, Pikor LA, Lam S, Lam WL.** 2015. Disruption of KEAP1/CUL3/RBX1 E3-ubiquitin ligase complex components by multiple genetic mechanisms: Association with poor prognosis in head and neck cancer. Head Neck **37:**727-734.

199. **Padmanabhan B, Tong KI, Ohta T, Nakamura Y, Scharlock M, Ohtsuji M, Kang MI, Kobayashi A, Yokoyama S, Yamamoto M.** 2006. Structural basis for defects of Keap1 activity provoked by its point mutations in lung cancer. Mol Cell **21:**689-700.

200. **Ohta T, Iijima K, Miyamoto M, Nakahara I, Tanaka H, Ohtsuji M, Suzuki T, Kobayashi A, Yokota J, Sakiyama T, Shibata T, Yamamoto M, Hirohashi S.** 2008. Loss of Keap1 function activates Nrf2 and provides advantages for lung cancer cell growth. Cancer Res **68:**1303-1309.

201. **Chen W, Sun Z, Wang XJ, Jiang T, Huang Z, Fang D, Zhang DD.** 2009. Direct interaction between Nrf2 and p21(Cip1/WAF1) upregulates the Nrf2-mediated antioxidant response. Mol Cell **34:**663-673.

202. **Esposito F, Cuccovillo F, Russo L, Casella F, Russo T, Cimino F.** 1998. A new p21waf1/cip1 isoform is an early event of cell response to oxidative stress. Cell Death Differ **5:**940-945.

203. **Villeneuve NF, Sun Z, Chen W, Zhang DD.** 2009. Nrf2 and p21 regulate the fine balance between life and death by controlling ROS levels. Cell Cycle **8:**3255-3256.

204. **Camp ND, James RG, Dawson DW, Yan F, Davison JM, Houck SA, Tang X, Zheng N, Major MB, Moon RT.** 2012. Wilms tumor gene on X chromosome (WTX) inhibits degradation of NRF2 protein through competitive binding to KEAP1 protein. J Biol Chem **287:**6539-6550.

205. **Kinch L, Grishin NV, Brugarolas J.** 2011. Succination of Keap1 and activation of Nrf2-dependent antioxidant pathways in FH-deficient papillary renal cell carcinoma type 2. Cancer Cell **20:**418-420.

206. **Lu MC, Ji JA, Jiang ZY, You QD.** 2016. The Keap1-Nrf2-ARE Pathway As a Potential Preventive and Therapeutic Target: An Update. Med Res Rev **36:**924-963.

207. **Singh A, Boldin-Adamsky S, Thimmulappa RK, Rath SK, Ashush H, Coulter J, Blackford A, Goodman SN, Bunz F, Watson WH, Gabrielson E, Feinstein E, Biswal S.** 2008. RNAi-mediated silencing of nuclear factor erythroid-2-related factor 2 gene expression in non-small cell lung cancer inhibits tumor growth and increases efficacy of chemotherapy. Cancer Res **68:**7975-7984.

208. **Tang X, Wang H, Fan L, Wu X, Xin A, Ren H, Wang XJ.** 2011. Luteolin inhibits Nrf2 leading to negative regulation of the Nrf2/ARE pathway and sensitization of human lung carcinoma A549 cells to therapeutic drugs. Free Radic Biol Med **50:**1599-1609.

209. **Cescon DW, She D, Sakashita S, Zhu CQ, Pintilie M, Shepherd FA, Tsao MS.** 2015. NRF2 Pathway Activation and Adjuvant Chemotherapy Benefit in Lung Squamous Cell Carcinoma. Clin Cancer Res **21:**2499-2505.

210. **Guntas G, Lewis SM, Mulvaney KM, Cloer EW, Tripathy A, Lane TR, Major MB, Kuhlman B.** 2016. Engineering a genetically encoded competitive inhibitor of the KEAP1-NRF2 interaction via structure-based design and phage display. Protein Eng Des Sel **29:**1-9.

211. **Wen X, Thorne G, Hu L, Joy MS, Aleksunes LM.** 2015. Activation of NRF2 Signaling in HEK293 Cells by a First-in-Class Direct KEAP1-NRF2 Inhibitor. J Biochem Mol Toxicol **29:**261-266.

212. **Hu L, Magesh S, Chen L, Wang L, Lewis TA, Chen Y, Khodier C, Inoyama D, Beamer LJ, Emge TJ, Shen J, Kerrigan JE, Kong AN, Dandapani S, Palmer M, Schreiber SL, Munoz B.** 2013. Discovery of a small-molecule inhibitor and cellular probe of Keap1-Nrf2 protein-protein interaction. Bioorg Med Chem Lett **23:**3039-3043.

213. **Jnoff E, Albrecht C, Barker JJ, Barker O, Beaumont E, Bromidge S, Brookfield F, Brooks M, Bubert C, Ceska T, Corden V, Dawson G, Duclos S, Fryatt T, Genicot C, Jigorel E, Kwong J, Maghames R, Mushi I, Pike R, Sands ZA, Smith MA, Stimson CC, Courade JP.** 2014. Binding mode and structure-activity relationships around direct inhibitors of the Nrf2-Keap1 complex. ChemMedChem **9:**699-705.

214. **East DA, Fagiani F, Crosby J, Georgakopoulos ND, Bertrand H, Schaap M, Fowkes A, Wells G, Campanella M.** 2014. PMI: a DeltaPsim independent pharmacological regulator of mitophagy. Chem Biol **21:**1585-1596.

215. **Probst BL, Trevino I, McCauley L, Bumeister R, Dulubova I, Wigley WC, Ferguson DA.** 2015. RTA 408, A Novel Synthetic Triterpenoid with Broad Anticancer and Anti-Inflammatory Activity. PLoS One **10:**e0122942.

216. **Luo Z, Pan Y, Jeong LS, Liu J, Jia L.** 2012. Inactivation of the Cullin (CUL)-RING E3 ligase by the NEDD8-activating enzyme inhibitor MLN4924 triggers protective autophagy in cancer cells. Autophagy **8:**1677-1679.

217. **Zhao Y, Xiong X, Jia L, Sun Y.** 2012. Targeting Cullin-RING ligases by MLN4924 induces autophagy via modulating the HIF1-REDD1-TSC1-mTORC1-DEPTOR axis. Cell Death Dis **3:**e386.

218. **Lu MC, Ji JA, Jiang YL, Chen ZY, Yuan ZW, You QD, Jiang ZY.** 2016. An inhibitor of the Keap1-Nrf2 protein-protein interaction protects NCM460 colonic cells and alleviates experimental colitis. Sci Rep **6:**26585.

219. **Lu MC, Yuan ZW, Jiang YL, Chen ZY, You QD, Jiang ZY.** 2016. A systematic molecular dynamics approach to the study of peptide Keap1-Nrf2 protein-protein interaction inhibitors and its application to p62 peptides. Mol Biosyst **12:**1378-1387.

220. **Ramos-Gomez M, Dolan PM, Itoh K, Yamamoto M, Kensler TW.** 2003. Interactive effects of nrf2 genotype and oltipraz on benzo[a]pyrene-DNA adducts and tumor yield in mice. Carcinogenesis **24:**461-467.

221. **Sharma S, Gao P, Steele VE.** 2006. The chemopreventive efficacy of inhaled oltipraz particulates in the B[a]P-induced A/J mouse lung adenoma model. Carcinogenesis **27:**1721-1727.

222. **Kelley MJ, Glaser EM, Herndon JE, 2nd, Becker F, Bhagat R, Zhang YJ, Santella RM, Carmella SG, Hecht SS, Gallot L, Schilder L, Crowell JA, Perloff M, Folz RJ, Bergan RC.** 2005. Safety and efficacy of weekly oral oltipraz in chronic smokers. Cancer Epidemiol Biomarkers Prev **14:**892-899.

223. **Bauer AK, Hill T, 3rd, Alexander CM.** 2013. The involvement of NRF2 in lung cancer. Oxid Med Cell Longev **2013:**746432.

224. **Menegon S, Columbano A, Giordano S.** 2016. The Dual Roles of NRF2 in Cancer. Trends Mol Med **22:**578-593.

225. **Bollong MJ, Yun H, Sherwood L, Woods AK, Lairson LL, Schultz PG.** 2015. A Small Molecule Inhibits Deregulated NRF2 Transcriptional Activity in Cancer. ACS Chem Biol **10:**2193-2198.

226. **Ren D, Villeneuve NF, Jiang T, Wu T, Lau A, Toppin HA, Zhang DD.** 2011. Brusatol enhances the efficacy of chemotherapy by inhibiting the Nrf2-mediated defense mechanism. Proc Natl Acad Sci U S A **108:**1433-1438.

227. **Choi EJ, Jung BJ, Lee SH, Yoo HS, Shin EA, Ko HJ, Chang S, Kim SY, Jeon SM.** 2017. A clinical drug library screen identifies clobetasol propionate as an NRF2 inhibitor with potential therapeutic efficacy in KEAP1 mutant lung cancer. Oncogene **36:**5285-5295.

CHAPTER 2: CANCER-DERIVED MUTATIONS IN THE KEAP1 UBIQUITIN LIGASE IMPAIR NRF2 DEGRADATION BUT NOT UBIQUITINATION

[1]2.A. Overview

NRF2 is a transcription factor that mediates stress responses. Oncogenic mutations in *NRF2* localize to one of its two binding interfaces with KEAP1, an E3 ubiquitin ligase that promotes proteasome-dependent degradation of NRF2. Somatic mutations in *KEAP1* occur commonly in human cancer, where *KEAP1* may function as a tumor suppressor. These mutations distribute throughout the KEAP1 protein but little is known about their functional impact. In this study, we characterized 18 *KEAP1* mutations defined in a lung squamous cell carcinoma tumor set. Four mutations behaved as wild-type KEAP1, thus are likely passenger events. R554Q, W544C, N469fs, P318fs, and G333C mutations attenuated binding and suppression of NRF2 activity. The remaining mutations exhibited hypomorphic suppression of NRF2, binding both NRF2 and CUL3. Proteomic analysis revealed that the R320Q, R470C, G423V, D422N, G186R, S243C, and V155F mutations augmented the binding of KEAP1 and NRF2. Intriguingly, these 'super-binder' mutants exhibited reduced degradation of NRF2. Cell-based and in vitro biochemical analyses demonstrated that despite its inability to suppress NRF2 activity, the R320Q 'superbinder' mutant maintained the ability to ubiquitinate NRF2. These data strengthen the genetic interactions between KEAP1 and NRF2 in cancer and provide new insight into KEAP1 mechanics.

---

[1] The following manuscript has been previously published in the journal of Cancer Research. The original citation for the manuscript, figures, and tables contained in this chapter is as follows: Hast BE, Cloer EW, et al., *Cancer-derived mutations in KEAP1 impair NRF2 degradation but no ubqituination.* Cancer Res, 2014. **74**(3): p. 808-817.

2.B. Introduction

In contrast to the mutational clustering seen in oncogenes, where a few residues are frequently affected, mutations in tumor suppressor proteins typically lack focal enrichment. This creates uncertainty as to the impact of specific mutations on protein function; mutations may be phenotypically silent 'passenger' events, they may result in a spectrum of hypomorphs, or produce a functionally dead protein. Catalogued associations between specific cancer genotypes and protein function will instruct many principles of cancer biology and oncology, including patient stratification for targeted therapy.

The Cancer Genome Atlas (TCGA) recently reported the characterization of 178 squamous cell lung carcinomas (SQCC), revealing at least 10 recurrently mutated genes. Among these were activating mutations in the *NFE2L2* (*NRF2*) oncogene and presumed loss-of-function mutations within the *KEAP1* tumor suppressor gene, at 15% and 12% of tumors, respectively (1). KEAP1 functions as a substrate recognition module within the CUL3-based E3 ubiquitin ligase, which targets the NRF2 transcription factor for proteosomal degradation (2). Regardless of tissue origin, nearly all somatic mutations within NRF2 fall to either the ETGE or the DLG motif, two regulatory short amino acid sequences within NRF2 that contact KEAP1 (3). As such, these mutations liberate NRF2 from KEAP1-mediated ubiquitination. Comparatively, a survey of cancer genomic data revealed 213 somatic mutations dispersed across the full length of the KEAP1 protein, a pattern consistent with the mutational spread often seen in tumor suppressor genes. Like many discoveries from genomic sequencing efforts, the functional consequences of these KEAP1 mutations are largely not known.

The lung SQCC analysis revealed that as expected, *KEAP1* mutations and *NRF2* mutations do not co-occur in the same tumor, and that tumors with *KEAP1* or *NRF2*

mutations express relatively high levels of NRF2-target mRNAs (1, 4). NRF2 target genes include a host of stress response genes, such as heme oxygenase 1 (*HMOX1*), NADPH dehydrogenase quinone 1 (*NQO1*), and genes involved in glutathione synthesis (5). The expression of these genes strengthens the cellular defense system to neutralize reactive oxygen species (ROS), clear xenobiotic agents, and reprogram protein degradation machinery to restore homeostasis. Recent studies also establish a role for NRF2 in modulating anabolic pathways to suit the metabolic demands of cancer cell growth, effectively yielding an increase in cancer cell proliferation (6). Although comprehensive data are not complete, several studies have reported that NRF2 activity correlates with poor prognosis and chemotherapeutic resistance (7-10).

The now established importance of KEAP1-NRF2 in promoting cancer cell growth and survival underscores the need to elucidate how cancer evolution leads to pathway activation. Several mechanisms are easily recognized from cancer genomic studies: activating mutations in NRF2 free it from KEAP1 association (11), copy number amplifications of the *NRF2* genomic locus increase protein expression, and *KEAP1* promoter hypermethylation decreases its mRNA and protein expression (12, 13). What remains uncertain is which somatic mutations within *KEAP1* affect its function, to what degree do they impact function, and mechanistically how its function is compromised. Recent efforts from several groups have identified correlations between cancer genotype and phenotype, and these findings may have a significant impact on clinical interventions (14-18). With these concepts in mind, we functionally tested and biochemically characterized *KEAP1* mutations found within lung SQCC. Our data connects cancer-derived *KEAP1* genotypes with NRF2 phenotype. Unexpectedly, we found that many KEAP1 mutant proteins bind and ubiquitinate NRF2, but do not promote its proteosomal degradation or suppress its transcriptional activity.

2.C. Materials and Methods

Tissue culture, transfections, and siRNAs

HEK293T, A549, and H2228 cells were obtained from the American Tissue and Culture Collection, which authenticates cells line using short tandem repeat analysis. Cell lines were not passaged for more than 6 months after resuscitation. The *Keap1*$^{-/-}$ MEFs were kindly provided by Thomas Kensler and Nobunao Wakabayshi. HEK293T cells were grown in Dulbecco's Modified Eagle's Medium, supplemented with 10% FBS and 1% GlutaMAX (Life Technologies) in a 37°C humidified incubator with 5% CO_2. *Keap1*$^{-/-}$ mouse embryo fibroblasts (MEF) were cultured in IMDM supplemented with 10% FBS. A549 and H2228 cells were grown in RPMI supplemented with 10% FBS. Expression constructs were transfected in HEK293T cells with Lipofectamine 2000 (Life Technologies). A549 cells and *Keap1*$^{-/-}$ MEFs were transfected with Fugene HD (Roche). Transfection of siRNA was done with Lipofectamine RNAiMAX (Life Technologies). siRNA sequences for CUL3 are as follows: (A) 5'-GGU CUC CUG AAU ACC UCU CAU UAU U, (B) 5'-GAA UGU GGA UGU CAG UUC ACG UCA A, (C) 5'-GGA UCG CAA AGU AUA CAC AUA UGU A.

Antibodies and buffers employed for Western blot analysis

Anti-FLAG M2 monoclonal (Sigma), anti-HA monoclonal (Roche), anti-βactin polyclonal (Sigma, A2066), anti-βtubulin monoclonal (Sigma, T7816), anti-KEAP1 polyclonal (ProteinTech, Chicago IL), anti-GFP (abcam, ab290), anti-NRF2 H300 polyclonal (Santa Cruz, Santa Cruz CA), anti-SLK (Bethyl, A300-499A), anti-DPP3 (abcam, ab97437), anti-MCM3 (Bethyl, A300-123A), anti-WTX (19), anti-IKKβ (Cell Signaling, 2678), anti-p62/SQSTM (Santa Cruz, sc25575), HMOX1 (abcam, ab13248), anti-CUL3 (Cell Signaling, 2759), anti-MEK1/2 (Cell Signaling, 8727), anti-histone 3 (Cell Signaling, 4499), anti-GST (Cell Signaling, 2622), and anti-VSV polyclonal (Bethyl, A190-131A). 0.1% NP-40 lysis buffer: 10% glycerol, 50mM HEPES, 150 mM NaCl, 2mM EDTA, 0.1% NP-40; RIPA buffer:

0.1% NP-40, 0.1% SDS, 10% glycerol, 25mM Tris HCl, 0.25% sodium deoxycholate, 150mM NaCl, 2mM EDTA.

Immunopurification, cell fractionation, and Western blotting

For FLAG immunopurification, cells were lysed in 0.1% NP-40 lysis buffer. Cell lysates were cleared by centrifugation and incubated with FLAG resin (Sigma) before washing with lysis buffer and eluting with NuPAGE loading buffer (Life Technologies). For immunoprecipitation of endogenous NRF2, cells were lysed in 0.1% NP-40 lysis buffer. Cell lysates were cleared by centrifugation, and pre-cleared for 1 hour with Protein A/G resin (Pierce). Lysates were then incubated with NRF2 H-300 antibody (Santa Cruz) overnight at 4 degree Celsius, and then incubated for 1 hour with Protein A/G resin before eluting with NuPAGE loading buffer. For siRNA, HEK293T cells were transiently transfected and lysed in RIPA buffer 60 hours post transfection. All antibodies and buffers used for Western analysis are listed in Supplementary Methods. Cell fractionation was performed using the NE-PER Nuclear and Cytoplasmic Extraction Reagent kit (Thermo Scientific).

Plasmids, expression vectors, and site-directed mutagenesis

Expression constructs for the *KEAP1* mutants were generated by PCR-based mutagenesis and sequence verified before use; primer sequences for the mutagenesis are shown in Table S.2.3. The TCGA tumor sample codes for each mutation are also shown in Table S.2.3. The reporter construct for human *hNQO1*-ARE-luciferase was a kind gift from Jeffrey Johnson.

ARE luciferase quantification

Cells were transfected with expression constructs, FLAG-KEAP1, FLAG-NRF2, *hNQO1*-ARE luciferase, and a control plasmid containing *Renilla* luciferase driven by a

constitutive cytomegalovirus (CMV) promoter. Approximately 24 hours post-transfection, NRF2-mediated transcription was measured as the ratio of Firefly to *Renilla* luciferase activity (Promega Dual-Luciferase Reporter Assay System).

NRF2 ubiquitination experiments

Ubiquitination of NRF2 under denaturing conditions was performed in HEK293T cells stably expressing FLAG-KEAP1 wild-type or R320Q, VSV-UB1, FLAG-NRF2, and Venus-NPM1. Cells were first lysed in denaturing buffer (25mM Tris, 150mM NaCl, 1% SDS, 1mM EDTA), then diluted with 0.1% NP-40 buffer, followed by immunoprecipitation of NRF2. For in vitro ubiquitination studies, GST-tagged wild-type Keap1 and the R320 mutant were over-expressed in Hi5 insect cells and purified using a glutathione affinity column. After removal of the GST tag, the proteins were further purified by ion exchange chromatography. For the *in vitro* ubiquitination assay, wild-type KEAP1 or the R320Q mutant was mixed with recombinant human E1, UbcH5, CUL3-RBX1, ubiquitin and GST-tagged NRF2 NEH2 domain (GST-NRF2-Neh2) in buffer containing 40 mM Tris-HCl pH 8.0, 5 mM MgCl2, 2 mM DTT and 4 mM ATP. Ubiquitination was carried out at 37 °C and the products were analyzed by Western blot with anti-GST antibody.

Immunonstaining

HEK293T cells were cotransfected with the indicated plasmids and plated on 10 μg/mL fibronectin-coated coverslips. Cells were fixed in 4% paraformaldehyde in cytoskeletal buffer for 15 minutes, and coverslips were mounted to slides using the Prolong Gold antifade reagent (Molecular Probes). Images were acquired using a Zeiss LSM5 Pascal Confocal Laser Scanning Microscope equipped with ×63/1.42 Oil PlanApo objective lenses.

Affinity purification and mass spectrometry

For streptavidin and FLAG affinity purification, cells were lysed in 0.1% NP-40 lysis. Cell lysates were incubated with streptavidin or FLAG resin and washed 5 times with lysis buffer. The precipitated proteins were trypsinized directly on beads using the FASP Protein Digestion Kit (Protein Discovery).

Protein identification, filtering, and bioinformatics

All raw data were converted to mzXML format before a search of the resultant spectra using SorcererTM-SEQUEST® (build 4.0.4, Sage N Research) and the Transproteomic Pipeline (TPP v4.3.1). Data were searched against the human UniProtKB/Swiss-Prot sequence database (Release 2011_08) supplemented with common contaminants, i.e. porcine (Swiss-Prot P00761) and bovine (P00760) trypsin, and further concatenated with its reversed copy as a decoy (40,494 total sequences). Search parameters used were a precursor mass between 400 and 4500 amu, up to 2 missed cleavages, precursor-ion tolerance of 3 amu, accurate mass binning within PeptideProphet, semi-tryptic digestion, a static carbamidomethyl cysteine modification, variable methionine oxidation, and variable phosphorylation of serines, threonines, and tyrosines. False discovery rates (FDR) were determined by ProteinProphet and minimum protein probability cutoffs resulting in a 1% FDR were selected individually for each experiment. PeptideProphet/ProteinProphet results for each APMS experiment were stored in a local Prohits database. To determine an interacting protein's abundance relative to WT, prey spectral counts were bait normalized by dividing by the bait spectral count, followed by calculating the number of standard deviations from WT (similar to a Z-score), where the standard deviation was computed for each prey individually. Unfiltered data and spectral count normalizations are provided as Supplementary Table S.2.2.

2.D. Results

2.D.1 Connecting cancer-derived KEAP1 mutations with NRF2 activity.

A search of the literature and public domain revealed 213 somatic mutations in *KEAP1*, observed across 17 cancer types and multiple cell lines (Table S.2.1). Mapping these mutations onto the KEAP1 primary amino acid sequence revealed a mostly uniform distribution of affected residues (Fig. 1A). The distribution of mutations specifically found in squamous cell lung carcinoma further reiterated the lack of a 'mutation cluster region' (Fig. 1A, blue ovals). Of the 18 mutations found in lung SQCC, only two mutations resulted in a truncated protein product (N469fs and P318fs). The remaining 16 missense mutations included the addition of three new cysteine residues (G333C, W544C, and S243C), which might alter KEAP1 reactivity to electrophilic agents. One mutation, V155F occurred in two separate tumors, and interestingly, none of the mutations in KEAP1 were in residues that directly interface with NRF2 (20). Given the importance of KEAP1-NRF2 signaling in cancer and our inability to predict the functional consequences of KEAP1 mutation, we cloned and comparatively evaluated each of the 18 lung SQCC mutations.

To test whether cancer-derived mutations in KEAP1 affect NRF2-driven transcription, we used an engineered reporter system, wherein the luciferase gene is expressed in a NRF2-dependent manner. Ectopic expression of wild-type KEAP1 suppressed NRF2-dependent luciferase expression in HEK293T cells (Fig. 1B). By comparison, the KEAP1 mutants displayed variable suppression of NRF2-driven transcription. Specifically, L231V, S224Y, P318L and R71L suppressed NRF2 as well as wild-type KEAP1; these genotypes represent possible passenger mutations within *KEAP1*. By contrast, N469fs, P318fs, and G333C exhibited a near-null phenotype. Most surprisingly, of the 18 mutants examined, 11 retained partial ability to suppress NRF2-driven transcription. To further validate these data, we tested the panel in the lung adenocarcinoma cell line A549, which express mutant and

inactive KEAP1^{G333C}, and in *Keap1* knockout mouse embryo fibroblasts (MEFs). In all three cell lines tested, which vary in *KEAP1* genotype, we observed a consistent pattern of KEAP1-mediated NRF2 suppression (Fig. 1C and D).

At its core, this work sought to isolate and functionally annotate specific *KEAP1* genotypes so that clinical correlations and predictions might be drawn from genome sequence data alone. As such, we tested whether the relative activities of each KEAP1 mutant correlated with the expression of 15 *NRF2* target genes within the lung SQCC TCGA cohort (1, 4). Comparing luciferase activity (Fig. 1B-D) to the NRF2 transcriptional gene signature, we found that mutants that suppress like wild-type KEAP1 associate with decreased NRF2 activity, whereas mutants unable to completely suppress NRF2 correlate with increased NRF2 target gene expression ($p=0.049$; two-sided Wilcoxon Rank Sum Test) (Fig. S1A). Any attempt to further segregate mutations based on luciferase activity did not show a statistically significant correlation in the patient data.

2.D.2. Biochemical characterization of the KEAP1 mutants.

Next, we sought molecular insight into how specific mutations differentially impacted KEAP1 function. First, we determined whether the mutants expressed at levels similar to wild-type KEAP1, as non-synonymous mutations often impair protein folding to decrease protein stability. Transient expression from plasmid DNA indicates that the majority of KEAP1 mutants expressed at levels similar to wild-type protein (Fig. 2A and S1B). Further study is required to determine if the reduced expression of mutants R554Q, W544C, N469fs, P318fs, G480W, and G333C is due to altered protein or mRNA stability. To extend these data, the subcellular localization of KEAP1 and each KEAP1 mutant was evaluated in HEK293T cells; all mutants exhibited a localization pattern indistinguishable from wild-type KEAP1 (Fig. S1C).

KEAP1 functions as a critical sensor of oxidative stress, wherein multiple cysteine residues act as biosensors for ROS and xenobiotic molecules (11, 21, 22). In cells, KEAP1 is thought to exist as a homodimer, creating a 2:1 stoichiometry with the NRF2 substrate. Following cysteine modification, either by reactive oxygen species or electrophilic agents like *tert*-butylhydroquinone (tBHQ), a conformational change within the KEAP1 homodimer creates an SDS-resistant form which is readily visualized under denaturing electrophoresis (23, 24). When treated with the pathway agonist, all 18 mutants formed an SDS-resistant dimer, suggesting that the mutations do not impair dimerization (Fig. 2A). To more rigorously test this, FLAG-tagged KEAP1 mutants were transfected into HEK293T cells stably expressing wild-type hemagglutinin epitope (HA) tagged KEAP1. FLAG immunopurification of the mutant protein, followed by Western blot for the HA-tagged wild-type protein was performed to evaluate KEAP1 dimerization (Fig. 2B). Each KEAP1 mutant protein retained the ability to dimerize with wild-type KEAP1.

The most likely molecular explanation for how KEAP1 mutations compromise its ability to suppress NRF2 is that the mutations impact either the KEAP1-NRF2 association or the KEAP1-CUL3 association. We evaluated whether the KEAP1 mutants maintain their ability to interact with endogenous CUL3 (Fig. S2A). Affinity purification and Western blot analysis revealed that all of the KEAP1 mutants interact with CUL3 (Fig. 2C). Further analysis is needed to determine if the subtle differences in CUL3 binding reflect differential affinities or expression variability (Fig 2C, compare lanes 15, 16, 19). Next we determined if the KEAP1-NRF2 association was maintained among the mutants. Western blot analysis of immunopurified KEAP1 and mutant KEAP1 protein complexes showed that the R554Q, W544C, N469fs, P318fs, and G333C mutants failed to bind NRF2 (Fig. 3A and S2B and S2C). Surprisingly, however, the remaining 13 KEAP1 mutants retained NRF2 binding. Together, these data suggest that with the exception of R554Q, W544C, N469fs, P318fs,

and G333C, SQCC-derived KEAP1 mutants maintain their ability to bind both NRF2 and CUL3.

Mass spectrometry-based proteomic analysis of KEAP1 revealed 42 high confidence associated proteins (4). To gather a global perspective of how the mutations affect KEAP1 protein interactions, we performed two experiments. First, we tested the association of 7 high confidence interacting proteins by affinity purification and Western blot analysis. The data show a distinct pattern among the KEAP1 mutants; those that do not bind NRF2 fail to bind several of the known interactors, including SLK, AMER1 (WTX), MCM3, DPP3, and IKBKB (IKKb) (Fig. 3A and S2C). Interestingly, all of these proteins contain an ETGE motif (4). Two mutations, G480W and S224Y, show decreased binding to SLK, MCM3, and DPP3 as compared to NRF2 (Fig. 3A, lanes 8, 15). Second, we employed affinity purification and shotgun mass spectrometry to define and compare the protein interaction network for wild-type KEAP1 and the following mutants: R554Q, R320Q, R470C, G480W, G423V, D422N, G186R, S243C, and V155F (Fig. 3B and Table S.2.2). The unbiased proteomic screens confirm the Western blot results and further expand the pattern of altered protein interactions.

2.D.3. A class of KEAP1 mutants with increased NRF2 binding.

We were particularly intrigued with a subset of mutants that consistently bound more NRF2 than wild-type KEAP1 (Fig. 3A, lanes 3, 5, 6, 9, 14, 16, 19, and Fig. S2C). We collectively refer to these mutants as the ‘superbinders’, although relative protein affinity is not meant to be inferred. The superbinder mutants include R320Q, R470C, G423V, D422N, G186R, S243C and V155F. Increased abundance of NRF2 within each superbinder protein complex was confirmed by immunoprecipitation and quantitative Western blot analysis (Fig. S3A and S3B). Additionally, label-free mass spectrometry comparing wild-type KEAP1 and

two superbinder mutants (R320Q and R470C) showed an increased abundance of NRF2 as compared to wild-type KEAP1; based on spectral counts, R320Q and R470C bound 3.3 and 3.2 fold more NRF2 than wild-type KEAP1, respectively (Fig. 3B and Table S.2.2). For comparative purposes, we performed quantitative proteomic analysis on two non-superbinder mutant proteins: R554Q, which cannot bind NRF2 and G480W, which binds NRF2 similarly to wild-type (Fig. 3B).

Despite an increased level of associated NRF2, the superbinder mutants were unable to suppress NRF2-mediated transcription of an artificial reporter gene (Fig. 1B-D). To confirm this using endogenous metrics of NRF2 activity, HEK293T cells, H2228 cells or A549 cells were transiently transfected with wild-type KEAP1 or the superbinder mutants before Western blot analysis of NRF2 and the NRF2 target gene HMOX1. Transient expression of each superbinder strongly increased the levels of NRF2 and HMOX1 in the H2228 and A549 cell lines (Fig. 4A and B). Subcellular fractionation of the HEK293T cells further revealed that KEAP1 superbinder expression increased the levels of NRF2 within the nuclear compartment (Fig. 4C and S3C).

2.D.4. KEAP1 'superbinder' mutants facilitate NRF2 ubiquitination but not degradation.

Our functional and biochemical examination revealed 7 KEAP1 mutations that show significantly impaired ability to suppress NRF2, but yet unexpectedly bind more NRF2 than wild-type KEAP1. To gain further insight, we evaluated NRF2 protein turnover and ubiquitination following KEAP1 superbinder expression. Using a cycloheximide pulse-chase approach, NRF2 protein half-life was evaluated in HEK293T cells stably expressing: 1) wild-type KEAP1, 2) the R320Q superbinder, 3) R470C superbinder, 3) R554Q which does not bind NRF2, or 5) G480W which behaves like wild-type. The expression of R320Q or R470C dramatically stabilized the NRF2 protein as compared to no exogenous KEAP1, wild-type

KEAP1 or G480W (Fig. S3D and Fig. 5A). The increased NRF2 stability occurred as a result of binding R320Q or R470C, as unbound NRF2 in the flow-through eluate showed elevated levels but dynamic turnover (Fig. 5B, compare flow-through to KEAP1 immunopurification). Together, these data suggest that the superbinder mutations within KEAP1 result in the stabilization of KEAP1-associated NRF2 and elevated levels of free NRF2, although the free NRF2 is still subject to dynamic turnover.

Given the increased NRF2 association and protein stability, we hypothesized that R320Q and other superbinder mutants impair NRF2 ubiquitination. To test this, we performed two complementary experiments to evaluate NRF2 ubiquitination by wild-type KEAP1 or the R320Q superbinder. First, Western blot analysis of immunoprecipitated NRF2, after denaturation, showed robust ubiquitination by both wild-type KEAP1 and R320Q (Fig. 5C). Second, we performed *in vitro* ubiquitination reactions using purified proteins (Fig. 5D). Remarkably, both experimental approaches demonstrate that wild-type KEAP1 and R320Q ubiquitinate NRF2.

2.E. Discussion

With some latitude, we can classify the 18 *KEAP1* mutations into three classes. First, the L231V, S224Y, P318L and R71L mutations did not impact the KEAP1-NRF2 association or the suppression of NRF2 activity. These mutations likely represent passenger events within KEAP1, at least with respect to NRF2. Second, and not surprisingly, the frame shift mutations N469fs and P318fs, as well as G333C, R554Q and W544C did not bind NRF2 and did not or weakly suppressed NRF2-mediated transcription. These genotypes represent null or near-null alleles. Third, the remaining nine mutations fell within a hypomorphic phenotypic range, with suppression occurring between 30-60% of the wild-type

KEAP1. Biochemically, the hypomorphic mutants displayed either reduced NRF2 binding or surprisingly, increased binding (the superbinders).

Mutations in tumor suppressor genes often results in complete loss of protein expression or the expression of a truncated protein product (25). It is therefore intriguing to consider why *KEAP1* is rarely lost through genomic deletion, despite being located between the *SMARCA4* and *STK11* tumor suppressor genes on 19p (cBioPortal). A number of loosely connected observations raise the possibility that KEAP1 may exert cancer-relevant functions that extend beyond regulation of oxidative stress and NRF2. First, we found that many KEAP1 mutations result in a hypomorphic phenotype, rather than a genetic null. Second, in general, these hypomorphic mutations do not affect the global KEAP1 protein interaction network, suggesting that some KEAP1 protein interactions are retained in the absence of NRF2 suppression (Fig. 3B and Table S.2.2). Indeed, KEAP1 associated proteins regulate a number of disparate cellular processes, including cell cycle, migration, and apoptosis (4, 26-34). Third, while the presence and importance of NRF2-independent KEAP1 functions remain unknown, we and others have established that several KEAP1 interacting proteins drive NRF2 activation via a competitive binding mechanism (4, 19, 35-37). Previously, we found that hypomorphic *KEAP1* mutants can be further inactivated by the ETGE-containing competitive binding protein, DPP3(4). Coupled with the observed over-expression of *DPP3* in lung squamous cell carcinoma, these observations suggest that from the perspective of cancer cell fitness, the presence of a hypomorphic *KEAP1* mutation may be more valuable than a null mutant.

The most surprising and perhaps exciting discovery we observed was the identification of the ‘superbinders’—those that do not suppress NRF2-mediated transcription, exhibit enhanced binding to NRF2, and facilitate NRF2 ubiquitination. Three

points of discussion are appropriate. First, by what mechanism could the 'superbinder' mutations affect NRF2 stability? Several possibilities exist, including an increased affinity between KEAP1 and NRF2 as a means to suppress substrate turn-over. Analogously, the expression of a superbinder variant SH2 domain antagonizes epidermal growth factor signaling via competitive inhibition (38). That said, although studies are ongoing, the lack of a focal enrichment within the tertiary structure casts some doubt on this possibility (Fig. 5E). Cullin ring E3 ubiquitin ligases cycle through an active and inactive state, and this neddylation-dependent transitioning is required for substrate turnover. A second possibility is that the superbinder mutations simply slow the rate of CUL3 neddylation. Finally, proteasome-mediated substrate degradation requires several steps, including recognition, unfolding, translocation, and deubiquitination prior to proteolysis (39). The striking observation that the enhanced NRF2 binding class of *KEAP1* mutants ubiquitinates NRF2 suggests that the mutations functionally hinder one of the steps prior to proteolysis, but after ubiquitination. Here, immediate questions include whether the superbinder mutations affect the ubiquitin chain linkage on NRF2 or whether they perturb the interaction of KEAP1 with the proteasome. All three of these putative mechanisms to describe the superbinder phenotype would inactivate KEAP1 and stabilize NRF2 in a manner consistent with the widely accepted "saturation model" (22). Importantly, as the *KEAP1* mutants described in this study exhibit hypomorphic phenotypes, the superbinders could represent a novel mechanism cancer cells employ to enhance cellular fitness without compromising all cellular functions of multifunctional proteins.

Second, it is now widely accepted that elevated levels of NRF2 are associated with enhanced cell viability in several tumor types (7, 10, 40-42). Although we show that 'superbinder' mutations result in NRF2 transcriptional activation, further studies are required to determine whether this KEAP1 mutant class is capable of enhancing cancer cell fitness *in*

vivo, and whether that depends upon prolonged activation of NRF2. Additionally, given emerging evidence identifying other putative KEAP1 substrates in cancer-relevant pathways, such as IKKb within NF-κB signaling (5, 43), investigating how—if at all—superbinder mutations impact these proteins could also have clinical significance. Looking at the full set of *KEAP1* mutant tumors and the expression of 15 NRF2 target genes, a marginal but statistically significant difference was observed between phenotypically 'silent' KEAP1 mutations and mutations which suppress KEAP1-driven NRF2 degradation (Fig. S1A). Our attempts to more precisely correlate *KEAP1* genotype with the cell-based phenotypic scoring failed to reach statistical significance. This is not surprising given the multitude of signaling and metabolic inputs that control KEAP1.

Third, from a structural perspective, we noted weak correlation between the tertiary position of a mutation and whether the mutation produced a KEAP1 superbinder (Fig. 5E). Although speculative, the superbinder mutations appear to be localized at positions that might orient the relative position of IVR and KELCH domains; experiments testing this model are ongoing. Intriguingly, of the 181 missense mutations reported in KEAP1, 6 directly target the R320 superbinder residue, making it the most commonly affected amino acid in KEAP1 (Fig. 1A). Beyond the superbinder mutations, mapping all SQCC 19 mutations onto the KEAP1 structure failed to reveal a discernible pattern. Likewise, side-chain biochemistry for the mutations varies widely, including those within the superbinder class. Cysteine reactivity depends upon the local chemical microenvironment, which is largely dictated by the surrounding amino acids in a protein tertiary structure. Hence, for a cysteine-dependent biosensor like KEAP1, oncogenesis may partially suppress KEAP1 activity by selecting for mutations which add cysteines (S243C, G333C, R470C) or which reduce the relative pKa of existing cysteines, making them more sensitive to electrophilic attack (44). Clearly, spatial constraints preclude the random addition of cysteines as a means to increase the reactivity

of KEAP1 to oxidative stress. New cancer-derived cysteines of functional importance would occupy specific localizations within the folded protein. By extension of this idea, cancer-derived mutations that create 'hyperactive' cysteines within KEAP1 would be expected to produce a hypomorphic phenotype, as we have observed. Further study is needed to support these ideas, perhaps through the functional and biochemical characterization of the other 213 cancer-derived mutations in *KEAP1*. To this end, medium-throughput functional analysis is facilitated by Gateway-based cloning, outsourced mutagenesis and a strong pathway-specific transcriptional reporter. The resulting data may better enable predictions of genotype-phenotype relationships. However, based on the KEAP1 data presented here, it is not yet possible to derive functional conclusions from the location of a mutation or the type of residue substitution.

In summary, we describe the functional and biochemical characteristics of 18 mutations in the E3 ligase adaptor protein KEAP1, which were found in patient-derived lung cancers. We show that while most of these mutations maintain similar protein interactions to wild-type KEAP1, all but four exhibit hypomorphic or null activity with respect to suppression of NRF2-mediated transcription. Intriguingly, a subset of these mutations exhibit enhanced binding to NRF2 despite an inability to suppress NRF2 activity. Functional analysis of one of these mutants, R320Q, revealed that these mutants are still able to ubiquitinate NRF2, but appear to be unable to facilitate its degradation. Further studies are required to elucidate the mechanism of this class of *KEAP1* mutations, including how they interact with the proteasome, as well as whether these mutants enhance viability of cancer cells via prolonged activation of NRF2.

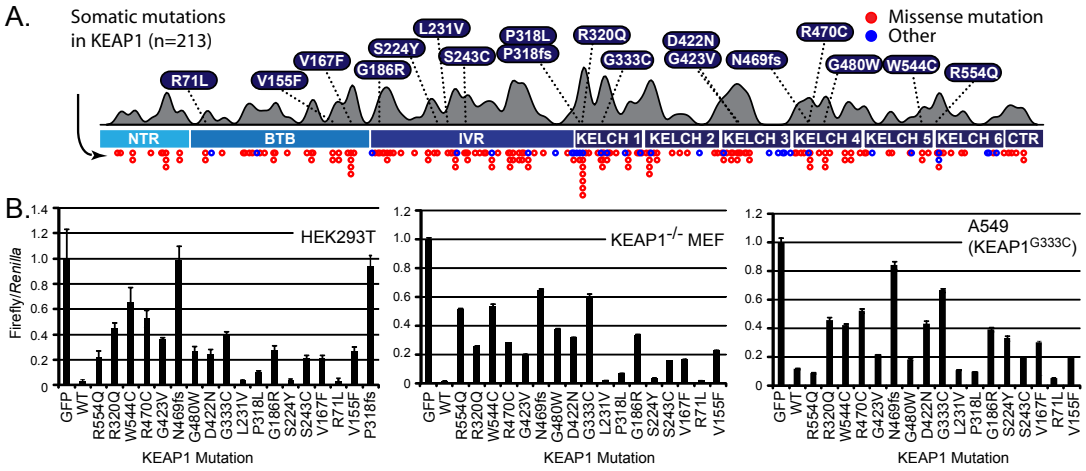

Figure 2.1. Mutations in KEAP1 positively correlate with increased NRF2 activity.
A. Probability density function of KEAP1 mutations were approximated using kernel density estimation. Lung SQCC mutations examined in this study are annotated above; all mutations from the public domain are shown below and in Supplementary Table S.2.1.
B. HEK293T cells, Keap1 knockout MEFs, and A549 cells were transiently transfected with the indicated plasmids along with constitutively expressed Renilla luciferase and the NQO1 promoter driving Firefly luciferase. Cells were lysed and Firefly luciferase values were normalized to the luciferase activity of the Renilla control. Error bars represent SD from the mean over 3 biologic replicates (NTR, N-terminal region; BTB, tramtrack and bric-a-brac; CTR, C-terminal region; IVR, intervening region).

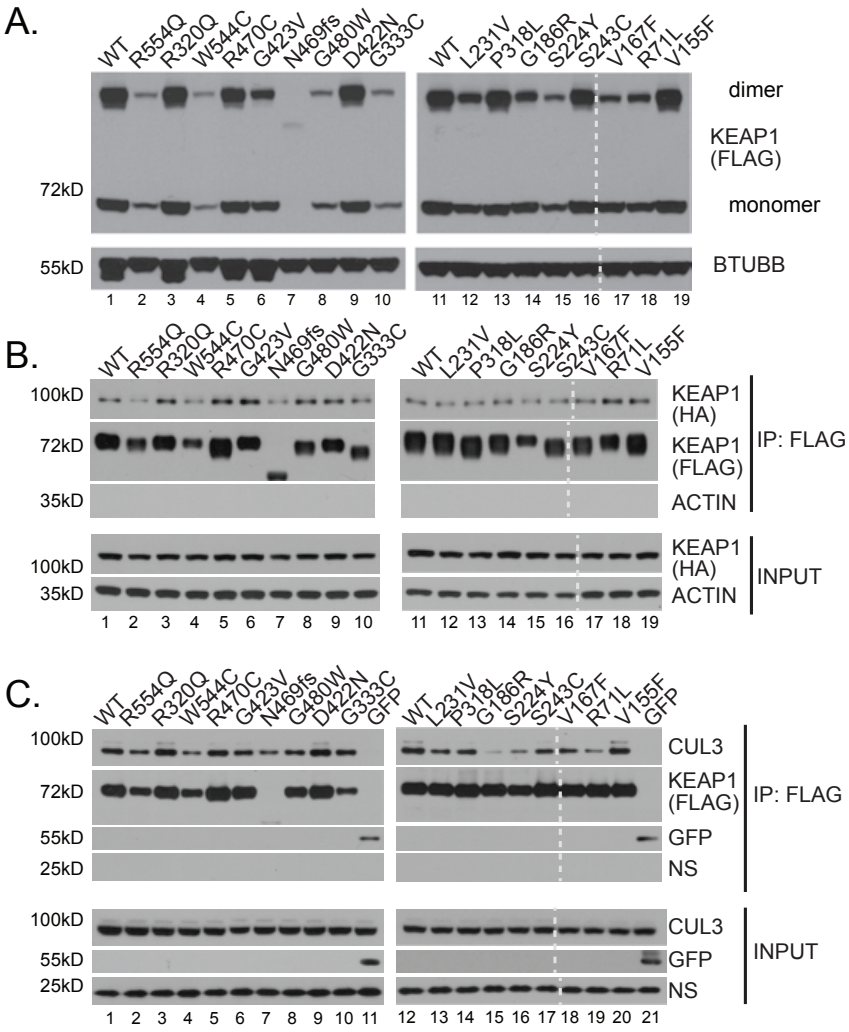

Figure 2.2. SQCC KEAP1 mutants retain the ability to dimerize and interact with the CUL3 E3 ubiquitin ligase.

A. HEK293T cells were transiently transfected with the indicated KEAP1 mutant plasmids, and treated with 50 mmol/L tBHQ for 1 hour. Cells were lysed in RIPA buffer and expression of FLAG-tagged mutants was analyzed by Western blot for the indicated proteins. The vertical dotted line depicts the digital removal of a KEAP1 mutant recently found not to exist. The correct mutation, P318fs, is shown in Supplementary Fig. S2.

B. HEK239T cells stably expressing WT HA-KEAP1 were transiently transfected with the indicated FLAG-tagged KEAP1mutants. Cells were lysed in 0.1% NP-40 buffer and immunoprecipitation (IP) of the FLAG-tagged protein complexes were analyzed by Western blot for the indicated proteins (HA, hemagglutinin).

C. FLAG-tagged protein complexes were immunopurified from HEK293Tcells transiently expressing the indicated KEAP1 mutants and analyzed by Western blot for the indicated proteins (NS,nonspecific).

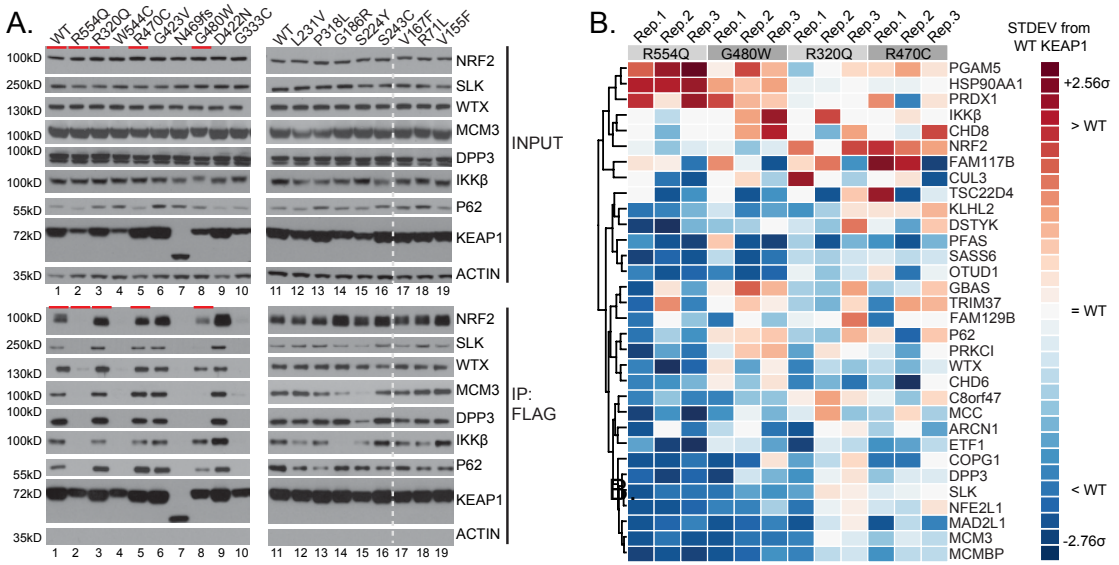

Figure 2.3. KEAP1 mutant proteins exhibit differential binding to interacting proteins.
A. HEK293T cells expressing the indicated KEAP1 mutants were treated with 10 **m**mol/L MG132 for 1 hour, followed by FLAG immunopurification. Protein complexes of the FLAG-tagged mutants were analyzed by Western blot for the indicated proteins. Red lines indicate KEAP1 mutants that were analyzed by mass spectrometry as indicated in B.
B. APMS experiments were performed via affinity purification of streptavidin-tagged KEAP1 mutants from stable HEK293T cells followed by mass spectrometry analysis of the bound proteins. Colors represent normalized spectral counts**—**semiquantitative values that reflect protein abundance**—**from the APMS experiments. Proteins displayed are previously identified high-confidence KEAP1 interactors.

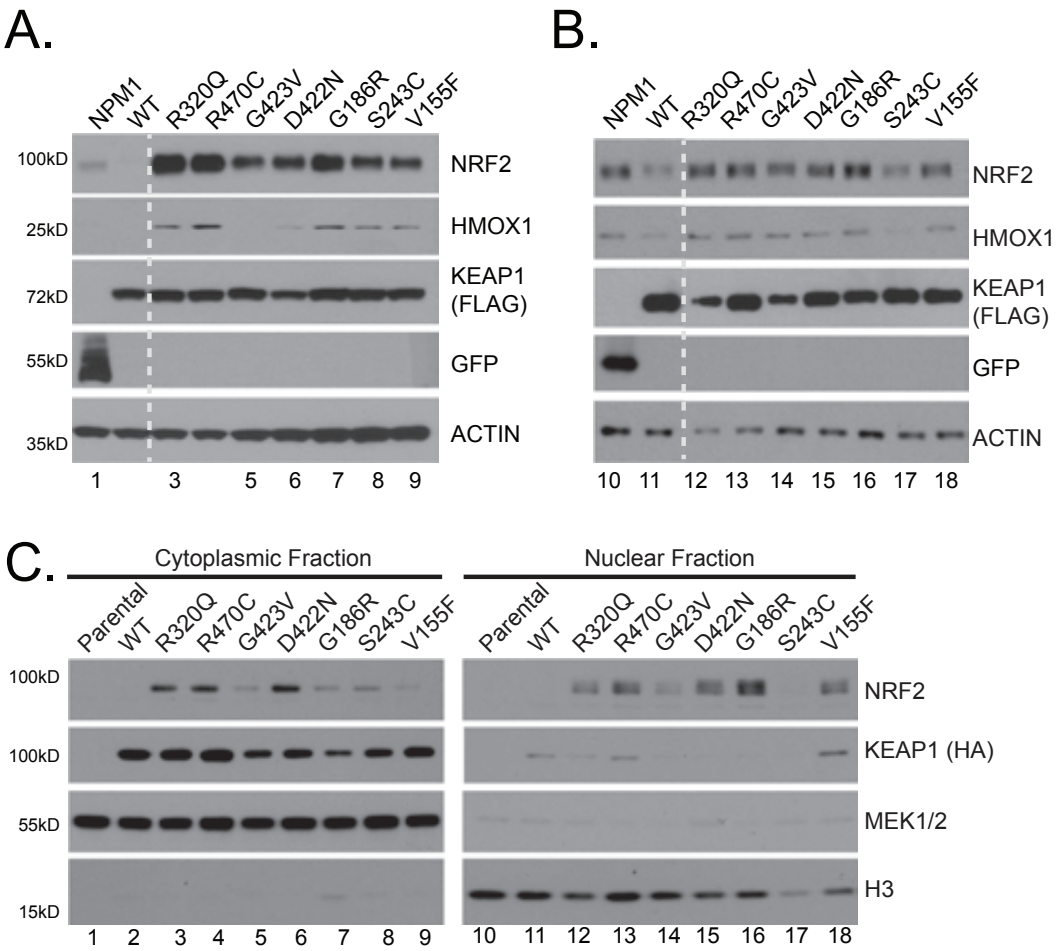

Figure 2.4. Expression of KEAP1 superbinder mutants enhances nuclear localization of NRF2.

A. H2228 cells were cotransfected with the indicated FLAG-tagged KEAP1 mutant plasmid or negative control Venus-NPM1, and NRF2 plasmid. Cells were lysed in RIPA buffer and analyzed by Western blot for the indicated proteins.

B. A549 cells were transiently transfected with the indicated KEAP1 mutants or Venus-NPM1, and protein lysates were analyzed as described in A.

C. HEK293T cells were transiently transfected with the indicated FLAG-tagged KEAP1 mutants. Cells were fractionated into nuclear and cytoplasmic fractions and lysates were analyzed by Western blot for the indicated endogenous (NRF2, MEK1/2, H3) and ectopically expressed proteins.

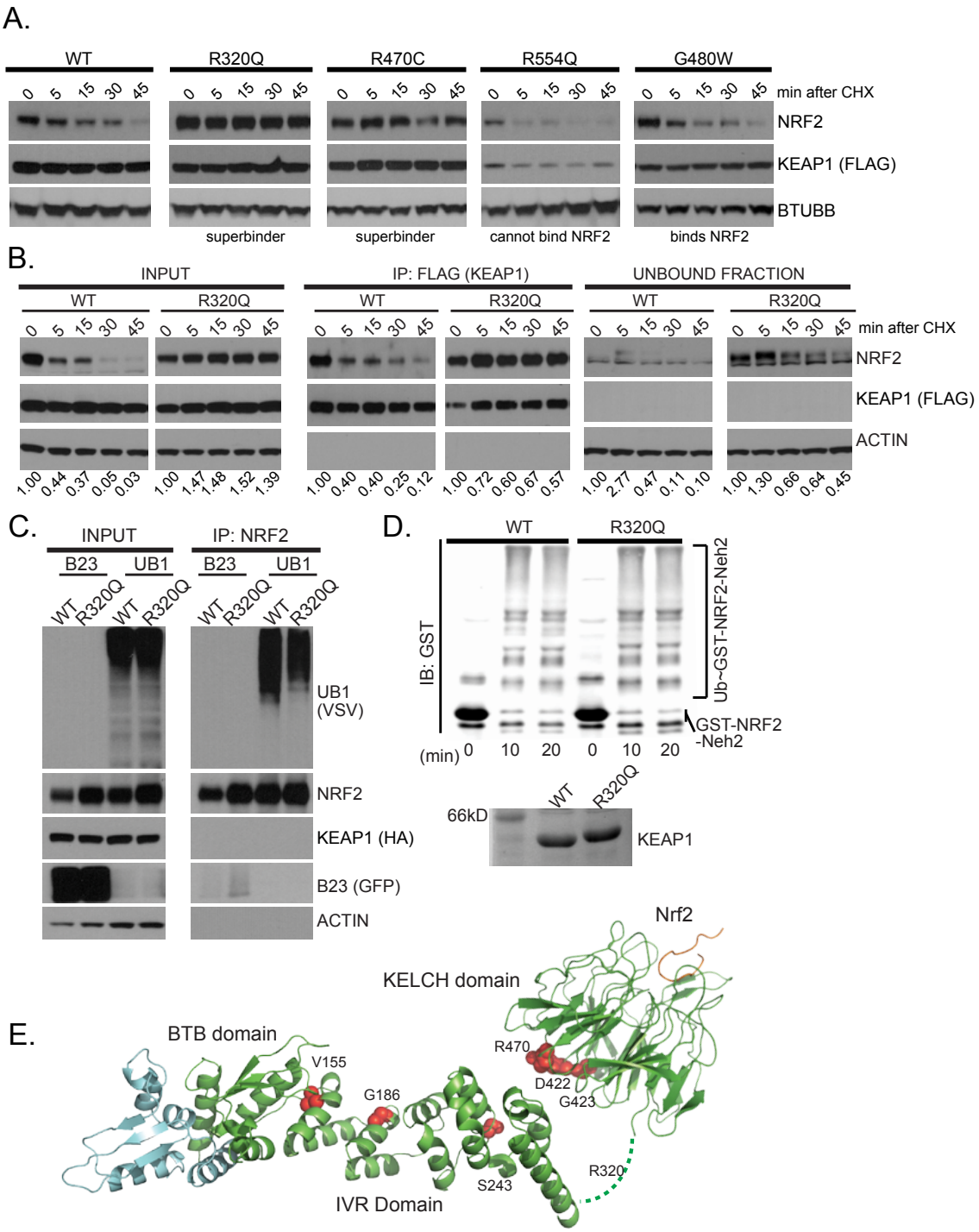
A.
WT
R320Q
R470C
R554Q
G480W
0 5 15 30 45
min after CHX
NRF2
KEAP1 (FLAG)
BTUBB
superbinder
superbinder
cannot bind NRF2
binds NRF2
B.
INPUT
IP: FLAG (KEAP1)
UNBOUND FRACTION
WT
R320Q
min after CHX
NRF2
KEAP1 (FLAG)
ACTIN
1.00 0.44 0.37 0.05 0.03
1.00 1.47 1.48 1.52 1.39
1.00 0.40 0.40 0.25 0.12
1.00 0.72 0.60 0.67 0.57
1.00 2.77 0.47 0.11 0.10
1.00 1.30 0.66 0.64 0.45
C.
INPUT
IP: NRF2
B23
UB1
WT
R320Q
UB1 (VSV)
NRF2
KEAP1 (HA)
B23 (GFP)
ACTIN
D.
WT
R320Q
IB: GST
Ub~GST-NRF2-Neh2
GST-NRF2 -Neh2
(min) 0 10 20 0 10 20
66kD
KEAP1
E.
Nrf2
KELCH domain
BTB domain
V155
G186
R470
D422
G423
S243
R320
IVR Domain

Figure 2.5. KEAP1 superbinder mutants cannot degrade NRF2 but maintain the ability to ubiquitinate NRF2.
A. HEK293T cells stably expressing the indicated
FLAG-tagged KEAP1mutantswere transiently transfected with NRF2. Cells were treated with 50 **m**g/mLCHX for the indicated time, and cell lysates were analyzed by Western blot for the specified proteins.
B. HEK293T cells stably expressing the indicated FLAG-tagged KEAP1 mutants were treated with CHX as described in A. FLAG immunopurification was performed to isolate protein complexes containing the indicated KEAP1 mutants. Whole cell lysate (INPUT), immunoprecipitated complexes (IP: FLAG), and eluate (UNBOUND FRACTION) were analyzed by Western blot for the indicated proteins. Values represent NRF2 quantitation relative to FLAG-tagged KEAP1 expression.
C. HEK293T cells stably expressing either FLAG-tagged wild-type KEAP1 or the R320Q mutant were transfected as described in A. Cells were lysed under denaturing conditions and then diluted to physiologic pH in 0.1% NP-40 lysis buffer. Immunopurification of NRF2 was performed, and protein complexes were analyzed by Western blot.
D. Purified KEAP1 or the R320Q mutant was mixed with recombinant human E1, UbcH5, CUL3-RBX1, ubiquitin, and GST-tagged NRF2 NEH2 domain. Ubiquitinated NRF2 was detected by Western blot analysis.
E. The BTB and intervening region (IVR) domains of KEAP1 (green) were modeled by the I-TASSER server. The BTB domain of the second copy of KEAP1 within the dimer is shown in cyan.Superbinder residues are shown in red spheres. R320 is located in a predicted short linker connecting the BTB**–**IVR domain and KELCH domain.

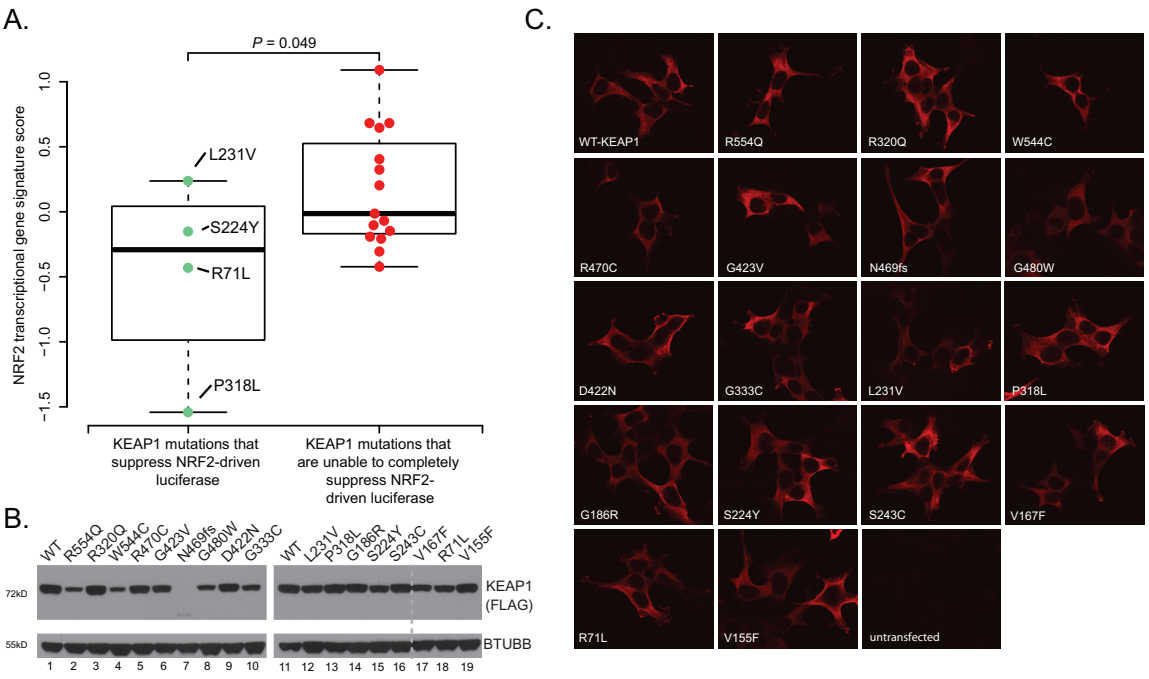

Figure S.2.1. SQCC KEAP1 mutant characterization.
A. Activity of KEAP1 mutants, as based on luciferase activity from Figure 1 B-D, positively correlates with NRF2 target gene expression (P=0.049, Kruskal-Wallis test).
B. HEK293T cells were transiently transfected with the indicated FLAG-tagged KEAP1 mutants and cell lysates were analyzed by Western blot.
C. HEK293T cells were transiently transfected with the indicated FLAG-KEAP1 mutants and stained for FLAG. Scale, 20 μm.

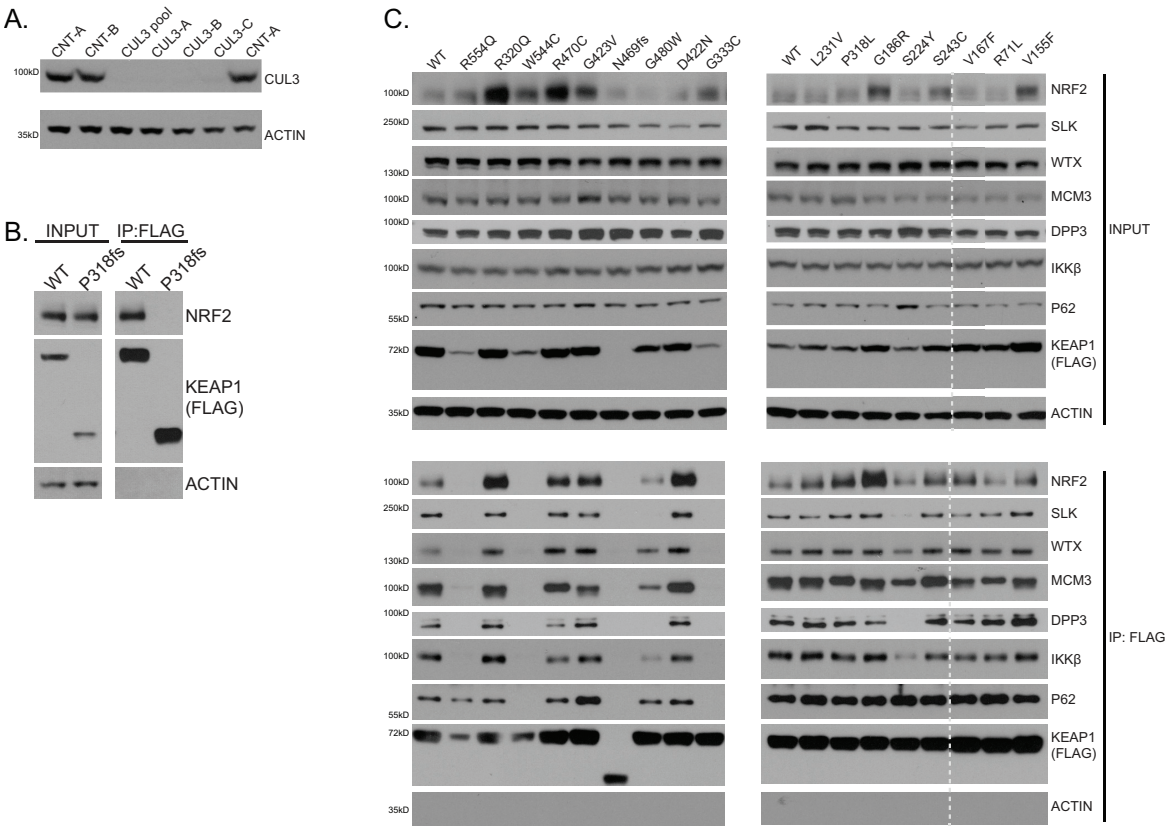

Figure S.2.2. KEAP1 mutants differentially bind to protein interactors.
A. Multiple CUL3 siRNAs silence CUL3 protein expression. HEK293T cells were transfected with 10nM of the indicated siRNAs before Western blot analysis.
B. Mutant P318fs was originally synthesized incorrectly, hence the dotted vertical line in Figures 2, 3A, 4A and B, S1, and S2C). The correct mutant was synthesized and HEK293T cells were transfected followed by immunopurification for the tagged mutant protein. Cell lysates and purified protein complexes were analyzed by Western blot to assess expression of the P318fs mutant, as well as NRF2 association.
C. HEK293T cells expressing the indicated FLAG-tagged KEAP1 mutants were purified and lysates were analyzed by Western blot.

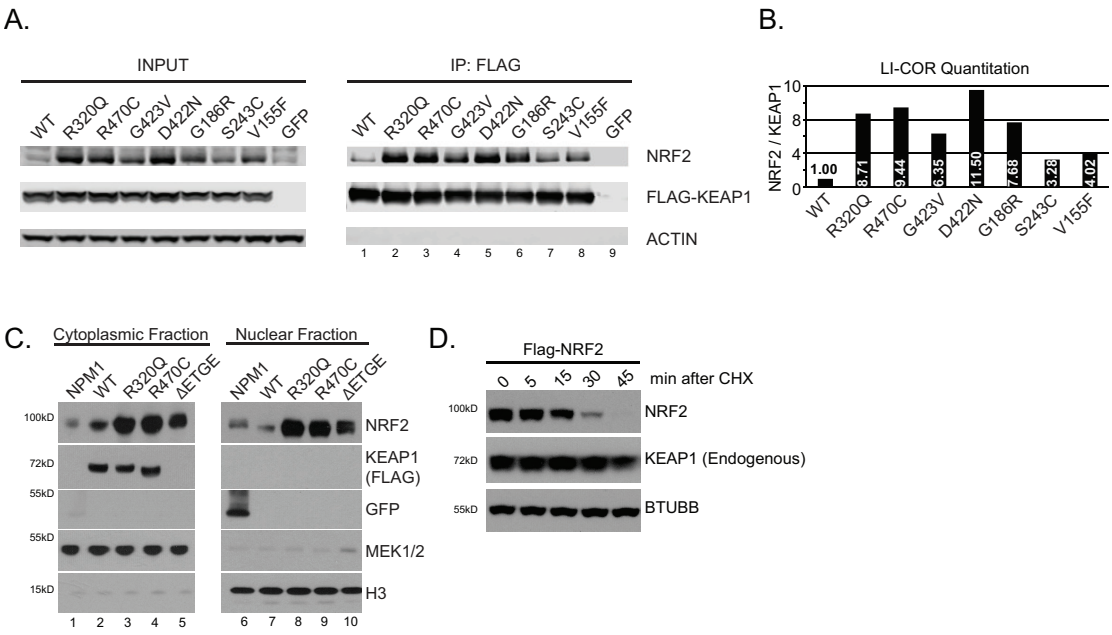

Figure S.2.3. KEAP1 superbinder mutants enhance ectopic NRF2 nuclear localization.
A. HEK293T cells were transfected with the indicated FLAG-tagged KEAP1 construct before lysis and quantitative Western blot analysis.
B. LI-COR-based quantitation of NRF2 and KEAP1 from Figure S3, panel A.
C. HEK293T cells were transiently co-transfected with the indicated FLAGtagged KEAP1 mutants and NRF2. Cells were fractionated into a cytoplasmic and nuclear fraction, and cell lysates were analyzed by Western blot.
D. HEK293T cells were transfected with FLAG-tagged NRF2 before treatment with cycloheximide for the indicated time, as was done in Fig. 5

REFERENCES

1. **The Cancer Genome Atlas.** 2012. Comprehensive genomic characterization of squamous cell lung cancers. Nature **489:**519-525.

2. **Furukawa M, Xiong Y.** 2005. BTB protein Keap1 targets antioxidant transcription factor Nrf2 for ubiquitination by the Cullin 3-Roc1 ligase. Mol Cell Biol **25:**162-171.

3. **Tong KI, Katoh Y, Kusunoki H, Itoh K, Tanaka T, Yamamoto M.** 2006. Keap1 recruits Neh2 through binding to ETGE and DLG motifs: characterization of the two-site molecular recognition model. Mol Cell Biol **26:**2887-2900.

4. **Hast BE, Goldfarb D, Mulvaney KM, Hast MA, Siesser PF, Yan F, Hayes DN, Major MB.** 2013. Proteomic analysis of ubiquitin ligase KEAP1 reveals associated proteins that inhibit NRF2 ubiquitination. Cancer Res **73:**2199-2210.

5. **Wakabayashi N, Slocum SL, Skoko JJ, Shin S, Kensler TW.** 2010. When NRF2 talks, who's listening? Antioxid Redox Signal **13:**1649-1663.

6. **Mitsuishi Y, Taguchi K, Kawatani Y, Shibata T, Nukiwa T, Aburatani H, Yamamoto M, Motohashi H.** 2012. Nrf2 redirects glucose and glutamine into anabolic pathways in metabolic reprogramming. Cancer Cell **22:**66-79.

7. **Jiang T, Chen N, Zhao F, Wang XJ, Kong B, Zheng W, Zhang DD.** 2010. High levels of Nrf2 determine chemoresistance in type II endometrial cancer. Cancer Res **70:**5486-5496.

8. **Mahaffey CM, Zhang H, Rinna A, Holland W, Mack PC, Forman HJ.** 2009. Multidrug-resistant protein-3 gene regulation by the transcription factor Nrf2 in human bronchial epithelial and non-small-cell lung carcinoma. Free Radic Biol Med **46:**1650-1657.

9. **Rushworth SA, Zaitseva L, Murray MY, Shah NM, Bowles KM, MacEwan DJ.** 2012. The high Nrf2 expression in human acute myeloid leukemia is driven by NF-kappaB and underlies its chemo-resistance. Blood **120:**5188-5198.

10. **Abazeed ME, Adams DJ, Hurov KE, Tamayo P, Creighton CJ, Sonkin D, Giacomelli AO, Du C, Fries DF, Wong KK, Mesirov JP, Loeffler JS, Schreiber SL, Hammerman PS, Meyerson M.** 2013. Integrative radiogenomic profiling of squamous cell lung cancer. Cancer Res doi:10.1158/0008-5472.CAN-13-1616.

11. **Hayes JD, McMahon M.** 2009. NRF2 and KEAP1 mutations: permanent activation of an adaptive response in cancer. Trends Biochem Sci **34:**176-188.

12. **Muscarella LA, Parrella P, D'Alessandro V, la Torre A, Barbano R, Fontana A, Tancredi A, Guarnieri V, Balsamo T, Coco M, Copetti M, Pellegrini F, De Bonis P, Bisceglia M, Scaramuzzi G, Maiello E, Valori VM, Merla G, Vendemiale G, Fazio VM.** 2011. Frequent epigenetics inactivation of KEAP1 gene in non-small cell lung cancer. Epigenetics **6:**710-719.

13. **Hanada N, Takahata T, Zhou Q, Ye X, Sun R, Itoh J, Ishiguro A, Kijima H, Mimura J, Itoh K, Fukuda S, Saijo Y.** 2012. Methylation of the KEAP1 gene promoter region in human colorectal cancer. BMC Cancer **12:**66.

14. **Jaiswal BS, Kljavin NM, Stawiski EW, Chan E, Parikh C, Durinck S, Chaudhuri S, Pujara K, Guillory J, Edgar KA, Janakiraman V, Scholz RP, Bowman KK, Lorenzo M, Li H, Wu J, Yuan W, Peters BA, Kan Z, Stinson J, Mak M, Modrusan Z, Eigenbrot C, Firestein R, Stern HM, Rajalingam K, Schaefer G, Merchant MA, Sliwkowski MX, de Sauvage FJ, Seshagiri S.** 2013. Oncogenic ERBB3 Mutations in Human Cancers. Cancer Cell **23:**603-617.

15. **Safaee M, Clark AJ, Oh MC, Ivan ME, Bloch O, Kaur G, Sun MZ, Kim JM, Oh T, Berger MS, Parsa AT.** 2013. Overexpression of CD97 Confers an Invasive Phenotype in Glioblastoma Cells and Is Associated with Decreased Survival of Glioblastoma Patients. PLoS One **8:**e62765.

16. **Hakimi AA, Ostrovnaya I, Reva BA, Schultz N, Chen YB, Gonen M, Liu H, Takeda S, Voss MH, Tickoo SK, Reuter VE, Russo P, Cheng EH, Sander C, Motzer RJ, Hsieh JJ.** 2013. Adverse Outcomes in Clear Cell Renal Cell Carcinoma with Mutations of 3p21 Epigenetic Regulators BAP1 and SETD2: a Report by MSKCC and the KIRC TCGA Research Network. Clin Cancer Res doi:1078-0432.CCR-12-3886 [pii]10.1158/1078-0432.CCR-12-3886.

17. **Meng X, Cai C, Wu J, Cai S, Ye C, Chen H, Yang Z, Zeng H, Shen Q, Zou F.** 2013. TRPM7 mediates breast cancer cell migration and invasion through the MAPK pathway. Cancer Lett **333:**96-102.

18. **Wu YM, Su F, Kalyana-Sundaram S, Khazanov N, Ateeq B, Cao X, Lonigro RJ, Vats P, Wang R, Lin SF, Cheng AJ, Kunju LP, Siddiqui J, Tomlins SA, Wyngaard P, Sadis S, Roychowdhury S, Hussain MH, Feng FY, Zalupski MM, Talpaz M, Pienta KJ, Rhodes DR, Robinson DR, Chinnaiyan AM.** 2013. Identification of Targetable FGFR Gene Fusions in Diverse Cancers. Cancer Discov doi:2159-8290.CD-13-0050 [pii]10.1158/2159-8290.CD-13-0050.

19. **Camp ND, James RG, Dawson DW, Yan F, Davison JM, Houck SA, Tang X, Zheng N, Major MB, Moon RT.** 2012. Wilms tumor gene on the X chromosome (WTX) inhibits the degradation of NRF2 through competitive binding to KEAP1. J Biol Chem doi:M111.316471 [pii]10.1074/jbc.M111.316471.

20. **Lo SC, Li X, Henzl MT, Beamer LJ, Hannink M.** 2006. Structure of the Keap1:Nrf2 interface provides mechanistic insight into Nrf2 signaling. EMBO J **25:**3605-3617.

21. **Cullinan SB, Gordan JD, Jin J, Harper JW, Diehl JA.** 2004. The Keap1-BTB protein is an adaptor that bridges Nrf2 to a Cul3-based E3 ligase: oxidative stress sensing by a Cul3-Keap1 ligase. Mol Cell Biol **24:**8477-8486.

22. **Zhang DD, Lo SC, Cross JV, Templeton DJ, Hannink M.** 2004. Keap1 is a redox-regulated substrate adaptor protein for a Cul3-dependent ubiquitin ligase complex. Mol Cell Biol **24:**10941-10953.

23. **Rachakonda G, Xiong Y, Sekhar KR, Stamer SL, Liebler DC, Freeman ML.** 2008. Covalent modification at Cys151 dissociates the electrophile sensor Keap1 from the ubiquitin ligase CUL3. Chem Res Toxicol **21:**705-710.

24. **Fourquet S, Guerois R, Biard D, Toledano MB.** 2010. Activation of NRF2 by nitrosative agents and H2O2 involves KEAP1 disulfide formation. J Biol Chem **285:**8463-8471.

25. **Levine AJ.** 1993. The tumor suppressor genes. Annu Rev Biochem **62:**623-651.

26. **Fujibuchi T, Abe Y, Takeuchi T, Imai Y, Kamei Y, Murase R, Ueda N, Shigemoto K, Yamamoto H, Kito K.** 2005. AIP1/WDR1 supports mitotic cell rounding. Biochem Biophys Res Commun **327:**268-275.

27. **Kato A, Kurita S, Hayashi A, Kaji N, Ohashi K, Mizuno K.** 2008. Critical roles of actin-interacting protein 1 in cytokinesis and chemotactic migration of mammalian cells. Biochem J **414:**261-270.

28. **Takei Y, Tsujimoto G.** 1998. Identification of a novel MCM3-associated protein that facilitates MCM3 nuclear localization. J Biol Chem **273:**22177-22180.

29. **Kubota Y, Mimura S, Nishimoto S, Takisawa H, Nojima H.** 1995. Identification of the yeast MCM3-related protein as a component of Xenopus DNA replication licensing factor. Cell **81:**601-609.

30. **Young MR, Tye BK.** 1997. Mcm2 and Mcm3 are constitutive nuclear proteins that exhibit distinct isoforms and bind chromatin during specific cell cycle stages of Saccharomyces cerevisiae. Mol Biol Cell **8:**1587-1601.

31. **Wagner S, Flood TA, O'Reilly P, Hume K, Sabourin LA.** 2002. Association of the Ste20-like kinase (SLK) with the microtubule. Role in Rac1-mediated regulation of actin dynamics during cell adhesion and spreading. J Biol Chem **277:**37685-37692.

32. **Wagner S, Storbeck CJ, Roovers K, Chaar ZY, Kolodziej P, McKay M, Sabourin LA.** 2008. FAK/src-family dependent activation of the Ste20-like kinase SLK is required for microtubule-dependent focal adhesion turnover and cell migration. PLoS One **3:**e1868.

33. **Sabourin LA, Rudnicki MA.** 1999. Induction of apoptosis by SLK, a Ste20-related kinase. Oncogene **18:**7566-7575.

34. **Hao W, Takano T, Guillemette J, Papillon J, Ren G, Cybulsky AV.** 2006. Induction of apoptosis by the Ste20-like kinase SLK, a germinal center kinase that activates apoptosis signal-regulating kinase and p38. J Biol Chem **281:**3075-3084.

35. **Ma J, Cai H, Wu T, Sobhian B, Huo Y, Alcivar A, Mehta M, Cheung KL, Ganesan S, Kong AN, Zhang DD, Xia B.** 2012. PALB2 interacts with KEAP1 to promote NRF2 nuclear accumulation and function. Mol Cell Biol **32:**1506-1517.

36. **Komatsu M, Kurokawa H, Waguri S, Taguchi K, Kobayashi A, Ichimura Y, Sou YS, Ueno I, Sakamoto A, Tong KI, Kim M, Nishito Y, Iemura S, Natsume T, Ueno T, Kominami E, Motohashi H, Tanaka K, Yamamoto M.** 2010. The selective autophagy substrate p62 activates the stress responsive transcription factor Nrf2 through inactivation of Keap1. Nat Cell Biol **12:**213-223.

37. **Chen W, Sun Z, Wang XJ, Jiang T, Huang Z, Fang D, Zhang DD.** 2009. Direct interaction between Nrf2 and p21(Cip1/WAF1) upregulates the Nrf2-mediated antioxidant response. Mol Cell **34:**663-673.

38. **Kaneko T, Huang H, Cao X, Li X, Li C, Voss C, Sidhu SS, Li SS.** 2012. Superbinder SH2 domains act as antagonists of cell signaling. Sci Signal **5:**ra68.

39. **Finley D.** 2009. Recognition and processing of ubiquitin-protein conjugates by the proteasome. Annu Rev Biochem **78:**477-513.

40. **Ohta T, Iijima K, Miyamoto M, Nakahara I, Tanaka H, Ohtsuji M, Suzuki T, Kobayashi A, Yokota J, Sakiyama T, Shibata T, Yamamoto M, Hirohashi S.** 2008. Loss of Keap1 function activates Nrf2 and provides advantages for lung cancer cell growth. Cancer Res **68:**1303-1309.

41. **Konstantinopoulos PA, Spentzos D, Fountzilas E, Francoeur N, Sanisetty S, Grammatikos AP, Hecht JL, Cannistra SA.** 2011. Keap1 mutations and Nrf2 pathway activation in epithelial ovarian cancer. Cancer Res **71:**5081-5089.

42. **Cong ZX, Wang HD, Wang JW, Zhou Y, Pan H, Zhang DD, Zhu L.** 2013. ERK and PI3K signaling cascades induce Nrf2 activation and regulate cell viability partly through Nrf2 in human glioblastoma cells. Oncol Rep doi:10.3892/or.2013.2485.

43. **Kim JE, You DJ, Lee C, Ahn C, Seong JY, Hwang JI.** 2010. Suppression of NF-kappaB signaling by KEAP1 regulation of IKKbeta activity through autophagic degradation and inhibition of phosphorylation. Cell Signal **22:**1645-1654.

44. **McMahon M, Lamont DJ, Beattie KA, Hayes JD.** 2010. Keap1 perceives stress via three sensors for the endogenous signaling molecules nitric oxide, zinc, and alkenals. Proc Natl Acad Sci U S A **107:**18838-18843.

CHAPTER 3: PATIENT-DERIVED KEAP1 SUPERBINDER MUTANTS STABILIZE KEAP1 STRUCTURE AND SEQUESTER NRF2 in P62-DEPENDENT CLUSTERS

3.A. Overview

Cancer-derived loss-of-function mutations in the *KEAP1* tumor suppressor gene stabilize the NRF2 transcription factor, resulting in a pro-survival gene expression program that alters cellular metabolism and neutralizes oxidative stress. In a previous study of *KEAP1* mutations observed in lung cancer, we classified 40% of the mutations as 'superbinders' (superbinders). These mutants bind and ubiquitylate NRF2 but do not promote NRF2 degradation. Here, we further investigated the molecular mechanism(s) driving the superbinder phenotype. BioID-based quantitative proteomic analysis of the R320Q and R470C superbinder mutations revealed increased co-complexed NRF2 without significant alteration to other KEAP1-associated proteins, including CUL3, VCP, and several ubiquitin receptors within the proteasome lid. Dynamic simulation modeling and limited proteolysis analyses suggest that superbinder mutations stabilize residues in KEAP1 that contact NRF2. In cells, KEAP1 R320Q and R470C mutants co-localize with NRF2, p62/SQSTM1 and polyubiquitin in spherical clusters that rapidly fuse and dissolve; localization to these clusters requires p62. Expression of R320Q and R470C in lung cancer cells provided resistance to the reactive oxygen species-inducing drug bleomycin. We present and discuss a model wherein superbinder mutations alter the conformational dynamics of the KEAP1-NRF2 complex to alter the cycling of KEAP1 between open and closed conformations, thus inhibiting NRF2 degradation.

3.B. Introduction

The National Cancer Institute projects more than 222,500 new cases of lung cancer, with mortalities in excess of 155,870 people for 2017 (1) Lung squamous cell carcinomas (LUSC) comprise 25-30% of all lung cancer cases with a 5-year survival rate of less than 5% for patients with Stage IV disease, thus demonstrating a clear need for earlier diagnostic measures and novel therapeutic treatments (2-4). Comprehensive studies conducted by The Cancer Genome Atlas (TCGA) revealed mutations in the Kelch-like ECH associated protein 1 (KEAP1) and nuclear factor erythroid 2-related factor 2 (NFE2L2/hereafter, NRF2) pathway in 34% of LUSC cases studied, underscoring the significance of this pathway in lung tumorigenesis (5).

KEAP1 functions as an intracellular sensor of oxidative stress (5-7). Under basal conditions, cytosolic KEAP1 exists as a homodimer and associates with the E3 ubiquitin ligase complex Cullin-3 (CUL3) and RBX1 via a three-box motif in its broad-complex, tramtrack, bric-à-brac (BTB) domain (6-10). Dimeric KEAP1 binds two different motifs within NRF2: a high-affinity ETGE and a low-affinity DLG. These motifs associate with KEAP1 via an arginine triad motif in the KELCH domains of KEAP1 (11-14). The prevailing theory is that the association of both motifs with a KEAP1 homodimer is essential to sterically position seven key lysine residues in NRF2 for ubiquitylation via the CUL3 complex (7-11, 13). Ubiquitylated NRF2 is then delivered to the proteasome for degradation, though mechanistic details of this transition are unresolved. Modifications to one or more of the 27 reactive cysteine residues in KEAP1 result in a conformational change that impairs NRF2 degradation (15-19). Because dimeric KEAP1 is no longer available to degrade NRF2, *de novo* synthesized NRF2 accumulates and translocates to the nucleus (11, 20, 21). Nuclear NRF2 heterodimerizes with small Maf proteins and binds to antioxidant response elements (ARE)/ electrophile response elements (EpRE) in the promoters of target genes, including

the phase II detoxifying enzyme NAD(P)H dehydrogenase [quinone] 1(*NQO1*), glutathione synthesis genes and heme oxygenase 1 (*HMOX1*) (20-22).

Live-cell imaging studies utilizing fluorescence lifetime imaging (FLIM) coupled with Förster resonance transfer (FRET) constructs established that KEAP1 cycles between two distinct conformations: open and closed (15). Initially, KEAP1 exists in the cytosol as a homodimer with a 1:1 stoichiometry with the CUL3 complex (Fig. 1.1) (15, 23, 24). As NRF2 protein levels increase, KEAP1 binds the ETGE motif of NRF2 and maintains an open conformation (Fig. 1.2) (15). Sequential binding of the low-affinity DLG motif generates the closed conformation of the complex in which ubiquitylation of NRF2 is sterically favorable (Fig. 1.3) (15). The closed complex delivers ubiquitylated NRF2 to the proteasome for degradation, and removal of the ubiquitylated substrate results in regeneration of free and open KEAP1, thus enabling cycling to continue (Fig. 1.4) (15). NRF2 inducers modify KEAP1 conformation resulting in impaired cycling and accumulation of the closed KEAP1-NRF2 complex (15). In order to re-establish redox-sensing capabilities, cells must regenerate free KEAP1 and remove KEAP1-NRF2 closed complexes; the mechanism of how this occurs has yet to be fully elucidated (15, 25, 26).

Due to its essential role in mitigating oxidative stress, a delicate balance of KEAP1-NRF2 signaling is required to maintain cellular homeostasis. Inappropriately low or high NRF2 activity is associated with a variety of disease conditions (5, 16, 27, 28). Diminished or absent NRF2 activity is associated with an increased risk for neurodegeneration and aging (16, 29, 30). In contrast, prolonged periods of NRF2 hyperactivation correlate with an increased risk for tumorigenesis (30-33). In greater than 30% of lung cancers, mutations in KEAP1 or NRF2 contribute to constitutive NRF2 activity which correlates with increased resistance to chemotherapy and poor patient outcome (5, 10, 30, 31, 34-36).

Although over 700 somatic mutations in KEAP1 have been identified in cancer, the mechanism and functional consequences of a majority of these mutations remains unknown (37). Analysis of 178 LUSC patients directed by the TCGA consortium revealed 18 mutations in KEAP1 (5). To determine the functional significance of these mutations in LUSC, we cloned and profiled the mutants to define their impact on NRF2 function and biochemical activity (38) . From these data, we identified three distinct functional classes: 1) silent mutations which most likely represent passenger events, 2) hypomorphic mutations, and 3) functionally dead proteins (38). Further interrogation of the hypomorphic mutant class revealed a subset of seven superbinder mutants which exhibit increased binding to NRF2, yet lack the ability to suppress NRF2 transcription (38). Remarkably, cell-based and *in vitro* studies revealed that the KEAP1 R320Q superbinder mutation retains the ability to ubiquitylate NRF2 (38).

From our analyses of the LUSC KEAP1 mutations, we estimate that KEAP1 superbinder mutations represent more than one third of patient-derived LUSC KEAP1 mutations; thus we pursued studies to examine the mechanism and phenotypic consequences of the superbinder mutants. Proximity-based proteomic analyses of KEAP1 superbinder complexes revealed exclusive enrichment for NRF2 with minimal comparable protein-protein interactions with key ubiquitin chaperones and receptors. Simulation data and biochemical studies suggest superbinder mutants stabilize KEAP1 tertiary structure, particularly at interfacing residues with NRF2. *In vivo*, superbinder mutants form clusters containing polyubiquitin, the autophagy cargo adaptor p62/SQSTM1 (p62), KEAP1, and NRF2. Surprisingly, the formation of these clusters is p62-dependent. Overexpression of KEAP1 superbinder mutants in lung adenocarcinoma cells protects from DNA-damaging agent bleomycin. These studies provide insight into how KEAP1 hypomorphic function

mutations sequester NRF2 in p62-dependent clusters thus potentially altering KEAP1-NRF2 conformational cycling.

3.C. Materials and Methods

Tissue culture and transfections

HEK 293T/17 and NCI-H1299 (H1299) cells were obtained from the American Type Culture Collection (ATCC, Manassas, VA) and authenticated by ATCC using short tandem repeat (STR) profiling. Cell lines were passaged for less than 3 months after resuscitation. The *Keap1*$^{-/-}$ mouse embryonic fibroblasts (MEFs) were derived in collaboration with Luke Chen at North Carolina Central University. HEK 293T/17 cells were grown in Dulbecco's Modified Eagle Medium (DMEM) supplemented with 10% fetal bovine serum (FBS). *Keap1*$^{-/-}$ MEFs were cultured in DMEM-F12 supplemented with 10% FBS, 1% non-essential amino acids, and 1% sodium pyruvate. H1299 cells were grown in RPMI-1640 supplemented with 10% FBS. All cells were grown in a 37°C humidified incubator with 5% CO_2. Expression constructs were transfected into HEK 293T/17 cells (7.50 x 10^6 cells/well in a 6-well format) with Lipofectamine® 2000 (Invitrogen 52887; Carlsbad, CA) according to the manufacturer's protocols. H1299 cells (3.0 x 10^6 cells/well in a 6-well format) and *Keap1*$^{-/-}$ MEFs (1.5 x 10^6 cells/well in a 6-well format) were transfected with FuGENE® HD (Promega E231A; Madison, WI) in accordance with the manufacturer's protocols. Transfection of siRNAs in HEK 293T/17 cells (2.0 x 10^6 in a 6-well format) was performed with Lipofectamine® RNAiMAX (Invitrogen, 56532) for 72 hr unless otherwise stated.

siRNA Seqences

Control (CNT) siRNA sequences are as follows: (A) 5' CGU ACG CGG AAU ACU UCG ACU UCG A 3' and (B) 5' UCG AAG UAU UCC GCG UAC GCU AAG U 3'. siRNA sequences for *NFE2L2* are as follows: (1) 5' CCG GGA CAG AGT CAC CAT TTG ATT T 3',

(2) 5’ CCC AGC AAT TCT ACC AGC CTC AAC T 3’, and (3) 5’ GCT ATG TTG GAT GAG ATC AGC CTT A 3’. The siRNA sequences for *PGAM5* are as follows: (1) 5’ ACG CGC GCC AUA GAG ACC ACC GAU A 3’, and (2) 5’ CAC CUG CCA GGC GUC UGC AAA GUC A 3’. siRNA sequences for p62/*SQSTM1* are as follows: (1) 5’ CAG AUG GAG UCG GAU AAC U 3’, (2) 5’ CAG UCU CUG GCG GAG CAG A 3’, and (3) 5’ GGC AGA AUC AGC UUC UGG U 3’. siRNA sequences for VCP are as follows: (1) 5’ GGU AGA AGA GGA UGA UCC A 3’, (2) 5’ CAG UUA CUA UGG AUG ACU U 3 ‘, and (3) 5’ GGU AGA UAU UGG AAU UCC U 3’.

Plasmids, expression vectors, and site-directed mutagenesis

Entry clones for KEAP1 R320Q and R470C were generated using pcDNA 3.1 FLAG-KEAP1 R320Q and R470C constructs as described previously (38). Phusion® High-Fidelity DNA Polymerase (NEB M0530; Ipswich, MA) was used to generate the PCR product for the TOPO cloning reaction using the pCR™8/GW/TOPO® TA Cloning™ Kit (Thermo Fisher Scientific 200517; Waltham, MA). TOPO cloning was performed according to the manufacturer’s instructions. Cloning primers were as follows: Forward 5’ ATG CAG CCA GAT CCC AGG 3’, and Reverse 5’ TCA ACA GGT ACA GTT CTG CTG GTC 3’. Resulting entry vectors were then gateway-cloned into a custom gateway lentiviral vector pHAGE-CMV-FLAG-BirA-DEST to generate expression constructs for BirA*-KEAP1 R320Q and R470C. Clones were sequence verified before use. The Keap1-mCh WT and EGFP-Nrf2 were a kind gift from Albena Dinkova-Kostova at the University of Dundee. R320Q and R470C mutants were generated from PCR-based mutagenesis using the QuikChange™ XL Site-Directed Mutagenesis Kit (Agilent 200517; Santa Clara, CA) according to the manufacturer’s instructions. Constructs were sequence verified before use; primer sequences for the mutagenesis are as follows: R320Q_Forward 5’ CCA CTT TGG GCG CCT GGC AGG GCA CTG C 3’, R320Q_Reverse 5’ GCA GTG CCC TGC CAG GCG CCC

AAA GTG G 3', R470C_Forward 5' CTG CAT ACA GCA AGC AGT TGA GCA CTG CCA C 3', and R470C_Reverse 5' GTG GCA GTG CTC AAC TGC TTG CTG TAT GCA G 3'.

Live cell imaging

HEK 293T/17 cells were co-transfected with mEGFP-Nrf2 and mKeap1-mCH R320 and imaged the following day. Time-lapse phase-contrast and fluorescence images were acquired every 5 min for 10 hr with an Olympus IX70 inverted fluorescence microscope enclosed within an environmental chamber controlled for temperature, relative humidity, and CO_2 and equipped with a 40X/0.6 Ph2 LCPlanFl objective lens and a Hamamatsu ORCA C4742-95 charge-coupled device camera. Data acquisition was carried out with Volocity (version 5.5.1; PerkinElmer), and image processing was performed with ImageJ and Adobe Photoshop CS software.

IncuCyte™ live cell imaging experiments were performed as reported previously with minor modifications (39). HEK 293T/17 cells (1.50×10^6 cells/well in 24-well format) were plated and transfected the next day with FLAG-KEAP1 WT, R320Q, or R470C (150 ng/well) along with mEGFP-Nrf2 or Venus-NRF2 (100 ng/well). Plates were immediately transferred into the IncuCyte™ ZOOM (Essen BioScience; Ann Arbor, MI) and housed inside a cell incubator at 37°C with 5% CO_2. Images were taken every hr for 24 hr with a 20X objective from four fields per well and from four technical replicates per condition in the phase and green channels (400 ms acquisition). Automated image processing on the fluorescence and phase channels was accomplished by applying an appropriate processing definition. Total Green Object Integrated Intensity (GCU X μm^2/Image) was normalized by cell confluence. Data presented represent the average of three biological replicates and are reported as mean ± standard error of the mean.

Immunopurification and Western blotting

For FLAG/mCherry immunopurification, HEK 293T/17 cells (7.5 x 10^6 cells/well in a 6-well format) or H1299 cells (3.0 x 10^6/well in a 6-well format) were seeded and transfected and/or treated the following day for for up to 24 hr . Cells were washed with DPBS and lysed in 255 µl (per well) of 0.1% NP- 40 lysis buffer (0.1% NP-40, 10% glycerol, 50 mM HEPES [pH 8.0], 150 mM NaCl, and 2mM EDTA) supplemented with Halt™ Protease Inhibitor Cocktail 100X (Thermo Scientific 78429), Halt™ Phosphatase Inhibitor Cocktail 100X (Thermo Scientific 78426), and 10 mM N-Ethylmaleimide (NEM) (Thermo Scientific 23030). Cells were lysed on ice for 30 mins followed by a 30 min centrifugation at 16,000g at 4°C. Cleared lysates were quantified using the Pierce BCA Protein Assay Kit (Thermo Scientific 23225) and incubated with EZview™ Red ANTI-FLAG™ M2 Affinity gel (Sigma F2426; St. Louis, MO) or 1 µg of mCherry antibody (Abcam; Cambridge, UK) prior to washing 4 times with 0.1% NP-40 lysis buffer and eluting with 4X NuPAGE™ LDS Sample buffer (Life Technologies NP0007; Carlsbad, CA). For immunoprecipitation of mKEAP1-mCh or mEGFP-Nrf2, cells were lysed and cleared as described above and pre-cleared for one hr with Pierce™ Protein A/G Agarose (Thermo Scientific 20421). Lysates were then incubated with mCherry antibody or GFP antibody (Abcam) overnight at 4°C. The following day, lysates were incubated for 1 hr with Pierce™ Protein A/G resin followed by elution with NuPAGE™ LDS Sample Buffer as described above. For siRNA experiments, HEK 293T/17 cells were lysed in RIPA buffer (1% NP-40, 0.1% SDS, 10% glycerol, 25 mM Tris-HCl pH [7-8], 0.25% sodium deoxycholate, 150 mM NaCl, and 2 mM EDTA) supplemented with protease and phosphatase inhibitor cocktails and 10 mM NEM 72 hr post-transfection.

Antibodies used for W. blot analysis

The GFP (ab290), HMOX1 (ab13243), mCherry (ab16745), and PGAM5 (ab126534) antibodies were purchased from Abcam (Cambridge, UK). The MCM3 (A300-192A), PALB2

(A301-246A), PSMD4 (A303-55A), p62/SQSTM1 A302-856A), and VSV-G (A190-131A) antibodies were purchased from Bethyl Laboratories (Montgomery, TX). The BCL2 (2876B), CUL3 (2759), IKBKB (2684), K48 linkage-specific polyubiquitin clone D9D5 (8081), LC3A/B clone D3U4C XP™ (12741), NBR1 clone D2E6 (9891), NRF1 (8052), p62/SQSTM1 (8025), VCP (2648), and VPS34 (4263) were purchased from Cell Signaling Technologies (Danvers, MA). The PSMD2 (PA5-27663) antibody was obtained from Invitrogen. The phosphor-p62 (SQSTM1) (Ser351) p62/SQSTM1 (PM074) antibody was obtained from MBL International (Woburn, MA). The KEAP1 (10503-2-AP) antibody was obtained from Proteintech (Rosemont, IL). The anti-hemagglutinin (HA) High Affinity Rat antibody (11 867 423 001) was purchased from Roche Diagnostics (Mannheim, Germany). The NRF2-H300 (SC-13032) antibody was purchased from Santa Cruz Biotechnology (Dallas, TX). The Actin (A5316), FLAG M2 (F1804), and Beta tubulin (T7816) antibodies were purchased from Sigma. The following secondary antibodies were purchased from Jackson Immunoresearch (West Grove, PA): Peroxidase-conjugated IgG Fraction Monoclonal Mouse Anti-Rabbit IgG, Light Chain Specific (211-032-171), Peroxidase AffiniPure Goat Anti-Mouse IgG, Light Chain Specific (115-035-174), Peroxidase AffiniPure Donkey Anit-Mouse IgG (H+L) (715-035-150), Peroxidase-conjugated AffiniPure Donkey Anti-Goat IgG (H+L) (705-035-003), Peroxidase-conjugated AffiniPure Donkey Anti-Rat IgG (H+L) (712-035-150), and Peroxidase-conjugated AffiniPure Donkey Anti-Rabbit IgG (H+L) (711-035-152). Secondary antibodies for LI-COR were purchased from LI-COR Biosciences (Lincoln, NE): IRDye® 680LT Goat anti Rabbit IgG (925-68021), IRDye® 680LT Goat anti Mouse IgG (925-68020), IRDye® 800CW Goat anti Mouse IgG (925-32210), and IRDye® 800CW Goat anti Rabbit IgG (925-32211). The following chemicals were purchased from Calbiochem (Darmstadt, Germany): MG-132 (474790), and MLN4924 (505477001).

Antibodies used for IF analysis

The LAMP2 antibody (555803) was obtained from BD Biosciences (Franklin, NJ). The LC3B (2775) and LC3B D11 XP™ (3868) were obtained from Cell Signaling Technology. The polyubiquitinylated conjugates clone FK1 antibody (BML-PW8805) was purchased from Enzo Life Sciences (Farmingdale, NY). The following secondary antibodies were all purchased from Jackson Immunoresearch Laboratories: Fluorescein (FITC) AffiniPure Donkey anti-Mouse IgG (715-095-150), Alexa Fluor® 647 AffiniPure Donkey anti-Rabbit IgG (711-605-152), Alexa Fluor® 647 AffiniPure Donkey anti-Mouse IgG (715-505-150), Rhodamine Red™-X (RRX) AffiniPure donkey anti-mouse IgG (715-295-150).

Small molecule reagents

The following chemicals were purchased from Cayman Chemicals (Ann Arbor, MI): Bleomycin sulfate (13877), cisplatin (13119), CB-5083 (19311), N^2,N^4-dibenzylquinazoline-2,4-diamine (DBeQ); 15318), and Eeyarestatin 1 (Eey1; 10012609). Cycloheximide (CHX; 1010083) was purchased from MP Biomedicals (Santa Ana, CA). The following chemicals were purchased from Sigma: Chloroquine (CQ; C6628), L-Sulforaphane (SFN; S6317), and *tert*-Butylhydroquinone (tBHQ; 112941). Bardoxolone methyl (CDDO; S8078) was obtained from Selleck Chemicals (Houston, TX). Paclitaxel (TXD01) was obtained from Cytoskeleton, Inc. (Denver, CO).

Immunostaining and Confocal Images

These experiments were performed as reported previously with minor modifications (39). Briefly, HEK 293T/17 or H1299 cells were plated on 10 µg/ml fibronectin-coated coverslips in the appropriate culture media and allowed to attach overnight. For experiments that required exogenous expression of tagged proteins, transfection was performed 24 hr post-plating, and cells were stained the following day. Cells were fixed in 4%

paraformaldehyde in cytoskeletal buffer (5 mM PIPES [pH 6.0], 137 mM NaCl, 5 mM KCl, 1.1 mM Na_2HPO_4, 0.4 mM KH_2PO_4, 0.4 mM $MgCl_2$, 0.4 mM $NaHCO_3$, 2 mM EGTA, and 50 mM glucose) for 15 min and permeabilized with 0.1% Triton X-100 in PBS for 5 min. After blocking with 1% BSA in PBS, cells were incubated overnight with the primary antibodies and then incubated with the appropriate fluorescence-conjugated secondary antibodies for 1 hr. The following primary antibodies were used: anti-FLAG (1:1000, Sigma), anti-p62 (1:150, Cell Signaling Technology), anti-p-S351-p62 (1:300, MBL International), anti-LC3B (1:150, Cell Signaling Technology), anti-LAMP2 (1:150, BD Biosciences), and anti-polyubiquitinylated conjugates FK1 (1:250, Enzo Life Sciences. Secondary antibodies were used at the following dilutions: FITC anti-mouse IgG (1:300), Alexa Fluor® 647 anti-Rabbit IgG (1:500), Alexa Fluor® 647 anti-mouse IgG (1:300), RRX anti-mouse IgG (1:2000). DAPI staining was performed for nuclear detection. Coverslips were mounted to slides using the ProLong™ gold antifade mountant with DAPI (P36935; Thermo Fisher Scientific), and images were acquired using a Zeiss LSM 710 confocal laser-scanning microscope equipped with 40X/1.3 Oil Plan Neo and 63X/1.4 Oil Plan Apo objective lenses.

Proximity Ligation Assays

For detection of KEAP1 and NRF2 interactions, proximity ligation was performed with the Duolink® II proximity ligation assay kit according to the protocol provided by the manufacturer (Sigma DUO092101). Briefly, HEK 293T/17 cells stably expressing FLAG-KEAP1 (WT or mutants) were plated on fibronectin-coated coverslips, allowed to attach, fixed, and permeabilized as described above. For the PLA experiments in H1299 cells, transfections with the desired plasmids were performed after plating cells on coverslips. Cells were then incubated in blocking solution in a humidified chamber at 37°C for 30 min, followed by overnight co-incubation with rabbit polyclonal antibodies against NRF2 (Santa Cruz 1:200) and mouse monoclonal antibody against FLAG (Sigma 1:1000) in antibody

diluent solution at 4°C. Cells were washed in buffer A and incubated with PLA probes (Sigma Duolink® In Situ PLA® Probe Anti-Rabbit PLUS (DUO92002) and Duolink® In Situ PLA® Probe Anti-Mouse MINUS (DUO92004) in antibody diluent (1: %dilution) for 1 hr at 37°C. They were then washed in buffer A and incubated with ligation solution (1:5 dilution of ligation buffer and 1:40 dilution of ligase in pure water) for 30 min at 37°C. After ligation, cells were washed in buffer A and subjected to amplification with Detection Reagents Red (1:5 dilution amplification stock and 1:80 dilution of polymerase in water) for 100 min at 37 °C. Amplified samples were washed in buffer B, washed in buffer A, and counterstained for microtubules using anti-tubulin-FITC antibodies (Sigma, 1:500 dilution). The coverslips were mounted with Duolink® II mounting medium with DAPI for nuclear detection. When analyzing PLA preparations in HEK 293T/17 cells, confocal Z-stack images of 10 μm thickness were taken with a Z-step of 0.5 μm (about 21 slices) at 512 x 512 pixels, using a Zeiss LSM710 spectral confocal laser-scanning microscope equipped with a ×40/1.4 Oil DIc M27PlanApo objective lens. ImageJ software was used to project all 21 slices per field into a 2D image. When analyzing PLA preparations in H1299 cells, a single optical slice was captured per field from a depth of 4-5 μm above the substrate to ensure that sampling was done from the same level for all preparations. Three channel images were taken for 9 random fields per condition. Experiments were done in three biological replicates. The number of nuclei and PLA dots per image were quantified using BlobFinder software (40). PLA dots/nuclei ratio was set to 1 in FLAG-KEAP1 WT-expressing cells (untreated or DMSO-treated) and used to calculate PLA dot fold-induction in cells expressing KEAP1 mutants or following treatment with NRF2 inducers.

KEAP1 ubiquitylation experiments

Ubiquitylation of KEAP1 under denaturing conditions was performed in HEK 293T/17 cells transiently transfected with VSV-Ub1 or Venus-NPM1 and SBPHA-KEAP1 WT, -

R320Q, or -R470C. Cells were lysed in pre-boiled SDS denaturing buffer (25 mM Tris, 150 mM NaCl, 1% SDS, and 1 mM EDTA) and boiled for 10 min. The cells were then diluted 1:5 in 0.5% NP-40 buffer (0.5% NP-40, 25 mM Tris-HCl [pH 7-8], and 150 mM NaCl) and normalized for protein content. 250 µg of protein was reserved for input, and 500 µg of the lysate was immunoprecipitated with FLAG antibody for two hr at 4°C. FLAG beads were washed 4X with SDS denaturing buffer diluted 1:10 in 0.5% NP-40 lysis buffer. FLAG beads were then eluted with NuPAGE™ Lysis Buffer and boiled for 10 min at 70°C.

BioID affinity purification and peptide generation

HEK 293T/17 cells stably expressing BirA*-KEAP1 WT, R320Q, or R470C were treated with 50 µM biotin (Sigma B4639) for 24 hr. Cells were lysed in RIPA buffer supplemented with protease and phosphatase inhibitors, 10 mM NEM, and 1 µl Benzonase (Sigma E1404), cleared with ultracentrifugation, and protein normalized. Five mg of protein was used for streptavidin affinity purification (AP). Streptavidin Sepharose™ High Performance beads (GE Healthcare 17-5113-01, Upssala, Sweden) were washed 3 times in RIPA buffer prior to AP overnight at 4°C with nutation. Beads were washed once with RIPA buffer, twice with TAP lysis buffer (10% glycerol, 50 mM HEPES [pH 8.0], 150 mM NaCl, 2 mM EDTA, and 0.1% NP-40), and three times with 50 mM ammonium bicarbonate (pH 8.0). The precipitated proteins were trypsinized with 1 µg of trypsin (Promega V5111) for 16 hr followed by another 0.5 µg of trypsin for 2 hr. Trypsinization was performed directly on beads using a modified FASP protocol followed by desalting via a Pierce™ C-18 spin column (Thermo 89870) and ethyl acetate cleanup.

Mass spectrometry, data filtering, and bioinformatics

Reverse-phase nano-HPLC coupled with a nanoACQUITY UPLC system (Waters Corporation; Milford, MA) were used to separate trypsinized peptides. Trapping and

separation of peptides was performed in a 2 cm column (Pepmap 100, 3 μm particle size, 100 Å pore size), and a 25 cm EASYspray analytical column (75 μm ID, 2.0 μm C18 particle size, 100 Å pore size) at 300 nl/min and 35˚C, respectively. Analysis of a 180 min gradient of 2-25% buffer B (0.1% formic acid in acetonitrile) was performed on an Orbitrap Elite mass spectrometer (Thermo Scientific). Data acquisition and ion source settings were previously published (41).

All raw mass spectrometry data were searched using MaxQuant version 1.5.2.6. Search parameters were as follows: UniProtKB/Swiss-Prot human canonical sequence database human_sp_072313, static carbamidomethyl cysteine modification, specific trypsin digestion with up to two missed cleavages, variable protein N-terminal acetylation and methionine oxidation, match between runs, and label free quantification (LFQ) with a minimum ratio count of two. Searched files were analyzed using Perseus version 1.5.1.6 for data filtering and visualization. Rows were filtered based on a Q value relation <0.01, and potential contaminants, decoys, and reverses were removed. LFQ intensities were log2-transformed and filtered for valid values. Missing values were imputed from a normal distribution using a down-shift of 1.8 and a distribution width of 0.4. Minimum protein probability cutoffs resulting in a 5% false discovery rate (FDR) were selected for each experiment. For volcano plots illustrating BioID/MS data, p-values were determined using a two-tailed t-test, and the FDR was calculated using the Benjamini-Hochberg procedure. MS data were filtered and normalized for R320Q and R470C (data not shown).

Sequence variability for NRF2 and KEAP1: The protein BLAST server (PMID: 8743682) was used to find 500 unique sequences for each gene and to analyze the sequence conservation for human NRF2 (UniProt ID: Q16236) and KEAP1 (UniProt ID: Q14145). All of the identified genes had at least 45% amino acid identity to the query

sequence. The PROMALS-3D webserver was used to create a multi-sequence alignment; default settings were used <PMID:18287115>. Shannon entropy was calculated for the multiple sequence alignments using the Protein Variability Server (PMID:17519246) with the default settings.

DMD simulation data

Five replicate discrete molecular dynamics (DMD) simulations of one million steps each for both KEAP1-WT and -R470C were performed in the presence of the NRF2 peptide (42).

Limited Proteolysis

Keap1$^{-/-}$ MEFs were seeded in 6-well plates and allowed to adhere overnight. The following day, cells were transfected with FLAG-KEAP1 constructs using FuGene HD according to the manufacturer's protocol. 24 hr post-transfection, cells were washed twice with PBS and harvested in PBSt (0.1% Triton X-100 in PBS). Cells were snap frozen in liquid nitrogen, thawed, and lysed for one hr at 4°C. Lysates were cleared at 16,000g for 10 min at 4°C and protein normalized. Lysates were diluted to 1 mg/mL, and 75 µl aliquots were taken. 25 µl of trypsin at indicated concentrations were added to each lysate, and limited proteolysis was allowed to proceed for 15 minutes on ice. Reactions were quenched with 100 µl of complete protease inhibitor and 100 µM PMSF. Samples were diluted with 4X LDS Sample buffer and DTT prior to boiling at 70°C for 10 min.

Triton X-100 Solubility Assays

Harvested cell pellets were lysed for 1 hr at 4˚C in 1% Triton X-100 lysis buffer (1% Triton X-100, 10% Glycerol, 25 mM Tris-Hcl pH 7-8 150 mM NACL, 2 mM EDTA) containing 10 µl RQ1 DNase (Promega). 45 µl of lysate was removed for 'total' sample and remaining

lysate was subjected to centrifugation at 20,000g for 15 minutes at 4˚C. Supernatant was removed and 45 µl was reserved for the 'soluble' fraction to which was added 20 µl of 4X LDS-sample buffer with 10 mM DTT. The insoluble fraction was dissolved in 200 µl of 1X SDS-sample buffer with DTT. Samples were sonicated with two 10-second pulses at 10% intensity using a digital sonifier (Branson) prior to SDS-PAGE.

Cell Viability Assays

H1299 (3500 cells/well in a 96-well format) were seeded and allowed to adhere overnight. Serial drug dilutions were prepared, and cells were treated for 72 hr. PrestoBlue™ Cell Viability Reagent (Life Technologies Corporation A13262) was added to wells according to the manufacturer's protocol. Measurements of resazurin conversion as a surrogate for mitochondrial respiration were measured by fluorescence on a Perkin Elmer Enspire™ plate reader (Perkin Elmer, Waltham, MA). All experiments were performed in technical quadruplicate and biological triplicate by two independent researchers. Resulting data were plotted and analyzed using GraphPad Prism software version 7.0.

3.D. Results

3.D.1. The mutational landscape of NRF2 and KEAP1

Across many cancer types, inactivating mutations in KEAP1 and activating mutations in NRF2 are mutually exclusive. Further, KEAP1 mutations lack positional enrichment, whereas mutations in NRF2 localize to the KEAP1 binding sites, features that are consistent with tumor suppressor and oncogene functions, respectively (5, 37, 38, 43-50). To illustrate these patterns, we compiled mutation data from cBioPortal into kernel density estimation (KDE) plots (Fig. 2A and 2B and Tables S.3.1 and S.3.2) (37). 448 mutations in NRF2 localize almost exclusively to the DLG and ETGE motifs which are required for binding to KEAP1 (Fig. 2A) (38). In contrast, the 718 mutations identified in KEAP1 lack appreciable

focal enrichment (Fig. 2B) (5, 37, 38, 45). Known superbinder mutations also do not localize to a specific domain of KEAP1. Two of the amino acid residues in KEAP1 with the highest mutational frequencies are R320 and R470, both of which result in a superbinder phenotype (Fig. 2B) (38).

We hypothesized that functionally relevant mutations in NRF2 and KEAP1 would also be evolutionarily conserved as compared to passenger mutations or non-mutated residues. To test this, we examined the correlation between mutational frequency (MF) and evolutionary conservation as estimated by Shannon entropy (SE) for a given amino acid residue (Fig. 2C-2F) (37, 51, 52). MF versus SE plots for NRF2 and KEAP1 revealed a general trend of cancer-derived mutations affecting evolutionarily conserved residues (Fig. 2C and 2D). For both NRF2 and KEAP1, the difference between SE for non-mutated and mutated residues was statistically significant (Fig. 2E and 2F). Although multiple amino acid substitutions are observed at the superbinder residues R320 and R470, we chose to further characterize R320Q and R470C.

3.D.2. Biochemical characterization of the KEAP1 superbinder mutants

To explore the mechanism of the superbinder mutants, we examined NRF2 stability and KEAP1-NRF2 association. We first probed the dynamics of NRF2 stabilization using live-cell imaging. HEK 293T/17 cells transiently overexpressing murine EGFP-Nrf2 (mEGFP-Nrf2) or human Venus-NRF2 (Venus-NRF2) were monitored every hour for 24 hours, and NRF2 stabilization was plotted as a function of green fluorescence intensity. Analysis of fluorescent NRF2 intensity confirmed that KEAP1 R320Q and R470C rapidly stabilized NRF2 within hours of transfection (Fig. 3A). Moreover, elevated NRF2 protein was sustained for up to 24 hours post-transfection (Fig. 3A). NRF2 stabilization in the presence of KEAP1

R320Q overexpression was also observed in fixed HEK 293T/17 cells using immunofluorescence (IF) (Fig. S1A).

Next, we compared KEAP1-NRF2 association using two complementary approaches: immunopurification followed by Western blot (IP/W.blot) and proximity ligation assay (PLA). Analysis of IP/W.blot for FLAG-KEAP1 complexes from HEK 293T/17 cells demonstrated that with the exception of G423V and G186R, the remaining five superbinder mutations express comparably to WT. Furthermore, all superbinder mutants stabilize NRF2 in the total cell lysate (Fig. 3B lanes 3-9) although not to the same extent as KEAP1 WT treated with the proteasome inhibitor MG-132 (Fig. 3B, lanes, 10, 20, and 30). Analysis of the immunopurified complex demonstrated increased association of NRF2 with all seven superbinder mutants (Fig. 3B, lanes 13-19) and increased NRF2 protein levels in the unbound fraction (Fig. 3B, lanes 23-29). Examination of the bound NRF2 suggests that there are two distinct classes of superbinders (Fig. 3B). In the first class, R320Q, R470C, D422N, and G186R consistently bound more NRF2 than the second superbinder class consisting of G423V, S243C, and V155F (Fig. 3B compare lanes 3, 4, 6, 7 with 5, 8, and 9).

To determine localization and to further quantify KEAP1-NRF2 complex formation, the proximity ligation assay (PLA) (53, 54)PLA was employed. Consistent with reported literature, confocal imaging analysis of the PLA puncta demonstrated KEAP1-NRF2 complex formation primarily within the cytosol (Fig. 3C) (15, 18, 23-25, 53, 54). Quantification of the PLA signal confirmed greater than a two-fold increase in R320Q KEAP1-NRF2 complex formation as compared to WT (Fig. 3D). To confirm the increased association of NRF2 with KEAP1 superbinders in a more clinically relevant cell line, we performed PLA in the lung adenocarcinoma cell line NCI-H1299 (H1299). PLA of KEAP1 R320Q and R470C with endogenous NRF2 demonstrated increased KEAP1-NRF2 complex

formation within the cytosol of the cell as compared to WT (Fig. 3D). Additionally, we compared the stabilization of the KEAP1-NRF2 complex in the presence of the superbinders with a panel of NRF2 inducers: sulforaphane (SFN), bardoxolone-methyl (CDDO), MLN4924, and MG-132 (55, 56). The neddylation inhibitor MLN4924 was the most potent NRF2 inducer (Fig. 3E and 3F) (55, 56). Cysteine modifying compounds SFN and CDDO also stabilized the KEAP1-NRF2 complex but to a lesser extent when compared to MLN4924 (19, 57-59). Moreover, R320Q and R470C stabilized the KEAP1-NRF2 interaction comparably to treatment with the proteasomal inhibitor MG-132 (Fig. 3F and 3G) (60). IF and WB were used to confirm equivalent expression of the FLAG-KEAP1 constructs as well as to assess NRF2 stabilization in H1299 cells (Fig. S1 panels B-D).

3.D.3. Defining protein-protein interactions of KEAP1 superbinders

Substrates targeted for ubiquitylation are often low abundant proteins or transient interactions that are difficult to detect by traditional immunopurification mass spectrometry (IP/MS); therefore, we employed an unbiased MS approach to probe for additional KEAP1 substrates and/or interacting proteins with altered association with the superbinder mutants. BioID is a novel technique employing the use of a promiscuous biotin ligase fused to a bait protein (61-63). Proteins that associate proximally with the bait will be biotinylated by the ligase and can be affinity purified using streptavidin and detected by MS or W.blot analyses (Fig. 4A) (61-63). Biotinylated complexes from HEK 293T/17 cells stably overexpressing BirA*-KEAP1 WT, R320Q, or R470C were affinity purified using streptavidin, and eluted peptides were analyzed using LC-MS/MS. Proteomic analysis revealed NRF2 as the only protein significantly increased within KEAP1 R320Q and R470C protein complexes when using a FDR of 5% (Fig. 4B and 4C and Tables S.3.3 and S.3.4).

To evaluate known KEAP1 substrates, IP/W.blot for all putative substrates was performed. IP/W.blot from HEK 293T/17 cells overexpressing FLAG-KEAP1 WT or all seven superbinders confirmed that only NRF2 association increased with KEAP1 superbinder overexpression (Fig. 4D). Stabilization of PALB2, MCM3, NRF1, IKBKB, PGAM5, or BCL2 in the input or in the bound complex was not observed (Fig. 4D) (41, 64-71), NRF1 and PGAM5 antibodies were confirmed using siRNAs (Fig. S2). Endogenous NRF1 protein levels were undetectable in the lysate but were detectable following MG-132 treatment (Fig. 4D and Fig. S2).

3.D.4. Probing mechanistic steps in KEAP1 cycling

Our data indicate that KEAP1 superbinders stabilize NRF2 while maintaining levels of NRF2 ubiquitylation, suggesting that superbinders may impair KEAP1 cycling. To test this hypothesis, different biochemical steps of the cycling process were systematically evaluated. We first confirmed that KEAP1 superbinder mutants can homodimerize by overexpressing streptavidin binding peptide and hemagglutinin-tagged KEAP1 (SBPHA-KEAP1) and FLAG-KEAP1 in *Keap1*$^{-/-}$ mouse embryonic fibroblasts (MEFs). These experiments were conducted in a KEAP1 null cell line to eliminate potential contributions from endogenous KEAP1. First of all, IP/W.blot demonstrated that KEAP1 superbinders retain the ability to homodimerize (Fig. 5A). Secondly, KEAP1/CUL3 association was examined using transient overexpression of FLAG-KEAP1 superbinder mutants in *Keap1*$^{-/-}$ MEFs. IP/W. blot analyses confirmed that KEAP1 superbinder mutants associate with CUL3 comparably to KEAP1 WT (Fig. 5B). Thirdly, given the previously reported interaction between KEAP1 and the proteasomal chaperone HSP90, the interaction between KEAP1 WT or R320Q and HSP90 was assessed (38, 72). Interactions between HSP90 and KEAP1 WT or R320Q were not observed (Fig. S3 panel A) (38, 72).

A recent report details the mechanism by which p97/Valosin containing protein (VCP) and co-factors UFD1/NPL4 and UBXN7 remove ubiquitylated NRF2 from the KEAP1-CUL3 complex for proteasomal delivery (73). These data were consistent with our hypothesis that KEAP1 superbinder mutants impair proteasomal degradation downstream of ubiquitylation but prior to proteolysis; consequently, interaction between KEAP1 and VCP was examined (73). In both HEK 293T/17 and *Keap1*$^{-/-}$ MEFs, we observed that KEAP1 WT, R320Q, and R470C bind VCP; however, there was no appreciable difference in VCP association between KEAP1 WT and the two superbinders (Fig. 5C and 5D). Treatment with VCP inhibitors CB-5083, DBeQ, or Eeyrestatin (Eey1) had no effect on VCP, KEAP1, or NRF2 protein levels (Fig. 5E, lanes 2-4, and 7-9) or association with KEAP1 WT or R320Q (Fig. 5E, lanes 12-14, and 17-19) (74-77). Finally, MG-132 treatment had no impact on VCP or KEAP1 levels or association (Fig. 5E, lanes 5, 10, 15, and 20). VCP siRNAs were used to validate the VCP antibody (Fig. S3B).

To test KEAP1 association with the proteasome, IP/W. blot for ubiquitin receptors PSMD2 and PSMD4 was performed (78-85) . IP/W.blot of FLAG-KEAP1 WT, R320Q, or R470C demonstrated no differences in association with either PSMD2 or PSMD4 between KEAP1 WT or the superbinders (Fig. 5F, lanes 7-9). Treatment with MG-132 did not lead to increased association of KEAP1 WT with either PSMD2 or PSMD4 (Fig. 5F, lane 10).

3.D.5. Assessing KEAP1 superbinder structure

Modifications to essential cysteines are known to reorganize KEAP1 architecture and impair KEAP1 function through conformational changes (19, 27, 59, 86). Mutations impacting cysteine reactivity or causing structural deformation of KEAP1 could result in the superbinder phenotype. The lack of an available full-length crystal structure for KEAP1 precluded molecular modeling to determine how R320Q impacts KEAP1 structure; however,

molecular modeling and simulations of the KEAP1 KELCH domain could be used to investigate how the R470C superbinder mutation may impact KEAP1 structure when complexed with NRF2.

Discrete molecular dynamics (DMD) simulation demonstrated that the R470C mutation significantly reduced root mean square fluctuations (RMSF) of several residues between amino acid residue numbers 500 and 550 (Fig. 6A) (42). A decrease in RMSF corresponds to reduced motion, suggesting that the R470C mutation has a stabilizing effect on these residues. When mapped to the crystal structure, several decreases in RMSF were observed to propagate throughout the KEAP1 KELCH domain and to contact loops with the NRF2 degron (Fig. 6B). Examination of potential interactions with R470 revealed two acidic residues, D422 and E493 that are capable of forming a salt bridge with R470 (Fig. 6B).

To further confirm the effects of KEAP1 superbinder mutations on KEAP1 tertiary structure, low resolution limited trypsin proteolysis was performed (87). Lysates from *Keap1*$^{-/-}$ MEFs transiently overexpressing FLAG- KEAP1 WT, R320Q, or R470C were exposed to increasing concentrations of trypsin which cleaves at exposed arginine and lysine residues. Although the molecular weight banding patterns generated by trypsin were similar between WT and the two superbinder mutants, the intensity for bands between 50 and 70 kDa differed between KEAP1 WT and the superbinders. The increased intensity observed with KEAP1 R320Q and R470C indicated decreased susceptibility to proteolysis, suggesting that the structure is less available for trypsin cleavage (Fig. 6C, compare lanes 2-4 with lanes 6-8 and 10-12) and supporting the DMD simulation theory.

KEAP1 stability and ubiquitylation were also assessed. Cycloheximide (CHX) chase experiments under basal and oxidative stress-inducing tert-Butylhydroquinone (tBHQ)

conditions confirmed that KEAP1 R320Q does not alter KEAP1-half-life (Fig. S4 panels A and B) (88, 89). IP/W.blot for ubiquitylated KEAP1 under native conditions demonstrated that KEAP1 superbinder mutants did not alter KEAP1 ubiquitylation under basal or induced (tBHQ and MG-132) conditions (Fig. S4Cm lanes 15-16, 19-20, and 23-24) nor did they alter KEAP1 K48 or K63 ubiquitin chain formation (Fig. S4D lanes 11-16). KEAP1 K48 ubiquitylation was further confirmed under near denaturing conditions using an antibody for endogenous K48 ubiquitin (Fig. S4D lanes 6-8).

3.D.6. KEAP1 superbinders form p62-dependent insoluble clusters

The proposed impairment to KEAP1 structure led us to investigate KEAP1 localization in the presence of the superbinders. We utilized validated fluorescent constructs to visualize the KEAP1-NRF2 complex in real time (15). We first tested the localization by independently overexpressing murine EGFP-Nrf2 (mEGFP-Nrf2), murine Keap1-mCherry (mKeap1-mCh) WT, R320Q, or R470C independently. Consistent with recent reports, in both HEK 293T/17 and H1299, overexpression of mEGFP-Nrf2 alone resulted in a primarily nuclear subcellular localization with nuclear foci observed in H1299 (Fig. S5, panels A and B). In contrast, overexpression of all of the mKeap1-mCh constructs resulted in a diffuse cytosolic subcellular localization with increased Keap1 positive clusters observed in H1299 cells as compared to HEK 293T/17 (Fig. S5 panels, A and B) (15). Next, overexpression of mEGFP-Nrf2 in the presence of mKeap1-WT, R320Q, or R470C was examined. A distinct increase in Keap1-Nrf2 containing clusters was observed when mEGFP-Nrf2 was overexpressed in the presence of the superbinder mutants in both HEK 293T/17 and H1299 cells (Fig. 7A and Fig. S5 panel C).

Cytoplasmic inclusions are characterized by insoluble protein aggregates; thus, the Triton X-100 solubility assay was used to identify the localization of these clusters within the

cell ((90). Similar accumulation within the insoluble fraction for all of the FLAG-KEAP1 constructs was observed (Fig. 7B lanes 12-14). However, NRF2 accumulation within the insoluble fraction only occurred in the presence of R320Q and R470C, or with KEAP1 WT treated with MG-132 (Fig. 7B lanes 12-14).

In order to visualize the formation of these complexes, mEGFP-Nrf2 and mKeap1-mCh R320Q were overexpressed in HEK 293T/17 cells for live cell imaging studies. These movies revealed that the smaller punctate structures combined to form larger clusters that are ultimately cleared by the cell within two hours (Fig. 7C). Moreover, accumulation of these aggregates was not cytotoxic as several instances of cells proceeding through another round of division following aggregate clearance were observed (Supplemental Movie).

Insoluble inclusion bodies and aggregate structures are often a hallmark of autophagy, a bulk cellular recycling pathway involved in protein homeostasis (91-94). KEAP1 binds the autophagy ubiquitin cargo adaptor p62/SQSTM1 (p62) via a KEAP1-interaction region (KIR) in p62 and is itself degraded by autophagy (95-98). We hypothesized that these clusters could represent autophagic flux of the KEAP1-NRF2 complexes with superbinder mutants. To evaluate KEAP1 association with components of the autophagy pathway, we performed IP/W.blot. Analysis of immunopurified complexes revealed that KEAP1 WT, R320Q, and R470C bound the autophagy cargo adapters next to BRCA-1 (NBR1), p62 and an autophagy specific phosphorylated form of p62 pS351 (99-101) (Fig. 7D) Furthermore, KEAP1 WT, R320Q, and R470C bound VPS34, a class III phosphatidylinositol (PI) 3-kinase involved in the initial formation of the autophagophore (93, 94, 102) (Fig. 7D).

Upon formation of the autophagophore, p62 and NBR1 bind to and transport ubiquitylated substrates from the phagophore to the autophagosome, where the substrates are tethered to a lipidated form of light chain 3 (LC3) (93, 103). Lipidated LC3 can be detected via W.blot as a faster migrating band, and conversion of LC3 I-II is routinely used as a marker of autophagic flux (91, 93, 103). KEAP1 WT, R320Q, and R470C were all deficient for binding with LC3 (Fig. 7D lanes 6-8).

Overexpression of KEAP1 WT, R320Q, and R470C did not alter the total protein levels of NBR1 or VPS34; however, overexpression of KEAP1 WT, R320Q, and R470C resulted in increased p62 and LC3 I to II conversion levels and decreased levels of p62 pS351 (Fig. 7D, compare lane 1 with lanes 2-4). There were no appreciable differences in the effect of KEAP1 WT as compared to R320Q and R470C with any of the autophagy proteins (Fig. 7D, compare lane 2 with lanes 3-4).

To identify the proteins contained in the insoluble clusters, IF analysis of mKeap1-mCh and mEGFP-Nrf2 in H1299 cells was performed, and results confirmed that both Keap1 and Nrf2 co-localize in the clusters (Fig. 8A). Moreover, IF analyses of FLAG-NRF2 and mKeap1-mCh R320Q revealed spherical clusters coated with endogenous poly-ubiquitin (poly-Ub), p62, and p62 pS351 (Fig. 8B). These clusters co-localized with overexpressed EGFP-LC3 but not with endogenous LC3, or lysosomal markers LAMP2 or lysotracker under basal conditions or following treatment with the autophagy inhibitor chloroquine (CQ) (Fig. S6 panels A-C) (91, 92, 104). Knockdown of p62 via siRNA resulted in the absence of Keap1-NRF2 clusters suggesting that cluster formation is p62-dependent (Fig. 8C and Fig. S6 panel D). Taken together, these data support the p62-dependent formation of spherical clusters that can be graphically represented as containing multiple

subunits of p62, p62 pS351, polyUb, and NRF2 on the periphery with a primarily KEAP1 positive core (Fig. 8D).

3.D.7. KEAP1 superbinder mutants protect against chemotherapies that induce oxidative stress

Prolonged NRF2 activation correlates with an increased resistance to chemotherapy and radiation treatment (22, 30-32, 35, 105-107). To determine the impact of superbinders on cell viability, H1299 cells stably overexpressing mKeap1-mCh WT, R320Q, R470C, or mEGFP-Nrf2 were generated and validated (Fig. S7 panel A). The H1299 stably expressing cell lines were then treated with bleomycin which induces DNA-damage via oxidative stress (108) cell viability and apoptotis were then assayed by PrestoBlue and Caspase 3/7 Glo assays, respectively. Analysis of EC50 values for bleomycin demonstrated that KEAP1 R470C and R320Q exhibit increased cell viability as compared to KEAP1 WT, and the difference in EC50 for KEAP1 WT and R470C was statistically significant at $p<0.0001$ (Fig. 9A). KEAP1 R320Q demonstrated a similar effect, though the increased EC50 value for R320Q compared to WT was not statistically significant (Fig. 9A) To complement the cell viability data, levels of apoptotic induction were quantified using Caspase 3/7 Glo. R470C exhibited decreased activation of executioner caspases, which was significantly different from WT at $p=0.0002$ (Fig. 9B). KEAP1 R320Q also exhibited lower levels of activated caspases; however, the difference with KEAP1 WT did not reach statistical significance (Fig. 9B). Intriguingly, the protection conferred by the superbinders was specific to bleomycin as similar effects were not observed with either the DNA damaging agent cisplatin or the microtubule destabilizer paclitaxel (Fig. S7 panels B and C).

3.E. Discussion

Through biochemical examination, we have defined five main attributes of the KEAP1 superbinder class. First, KEAP1 superbinders occur at well-conserved and frequently mutated residues within KEAP1. Second, KEAP1 superbinders exclusively exhibit increased KEAP1-NRF2 complex formation. Third, KEAP1 superbinders have a stabilizing effect on KEAP1 structure that decreases flexibility at key residues interfacing with NRF2. Fourth, the superbinder mutants form p62-dependent clusters that are spherical in shape and contain p62, p62 pS351, polyUb, and NRF2. Fifth, KEAP1 superbinders show increased resistance to bleomycin treatment but not to cisplatin or paclitaxel.

Although expected, the high correlation between mutational frequency and conservation appears to indicate biologically functional residues. Within NRF2, 19 of the top 20 frequently mutated residues (with the exception of R499) localize to the ETGE or DLG motif, which are required for KEAP1 association. Similarly, there is enrichment for superbinder residues and known KEAP1 inactivating mutations such as G333 and G480 within the top 20 frequently mutated residues in KEAP1 (38, 46, 47, 109). We hypothesize that highly conserved and frequently mutated residues impact protein function and that this approach can be used to prioritize mutations for further study.

Unexpectedly, excluding NRF2, results from the unbiased BioID/MS approach and targeted interrogation of key protein-protein interactions suggest that the superbinder mutants are almost indistinguishable from KEAP1 WT in terms of biochemical interaction profiles. We would have predicted that other ETGE-containing substrates similar to NRF2 would have been predicted to also exhibit increased association with KEAP1 superbinders. In fact, appreciable differences were not detected between superbinders and NRF1, which contains both the DLG and ETGE motifs (65, 110).

To date, the exact mechanism of how ubiquitylated NRF2 is delivered to the proteasome has not been described; however, we characterized novel KEAP1 interactions with the ubiquitin chaperone VCP and with two proteasomal ubiquitin receptors, PSMD2 and PSMD4. The KEAP1-VCP interaction merits further examination as a recent report details the roles of VCP and ubiquitin cofactors UFD1/NPL4 and UBXN7 in removing ubiquitylated NRF2 from the KEAP1-CUL3 complex (73). In our studies, VCP depletion and inhibition had no effect on NRF2 protein levels in the presence of KEAP1 WT or R320Q, suggesting that VCP may not play a critical role in HEK 293T/17 or H1299 cells. The interaction between KEAP1 superbinders and PSMD2 and PSMD4 indicates that superbinders retain the ability to interact with the proteasome, which raises several possibilities for how the superbinders may impair NRF2 degradation. First, ubiquitin removal and substrate unfolding may require ATP-dependent reactions or additional chaperone proteins that were not identified by the BioID approach. Second, the stabilized KEAP1 tertiary structure predicted by our simulation modeling and supported by the limited proteolysis may preclude the removal of ubiquitin from NRF2 or the dissociation of the E3 complex after the superbinder attempts to present ubiquitylated NRF2 to the proteasome for degradation. Decreased flexibility at NRF2 contact points is a plausible explanation for the observed superbinder phenotype. It is possible that the R470C mutation disrupts salt bridge formation between amino acid residues D422 and/or E493, resulting in the observed stabilization. This mechanism of action is particularly attractive as the KEAP1 D422N mutation also results in a superbinder phenotype (38). Intriguingly, patient mutations of KEAP1 E493 have been reported, and we speculate that these mutations may also result in a superbinder phenotype. Experiments testing this hypothesis are currently ongoing. Alterations to KEAP1 architecture and NRF2 contact residues support the hypothesis that superbinders modify KEAP1 structure resulting in impaired KEAP1 conformational cycling.

The identification of p62-dependent clusters was an unexpected phenotype observed with the superbinders. These clusters are not specific to superbinders as they were also observed with KEAP1 WT in the H1299 cells; however, superbinder mutations increased the accumulation of these clusters regardless of the cell type studied. The exact nature of these clusters is intriguing given the unique shape and ordering of proteins within the clusters. Confocal imaging established that the clusters are circular and contain KEAP1 in the center, surrounded by rings of p62, p62 pS351, poly-Ub, and in some instances NRF2. Identification of the stoichiometric ratios of these proteins within the cluster would help to determine whether the clusters contain multimeric units of KEAP1-NRF2-p62 complexes. Biochemical isolation of the clusters would be informative for the identification of additional proteins as well as post-translational modifications of proteins within the clusters.

Given the dependence on p62 for cluster formation, it is possible that these clusters may represent an intermediate between proteasomal and autophagic degradation pathways (101, 111-113). In fact, dynamic crosstalk between proteasomal and autophagic degradation pathways is critical for cellular homeostasis, and proteotoxic stress has been shown to lead to increased autophagic flux (101, 111, 112). A recent report found that KEAP1/CUL3 ubiquitylates p62 on its ubiquitin-associated domain (UBA) and that this interaction is crucial for the recruitment of p62 into the autophagosome (114, 115). Conformationally strained KEAP1 due to superbinder mutations may result in decreased or absent p62 ubiquitylation, preventing tethering to LC3 for autophagosome formation and maturation

KEAP1 superbinder mutations are known to increase NRF2 transcriptional activity, which has been shown to be protective against chemotherapeutic insults (22, 30-32, 35, 105-107). Surprisingly, of the three cytotoxic drugs tested, KEAP1 superbinder mutations only conferred protection against bleomycin treatment, which induces DNA damage in cells

through upregulating oxidative stress. This result was initially perplexing given the extensive body of literature demonstrating cytoprotective effects from elevated NRF2 transcriptional activity (22, 30-32, 35, 105-107); however, this finding raises several interesting points for discussion. First, mutations in KEAP1 result in a spectrum of phenotypes: functionally silent/WT, hypomorphs, and functionally dead (38). Approximately 25% of the KEAP1 LUSC mutations identified from the TCGA studies behaved comparably to KEAP1 WT (38). These silent mutations result in high levels of KEAP1 conformational cycling and low levels of nuclear NRF2 and NRF2 transcriptional activity (Fig. 9C-I). Hypomorphic mutations constitute 50% of KEAP1 LUSC mutations and include the superbinder mutations. These hypomorph mutations result in impaired NRF2 degradation and may therefore impair KEAP1 cycling. As such, these mutations result in moderate levels of nuclear NRF2 and NRF2 transcriptional activity (Fig. 9C-II). Functionally dead mutations represent 25% of LUSC KEAP1 mutations. These KEAP1 mutants are unable to bind NRF2 and do not cycle; consequently, they exhibit elevated levels of both cytosolic and nuclear NRF2 with maximal NRF2 transcriptional activity (Fig. 9C-III). Second, genes that are transcriptionally upregulated in the presence of superbinders may not be the same target genes as those upregulated in the presence of functionally dead mutations. Identification of these differentially expressed genes may provide further mechanistic understanding of superbinder mutations as well as reveal novel targets for clinical intervention.

In summary, through careful biochemical examination, we have defined novel interactions for KEAP1 with VCP, PSMD2, and PSMD4. Furthermore, we determined that KEAP1 superbinder mutations exclusively impact NRF2 association, appear to stabilize KEAP1 tertiary structure, and form p62-dependent spherical clusters containing a KEAP1-positive core surrounded by unmodified and phosphorylated p62, poly-Ub, and NRF2. These superbinder mutants are uniquely resistant to bleomycin treatment. These studies

reveal molecular insights into KEAP1 regulation and subcellular localization and suggest potential relationships between KEAP1 mutation function and KEAP1 conformational cycling.

Supplemental Tables

1. Curated list of *NFE2L2* mutations downloaded from CBioPortal.
2. Curated list of *KEAP1* mutations downloaded from CBioPortal.
3. Determination of NRF2 Shannon entropy from PROMALS alignment.
4. Determination of KEAP1 Shannon entropy from PROMALS alignment.

Authors' Contributions

Conceptualization: EWC and MBM

Experimental Design: EWC, PFS, EMC, DG, and MBM.

Shannon entropy analysis: JSH and BK

Cell imaging studies: PFS

Mass spectrometry studies: EWC and DG

Data analysis: EWC, DG, PFS, and MBM

DMD simulation studies: DDM and NVD

Writing: EWC and MBM

Supervision: MBM

Funding support: EWC and MBM

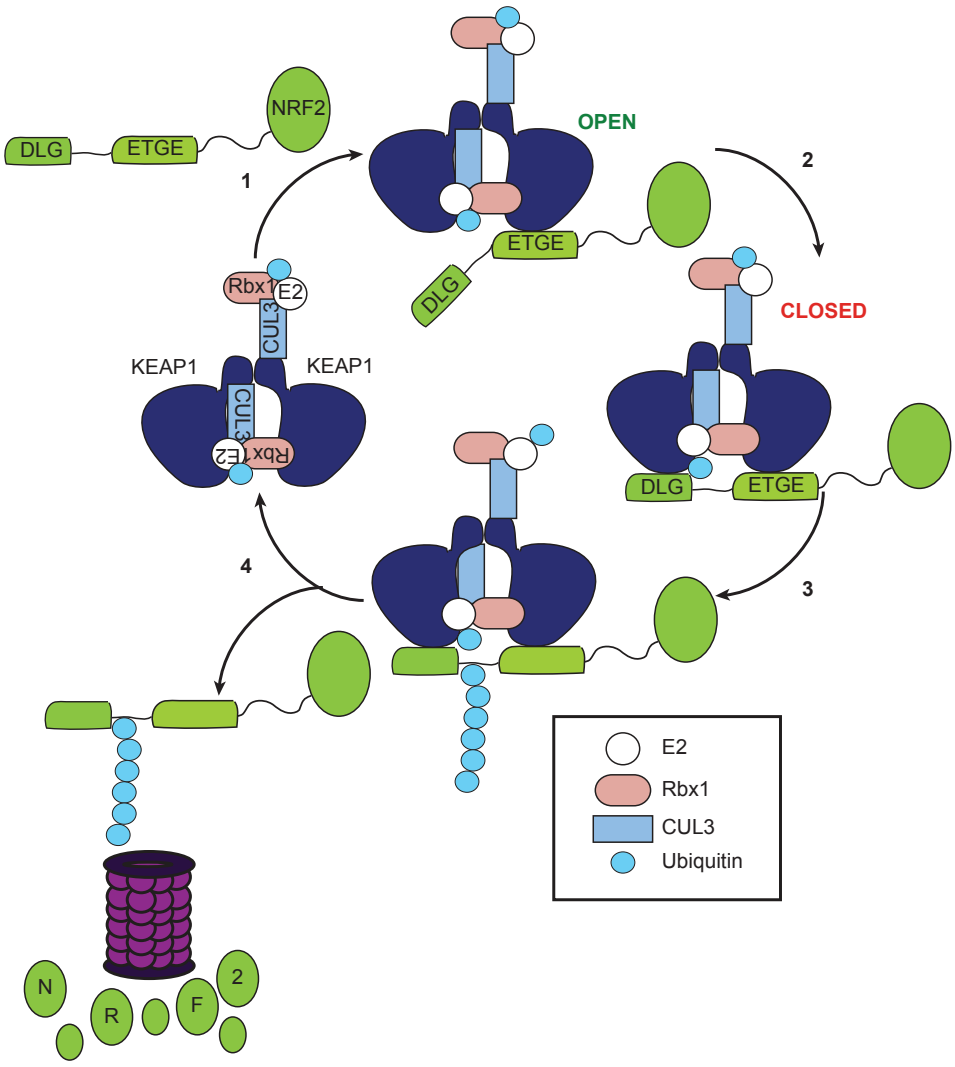

Figure 3.1. KEAP1 cycles between open and closed conformations.
Cartoon schematic of KEAP1 conformational cycling (15). 1) Dimeric KEAP1 is associated with the E3 ubiquitin ligase CUL3/RBX1 and is primed to scavenge newly synthesized NRF2. As NRF2 levels increase, KEAP1 binds the ETGE motif in the Neh2 domain of NRF2 to generate the open conformation. 2) Sequential binding of the DLG motif of NRF2 generates the closed conformation of the KEAP1-NRF2 complex. 3) The closed conformation is favorable for NRF2 ubiquitylation by CUL3. 4) Ubiquitylated NRF2 is released from the complex and subsequently degraded by the proteasome, allowing cycling to proceed again.

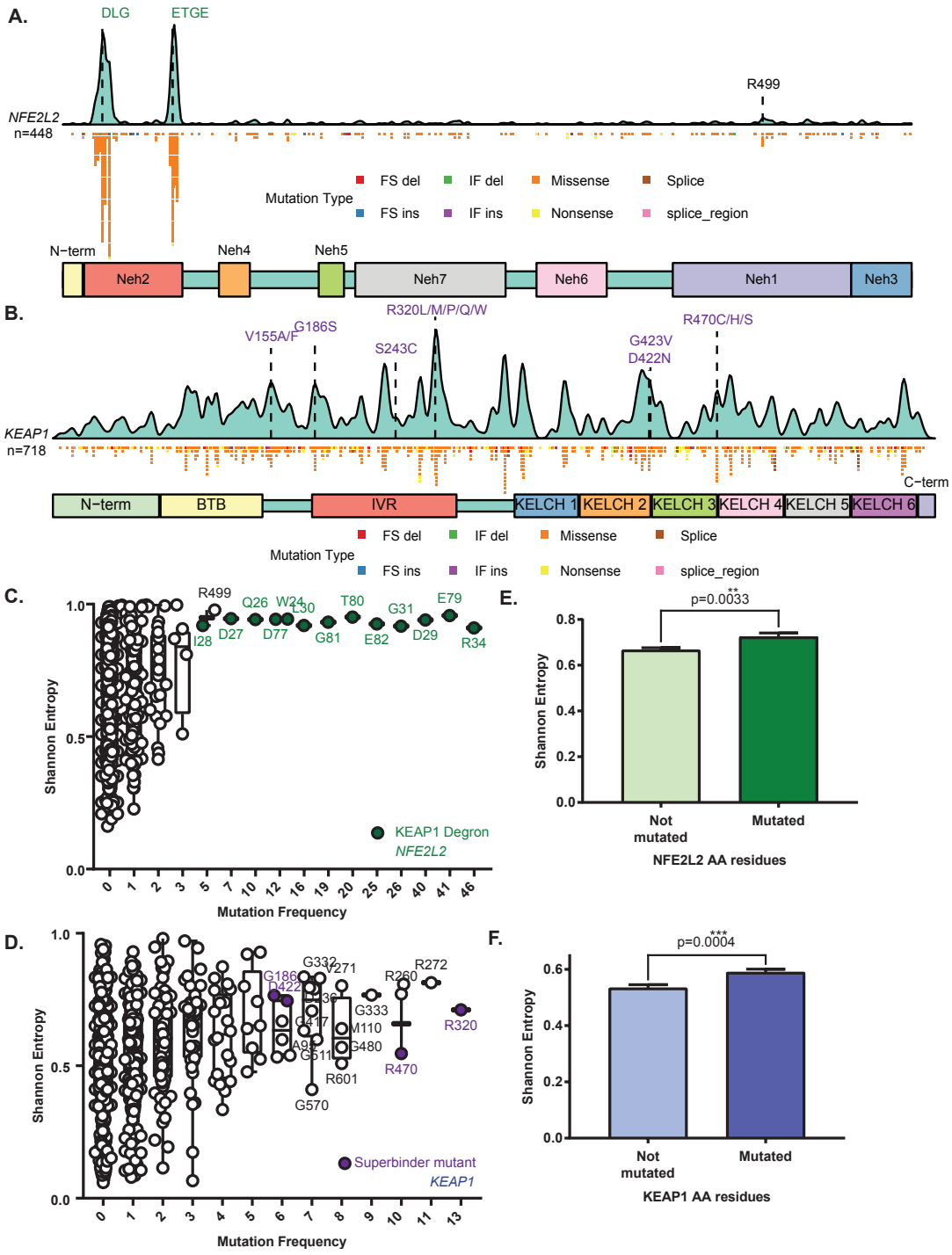
A.
DLG
ETGE
R499
NFE2L2
n=448
Mutation Type
FS del
IF del
Missense
Splice
FS ins
IF ins
Nonsense
splice_region
N−term
Neh2
Neh4
Neh5
Neh7
Neh6
Neh1
Neh3
B.
R320L/M/P/Q/W
V155A/F
G186S
S243C
G423V
D422N
R470C/H/S
KEAP1
n=718
C−term
N−term
BTB
IVR
KELCH 1
KELCH 2
KELCH 3
KELCH 4
KELCH 5
KELCH 6
C.
R499
Q26
W24
L30
T80
G31
E79
I28
D27
D77
G81
E82
D29
R34
Shannon Entropy
KEAP1 Degron
NFE2L2
Mutation Frequency
D.
G332
V271
R272
R260
G186
D422
G333
M110
G480
R320
R470
R601
G570
Superbinder mutant
KEAP1
Shannon Entropy
Mutation Frequency
E.
p=0.0033
Shannon Entropy
Not mutated
Mutated
NFE2L2 AA residues
F.
p=0.0004
Shannon Entropy
Not mutated
Mutated
KEAP1 AA residues

Figure 3.2. Defining the mutational landscape of NRF2 and KEAP1.
A. Kernel density estimation (KDE) of 448 NRF2 somatic mutations demonstrates focal enrichment of mutations at the DLG and ETGE motifs, which are required for KEAP1 association. 14 patients exhibited in-frame deletions across the DLG and/or ETGE; five patients had *NFE2L2* intragenic fusion events, and one patient had a *ZNF385B-NFE2L2* fusion. Data from these patients were not included in the KDE analysis. Data were downloaded from cBioPortal and represent *NFE2L2* mutations across 59 studies investigating 37 different cancer types (Table S.3.1) (37).
B. KDE of 718 KEAP1 somatic mutations identified in patient samples reveals elevated mutational frequencies at superbinder residues R320 and R470. Data were downloaded from cBioPortal and represent *KEAP1* mutations across 68 studies investigating 33 different cancer types (Table S.3.2) (37).
C. Plot of NRF2 mutational frequency versus Shannon Entropy. Shannon entropy was determined using PROMALS alignment, and mutational frequencies per residue were determined from cBioPortal data (Table S.3.3).
D. Comparison of Shannon entropy values for all non-mutated residues in NRF2 (n=459) versus mutated residues (n=146). Error bars represent the standard error of the mean (SEM). The difference is statistically significant at p=0.0033 using an unpaired t-test.
E. Plot of KEAP1 mutational frequency versus Shannon Entropy. Data were analyzed as in C (Table S.3.4).
F. Comparison of Shannon entropy values for all non-mutated residues (n=306) in KEAP1 versus mutated residues (n=318). Error bars represent the standard error of the means (SEM). The difference is statistically significant at p=0.0004 using an unpaired t-test.

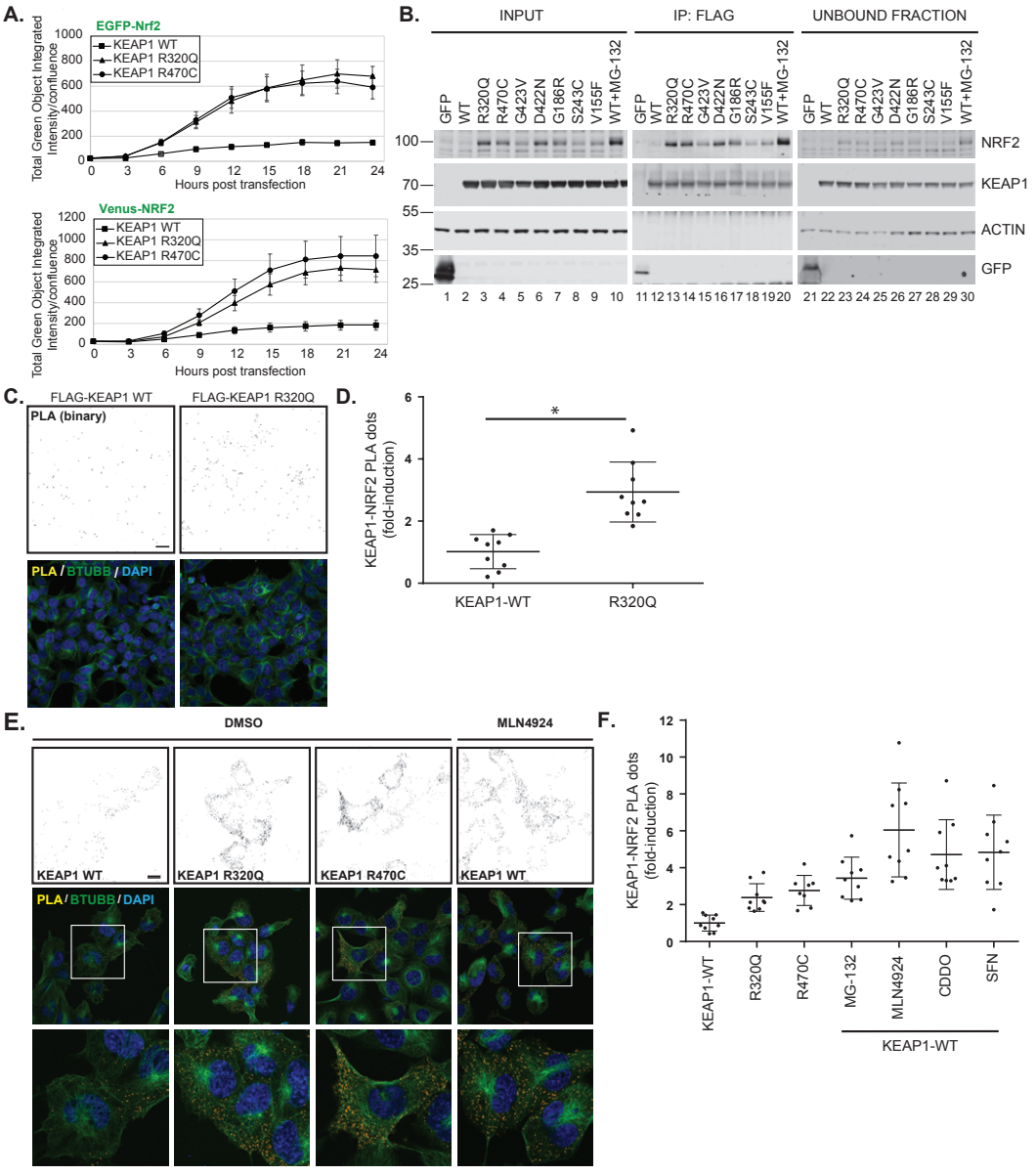
A.
EGFP-Nrf2
KEAP1 WT
KEAP1 R320Q
KEAP1 R470C
Total Green Object Integrated Intensity/confluence
Hours post transfection
Venus-NRF2
B.
INPUT
IP: FLAG
UNBOUND FRACTION
GFP
WT
R320Q
R470C
G423V
D422N
G186R
S243C
V155F
WT+MG-132
NRF2
KEAP1
ACTIN
GFP
C.
FLAG-KEAP1 WT
FLAG-KEAP1 R320Q
PLA (binary)
PLA / BTUBB / DAPI
D.
KEAP1-NRF2 PLA dots (fold-induction)
KEAP1-WT
R320Q
E.
DMSO
MLN4924
KEAP1 WT
KEAP1 R320Q
KEAP1 R470C
KEAP1 WT
PLA / BTUBB / DAPI
F.
KEAP1-NRF2 PLA dots (fold-induction)
KEAP1-WT
R320Q
R470C
MG-132
MLN4924
CDDO
SFN
KEAP1-WT

Figure 3.3. KEAP1 superbinder mutants stabilize NRF2 and increase KEAP1-NRF2 association.
A. HEK 293T/17 cells were co-transfected with FLAG-KEAP1 WT, R320Q, or R470C and either EGFP-Nrf2 or Venus-NRF2 and immediately subjected to image acquisition using the IncuCyteTM Zoom. GFP and phase images were acquired every hr at 20x with four fields/well. Data were plotted for every three hr, and total green object integrated intensity values were normalized by percentage confluence. Each graph represents the average of three biological replicates, with four technical replicates per condition for each experiment. Error bars represent standard errors of triplicates.
B. IP/W.blot of HEK 293T/17 transfected with indicated FLAG-KEAP1 constructs. 18 hours post-transfection, cells were treated with DMSO or 10 μM MG-132 for six hr prior to harvest. Data are representative of a single experiment performed in biological triplicate.
C. HEK 293T/17 cells stably expressing FLAG-KEAP1 WT or R320Q were subjected to PLA using FLAG and NRF2 antibodies for detection of endogenous NRF2 interactions (yellow). Images represent maximum intensity projections of Z-stacks acquired using a confocal microscope. For clarity, both color and black-and-white images of the PLA dots are provided. Nuclei were stained with DAPI (blue), and microtubules were counterstained with anti-Tubulin (green). Scale bar = 20 μm.
D. Fold induction relative to WT of KEAP1-NRF2 interaction in cells expressing R320Q. PLA dots were quantified and normalized by cell number prior to calculation of fold induction. Data are presented as means ± SDM. *$p < 0.001$. Data are representative of a single experiment performed in biological triplicate.
E. H1299 cells were transfected with FLAG-KEAP1 WT, R320Q, or R470C. The following day, cells were treated with either DMSO (control) or a panel of NRF2 inducers: 10 μM MG-132, 5 μM MLN4924, 375 nM CDDO, 50 μM tBHQ, or 20 μM SFN for six hours. Cells were then fixed and subjected to PLA using FLAG and NRF2 antibodies for detection of KEAP1 interactions with endogenous NRF2 (yellow). Images represent a single optical slice acquired using a confocal microscope as in C. Scale bar = 20 μm.
F. Fold induction relative to WT of KEAP1-NRF2 interaction in cells expressing untreated WT, R320Q, R470C, or NRF2 inducer-treated WT. PLA dots were quantified and normalized by cell number prior to calculation of fold induction. Data are presented as means ± SDM. *$p < 0.001$. Data are representative of a single experiment performed in biological triplicate.

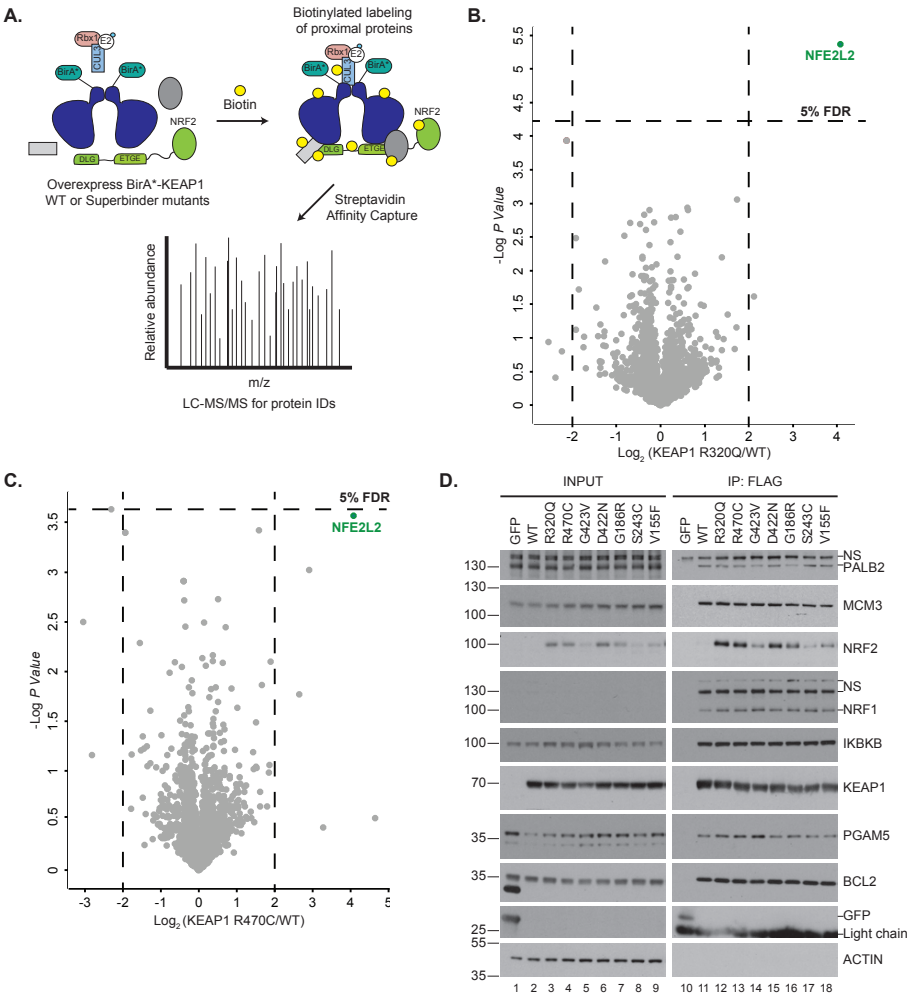

Figure 3.4. **NRF2 is the only KEAP1 substrate to exhibit a superbinder phenotype.**
A. Cartoon schematic of BioID MS approach. N-terminally tagged BirA*-KEAP1 WT, -R320Q, or -R470C constructs were stably overexpressed in HEK 293T/17 cells. Addition of exogenous biotin enabled the biotinylation of proximally associated proteins that were affinity captured using streptavidin. Bound complexes were subjected to LC-MS/MS for protein identification and analysis.
B. Volcano plot of BirA*-KEAP1 R320Q versus BirA*-KEAP1 WT. Experiments were performed in biological triplicate using HEK 293T/17 cells stably expressing BirA*-KEAP1 WT or R320Q and treated with 50 μM biotin for 24. Biotinylated proteins were affinity purified using streptavidin, and the bound complexes were subjected to LC-MS/MS. Dashed vertical lines indicate a 2-fold change cutoff. The horizontal dashed line indicates a 5% FDR threshold determined using the Benjamini-Hochberg procedure. P-values were determined using the two-tailed t-test.
C. Volcano plot of BirA*-KEAP1 R470C versus BirA*-KEAP1 WT. Experiments were performed and analyzed as described in B.
D. IP/W.blot of HEK 293T/17 cells transiently transfected with the indicated FLAG-KEAP1 constructs. FLAG-KEAP1 complexes were immunopurified and probed for endogenous substrate proteins as indicated. Data are representative of a single experiment performed in biological triplicate.

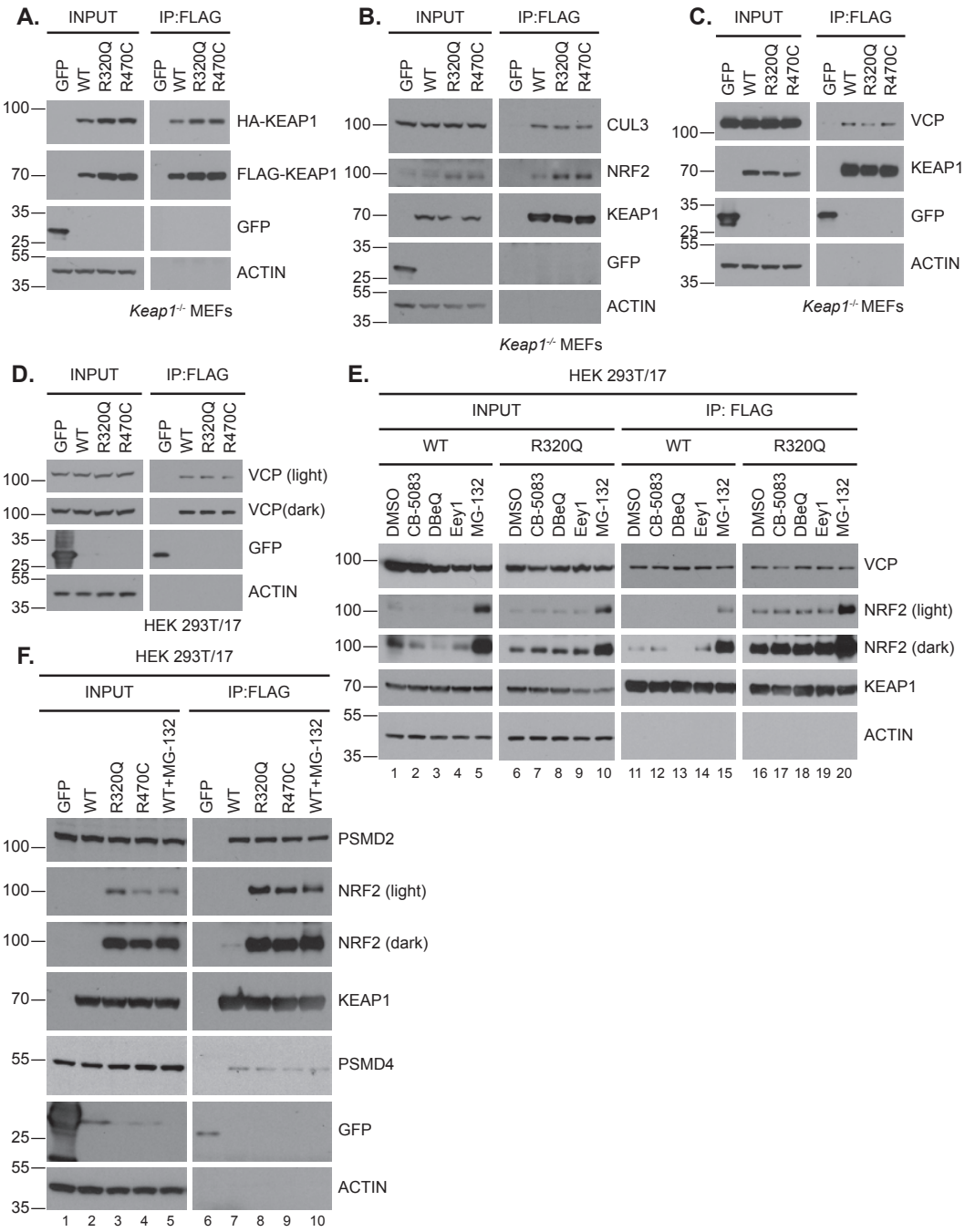
A.
INPUT
IP:FLAG
GFP
WT
R320Q
R470C
HA-KEAP1
FLAG-KEAP1
GFP
ACTIN
Keap1-/- MEFs
B.
CUL3
NRF2
KEAP1
C.
VCP
D.
VCP (light)
VCP(dark)
HEK 293T/17
E.
HEK 293T/17
IP: FLAG
DMSO
CB-5083
DBeQ
Eey1
MG-132
NRF2 (light)
NRF2 (dark)
F.
WT+MG-132
PSMD2
PSMD4

Figure 3.5. KEAP1 superbinders R320Q and R470C exhibit similar biochemical interactions to KEAP1 WT.
A. IP/W.blot of *Keap1*$^{-/-}$ MEFs transiently co-transfected with the indicated FLAG-KEAP1 and SBPHA-KEAP1 constructs. FLAG-KEAP1 complexes were immunopurified and probed for HA-KEAP1 to determine homodizeration. Data are representative of a single experiment performed in biological triplicate.
B. IP/W.blot of *Keap1*$^{-/-}$ MEFs transiently transfected with the indicated FLAG-KEAP1 constructs. FLAG-KEAP1 complexes were immunopurified and probed for association with endogenous CUL3. Data are representative of a single experiment performed in biological triplicate.
C-D. IP/W.blot of *Keap1*$^{-/-}$ MEFs or HEK 293T/17 cells transiently transfected with the indicated FLAG-KEAP1 constructs. FLAG-KEAP1 complexes were immunopurified and probed for association with endogenous VCP. Data are representative of a single experiment performed in biological triplicate.
E. IP/W.blot of HEK 293T/17 cells transiently transfected with the indicated FLAG-KEAP1 constructs. Cells were treated with the following inhibitors: 1 μM CB-5083, 10 μM DBeQ, 10 μM Eey1, or 10 μM MG-132 for six. Data are representative of a single experiment performed in biological duplicate.
F. IP/W. blot of HEK 293T/17 cells transiently transfected with the indicated FLAG-KEAP1 constructs. Cells were treated with 10 μM MG-132 for six hours. FLAG-KEAP1 complexes were immunopurified and probed for association with ubiquitin receptors. Data are representative of a single experiment performed in biological triplicate.

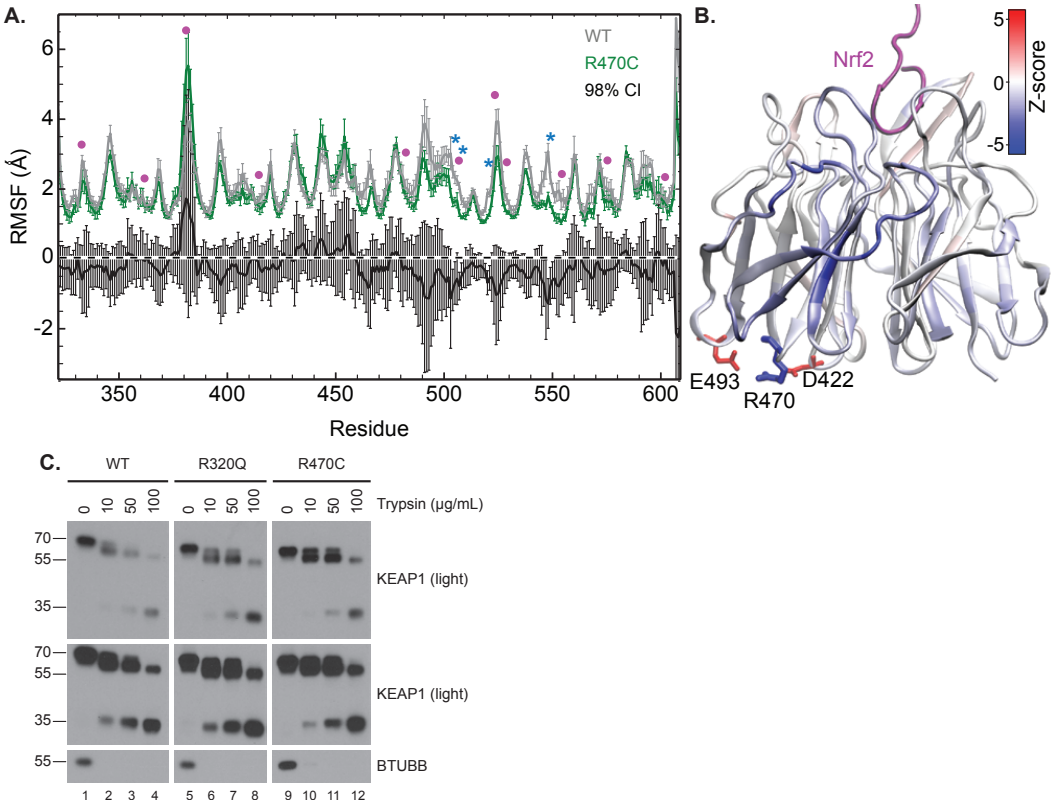

Figure 3.6. KEAP1 superbinder mutants stabilize KEAP1 structure.
A. Plot of the root mean square fluctuations (RMSF) at each residue for KEAP1-WT (grey) and -R470C (green). For each system, the mean and standard error of five replicates, each with one million steps, was plotted. Magenta circles denote the contact points with NRF2 in the crystal structure (PDB ID: 4IFL). The black line corresponds to the difference between the means for R470C and WT simulations, and error bars correspond to the 98% confidence interval (CI) for the difference between the means. Blue stars indicate statistically significant decreases in RMSF ($p<0.02$).
B. Cartoon representation of the KEAP1-NRF2 crystal structure colored by the Z-score for the RMSF difference between KEAP1 mutant and WT. The bound NRF2 peptide is colored magenta. The mutated residue R470 and the potential salt bridge partners are shown as sticks (red: acidic resides, blue: basic residues).
C. W.blot of lysates from imited proteolysis of *Keap1*$^{-/-}$ MEFs transiently transfected with FLAG-KEAP1 constructs and exposed to various concentrations of trypsin for 15 min.

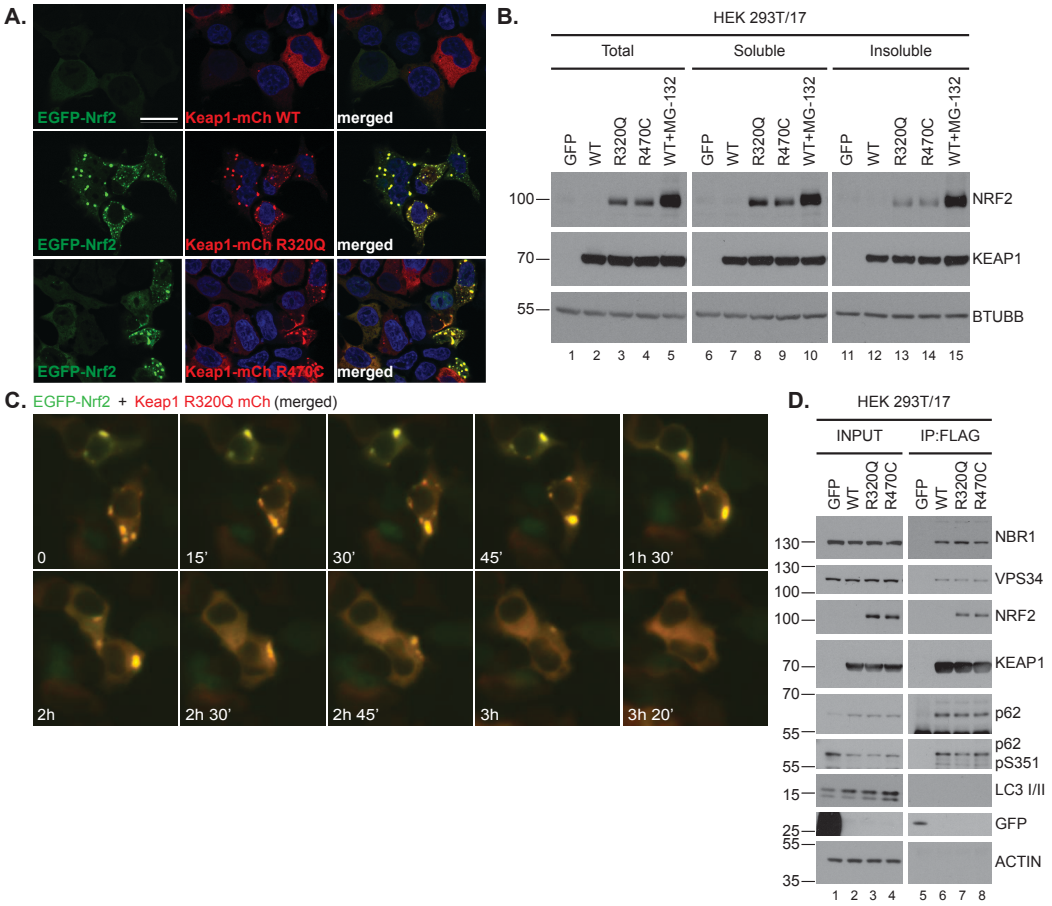

Figure 3.7. KEAP1 superbinder mutants form insoluble clusters with NRF2 and interact with proteins involved in autophagy.

A. HEK 293T/17 were transiently co-transfected with EGFP-Nrf2 (green) and Keap1-mCh WT, R320Q, or with DAPI to visualize nuclei (blue). Scale bar = 20 μm.

B. Triton X-100 solubility assay of HEK 293T/17 cells transiently transfected with the indicated FLAG-KEAP1 constructs. 16 hours post-transfection, cells were treated with DMSO or 10 μM MG-132 for eight hr. Data shown are representative of a single experiment performed in biological triplicate.

C. Time-lapse clearance of HEK 293T/17 co-transfected with EGFP-Nrf2 (green) and Keap1-R320Q mCh (red). Image acquisition was started 24-hr post-transfection, and images were acquired every four min. Scale bar = 20 μm.

D. IP/W.blot of HEK 293T/17 cells transfected with the indicated FLAG-KEAP1 constructs. FLAG-KEAP1 complexes were immunopurified and probed for the indicated proteins. Data shown are representative of a single experiment performed in biological triplicate.

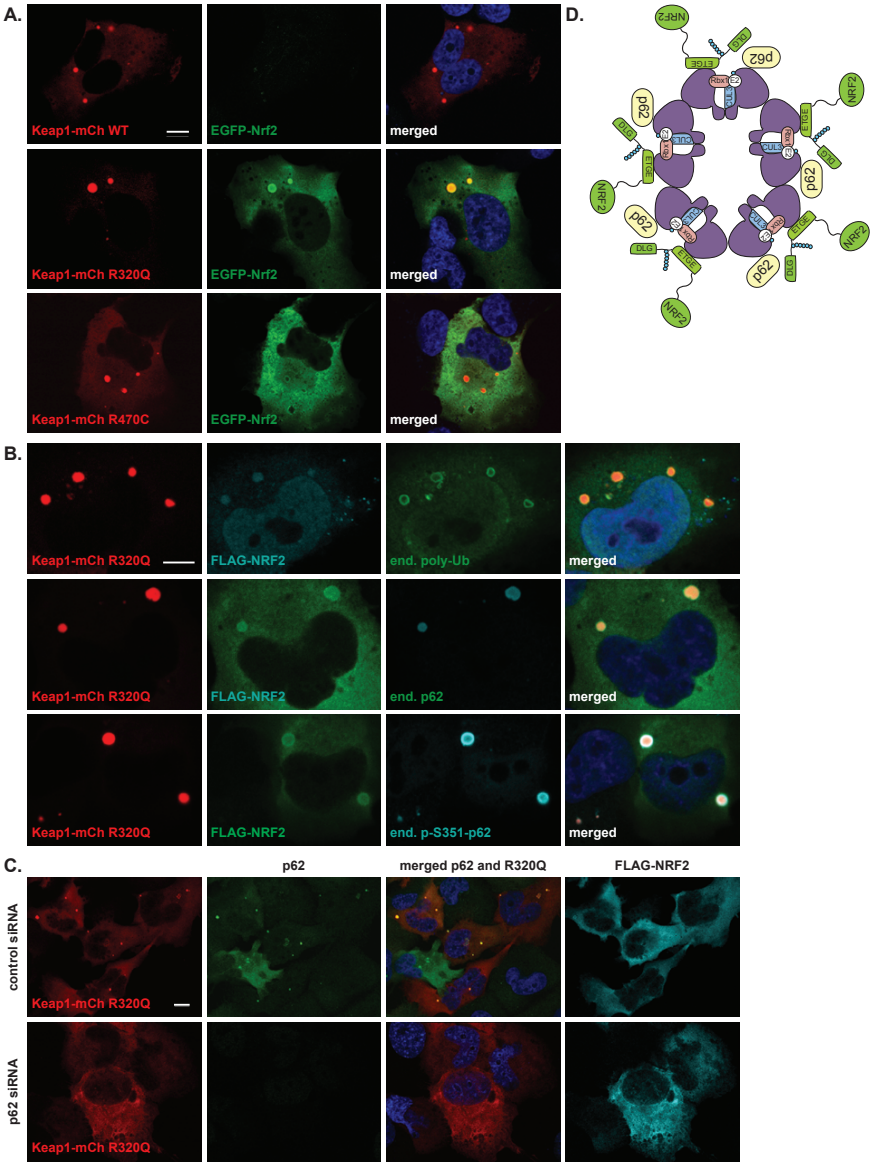

Figure 3.8. KEAP1- and NRF2-positive clusters are positive for endogenous p62 and require p62 to form.

A. H1299 cells were co-transfected with Keap1-mCh WT, R320Q, or R470C (red), and EGFP-NRF2 (green). Nuclei were stained with DAPI (blue). Scale bar = 10 μm, confocal images.

B. H1299 cells were co-transfected with Keap1-mCh R320Q (red) and FLAG-NRF2 (green or cyan) and stained for endogenous p62 and p62 pS351. Nuclei were stained with DAPI (blue). Scale bar = 10 μm, confocal images.

C. H1299 cells were transfected with either control or p62 siRNA followed by co-transfection of Keap1-mCh R320Q (red) and FLAG-NRF2 (cyan).
Transfected cells were stained for endogenous p62 (green). Scale bar = 20 μM, confocal images Nuclei were stained with DAPI (blue).

D. Cartoon schematic of p62-dependent clusters containing KEAP1, NRF2, p62, and polyUb.

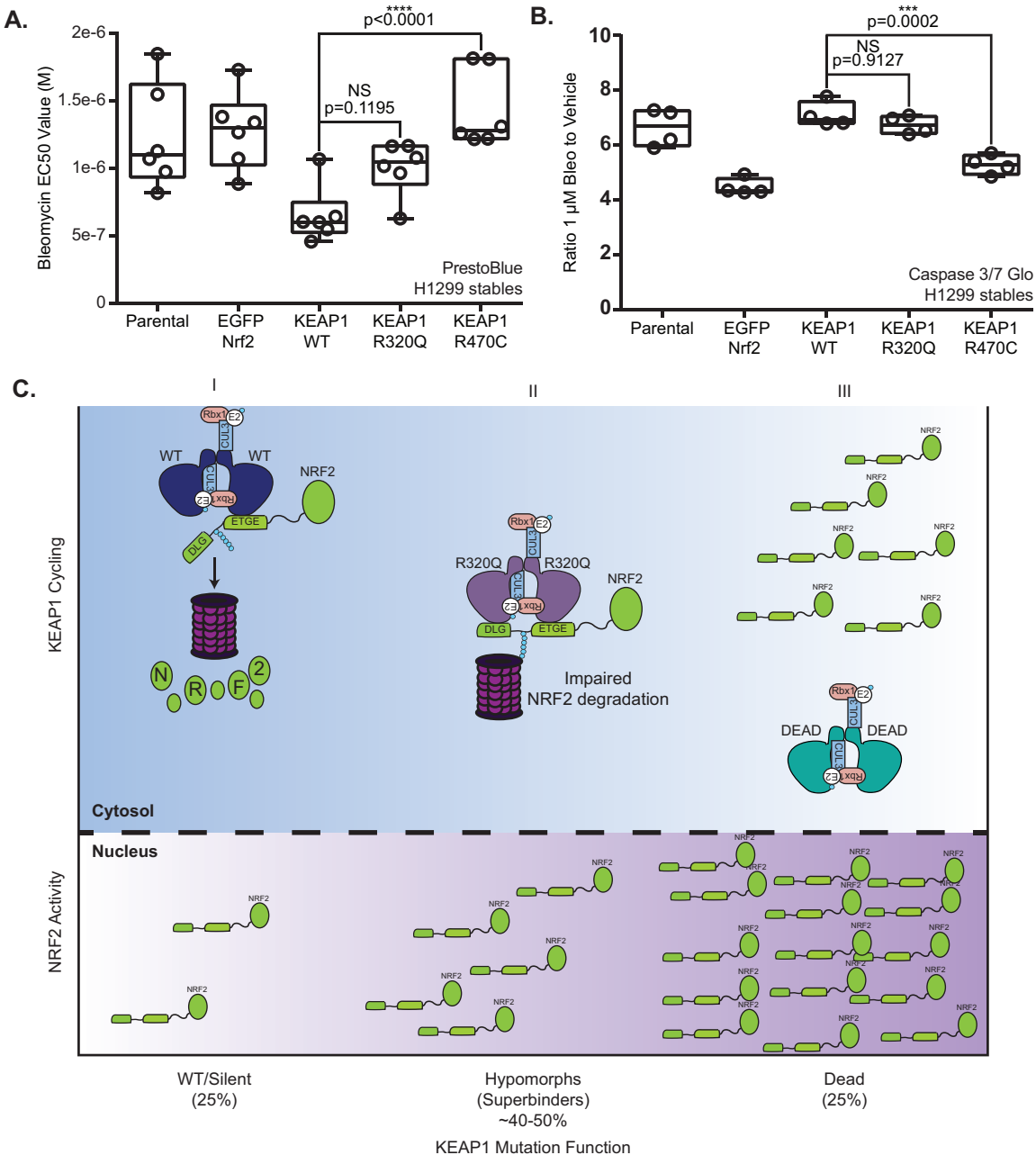
A.
Bleomycin EC50 Value (M)
2e-6
1.5e-6
1e-6
5e-7
0
****
p<0.0001
NS
p=0.1195
PrestoBlue
H1299 stables
Parental
EGFP Nrf2
KEAP1 WT
KEAP1 R320Q
KEAP1 R470C
B.
Ratio 1 µM Bleo to Vehicle
10
8
6
4
2
0
***
p=0.0002
NS
p=0.9127
Caspase 3/7 Glo
H1299 stables
Parental
EGFP Nrf2
KEAP1 WT
KEAP1 R320Q
KEAP1 R470C
C.
I
II
III
KEAP1 Cycling
NRF2 Activity
WT
WT
NRF2
ETGE
DLG
Rbx1
E2
CUL3
R320Q
R320Q
Impaired
NRF2 degradation
DEAD
DEAD
Cytosol
Nucleus
WT/Silent
(25%)
Hypomorphs
(Superbinders)
~40-50%
Dead
(25%)
KEAP1 Mutation Function

Figure 3.9. **Potential genotype-phenotype correlations of KEAP1 superbinder mutants.**
A. EC50 values of H1299 cells stably expressing indicated constructs and treated with bleomycin for 72 hr. PrestoBlue measurements were plotted and fit to determine EC50 values. Each point represents the mean of technical quadruplicates performed in biological triplicate by two independent researchers. Error bars represent the standard error of the means. P-values were determined using a one-way ANOVA with a Tukey's multiple comparison test.
B. H1299 cells stably expressing indicated constructs were treated with 1 μM bleomycin for 72 hours. Caspase 3/7 Glo assay was used to measure levels of apoptosis. Each point represents the mean from a single experiment performed in technical quadruplicate. Error bars represent the SEM. P-values were determined using a one-way ANOVA with a Tukey's multiple comparison test.
C. Proposed model correlating KEAP1 cycling dynamics with NRF2 activity and KEAP1 mutation function. I) Passenger or silent mutations are estimated to represent 25% of the mutations identified in LUSC. Functionally silent mutations result in low levels of nuclear NRF2 and maintain normal rates of KEAP1 conformational cycling. II) KEAP1 hypomorphs are estimated to represent 40-50% of LUSC mutations. We hypothesize that the superbinder mutations result in impaired or delayed cycling and form p62-dependent clusters that may represent intermediate aggregates between proteasomal and autophagic degradation. Consequently, KEAP1 hypomorphs exhibit elevated but not maximal levels of nuclear NRF2. III) Functionally dead mutations are unable to bind NRF2 and as such do not cycle; consequently, they exhibit maximal levels of nuclear NRF2 activity and provide protection against DNA-damaging agents.

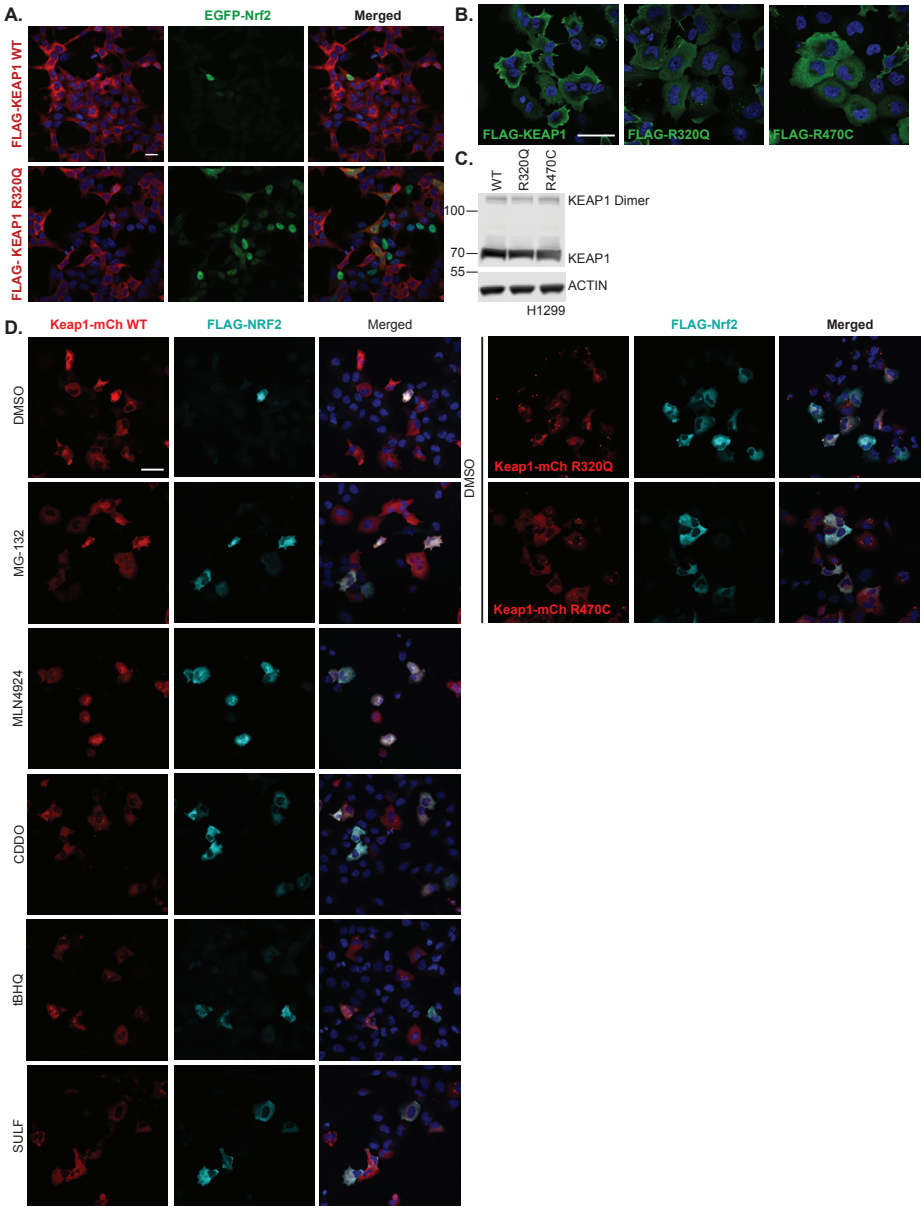

Figure 3.S.1. Supplemental data for Figure 3.2.
A. HEK 293T/17 cells stably expressing FLAG-KEAP1 WT or R320Q were transfected with EGFP-Nrf2 (mouse) or Venus-NRF2 (human). FLAG antibody immunostaining was performed to detect KEAP1 WT or R320Q. Images represent maximum intensity projections of Z-stacks. Nuclei were stained with DAPI (blue). Scale bar = 20 μm.
B-C. H1299 cells were transfected with FLAG-KEAP1 WT, R320Q, or R470C and subjected to IF (B) or W.blot (C) analyses with FLAG antibody. Nuclei were stained with DAPI (blue). Scale bar = 20 μm; confocal images.
D. H1299 cells were co-transfected with FLAG-NRF2 and either Keap1-mCh WT, R320Q, or R70C. The following day, cells were treated with either DMSO (control) or a panel of NRF2 inducers (10 μm MG-132, 5 μm MLN4924, 375 nM CDDO, 50 μm tBHQ, or 20 μmM SULF) for six hr. Fixed cells were stained with FLAG antibody for detection of NRF2 (cyan). Nuclei were stained with DAPI (blue). Scale bar = 50 μm, confocal images.

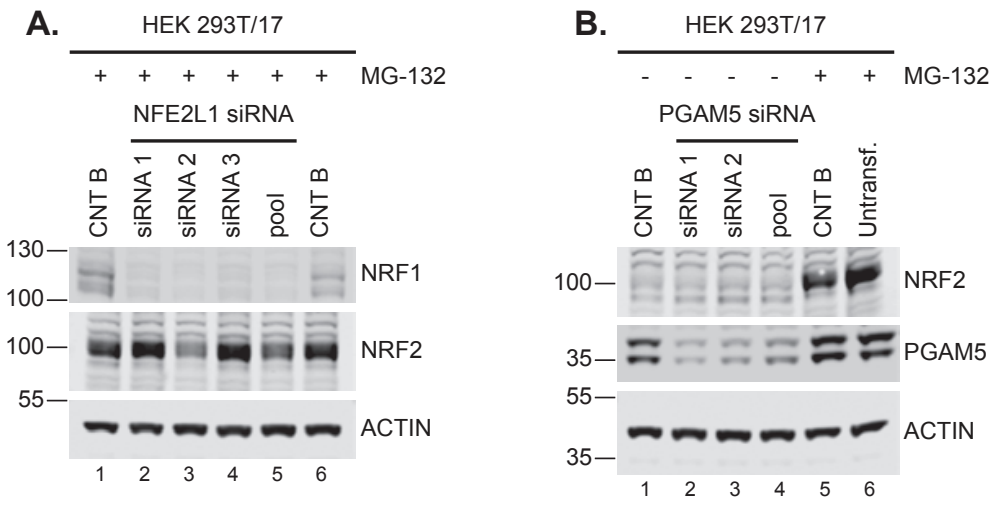

Figure 3.S.2. Validation of antibodies for KEAP1 substrates.
A. Validation of NRF1 siRNAs. HEK 293T/17 were transfected with 10 nM siRNA for 66 hr. Cells were treated with 10 μM MG-132 for six hr, and cleared lysates were analyzed by W.blot for the indicated proteins.
B. Validation of PGAM5 siRNAs. HEK 293T/17 were transfected with 10 nM siRNA and treated with 10 μM MG-132 prior to W. blot analysis as described in B.

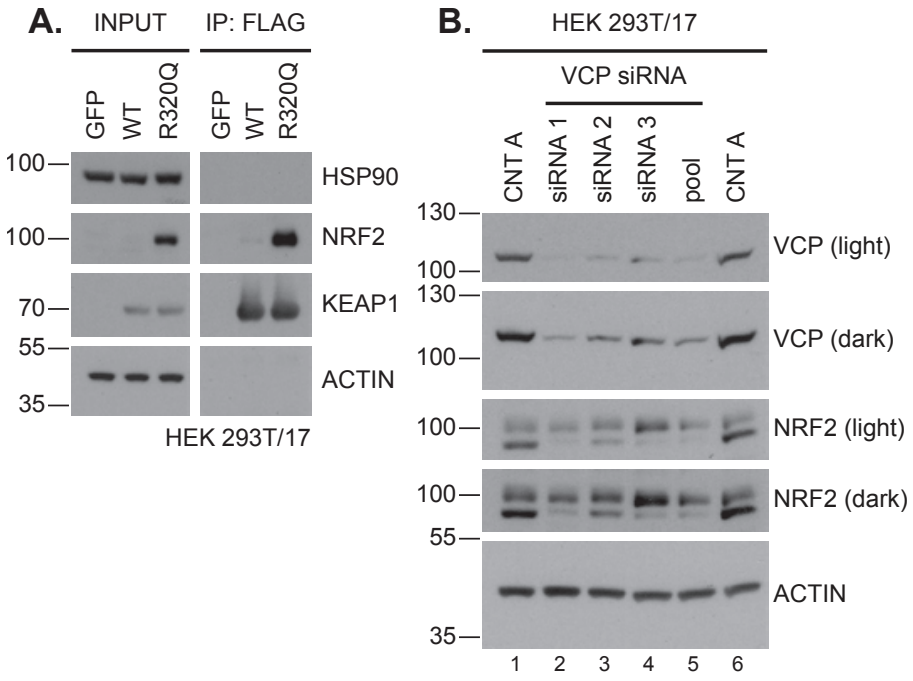

Figure 3.S.3. Supplemental data for Figure 3.5.
A. IP/W.blot of HEK 293T/17 cells transfected with the indicated FLAG-KEAP1 constructs. FLAG-KEAP1 complexes were immunopurified and probed for association with endogenous HSP90. Data are representative of a single experiment performed in biological duplicate.
B. Validation of VCP siRNAs. HEK 293T/17 were transfected with 20 nM siRNA for 72 hr. Cleared lysates were analyzed by W.blot for the indicated proteins.

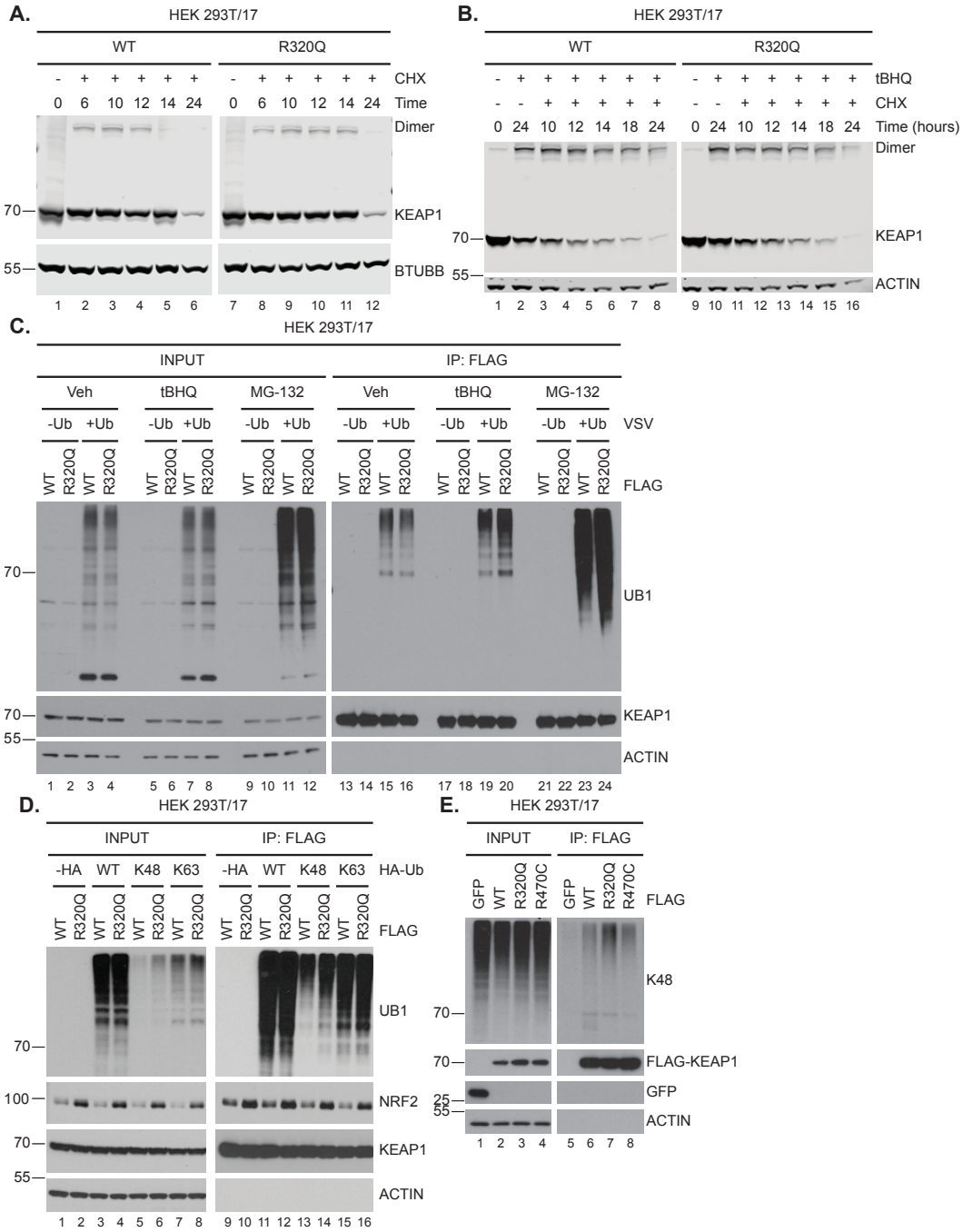
A.
HEK 293T/17
WT
R320Q
CHX
Time
Dimer
KEAP1
BTUBB
70
55
B.
HEK 293T/17
WT
R320Q
tBHQ
CHX
Time (hours)
Dimer
KEAP1
ACTIN
C.
HEK 293T/17
INPUT
IP: FLAG
Veh
tBHQ
MG-132
-Ub
+Ub
VSV
FLAG
UB1
KEAP1
ACTIN
D.
HEK 293T/17
INPUT
IP: FLAG
-HA
WT
K48
K63
HA-Ub
FLAG
UB1
NRF2
KEAP1
ACTIN
100
E.
HEK 293T/17
INPUT
IP: FLAG
GFP
WT
R320Q
R470C
FLAG
K48
FLAG-KEAP1
GFP
ACTIN
25

Figure 3.S.4. KEAP1 superbinder mutants do not dramatically alter KEAP1 half-life or ubiquitylation under basal or induced conditions.
A. Cycloheximide (CHX) chase of HEK 293T/17 cells stably expressing FLAG-KEAP1 WT or R320Q. Cells were treated with 50 μg/mL CHX for the indicated times. Lysates were analyzed by quantitative W.blot for the indicated proteins. Image shown is representative of a single experiment performed in biological triplicate.
B. Cycloheximide (CHX) chase of HEK 293T/17 cells stably expressing FLAG-KEAP1 WT or R320Q. Cells were treated with 50 μg/mL CHX and 50 μM tBHQ for the indicated times. Lysates were analyzed as in (A). Image shown is representative of a single experiment performed in biological triplicate.
C. HEK 293T/17 cells stably expressing FLAG-KEAP1 WT or R320Q were transiently transfected with VSV-UB1. 18 hr-post transfection, cells were treated with 50 μM tBHQ or 10 μM MG-132 for 2 hr. Immunopurified FLAG-KEAP1 complexes were probed for the indicated proteins.
D. HEK 293T/17 cells stably expressing FLAG-KEAP1 WT or R320Q were transiently transfected with HA-UB1 lysine chain-specific constructs as indicated. Immunopurified FLAG-KEAP1 complexes were probed for the indicated proteins.
E. HEK 293T/17 cells were transfected with FLAG-KEAP1 WT, R320Q, or R470C. 24 hr following transfection, cells were harvested under near-denaturing conditions. FLAG-immunopurified KEAP1 complexes were probed for indicated proteins.

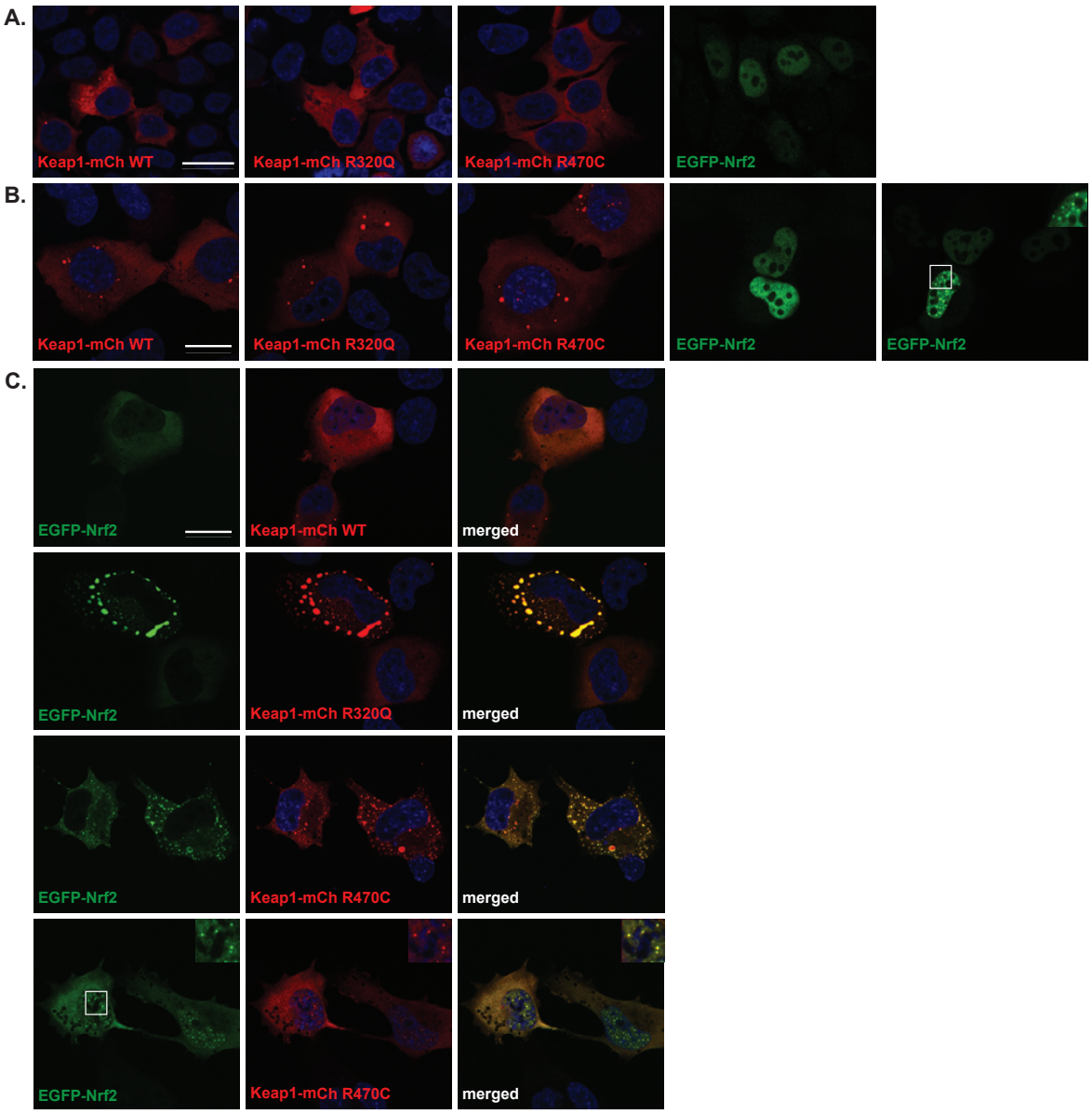

Figure 3.S.5. Supplemental data for Figure 3.7.
A. H1299 cells stably expressing Keap1-mCh WT, R320Q, R470C, or EGFP-Nrf2 were fixed and subjected to IF. Nuclei were stained with DAPI (blue). Scale bar = 20 μm; confocal images.
B. H1299 cells stably expressing Keap1-mCh R470C were transfected with EGFP-Nrf2. Scale bar = 20 μm; confocal images.
C. H1299 cells were co-transfected with EGFP-Nrf2 and Keap1-mCh WT, R320Q, or R470C. Keap1-Nrf2 nuclear foci were also occasionally observed (inset). Nuclei were stained with DAPI (blue). Scale bar = 20 μm; confocal images.

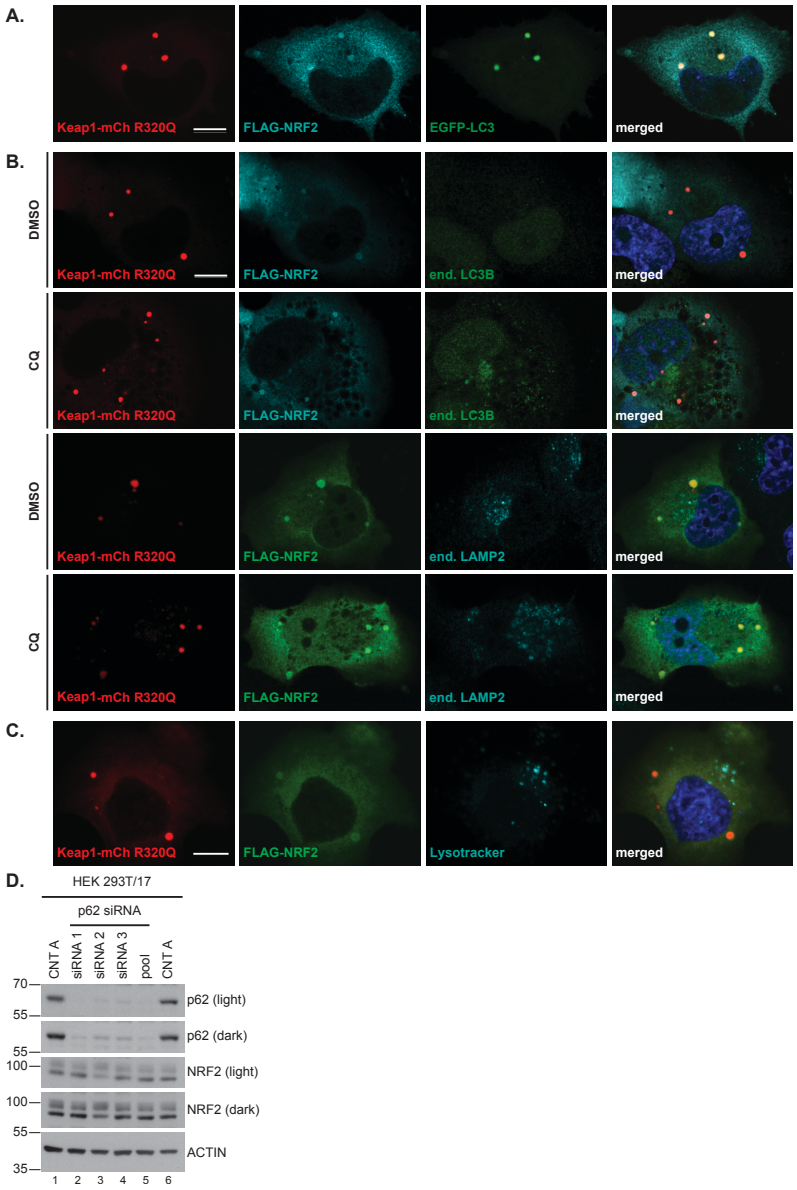

Figure 3.S.6. Supplemental data for Figure 8: KEAP1- and NRF2-positive clusters are positive for endogenous p62, but not for LC3B or LAMP2.

A. H1299 cells were co-transfected with Keap1-mCh R320Q (red), FLAG-NRF2 (cyan), and GFP-LC3 (green) and stained for FLAG. Keap1-positive and NRF2-positive puncta are positive for exogenous EGFP-LC3. Scale bar = 10 μm.

B. H1299 cells were co-transfected with Keap1-mCh R320Q (red) and FLAG-NRF2 (green or cyan), treated with either DMSO or 50 μM chloroquine (CQ) overnight and stained for FLAG-NRF2 (cyan/green), endogenous LC3B (green), or endogenous LAMP2 (cyan). Keap1-positive and NRF2-positive clusters are negative for endogenous LC3B and LAMP2.

C. H1299 cells were co-transfected with Keap1-mCh R320Q (red) and FLAG-NRF2 (green) and stained with FLAG antibody and Lysotracker AlexaFluor647.
Nuclei were stained with DAPI (blue). Scale bar = 10μM, confocal images.

D. Validation of p62 siRNAs. HEK 293T/17 were transfected with 20 nM siRNA for 72 hr. Cleared lysates were analyzed by W.blot for the indicated proteins.

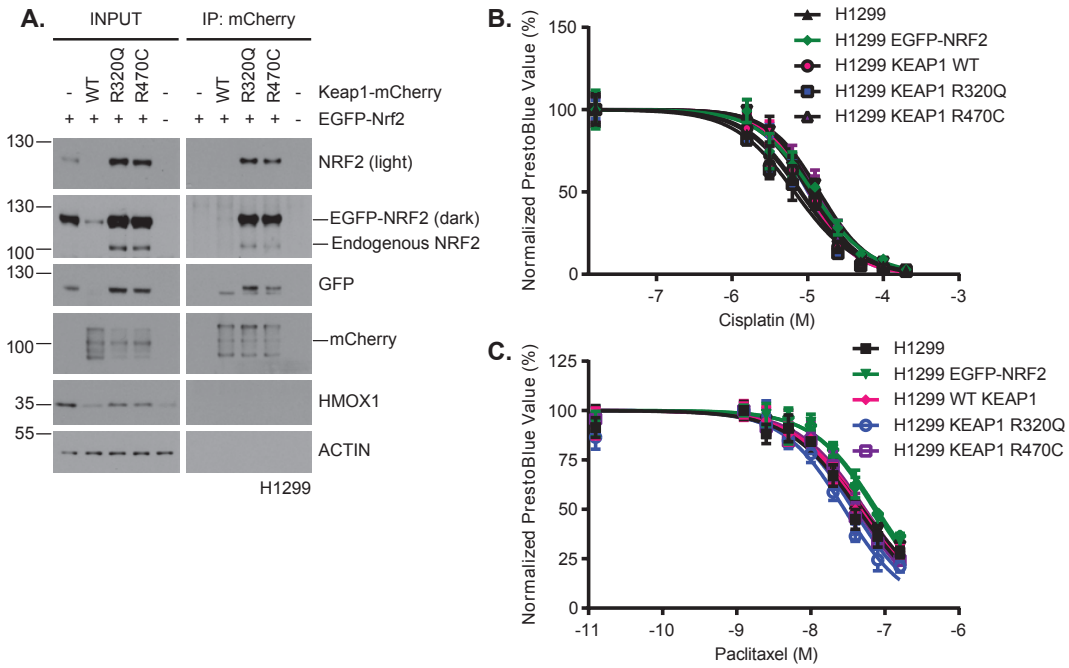

Figure 3.S.7. **Supplemental data for Figure 9.**
A. H1299 cells were co-transfected with Keap1-mCh R320Q and EGFP-Nrf2. Keap1 complexes were immunopurified using mCherry antibody and probed for indicated proteins. **B-C.** Dose-response curves of H1299 cells stably expressing indicated constructs and treated with varying doses of cisplatin (B) or paclitaxel (C) for 72 hr. PrestoBlue measurements were used as an indicator of cell viability, and measured values were plotted to determine EC50 values. Each point represents the mean of technical quadruplicates performed in biological triplicate by two independent researchers. Error bars represent the standard error of the means.

REFERENCES

1. **Howlader N, Noone AM, Krapcho M, Miller D, Bishop K, Kosary CL, Yu M, Ruhl J, Tatalovich Z, Mariotto A, Lewis DR, Chen HS, Feuer EJ, Cronin KA (eds).** SEER Cancer Statistics Review, 1975-2014, National Cancer Institute. Bethesda, MD, https://seer.cancer.gov/csr/1975_2014/, based on November 2016 SEER data submission, posted to the SEER web site, April 2017.

2. **Herbst RS, Heymach JV, Lippman SM.** 2008. Lung cancer. N Engl J Med **359:**1367-1380.

3. **Alberg AJ, Ford JG, Samet JM, American College of Chest P.** 2007. Epidemiology of lung cancer: ACCP evidence-based clinical practice guidelines (2nd edition). Chest **132:**29S-55S.

4. **Ries LAG YJ, Keel GE, Eisner MP, Lin YD, Horner M-J (editors). .** 2007. SEER Survival Monograph: Cancer Survival Among Adults: U.S. SEER Program, Chapter 9: Cancer of the Lung, 1988-2001, Patient and Tumor Characteristics. National Cancer Institute, SEER Program, NIH Pub No 07-6215.

5. **Cancer Genome Atlas Research N.** 2012. Comprehensive genomic characterization of squamous cell lung cancers. Nature **489:**519-525.

6. **Itoh K, Mimura J, Yamamoto M.** 2010. Discovery of the negative regulator of Nrf2, Keap1: a historical overview. Antioxid Redox Signal **13:**1665-1678.

7. **Cullinan SB, Gordan JD, Jin J, Harper JW, Diehl JA.** 2004. The Keap1-BTB protein is an adaptor that bridges Nrf2 to a Cul3-based E3 ligase: oxidative stress sensing by a Cul3-Keap1 ligase. Mol Cell Biol **24:**8477-8486.

8. **Furukawa M, Xiong Y.** 2005. BTB protein Keap1 targets antioxidant transcription factor Nrf2 for ubiquitination by the Cullin 3-Roc1 ligase. Mol Cell Biol **25:**162-171.

9. **Zhang DD, Lo SC, Cross JV, Templeton DJ, Hannink M.** 2004. Keap1 is a redox-regulated substrate adaptor protein for a Cul3-dependent ubiquitin ligase complex. Mol Cell Biol **24:**10941-10953.

10. **Kobayashi A, Kang MI, Okawa H, Ohtsuji M, Zenke Y, Chiba T, Igarashi K, Yamamoto M.** 2004. Oxidative stress sensor Keap1 functions as an adaptor for Cul3-based E3 ligase to regulate proteasomal degradation of Nrf2. Mol Cell Biol **24:**7130-7139.

11. **Taguchi K, Motohashi H, Yamamoto M.** 2011. Molecular mechanisms of the Keap1-Nrf2 pathway in stress response and cancer evolution. Genes Cells **16:**123-140.

12. **Lo SC, Li X, Henzl MT, Beamer LJ, Hannink M.** 2006. Structure of the Keap1:Nrf2 interface provides mechanistic insight into Nrf2 signaling. EMBO J **25:**3605-3617.

13. **Tong KI, Kobayashi A, Katsuoka F, Yamamoto M.** 2006. Two-site substrate recognition model for the Keap1-Nrf2 system: a hinge and latch mechanism. Biol Chem **387:**1311-1320.

14. **Tong KI, Katoh Y, Kusunoki H, Itoh K, Tanaka T, Yamamoto M.** 2006. Keap1 recruits Neh2 through binding to ETGE and DLG motifs: characterization of the two-site molecular recognition model. Mol Cell Biol **26:**2887-2900.

15. **Baird L, Lleres D, Swift S, Dinkova-Kostova AT.** 2013. Regulatory flexibility in the Nrf2-mediated stress response is conferred by conformational cycling of the Keap1-Nrf2 protein complex. Proc Natl Acad Sci U S A **110:**15259-15264.

16. **Kensler TW, Wakabayashi N, Biswal S.** 2007. Cell survival responses to environmental stresses via the Keap1-Nrf2-ARE pathway. Annu Rev Pharmacol Toxicol **47:**89-116.

17. **Ogura T, Tong KI, Mio K, Maruyama Y, Kurokawa H, Sato C, Yamamoto M.** 2010. Keap1 is a forked-stem dimer structure with two large spheres enclosing the intervening, double glycine repeat, and C-terminal domains. Proc Natl Acad Sci U S A **107:**2842-2847.

18. **Watai Y, Kobayashi A, Nagase H, Mizukami M, McEvoy J, Singer JD, Itoh K, Yamamoto M.** 2007. Subcellular localization and cytoplasmic complex status of endogenous Keap1. Genes Cells **12:**1163-1178.

19. **Zhang DD, Hannink M.** 2003. Distinct cysteine residues in Keap1 are required for Keap1-dependent ubiquitination of Nrf2 and for stabilization of Nrf2 by chemopreventive agents and oxidative stress. Mol Cell Biol **23:**8137-8151.

20. **Nguyen T, Sherratt PJ, Huang HC, Yang CS, Pickett CB.** 2003. Increased protein stability as a mechanism that enhances Nrf2-mediated transcriptional activation of the antioxidant response element. Degradation of Nrf2 by the 26 S proteasome. J Biol Chem **278:**4536-4541.

21. **McMahon M, Itoh K, Yamamoto M, Hayes JD.** 2003. Keap1-dependent proteasomal degradation of transcription factor Nrf2 contributes to the negative regulation of antioxidant response element-driven gene expression. J Biol Chem **278:**21592-21600.

22. **Taguchi K, Yamamoto M.** 2017. The KEAP1-NRF2 System in Cancer. Front Oncol **7:**85.

23. **Iso T, Suzuki T, Baird L, Yamamoto M.** 2016. Absolute Amounts and Status of the Nrf2-Keap1-Cul3 Complex within Cells. Mol Cell Biol **36:**3100-3112.

24. **Baird L, Dinkova-Kostova AT.** 2013. Diffusion dynamics of the Keap1-Cullin3 interaction in single live cells. Biochem Biophys Res Commun **433:**58-65.

25. **Baird L, Swift S, Lleres D, Dinkova-Kostova AT.** 2014. Monitoring Keap1-Nrf2 interactions in single live cells. Biotechnol Adv **32:**1133-1144.

26. **Baird L, Dinkova-Kostova AT.** 2011. The cytoprotective role of the Keap1-Nrf2 pathway. Arch Toxicol **85:**241-272.

27. **Kobayashi M, Yamamoto M.** 2006. Nrf2-Keap1 regulation of cellular defense mechanisms against electrophiles and reactive oxygen species. Adv Enzyme Regul **46:**113-140.

28. **Singh A, Misra V, Thimmulappa RK, Lee H, Ames S, Hoque MO, Herman JG, Baylin SB, Sidransky D, Gabrielson E, Brock MV, Biswal S.** 2006. Dysfunctional KEAP1-NRF2 interaction in non-small-cell lung cancer. PLoS Med **3:**e420.

29. **Sykiotis GP, Bohmann D.** 2010. Stress-activated cap'n'collar transcription factors in aging and human disease. Sci Signal **3:**re3.

30. **Solis LM, Behrens C, Dong W, Suraokar M, Ozburn NC, Moran CA, Corvalan AH, Biswal S, Swisher SG, Bekele BN, Minna JD, Stewart DJ, Wistuba, II.** 2010. Nrf2 and Keap1 abnormalities in non-small cell lung carcinoma and association with clinicopathologic features. Clin Cancer Res **16:**3743-3753.

31. **Wang XJ, Sun Z, Villeneuve NF, Zhang S, Zhao F, Li Y, Chen W, Yi X, Zheng W, Wondrak GT, Wong PK, Zhang DD.** 2008. Nrf2 enhances resistance of cancer cells to chemotherapeutic drugs, the dark side of Nrf2. Carcinogenesis **29:**1235-1243.

32. **Ohta T, Iijima K, Miyamoto M, Nakahara I, Tanaka H, Ohtsuji M, Suzuki T, Kobayashi A, Yokota J, Sakiyama T, Shibata T, Yamamoto M, Hirohashi S.** 2008. Loss of Keap1 function activates Nrf2 and provides advantages for lung cancer cell growth. Cancer Res **68:**1303-1309.

33. **Satoh H, Moriguchi T, Takai J, Ebina M, Yamamoto M.** 2013. Nrf2 prevents initiation but accelerates progression through the Kras signaling pathway during lung carcinogenesis. Cancer Res **73:**4158-4168.

34. **Lau A, Villeneuve NF, Sun Z, Wong PK, Zhang DD.** 2008. Dual roles of Nrf2 in cancer. Pharmacol Res **58:**262-270.

35. **Homma S, Ishii Y, Morishima Y, Yamadori T, Matsuno Y, Haraguchi N, Kikuchi N, Satoh H, Sakamoto T, Hizawa N, Itoh K, Yamamoto M.** 2009. Nrf2 enhances cell proliferation and resistance to anticancer drugs in human lung cancer. Clin Cancer Res **15:**3423-3432.

36. **Zhang DD.** 2010. The Nrf2-Keap1-ARE signaling pathway: The regulation and dual function of Nrf2 in cancer. Antioxid Redox Signal **13:**1623-1626.

37. **Gao J, Aksoy BA, Dogrusoz U, Dresdner G, Gross B, Sumer SO, Sun Y, Jacobsen A, Sinha R, Larsson E, Cerami E, Sander C, Schultz N.** 2013. Integrative analysis of complex cancer genomics and clinical profiles using the cBioPortal. Sci Signal **6:**pl1.

38. **Hast BE, Cloer EW, Goldfarb D, Li H, Siesser PF, Yan F, Walter V, Zheng N, Hayes DN, Major MB.** 2014. Cancer-derived mutations in KEAP1 impair NRF2 degradation but not ubiquitination. Cancer Res **74:**808-817.

39. **Chen PH, Smith TJ, Wu J, Siesser PF, Bisnett BJ, Khan F, Hogue M, Soderblom E, Tang F, Marks JR, Major MB, Swarts BM, Boyce M, Chi JT.** 2017. Glycosylation of KEAP1 links nutrient sensing to redox stress signaling. EMBO J **36:**2233-2250.

40. **Allalou A, Wahlby C.** 2009. BlobFinder, a tool for fluorescence microscopy image cytometry. Comput Methods Programs Biomed **94:**58-65.

41. **Mulvaney KM, Matson JP, Siesser PF, Tamir TY, Goldfarb D, Jacobs TM, Cloer EW, Harrison JS, Vaziri C, Cook JG, Major MB.** 2016. Identification and Characterization of MCM3 as a Kelch-like ECH-associated Protein 1 (KEAP1) Substrate. J Biol Chem **291:**23719-23733.

42. **Sharma S, Ding F, Nie H, Watson D, Unnithan A, Lopp J, Pozefsky D, Dokholyan NV.** 2006. iFold: a platform for interactive folding simulations of proteins. Bioinformatics **22:**2693-2694.

43. **Forbes SA, Beare D, Gunasekaran P, Leung K, Bindal N, Boutselakis H, Ding M, Bamford S, Cole C, Ward S, Kok CY, Jia M, De T, Teague JW, Stratton MR, McDermott U, Campbell PJ.** 2015. COSMIC: exploring the world's knowledge of somatic mutations in human cancer. Nucleic Acids Res **43:**D805-811.

44. **Forbes SA, Bhamra G, Bamford S, Dawson E, Kok C, Clements J, Menzies A, Teague JW, Futreal PA, Stratton MR.** 2008. The Catalogue of Somatic Mutations in Cancer (COSMIC). Curr Protoc Hum Genet **Chapter 10:**Unit 10 11.

45. **Levine AJ.** 1993. The tumor suppressor genes. Annu Rev Biochem **62:**623-651.

46. **Padmanabhan B, Tong KI, Ohta T, Nakamura Y, Scharlock M, Ohtsuji M, Kang MI, Kobayashi A, Yokoyama S, Yamamoto M.** 2006. Structural basis for defects of Keap1 activity provoked by its point mutations in lung cancer. Mol Cell **21:**689-700.

47. **Hayes JD, McMahon M.** 2009. NRF2 and KEAP1 mutations: permanent activation of an adaptive response in cancer. Trends Biochem Sci **34:**176-188.

48. **Imielinski M, Berger AH, Hammerman PS, Hernandez B, Pugh TJ, Hodis E, Cho J, Suh J, Capelletti M, Sivachenko A, Sougnez C, Auclair D, Lawrence MS, Stojanov P, Cibulskis K, Choi K, de Waal L, Sharifnia T, Brooks A, Greulich H, Banerji S, Zander T, Seidel D, Leenders F, Ansen S, Ludwig C, Engel-Riedel W, Stoelben E, Wolf J, Goparju C, Thompson K, Winckler W, Kwiatkowski D, Johnson BE, Janne PA, Miller VA, Pao W, Travis WD, Pass HI, Gabriel SB, Lander ES, Thomas RK, Garraway LA, Getz G, Meyerson M.** 2012. Mapping the hallmarks of lung adenocarcinoma with massively parallel sequencing. Cell **150:**1107-1120.

49. **Berger AH, Brooks AN, Wu X, Shrestha Y, Chouinard C, Piccioni F, Bagul M, Kamburov A, Imielinski M, Hogstrom L, Zhu C, Yang X, Pantel S, Sakai R, Watson J, Kaplan N, Campbell JD, Singh S, Root DE, Narayan R, Natoli T, Lahr DL, Tirosh I, Tamayo P, Getz G, Wong B, Doench J, Subramanian A, Golub TR, Meyerson M, Boehm JS.** 2016. High-throughput Phenotyping of Lung Cancer Somatic Mutations. Cancer Cell **30:**214-228.

50. **Campbell JD, Alexandrov A, Kim J, Wala J, Berger AH, Pedamallu CS, Shukla SA, Guo G, Brooks AN, Murray BA, Imielinski M, Hu X, Ling S, Akbani R, Rosenberg M, Cibulskis C, Ramachandran A, Collisson EA, Kwiatkowski DJ, Lawrence MS, Weinstein JN, Verhaak RG, Wu CJ, Hammerman PS, Cherniack AD, Getz G, Cancer Genome Atlas Research N, Artyomov MN, Schreiber R, Govindan R, Meyerson M.** 2016. Distinct patterns of somatic genome alterations in lung adenocarcinomas and squamous cell carcinomas. Nat Genet **48:**607-616.

51. **Valdar WS.** 2002. Scoring residue conservation. Proteins **48:**227-241.

52. **Capra JA, Singh M.** 2007. Predicting functionally important residues from sequence conservation. Bioinformatics **23:**1875-1882.

53. **Bellucci A, Fiorentini C, Zaltieri M, Missale C, Spano P.** 2014. The "in situ" proximity ligation assay to probe protein-protein interactions in intact tissues. Methods Mol Biol **1174:**397-405.

54. **Pacchiana R, Abbate M, Armato U, Dal Pra I, Chiarini A.** 2014. Combining immunofluorescence with in situ proximity ligation assay: a novel imaging approach to monitor protein-protein interactions in relation to subcellular localization. Histochem Cell Biol **142:**593-600.

55. **Zhao Y, Xiong X, Jia L, Sun Y.** 2012. Targeting Cullin-RING ligases by MLN4924 induces autophagy via modulating the HIF1-REDD1-TSC1-mTORC1-DEPTOR axis. Cell Death Dis **3:**e386.

56. **Luo Z, Pan Y, Jeong LS, Liu J, Jia L.** 2012. Inactivation of the Cullin (CUL)-RING E3 ligase by the NEDD8-activating enzyme inhibitor MLN4924 triggers protective autophagy in cancer cells. Autophagy **8:**1677-1679.

57. **Eggler AL, Liu G, Pezzuto JM, van Breemen RB, Mesecar AD.** 2005. Modifying specific cysteines of the electrophile-sensing human Keap1 protein is insufficient to disrupt binding to the Nrf2 domain Neh2. Proc Natl Acad Sci U S A **102:**10070-10075.

58. **Dinkova-Kostova AT, Kostov RV, Canning P.** 2017. Keap1, the cysteine-based mammalian intracellular sensor for electrophiles and oxidants. Arch Biochem Biophys **617:**84-93.

59. **Cleasby A, Yon J, Day PJ, Richardson C, Tickle IJ, Williams PA, Callahan JF, Carr R, Concha N, Kerns JK, Qi H, Sweitzer T, Ward P, Davies TG.** 2014. Structure of the BTB domain of Keap1 and its interaction with the triterpenoid antagonist CDDO. PLoS One **9:**e98896.

60. **Cui W, Bai Y, Luo P, Miao L, Cai L.** 2013. Preventive and therapeutic effects of MG132 by activating Nrf2-ARE signaling pathway on oxidative stress-induced cardiovascular and renal injury. Oxid Med Cell Longev **2013:**306073.

61. **Roux KJ, Kim DI, Raida M, Burke B.** 2012. A promiscuous biotin ligase fusion protein identifies proximal and interacting proteins in mammalian cells. J Cell Biol **196:**801-810.

62. **Kim DI, Birendra KC, Zhu W, Motamedchaboki K, Doye V, Roux KJ.** 2014. Probing nuclear pore complex architecture with proximity-dependent biotinylation. Proc Natl Acad Sci U S A **111:**E2453-2461.

63. **Kim DI, Jensen SC, Noble KA, Kc B, Roux KH, Motamedchaboki K, Roux KJ.** 2016. An improved smaller biotin ligase for BioID proximity labeling. Mol Biol Cell **27:**1188-1196.

64. **Ma J, Cai H, Wu T, Sobhian B, Huo Y, Alcivar A, Mehta M, Cheung KL, Ganesan S, Kong AN, Zhang DD, Xia B.** 2012. PALB2 interacts with KEAP1 to promote NRF2 nuclear accumulation and function. Mol Cell Biol **32:**1506-1517.

65. **Zhang Y, Crouch DH, Yamamoto M, Hayes JD.** 2006. Negative regulation of the Nrf1 transcription factor by its N-terminal domain is independent of Keap1: Nrf1, but not Nrf2, is targeted to the endoplasmic reticulum. Biochem J **399:**373-385.

66. **Tian H, Zhang B, Di J, Jiang G, Chen F, Li H, Li L, Pei D, Zheng J.** 2012. Keap1: one stone kills three birds Nrf2, IKKbeta and Bcl-2/Bcl-xL. Cancer Lett **325:**26-34.

67. **Jiang ZY, Chu HX, Xi MY, Yang TT, Jia JM, Huang JJ, Guo XK, Zhang XJ, You QD, Sun HP.** 2013. Insight into the intermolecular recognition mechanism between Keap1 and IKKbeta combining homology modelling, protein-protein docking, molecular dynamics simulations and virtual alanine mutation. PLoS One **8:**e75076.

68. **Lo SC, Hannink M.** 2006. PGAM5, a Bcl-XL-interacting protein, is a novel substrate for the redox-regulated Keap1-dependent ubiquitin ligase complex. J Biol Chem **281:**37893-37903.

69. **Wang Z, Jiang H, Chen S, Du F, Wang X.** 2012. The mitochondrial phosphatase PGAM5 functions at the convergence point of multiple necrotic death pathways. Cell **148:**228-243.

70. **Niture SK, Jaiswal AK.** 2011. INrf2 (Keap1) targets Bcl-2 degradation and controls cellular apoptosis. Cell Death Differ **18:**439-451.

71. **Niture SK, Jaiswal AK.** 2011. Inhibitor of Nrf2 (INrf2 or Keap1) protein degrades Bcl-xL via phosphoglycerate mutase 5 and controls cellular apoptosis. J Biol Chem **286:**44542-44556.

72. **Niture SK, Jaiswal AK.** 2010. Hsp90 interaction with INrf2(Keap1) mediates stress-induced Nrf2 activation. J Biol Chem **285:**36865-36875.

73. **Tao S, Liu P, Luo G, Rojo de la Vega M, Chen H, Wu T, Tillotson J, Chapman E, Zhang DD.** 2017. p97 Negatively Regulates NRF2 by Extracting Ubiquitylated NRF2 from the KEAP1-CUL3 E3 Complex. Mol Cell Biol **37**.

74. **Chou TF, Li K, Nordin BE, Porubsky P, Frankowski K, Patricelli MP, Aube J, Schoenen FJ, Deshaies R.** 2010. Selective, reversible inhibitors of the AAA ATPase p97, Probe Reports from the NIH Molecular Libraries Program, Bethesda (MD).

75. **Chou TF, Brown SJ, Minond D, Nordin BE, Li K, Jones AC, Chase P, Porubsky PR, Stoltz BM, Schoenen FJ, Patricelli MP, Hodder P, Rosen H, Deshaies RJ.** 2011. Reversible inhibitor of p97, DBeQ, impairs both ubiquitin-dependent and autophagic protein clearance pathways. Proc Natl Acad Sci U S A **108:**4834-4839.

76. **Chapman E, Maksim N, de la Cruz F, La Clair JJ.** 2015. Inhibitors of the AAA+ chaperone p97. Molecules **20:**3027-3049.

77. **Chou TF, Deshaies RJ.** 2011. Development of p97 AAA ATPase inhibitors. Autophagy **7:**1091-1092.

78. **Pickart CM, Cohen RE.** 2004. Proteasomes and their kin: proteases in the machine age. Nat Rev Mol Cell Biol **5:**177-187.

79. **Budenholzer L, Cheng CL, Li Y, Hochstrasser M.** 2017. Proteasome Structure and Assembly. J Mol Biol doi:10.1016/j.jmb.2017.05.027.

80. **Murata S, Yashiroda H, Tanaka K.** 2009. Molecular mechanisms of proteasome assembly. Nat Rev Mol Cell Biol **10:**104-115.

81. **Collins GA, Goldberg AL.** 2017. The Logic of the 26S Proteasome. Cell **169:**792-806.

82. **Ciechanover A, Stanhill A.** 2014. The complexity of recognition of ubiquitinated substrates by the 26S proteasome. Biochim Biophys Acta **1843:**86-96.

83. **Mayor T, Lipford JR, Graumann J, Smith GT, Deshaies RJ.** 2005. Analysis of polyubiquitin conjugates reveals that the Rpn10 substrate receptor contributes to the turnover of multiple proteasome targets. Mol Cell Proteomics **4:**741-751.

84. **Verma R, Oania R, Graumann J, Deshaies RJ.** 2004. Multiubiquitin chain receptors define a layer of substrate selectivity in the ubiquitin-proteasome system. Cell **118:**99-110.

85. **Elsasser S, Finley D.** 2005. Delivery of ubiquitinated substrates to protein-unfolding machines. Nat Cell Biol **7:**742-749.

86. **Yamamoto T, Suzuki T, Kobayashi A, Wakabayashi J, Maher J, Motohashi H, Yamamoto M.** 2008. Physiological significance of reactive cysteine residues of Keap1 in determining Nrf2 activity. Mol Cell Biol **28:**2758-2770.

87. **Fontana A, de Laureto PP, Spolaore B, Frare E, Picotti P, Zambonin M.** 2004. Probing protein structure by limited proteolysis. Acta Biochim Pol **51:**299-321.

88. **Morimoto T, Tashiro Y, Matsuura S.** 1967. Chase of newly synthesized proteins in guinea-pig pancreas with cycloheximide. Biochim Biophys Acta **138:**631-633.

89. **Eftekharzadeh B, Maghsoudi N, Khodagholi F.** 2010. Stabilization of transcription factor Nrf2 by tBHQ prevents oxidative stress-induced amyloid beta formation in NT2N neurons. Biochimie **92:**245-253.

90. **Fink AL.** 1998. Protein aggregation: folding aggregates, inclusion bodies and amyloid. Fold Des **3:**R9-23.

91. **Mizushima N.** 2007. Autophagy: process and function. Genes Dev **21:**2861-2873.

92. **Mizushima N, Komatsu M.** 2011. Autophagy: renovation of cells and tissues. Cell **147:**728-741.

93. **Mizushima N.** 2010. Autophagy. FEBS Lett **584:**1279.

94. **Yin Z, Pascual C, Klionsky DJ.** 2016. Autophagy: machinery and regulation. Microb Cell **3:**588-596.

95. **Komatsu M, Kurokawa H, Waguri S, Taguchi K, Kobayashi A, Ichimura Y, Sou YS, Ueno I, Sakamoto A, Tong KI, Kim M, Nishito Y, Iemura S, Natsume T, Ueno T, Kominami E, Motohashi H, Tanaka K, Yamamoto M.** 2010. The selective autophagy substrate p62 activates the stress responsive transcription factor Nrf2 through inactivation of Keap1. Nat Cell Biol **12:**213-223.

96. **Lau A, Wang XJ, Zhao F, Villeneuve NF, Wu T, Jiang T, Sun Z, White E, Zhang DD.** 2010. A noncanonical mechanism of Nrf2 activation by autophagy deficiency: direct interaction between Keap1 and p62. Mol Cell Biol **30:**3275-3285.

97. **Stepkowski TM, Kruszewski MK.** 2011. Molecular cross-talk between the NRF2/KEAP1 signaling pathway, autophagy, and apoptosis. Free Radic Biol Med **50:**1186-1195.

98. **Taguchi K, Fujikawa N, Komatsu M, Ishii T, Unno M, Akaike T, Motohashi H, Yamamoto M.** 2012. Keap1 degradation by autophagy for the maintenance of redox homeostasis. Proc Natl Acad Sci U S A **109:**13561-13566.

99. **Kirkin V, Lamark T, Sou YS, Bjorkoy G, Nunn JL, Bruun JA, Shvets E, McEwan DG, Clausen TH, Wild P, Bilusic I, Theurillat JP, Overvatn A, Ishii T, Elazar Z, Komatsu M, Dikic I, Johansen T.** 2009. A role for NBR1 in autophagosomal degradation of ubiquitinated substrates. Mol Cell **33:**505-516.

100. **Lippai M, Low P.** 2014. The role of the selective adaptor p62 and ubiquitin-like proteins in autophagy. Biomed Res Int **2014:**832704.

101. **Ichimura Y, Waguri S, Sou YS, Kageyama S, Hasegawa J, Ishimura R, Saito T, Yang Y, Kouno T, Fukutomi T, Hoshii T, Hirao A, Takagi K, Mizushima T, Motohashi H, Lee MS, Yoshimori T, Tanaka K, Yamamoto M, Komatsu M.** 2013. Phosphorylation of p62 activates the Keap1-Nrf2 pathway during selective autophagy. Mol Cell **51:**618-631.

102. **Jiang X, Bao Y, Liu H, Kou X, Zhang Z, Sun F, Qian Z, Lin Z, Li X, Liu X, Jiang L, Yang Y.** 2017. VPS34 stimulation of p62 phosphorylation for cancer progression. Oncogene doi:10.1038/onc.2017.295.

103. **Yoshii SR, Mizushima N.** 2017. Monitoring and Measuring Autophagy. Int J Mol Sci **18**.

104. **Klionsky DJ, Baehrecke EH, Brumell JH, Chu CT, Codogno P, Cuervo AM, Debnath J, Deretic V, Elazar Z, Eskelinen EL, Finkbeiner S, Fueyo-Margareto J, Gewirtz D, Jaattela M, Kroemer G, Levine B, Melia TJ, Mizushima N, Rubinsztein DC, Simonsen A, Thorburn A, Thumm M, Tooze SA.** 2011. A comprehensive glossary of autophagy-related molecules and processes (2nd edition). Autophagy **7:**1273-1294.

105. **Jiang T, Chen N, Zhao F, Wang XJ, Kong B, Zheng W, Zhang DD.** 2010. High levels of Nrf2 determine chemoresistance in type II endometrial cancer. Cancer Res **70:**5486-5496.

106. **Shibata T, Kokubu A, Gotoh M, Ojima H, Ohta T, Yamamoto M, Hirohashi S.** 2008. Genetic alteration of Keap1 confers constitutive Nrf2 activation and resistance to chemotherapy in gallbladder cancer. Gastroenterology **135:**1358-1368, 1368 e1351-1354.

107. **Choi B-h, Kwak M-K.** 2016. Shadows of NRF2 in cancer: Resistance to chemotherapy. Current Opinion in Toxicology **1:**20-28.

108. **Lee YS, Yoon S, Park MS, Kim JH, Lee JH, Song CW.** 2010. Influence of p53 expression on sensitivity of cancer cells to bleomycin. J Biochem Mol Toxicol **24:**260-269.

109. **Shibata T, Ohta T, Tong KI, Kokubu A, Odogawa R, Tsuta K, Asamura H, Yamamoto M, Hirohashi S.** 2008. Cancer related mutations in NRF2 impair its recognition by Keap1-Cul3 E3 ligase and promote malignancy. Proc Natl Acad Sci U S A **105:**13568-13573.

110. **Katsuoka F, Yamazaki H, Yamamoto M.** 2016. Small Maf deficiency recapitulates the liver phenotypes of Nrf1- and Nrf2-deficient mice. Genes Cells **21:**1309-1319.

111. **Kageyama S, Sou YS, Uemura T, Kametaka S, Saito T, Ishimura R, Kouno T, Bedford L, Mayer RJ, Lee MS, Yamamoto M, Waguri S, Tanaka K, Komatsu M.** 2014. Proteasome dysfunction activates autophagy and the Keap1-Nrf2 pathway. J Biol Chem **289:**24944-24955.

112. **Liu WJ, Ye L, Huang WF, Guo LJ, Xu ZG, Wu HL, Yang C, Liu HF.** 2016. p62 links the autophagy pathway and the ubiqutin-proteasome system upon ubiquitinated protein degradation. Cell Mol Biol Lett **21:**29.

113. **Seguin SJ, Morelli FF, Vinet J, Amore D, De Biasi S, Poletti A, Rubinsztein DC, Carra S.** 2014. Inhibition of autophagy, lysosome and VCP function impairs stress granule assembly. Cell Death Differ **21:**1838-1851.

114. **Peng H, Yang J, Li G, You Q, Han W, Li T, Gao D, Xie X, Lee BH, Du J, Hou J, Zhang T, Rao H, Huang Y, Li Q, Zeng R, Hui L, Wang H, Xia Q, Zhang X, He Y, Komatsu M, Dikic I, Finley D, Hu R.** 2017. Ubiquitylation of p62/sequestosome1 activates its autophagy receptor function and controls selective autophagy upon ubiquitin stress. Cell Res **27:**657-674.

115. **Lee Y, Chou TF, Pittman SK, Keith AL, Razani B, Weihl CC.** 2017. Keap1/Cullin3 Modulates p62/SQSTM1 Activity via UBA Domain Ubiquitination. Cell Rep **20:**1994.

CHAPTER IV: DISCUSSION

4.A. The identification and mechanism(s) of KEAP1 superbinder mutants

4.A.1.Summary of findings

This dissertation discusses a previously described high-throughput platform for profiling patient-derived KEAP1 mutants (1). This platform combines two assays for KEAP1 function: 1) NRF2 transcriptional activity and 2) NRF2 association with KEAP1 as measured by IP/W.blot (1, 2). Integration of these two metrics enables the binning of KEAP1 mutations into three distinct functional classes: 1) passenger or silent mutations that are functionally equivalent to KEAP1 WT, 2) hypomorphic mutations which increase KEAP1-NRF2 protein association but cannot suppress NRF2 transcriptional activity, and 3) inactivating mutations which result in functionally dead proteins. Further examination of the hypomorphic class revealed a subset of six mutants: V155F, G186S, R320Q, D422N, G423V, and R470C. These mutants retain the ability to ubiquitylate NRF2 but are deficient in their ability to target NRF2 for proteasomal degradation; we have termed these KEAP1 ‘superbinders’. Two of these KEAP1 mutants, the R320Q and R470C superbinders, occur at amino acid residues determined to be frequently mutated in cancer. Moreover, we estimate that the superbinder class of KEAP1 mutations constitutes nearly 40% of the mutations identified in LUSC (1). The primary objective of this dissertation was to investigate the mechanism(s) of the class of KEAP1 superbinders by interrogating four aspects of these mutants: 1) protein-protein interactions, 2) structural analyses, 3) subcellular localization, and 4) response to chemotherapeutic insults.

KEAP1 protein interaction alterations may result in the superbinder phenotype. To test this hypothesis, unbiased BioID/MS analyses of proximal proteins and targeted IP/W.blot of the superbinders were performed. These studies concluded that superbinder mutants do not disrupt CUL3 association, KEAP1 homodimerization, or associations with six established substrates: PALB2, MCM3, NRF1, IKBKB, PGAM5, and BCL2. Furthermore, as compared to WT, superbinders were not altered in their association with three novel interactors: the ATPase VCP and two ubiquitin receptors on the proteasome lid, PSMD2 and PSMD4.

Conformational changes to KEAP1 impair NRF2 degradation; consequently, modifications to KEAP1 tertiary structure may contribute to the superbinder phenotype (3-9). Dynamic simulation and limited proteolysis studies of full-length KEAP1 were used to probe KEAP1 superbinder structure. Due to the availability of a crystal structure for the KEAP1 KELCH domain, simulation studies could be performed with the R470 superbinder mutant as this mutation lies within the KELCH domain that is required for NRF2 association. These studies revealed that mutations at R470 reduced flexibility throughout the KELCH domain, potentially through salt bridge formations with acidic residues D422 and E493 in KEAP1. Intriguingly, mutations to the D422 residue also result in a superbinder phenotype. Moreover, the reduction in KEAP1 flexibility is predicted to impact residues that associate with NRF2 and may impair the dissociation of ubiquitylated NRF2 from KEAP1. As a complementary approach, limited proteolysis of full-length superbinders R320Q and R470C was performed. KEAP1 superbinders were more resistant to trypsin-mediated limited proteolysis as compared to KEAP1 WT, providing biochemical data supportive of the simulation studies. Taken together, these data suggest that superbinder mutants may stabilize KEAP1 structure, particularly at sites contacting the NRF2 degron.

Next, we employed live cell imaging of fluorescent constructs and IF analyses to examine the mechanism by which KEAP1 superbinder mutants impact subcellular localization of the KEAP1-NRF2 complex. These studies revealed that overexpression of KEAP1 superbinders induces the formation of p62-dependent circular clusters that contain KEAP1, NRF2, p62, an autophagy-specific phosphorylated form of p62 (p62 pS351), and polyubiquitin. Moreover, these clusters do not colocalize with markers of autophagy (LC3) or lysosomal degradation (LAMP2 and lysotracker).

Hyperactivation of NRF2 in cancer cells is protective against chemotherapeutic insult (10-19). To determine the phenotypic consequence of KEAP1 superbinder mutations, we compared dose-response curves of cells overexpressing KEAP1 WT or superbinder mutants for three chemotherapeutic drugs: cisplatin, paclitaxel, and bleomycin. Of the three drugs tested, superbinder mutants conferred resistance only to the oxidative stressor bleomycin as measured by cell viability using two complementary assays: 1) PrestoBlue as a surrogate for mitochondrial metabolism and 2) the Caspase 3/7 Glo assay which measures apoptotic induction. No differential sensitivity was observed for cisplatin and paclitaxel in WT- or superbinder-overexpressing cells.

The mechanistic studies of the R320Q and R470C superbinder mutants revealed five defining traits for the superbinder class. First, superbinder mutants exhibit a high correlation between mutational frequency and sequence conservation; two of the three most frequently mutated residues within KEAP1 are superbinder mutants. Second, superbinder mutants increase NRF2 association without disrupting KEAP1 associations with other proteins. Third, superbinder mutants likely stabilize KEAP1 tertiary structure, thus altering association with the NRF2 degron. Fourth, overexpression of KEAP1 superbinder mutants results in the formation of p62-dependent clusters that contain KEAP1 enclosed by a ring of

p62, autophagy-specific phosphorylated p62, polyubiquitin, and occasionally NRF2. Fifth, overexpression of KEAP1 superbinder mutants protects lung cancer cells from bleomycin-induced DNA damage (20).

4.A.2 Proposed future studies of superbinder mutants

Identification of genotype-phenotype relationships

The correlation between mutation frequency and sequence conservation is intriguing and lends itself to two follow-up studies: 1) biochemical profiling of frequently mutated and conserved residues in NRF2 and KEAP1 with unknown biological function, and 2) comparative analyses of mutational frequency and conservation for additional tumor suppressors and oncogenes. Mutations known to impact protein function appear to be enriched in frequently mutated and conserved residues for both NRF2 and KEAP1. Of the top 20 frequently mutated and conserved residues in NRF2, 19 are localized to the DLG and ETGE motifs required for KEAP1 association (R499 is the lone exception, Figure 3.2A). Our lab and others have established that mutations within the DLG and ETGE residues abolish KEAP1 association and result in elevated NRF2 transcriptional activity (21-28). The R499 residue is located within the Neh3 domain of NRF2 which is responsible for DNA binding and dimerization (29-31). Future studies to clone this mutation and determine its impact on NRF2 subcellular localization, NRF2 transcriptional activity, and association with small MAF (sMAF) proteins or KEAP1 are warranted. Based on the location of the mutation, I would predict that R499 mutations would have no impact on KEAP1 association; however, these mutations could potentially block heterodimerization with sMAF proteins, thus blocking DNA binding and suppressing NRF2-dependent transcription. Additionally, 9 of the top 20 frequently mutated residues in KEAP1 are known to impact KEAP1 function; these 20 mutations are highly conserved across 500 protein sequences bearing at least 45% identity to human KEAP1. These residues include 5 hypomorphs (G480 and 4 superbinders: G186,

R320, D422, and R470) and 4 functionally dead mutant residues (G333, G417, R601, and R603) (Figure 3.2B) (1, 11, 16-18, 32-35). Cloning and profiling of mutations occurring in the remaining 11 top frequently mutated and conserved residues would be predicted to reveal residues impacting biological function (1, 11, 16-18, 32-36). The E493 residue is of particular interest because DMD simulation studies performed in Chapter 3 of this dissertation identified salt bridge formations and electrostatic interactions between E493 and the R470C superbinder; furthermore, E493 is the 19th most mutated residue in KEAP1. As such, patient-derived E493 mutations would be predicted to phenocopy superbinder mutations.

The second future study involves comparing mutational frequency and Shannon entropy for other tumor suppressors (i.e. *TP53* and *PTEN*) and oncogenes (i.e. *KRAS* and *BRAF)*. It would be informative to determine whether frequently mutated and highly conserved residues in known oncogenes and tumor suppressors impair their function. If true, comparison of mutational frequency with Shannon entropy could be used to prioritize patient-derived mutations for molecular studies for additional tumor suppressors and oncogenes.

KEAP1 structural studies

Though the exact mechanism by which the KEAP1 superbinder mutants alter KEAP1 tertiary structure has not yet been elucidated, the limited proteolysis analysis and DMD simulations are both suggestive of KEAP1 structure alterations that result in changes to the NRF2 interface. Surface plasmon resonance (SPR) of the recombinant NRF2 Neh2 domain with the KEAP1 KELCH WT or R470C domain should be considered to determine the affinity of the complex. Purification of full-length recombinant KEAP1 is challenging given the number of cysteine residues within the protein (6, 37-41). Although we were successful in

purifying small amounts of CUL3, NRF2, and KEAP1, SPR analyses proved difficult because biotinylation of full-length KEAP1 for SPR chip immobilization impaired its association with full-length NRF2 (data not shown). As an alternative to SPR analysis, KEAP1-NRF2 affinity estimates were attempted via dissociation of immunopurified KEAP1-NRF2 complexes using salt and urea titration curves. Surprisingly, the KEAP1 WT-NRF2 or KEAP1 superbinder-NRF2 complexes did not fully dissociate even with the addition of 2.5 M NaCl or 8 M urea washes (data not shown). These data support an extremely tight association between KEAP1-NRF2 that may be near covalent in strength. As a complementary approach, KEAP1-NRF2 complexes could be exposed to increasing amounts of the reducing agent dithiothreitol (DTT) to determine if increased DTT can dissociate KEAP1-NRF2.

Our prevailing theory is that superbinder mutants impair KEAP1 conformational cycling (7-9, 42). The rate of KEAP1 conformational cycling within an individual cell can be determined using fluorescence lifetime imaging (FLIM) and Förster resonance energy transfer (FRET) to calculate FRET efficiency (e-FRET) (8). Although constructs to test this hypothesis have been generated and validated, the resources and expertise to perform these experiments are not currently available at UNC. As such, we have an ongoing collaboration with the Dinkova-Kostova laboratory at the University of Dundee, and we are eagerly awaiting results of these studies. The Dinkova-Kostova group originally characterized KEAP1 conformational cycling using FLIM-FRET (7). Thus far, our collaborators have established that KEAP1 superbinder mutants do not alter fluorescence recovery after photobleaching (FRAP) when compared to KEAP1 WT (data not shown). However, proteasome inhibition via MG-132 results in statistically significant alterations in the mobility of KEAP1 WT and superbinder mutants as measured by FRAP analysis (data not shown). These alterations suggest that proteasome inhibition impairs KEAP1-NRF2

complex mobility within the cell, which merits further investigation. Future experiments testing superbinder mutants should be performed in *Keap1*$^{-/-}$ MEFs or other KEAP1 genetically null cell lines in order to exclude contributions from KEAP1 WT-superbinder heterodimers.

Additional studies of p62-dependent KEAP1-NRF2 clusters

One of the more intriguing findings in this dissertation is the accumulation of the p62-dependent clusters in the presence of the KEAP1 superbinder mutants (discussed in Chapter 3). The exact nature and biological significance of these clusters is yet to be determined. We observed that cluster formation was cell line-dependent. In HEK 293T/17 cells, clusters were observed only in the presence of overexpressed KEAP1 superbinders. In contrast, lung adenocarcinoma H1299 cells revealed KEAP1-NRF2- positive clusters even in the presence of KEAP1 WT, though KEAP1 WT resulted in the formation of fewer clusters as compared to KEAP1 superbinders. Because cluster formation requires p62, it is possible that H1299 cells have higher levels of endogenous p62 compared to HEK 293T/17 cells. Western blot analysis of HEK 293T/17 and a panel of lung line lysates would be an appropriate experiment to test this hypothesis. These lysates should also be probed for differential expression of KEAP1, NRF2, p62 pS351, and LC3I-II. Cell lines expressing higher levels of endogenous p62 and NRF2 would be predicted to form clusters in the presence of KEAP1 superbinder overexpression.

Given that KEAP1 binds to p62 and that the formation of these clusters is p62-dependent, we predicted that autophagy was being engaged to clear the clusters. However, studies examining the colocalization of these clusters with markers of the autophagosome (LC3) or lysosome (LysoTracker or LAMP2) were negative (43-49). Moreover, autophagy inducers (wortmannin, serum starvation, and rapamycin) or inhibitors (chloroquine [CQ] and

bafilomycin A1) did not impact cluster formation or clearance (data not shown) (44-49). Two key experiments for future studies are proposed here. First, the status of KEAP1-dependent p62 ubiquitylation and interactions in the presence of the superbinder mutants should be determined. P62 was recently reported to be ubiquitylated by the KEAP1-NRF2 complex (50-59). Furthermore, ubiquitylation of p62 is essential for p62 association with LC3; this interaction enables p62 to transport ubiquitylated cargo to the growing phagophores for autophagic clearance (44-47, 49, 51, 53-55, 57-62). It is possible that KEAP1-NRF2 superbinder complexes are competent for p62 association but are deficient for p62 ubiquitylation. As such, the KEAP1-NRF2-p62 clusters could represent intermediates between impaired proteasome-mediated and autophagic degradation. To conduct these experiments, p62 could be immunopurified under denaturing conditions in the presence of KEAP1 WT or superbinder overexpression. Immunopurified complexes would then be probed for polyubiquitin as well as ubiquitin chain-specific antibodies. It is feasible that KEAP1 superbinder mutants alter essential protein-protein interactions of p62. Therefore, p62 protein-protein interactions in the presence of KEAP1 WT or superbinders should be assessed through unbiased BioID/MS to identify changes in association of proximal proteins as well as through targeted IP/W.blot analyses to examine interactions between p62 and known interactors such as LC3.

Additional live cell imaging studies with NRF2 inducers or p62 siRNAs could provide information concerning the dynamics of the formation and clearance of KEAP1-NRF2-p62 clusters. High-resolution electron microscopy (EM) with immunogold staining or cryo-electron microscopy (cryo-EM) may resolve the dimensions and organization of proteins within the clusters. Accurate size analysis of the clusters might lead to theories regarding the stoichiometric ratios of proteins within these clusters. Given the observed size of the clusters, the clusters may contain multiple subunits of KEAP1-NRF2 complexes as well as

oligomerized p62. If technically feasible, biochemical fractionation and MS analyses of the clusters could reveal stoichiometric ratios, identify additional proteins localized within the clusters, and identify post-translational modifications of proteins within the clusters.

Generating cell lines and mice with KEAP1 superbinder mutations

There are currently no available cell lines expressing superbinder mutations from the endogenous KEAP1 promoter. As such, clustered regularly interspaced short palindromic repeats (CRISPR)/Cas9 gene editing could be employed to generate a panel of lung cancer cell lines expressing the KEAP1 R320Q and R470C superbinder mutations; KEAP1 WT isogenic cell lines would serve as controls. These cell lines could be evaluated for transformative potential using soft agar assays to measure anchorage-independent growth as well as clonogenic potential via colony formation assays. Genetic models of NRF2 hyperactivation alone do not result in spontaneous tumor formation; therefore, expression of the KEAP1 superbinders may need to be performed in conjunction with oncogenic mutation ($KRAS^{G12D}$) or tumor suppressor deletion ($TP53^{-/-}$) in order to observe a robust phenotype in transformative or clonogenic assays.

These cell lines could also be used in xenograft studies to evaluate tumorigenic potential and response to treatment *in vivo*. Generation of mice carrying a floxed allele with superbinder mutations would enable experiments testing the consequence of superbinder mutations during embryonic development. Mice born with superbinder mutations should exhibit moderate levels of NRF2 activation as compared to the lethal $Keap1^{-/-}$ (KO) mice. As such, these mice would be expected to survive and would be predicted to behave comparably to $Keap1^{flox/-}$(*Keap1*-KD) mice, which demonstrate moderate levels of NRF2 transcriptional activity and survive to adulthood (19). Furthermore, the floxed superbinder mice could be genetically crossed with mouse models of LUSC

(*Keap1*$^{flox/flox}$*::Trp53*$^{flox/flox}$*::R26*^{tdTomato}) and/or LUAD (*Kras*$^{LSL\text{-}G12D/+}$*::Tp53*$^{flox/flox}$) to test the role of superbinder mutations in tumor development *in vivo* (63-67). The increase in NRF2 stabilization and transcriptional activity caused by the superbinder mutations should increase tumor formation and burden in both the LUSC and LUAD mouse models. Moreover, the elevated expression of NRF2 target genes in tumors from mice with superbinder mutations should confer resistance to chemotherapy and radiotherapy similarly to the bleomycin resistance observed in cell lines overexpressing KEAP1 superbinders, which was discussed in Chapter 3.

4.B. Clinical application: Identification of a patient-derived NRF2 Functionally Active Mutant Signature (NRF2^{FAMS})

4.B.1. Rationale

The American Cancer Society estimated that more than 90,000 patients will be diagnosed with NRF2-active cancers in 2017; furthermore, NRF2-active cancers will account for more than 45,000 deaths this year (Figure 4.1). Mutations impacting NRF2 activity are found in more than 10 organs and are most prevalent in the lung (68-70). Over 30% of NSCLC patients harbor mutations in *KEAP1*, *NFE2L2*, or *CUL3* (32, 68, 71-77). Unfortunately, patients with increased NRF2 transcriptional activity are less responsive to chemo- and radiotherapy and have a worse prognosis (11, 17, 18, 34, 35, 78-82). Due to the prognostic value of identifying patients with KEAP1-NRF2 pathway alterations prior to chemo- or radiotherapy, there is a clear need to develop a patient-derived NRF2 target gene signature for use as a biomarker. The most established NRF2 signature was developed by the Biswal laboratory (Singh_NFE2L2_targets GSEA M2662, hereafter Singh signature) and is comprised of 15 genes identified from NRF2-depleted A549 and H460 lung adenocarcinoma cells which normally exhibit NRF2 hyperactivation due to inactivating mutations in KEAP1(17). Recent studies expanded this signature using patient data sets

from the gene expression omnibus (GEO) and The Cancer Genome Atlas (TCGA) (83-86). These additional signatures were derived through gene set enrichment analysis (GSEA) by segregating patient samples with WT or mutant *KEAP1*/*NFE2L2*/*CUL3* genes; however, these signatures treated functionally silent mutations as mutants, which likely impacted the analysis as approximately 20% of all KEAP1 LUSC mutations are predicted as functionally silent (1). Grouping mutations with WT function along with functionally inactive or hypomorphic mutations to derive a gene signature could result in missed opportunities for identifying novel target genes or in a target gene signature that is neither prognostic nor predictive (84). As an extension to the work describing KEAP1 superbinder function, a secondary goal was to establish a database with functional annotations for patient-derived *KEAP1*/*NFE2L2*/*CUL3* mutations. This was accomplished by utilizing insights gained from functional and biochemical characterization of 18 KEAP1 mutations identified in LUSC as well as literature-based evidence of mutation function in *KEAP1/NFE2L2/CUL3* samples (1).

4.B.2. Approach

Patient samples from the most recent TCGA-LUSC (n=489) dataset were binned into six classes based on RNA-seq and gene expression data: 1) *CUL3* homozygous deletions or activating mutations (n=9), 2) *KEAP1* inactivating mutations or deletions (n=20), 3) *NFE2L2* gain-of-function (GOF) mutations (n=83), 4) samples containing multiple mutations and/or amplifications and/or deletions (n=24), 5) *KEAP1/NFE2L2/CUL3* mutations of unknown function (n=69), and 6) normal samples, which incorporates known passenger or silent mutations (n=330) (Figure 4.2) (1, 10, 12, 16-18, 32, 34, 68, 71, 73, 76, 84, 87-91). Using a stringent false discovery rate (FDR) of 5% with median-centered values, differentially expressed genes (DEGs) were sorted by fold-change; this revealed 50 genes that are significantly upregulated in *KEAP1/NFE2L2/CUL3* mutant patient samples (Figure 4.3). We defined a gene signature using the top 30 DEGs as determined by log2-

transformed fold-change and termed it the NRF2 Functionally Annotated Mutant Signature ($NRF2^{FAMS}$).

Differential expression analyses of RNA-seq data were performed using the bioconductor R *LIMMA* package with voom transformation (92-94). Transcripts were quantified using RNA-seq by expectation maximation (RSEM) and restricted to at least a 75% or greater RSEM value of 5 (95). Note that all statistical analyses and figures were generated using R version 3.2.3 (94, 96).

4.B.3. Summary of findings

We compared the $NRF2^{FAMS}$ gene set to two well-established gene signature sets: 1) 15 genes derived from RT-PCR analysis of NRF2-depleted A549 and H460 lung cancer cell lines (Singh signature) and 2) 28 genes derived from a TCGA-LUSC dataset of 104 patients binned into either normal or mutant for *KEAP1/NFE2L2/CUL3* ($NRF2^{ACT}$ signature) (84). Only two genes from $NRF2^{FAMS}$ were observed to overlap with the Singh signature (*ABCC2* and *NQO1*), while 11 genes overlap with the $NRF2^{ACT}$ signature (Figure 4.4) (33, 84). Despite being derived from similar TCGA datasets, 70% of the genes identified in $NRF2^{FAMS}$ do not overlap with the $NRF2^{ACT}$ gene signature (84, 97). This difference is likely driven by two main factors. First, $NRF2^{FAMS}$ was derived from a patient cohort comprised of 489 TCGA-LUSC samples while $NRF2^{ACT}$ was derived from a patient cohort of 104 TCGA-LUSC samples (84). Second, $NRF2^{FAMS}$ was developed based on the inclusion of validated functional mutations only, thus underscoring the importance of rigorous classification prior to establishing the gene signature and training the dataset.

We next tested the prognostic value of the $NRF2^{FAMS}$ signature in the TCGA-LUSC data set. Using hierarchical clustering with pearson's correlation, patients were classified

according to NRF2^{FAMS} expression into two groups: NRF2^{FAMS} high (n=126) or NRF2^{FAMS} low (n=363). Kaplan-Meier analysis comparing overall survival (OS) revealed that NRF2^{FAMS} high patients have a lower probability of OS as compared to NRF2^{FAMS} low patients (Figure 4.5). This analysis demonstrated that NRF2^{FAMS} is prognostic of OS with a statistically significant p-value of 0.004 as calculated by a log-rank test (survival R package) (Figure 4.5) (98, 99).

4.B.4. Proposed studies for NRF2^{FAMS}

Identify and validate novel NRF2 transcriptional targets

Differentially expressed genes identified in NRF2-active patient samples compared to NRF2-normal samples may represent novel NRF2 target genes. A comprehensive comparison of NRF2^{FAMS} to established NRF2 signatures will identify previously unpublished NRF2 target genes (13, 84, 100-102). Bioinformatic analyses can be employed to probe for ARE consensus sequences in the promoters of candidate genes (17, 67, 89, 101, 103, 104). Identification of putative NRF2 target genes can be validated biochemically using assays described in Chapter 2 of this dissertation, which include: NRF2 transcriptional activity assays, quantitative PCR (qPCR) for well-established NRF2 target genes (i.e. *HMOX1* and *NQO1*), and quantitative Western blot analysis of cells treated with NRF2 inducers (tBHQ, SF, CDDO, MG-132, or MLN49224) for protein levels of NRF2 and NRF2 target genes (i.e. HMOX1, GCLC, and GCLM) (37, 67, 105-108). The identification of novel NRF2 target genes may reveal clinically actionable targets.

Determine genotype-phenotype correlations for novel functional mutations

Class 5 mutations (those of unknown function) can be predicted as functionally active or WT based on their expression of NRF2 target genes as defined by NRF2^{FAMS} (Figure 4.3). Of these mutations, predicted normal and predicted functionally active

mutations could then be cloned and biochemically profiled using NRF2 transcriptional activity assays coupled with KEAP1-NRF2 binding. These data will not only aid in the validation of the $NRF2^{FAMS}$ gene signature but may reveal additional superbinder or functionally inactivating KEAP1 mutations.

Determining the prognostic value of $NRF2^{FAMS}$ in additional data sets

Gene expression data for large patient cohorts are now readily and publicly available (68, 71). Independent validation of the prognostic nature of $NRF2^{FAMS}$ in additional datasets should be performed. The following four LUSC data sets contain RNA-seq expression data as well as information on recurrence-free survival: Korea (GSE8894, KOR), Canada (GSE50081, CAN), Sweden (GSE37745, SWE), and the United States (GSE3141, USA) (109-112). Expression data from these groups can be used to bin patients according to their $NRF2^{FAMS}$ signature and to generate Kaplan-Meier survival plots (85). These plots can then be used to evaluate the prognostic potential of $NRF2^{FAMS}$ with other NRF2 target gene signatures (84, 85, 102). This approach can be easily adapted to other tumor types with significant genetic alterations in KEAP1-NRF2 (i.e. head and neck squamous cell carcinoma (HNSCC) and liver). The prognostic value of $NRF2^{FAMS}$ in a TCGA-LUAD dataset of 510 patient samples is currently ongoing (68, 71, 76).

Correlation of NRF2 activity with smoking status

As discussed in Chapter 1, 90% of lung cancers are caused by cigarette smoke exposure (10, 69, 70, 78, 109, 110, 113-119). Smoking induces oxidative stress and results in the formation of DNA adducts on guanine (G); these G to thymidine (T) transversions are considered a hallmark of smoking (113, 114). Seven of the 18 KEAP1 LUSC mutations studied in Chapter 2 arise from G to T transversions. Of these 7 mutations, all but 1 inactivate KEAP1 function. As a class, more than 50% of the KEAP1 hypomorphs exhibit G

to T transversions. These findings suggest that G to T transversions may be a feature of KEAP1 inactivating and hypmorphic mutations. As such, further investigation is needed to determine if correlations between mutant function and G to T transversions exist in lung cancer patients with $NRF2^{FAMS}$ high signatures.

Comparing target gene profiles of KEAP1 mutant classes

In Chapter 3, the prevalence and nature of KEAP1 hypomorphic mutations were discussed; these mutations occur in 40-50% of LUSC samples and result in a gradient of elevated NRF2 transcriptional activity as compared to KEAP1 WT or KEAP1 functionally dead mutations (1). This gradient of NRF2 activity between mutant subclasses is suggestive of differential activation or expression of NRF2 target genes. Determination of the NRF2 target genes upregulated with KEAP1 hypomorphs compared to functionally dead KEAP1 mutations may reveal candidates for targeted therapies for patients with KEAP1 hypomorphs.

4.C. Perspectives

Studies conducted by the TCGA in 2012 raised awareness of KEAP1-NRF2 mutations in the development and progression of LUSC. In 2012, we curated the literature and identified 213 KEAP1 and 68 NRF2 mutations reported across 17 different cancer subtypes. Today, cBioPortal reports 853 missense mutations in KEAP1 and 555 missense mutations in NRF2 (68, 71). These numbers are constantly increasing and underscore the importance of understanding KEAP1-NRF2 regulation in cancer, particularly in lung cancer.

This dissertation work began in 2012 and coincided with the surging interest in KEAP1-NRF2 signaling as well as with the identification of the 18 KEAP1 mutations identified by the TCGA (73). The comprehensive characterization of the 18 KEAP1 mutants presented in Chapter 2 revealed the class of superbinder mutants that formed the basis for

this dissertation (1). Investigating the mechanism of the superbinder mutants has broadened our understanding of the molecular mechanisms and phenotypic consequences of KEAP1 superbinder mutations. Moreover, superbinder mutants are estimated to occur in 40% of LUSC tumors for which there are currently no targeted therapies (73, 120, 121). The ultimate goal of gene signature studies such as $NRF2^{FAMS}$ is the identification of clinically actionable targets for the development of targeted therapies for LUSC.

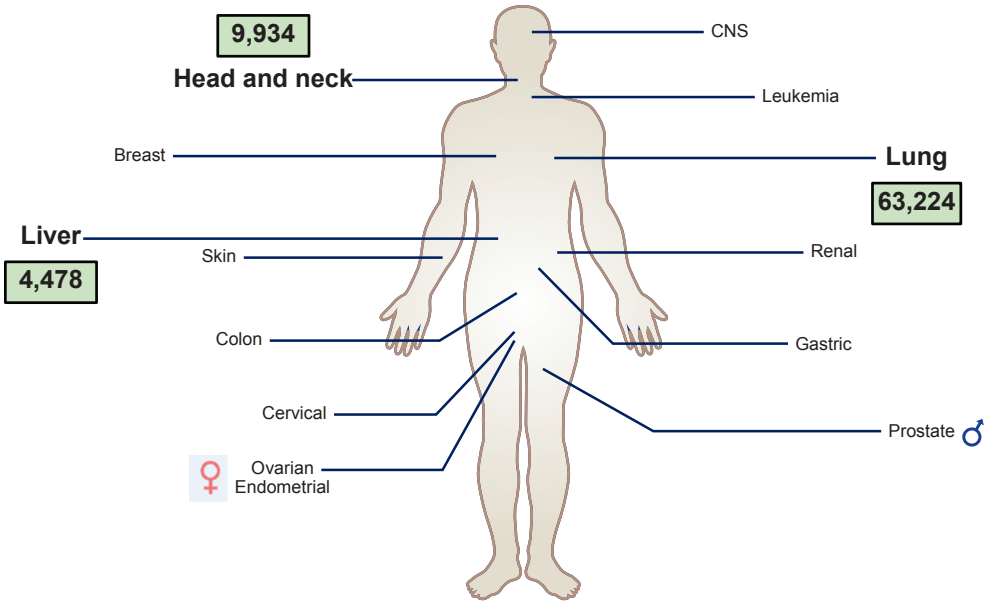

Figure 4.1. ACS estimates for NRF2-active cancer sites.
In 2017, ACS estimates that more than 90,000 patients will be diagnosed with NRF2-active cancers, impacting more than 10 different organs. Numbers reflect estimates from American Cancer Society (ACS) data.

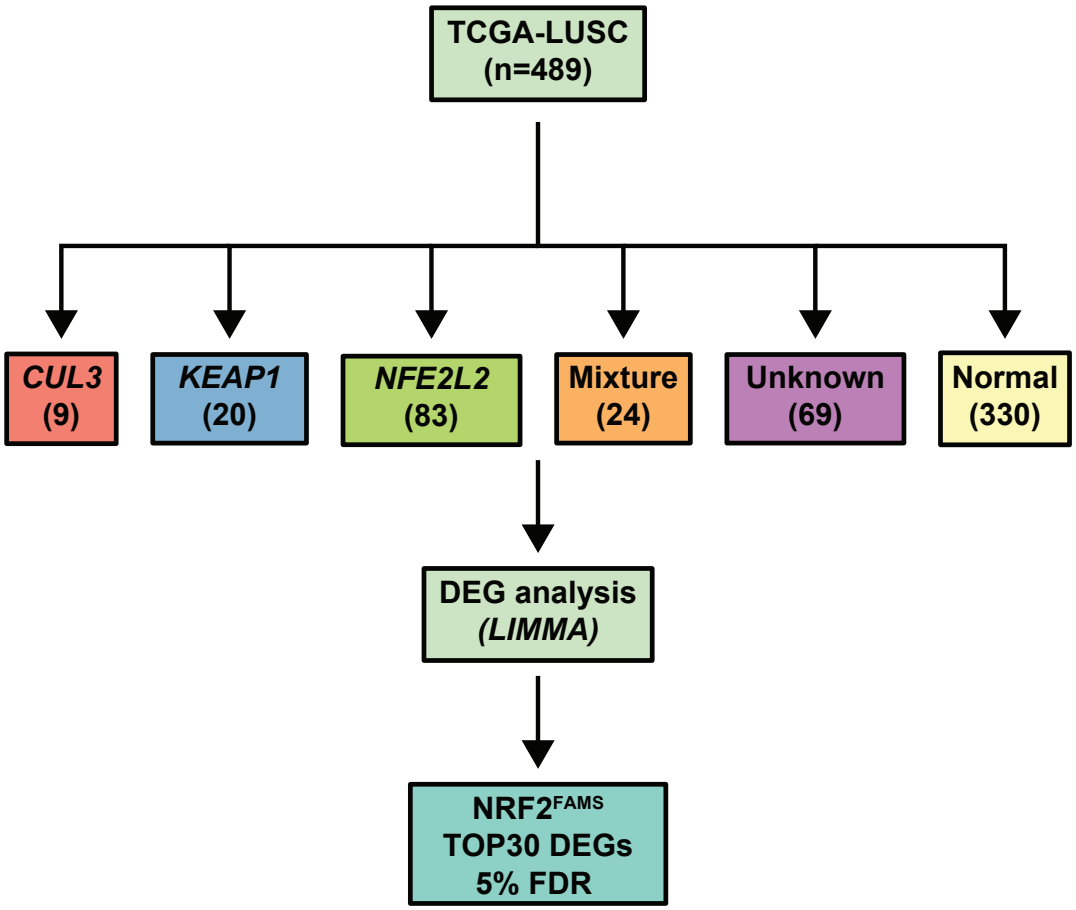

Figure 4.2. Schematic of TCGA-LUSC binning of patient-derived mutations.
489 patient-derived mutations were binned according to gene mutation and function.

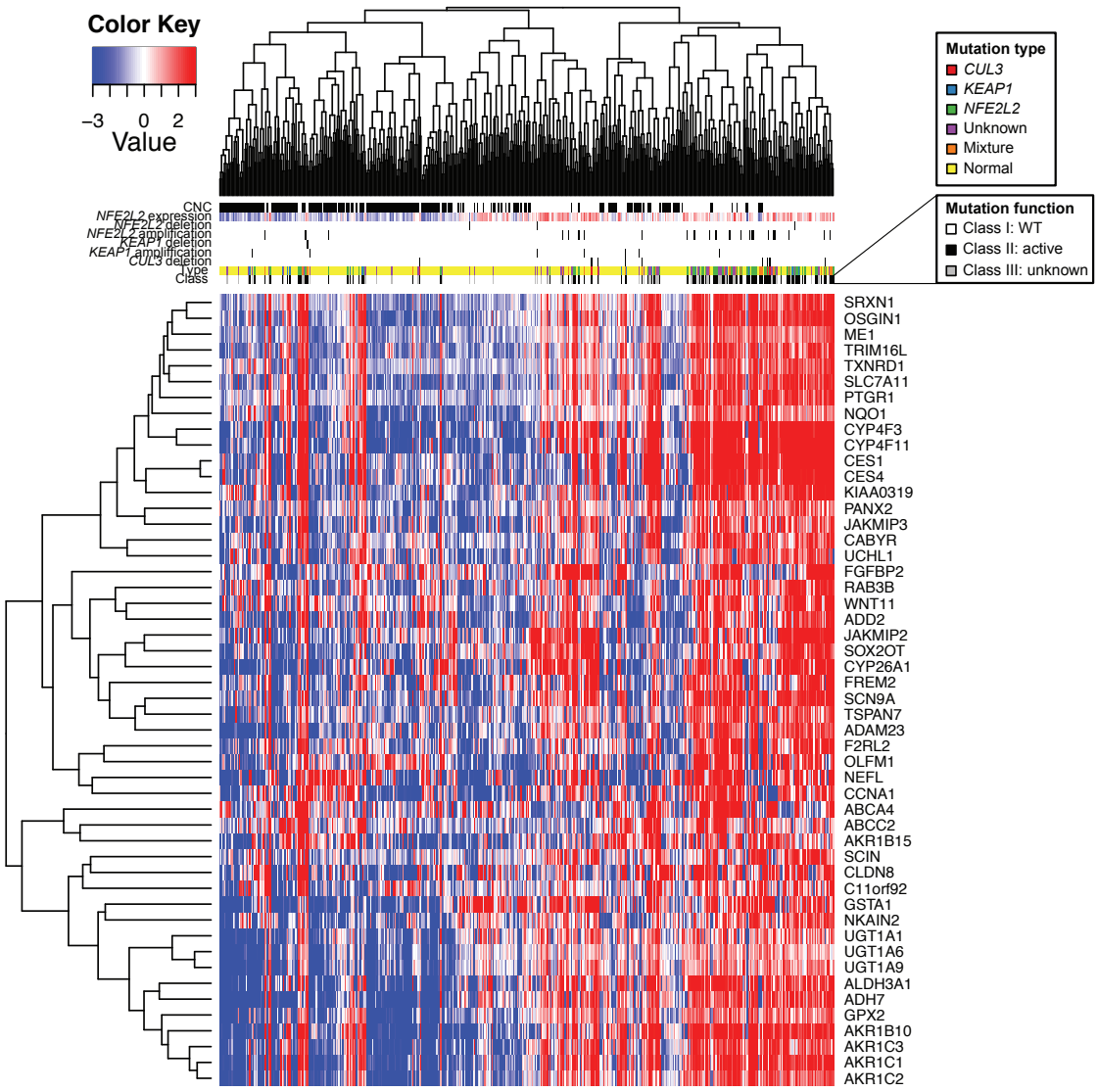

Figure 4.3. Identification of genes upregulated in NRF2-active LUSC.
Heatmap illustrating expression profiles and supervised hierarchical clustering of the top 50 differentially expressed genes (DEGs) upregulated in NRF2-active ($NRF2^{FAMS}$ high) TCGA-LUSC samples. 489 patient samples were included in the analysis.

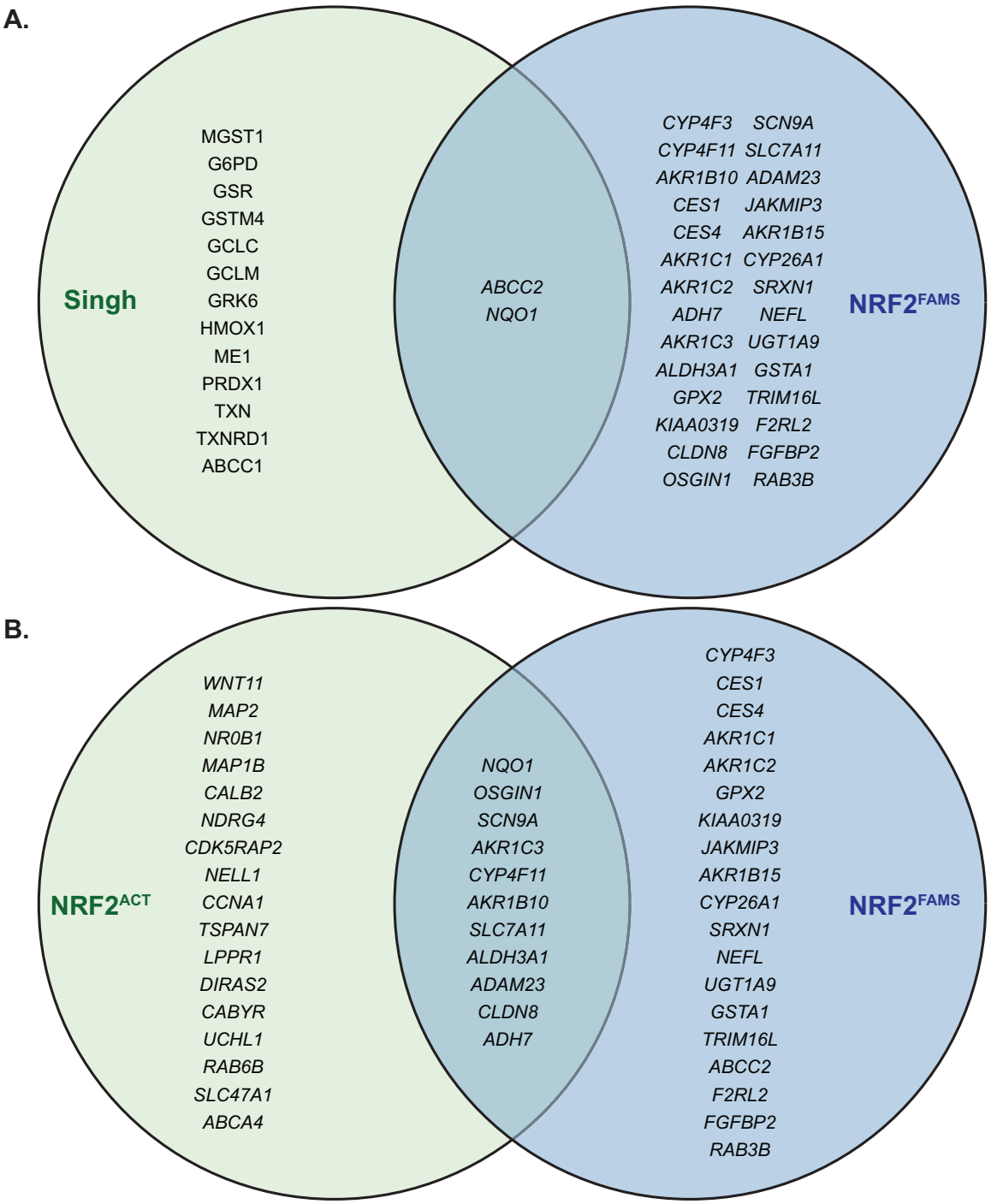

Figure 4.4. Comparison of NRF2 gene signatures.
A. Comparison of NRF2^{FAMS} with the Singh signature (33).
B. Comparison of NRF2^{FAMS} with the NRF2^{ACT} signature (84).
Venn diagrams were created using jvenn (97).

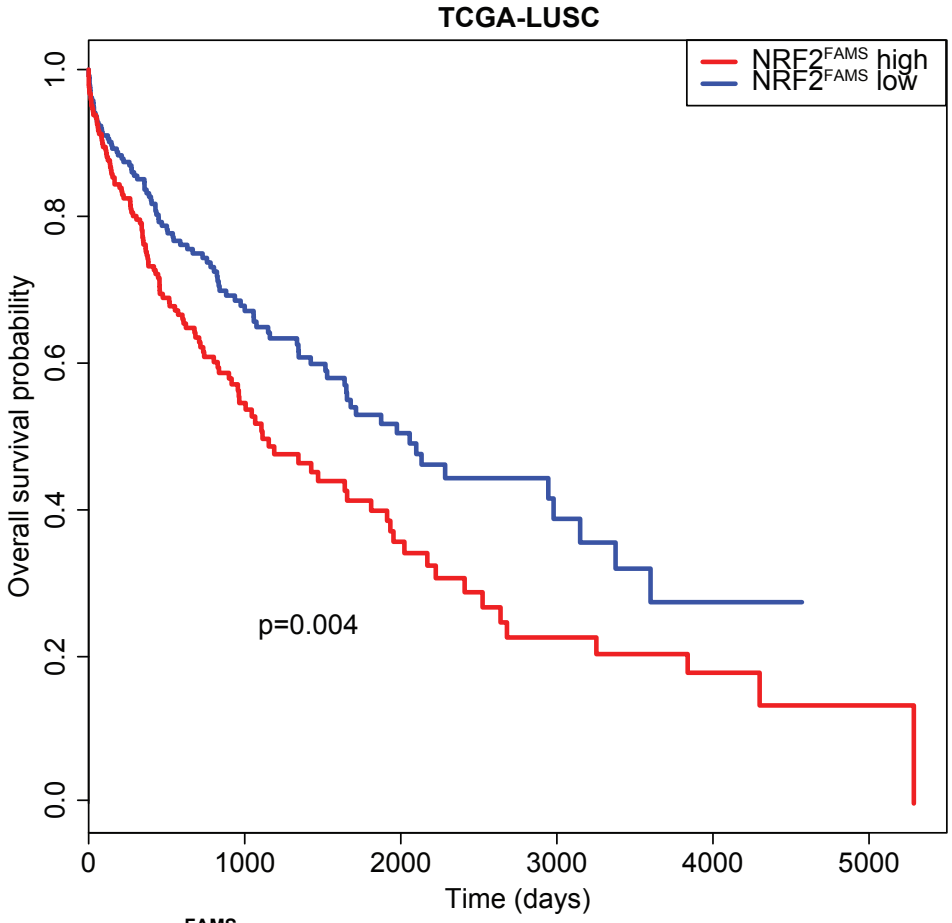

Figure 4.5. NRF2^{FAMS} is prognostic for overall survival.
Kaplan-Meier estimate of overall survival for the TCGA-LUSC cohort (n=489 patients). Log-rank test of the median difference in survival between patients classified as NRF2^{FAMS} high and NRF2^{FAMS} low is statistically significant at p=0.004.

REFERENCES

1. **Hast BE, Cloer EW, Goldfarb D, Li H, Siesser PF, Yan F, Walter V, Zheng N, Hayes DN, Major MB.** 2014. Cancer-derived mutations in KEAP1 impair NRF2 degradation but not ubiquitination. Cancer Res **74:**808-817.

2. **Lee JM, Moehlenkamp JD, Hanson JM, Johnson JA.** 2001. Nrf2-dependent activation of the antioxidant responsive element by tert-butylhydroquinone is independent of oxidative stress in IMR-32 human neuroblastoma cells. Biochem Biophys Res Commun **280:**286-292.

3. **Dinkova-Kostova AT, Holtzclaw WD, Cole RN, Itoh K, Wakabayashi N, Katoh Y, Yamamoto M, Talalay P.** 2002. Direct evidence that sulfhydryl groups of Keap1 are the sensors regulating induction of phase 2 enzymes that protect against carcinogens and oxidants. Proc Natl Acad Sci U S A **99:**11908-11913.

4. **Wakabayashi N, Dinkova-Kostova AT, Holtzclaw WD, Kang MI, Kobayashi A, Yamamoto M, Kensler TW, Talalay P.** 2004. Protection against electrophile and oxidant stress by induction of the phase 2 response: fate of cysteines of the Keap1 sensor modified by inducers. Proc Natl Acad Sci U S A **101:**2040-2045.

5. **Eggler AL, Liu G, Pezzuto JM, van Breemen RB, Mesecar AD.** 2005. Modifying specific cysteines of the electrophile-sensing human Keap1 protein is insufficient to disrupt binding to the Nrf2 domain Neh2. Proc Natl Acad Sci U S A **102:**10070-10075.

6. **Dinkova-Kostova AT, Holtzclaw WD, Wakabayashi N.** 2005. Keap1, the sensor for electrophiles and oxidants that regulates the phase 2 response, is a zinc metalloprotein. Biochemistry **44:**6889-6899.

7. **Baird L, Dinkova-Kostova AT.** 2011. The cytoprotective role of the Keap1-Nrf2 pathway. Arch Toxicol **85:**241-272.

8. **Baird L, Lleres D, Swift S, Dinkova-Kostova AT.** 2013. Regulatory flexibility in the Nrf2-mediated stress response is conferred by conformational cycling of the Keap1-Nrf2 protein complex. Proc Natl Acad Sci U S A **110:**15259-15264.

9. **Baird L, Swift S, Lleres D, Dinkova-Kostova AT.** 2014. Monitoring Keap1-Nrf2 interactions in single live cells. Biotechnol Adv **32:**1133-1144.

10. **Hayes JD, McMahon M.** 2009. NRF2 and KEAP1 mutations: permanent activation of an adaptive response in cancer. Trends Biochem Sci **34:**176-188.

11. **Homma S, Ishii Y, Morishima Y, Yamadori T, Matsuno Y, Haraguchi N, Kikuchi N, Satoh H, Sakamoto T, Hizawa N, Itoh K, Yamamoto M.** 2009. Nrf2 enhances cell proliferation and resistance to anticancer drugs in human lung cancer. Clin Cancer Res **15:**3423-3432.

12. **Jaramillo MC, Zhang DD.** 2013. The emerging role of the Nrf2-Keap1 signaling pathway in cancer. Genes Dev **27:**2179-2191.

13. **Jeong Y, Hoang NT, Lovejoy A, Stehr H, Newman AM, Gentles AJ, Kong W, Truong D, Martin S, Chaudhuri A, Heiser D, Zhou L, Say C, Carter JN, Hiniker SM, Loo BW, Jr., West RB, Beachy P, Alizadeh AA, Diehn M.** 2017. Role of KEAP1/NRF2 and TP53 Mutations in Lung Squamous Cell Carcinoma Development and Radiation Resistance. Cancer Discov **7:**86-101.

14. **Jiang T, Chen N, Zhao F, Wang XJ, Kong B, Zheng W, Zhang DD.** 2010. High levels of Nrf2 determine chemoresistance in type II endometrial cancer. Cancer Res **70:**5486-5496.

15. **Leinonen HM, Kansanen E, Polonen P, Heinaniemi M, Levonen AL.** 2014. Role of the Keap1-Nrf2 pathway in cancer. Adv Cancer Res **122:**281-320.

16. **Shibata T, Kokubu A, Saito S, Narisawa-Saito M, Sasaki H, Aoyagi K, Yoshimatsu Y, Tachimori Y, Kushima R, Kiyono T, Yamamoto M.** 2011. NRF2 mutation confers malignant potential and resistance to chemoradiation therapy in advanced esophageal squamous cancer. Neoplasia **13:**864-873.

17. **Singh A, Boldin-Adamsky S, Thimmulappa RK, Rath SK, Ashush H, Coulter J, Blackford A, Goodman SN, Bunz F, Watson WH, Gabrielson E, Feinstein E, Biswal S.** 2008. RNAi-mediated silencing of nuclear factor erythroid-2-related factor 2 gene expression in non-small cell lung cancer inhibits tumor growth and increases efficacy of chemotherapy. Cancer Res **68:**7975-7984.

18. **Solis LM, Behrens C, Dong W, Suraokar M, Ozburn NC, Moran CA, Corvalan AH, Biswal S, Swisher SG, Bekele BN, Minna JD, Stewart DJ, Wistuba, II.** 2010. Nrf2 and Keap1 abnormalities in non-small cell lung carcinoma and association with clinicopathologic features. Clin Cancer Res **16:**3743-3753.

19. **Taguchi K, Maher JM, Suzuki T, Kawatani Y, Motohashi H, Yamamoto M.** 2010. Genetic analysis of cytoprotective functions supported by graded expression of Keap1. Mol Cell Biol **30:**3016-3026.

20. **Lee YS, Yoon S, Park MS, Kim JH, Lee JH, Song CW.** 2010. Influence of p53 expression on sensitivity of cancer cells to bleomycin. J Biochem Mol Toxicol **24:**260-269.

21. **Fukutomi T, Takagi K, Mizushima T, Ohuchi N, Yamamoto M.** 2014. Kinetic, thermodynamic, and structural characterizations of the association between Nrf2-DLGex degron and Keap1. Mol Cell Biol **34:**832-846.

22. **Padmanabhan B, Tong KI, Kobayashi A, Yamamoto M, Yokoyama S.** 2008. Structural insights into the similar modes of Nrf2 transcription factor recognition by the cytoplasmic repressor Keap1. J Synchrotron Radiat **15:**273-276.

23. **Tong KI, Katoh Y, Kusunoki H, Itoh K, Tanaka T, Yamamoto M.** 2006. Keap1 recruits Neh2 through binding to ETGE and DLG motifs: characterization of the two-site molecular recognition model. Mol Cell Biol **26:**2887-2900.

24. **Tong KI, Kobayashi A, Katsuoka F, Yamamoto M.** 2006. Two-site substrate recognition model for the Keap1-Nrf2 system: a hinge and latch mechanism. Biol Chem **387:**1311-1320.

25. **Tong KI, Padmanabhan B, Kobayashi A, Shang C, Hirotsu Y, Yokoyama S, Yamamoto M.** 2007. Different electrostatic potentials define ETGE and DLG motifs as hinge and latch in oxidative stress response. Mol Cell Biol **27:**7511-7521.

26. **Hast BE, Goldfarb D, Mulvaney KM, Hast MA, Siesser PF, Yan F, Hayes DN, Major MB.** 2013. Proteomic analysis of ubiquitin ligase KEAP1 reveals associated proteins that inhibit NRF2 ubiquitination. Cancer Res **73:**2199-2210.

27. **Capra JA, Singh M.** 2007. Predicting functionally important residues from sequence conservation. Bioinformatics **23:**1875-1882.

28. **Valdar WS.** 2002. Scoring residue conservation. Proteins **48:**227-241.

29. **Itoh K, Mimura J, Yamamoto M.** 2010. Discovery of the negative regulator of Nrf2, Keap1: a historical overview. Antioxid Redox Signal **13:**1665-1678.

30. **Lo SC, Li X, Henzl MT, Beamer LJ, Hannink M.** 2006. Structure of the Keap1:Nrf2 interface provides mechanistic insight into Nrf2 signaling. EMBO J **25:**3605-3617.

31. **Taguchi K, Motohashi H, Yamamoto M.** 2011. Molecular mechanisms of the Keap1-Nrf2 pathway in stress response and cancer evolution. Genes Cells **16:**123-140.

32. **Berger AH, Brooks AN, Wu X, Shrestha Y, Chouinard C, Piccioni F, Bagul M, Kamburov A, Imielinski M, Hogstrom L, Zhu C, Yang X, Pantel S, Sakai R, Watson J, Kaplan N, Campbell JD, Singh S, Root DE, Narayan R, Natoli T, Lahr DL, Tirosh I, Tamayo P, Getz G, Wong B, Doench J, Subramanian A, Golub TR, Meyerson M, Boehm JS.** 2016. High-throughput Phenotyping of Lung Cancer Somatic Mutations. Cancer Cell **30:**214-228.

33. **Singh A, Misra V, Thimmulappa RK, Lee H, Ames S, Hoque MO, Herman JG, Baylin SB, Sidransky D, Gabrielson E, Brock MV, Biswal S.** 2006. Dysfunctional KEAP1-NRF2 interaction in non-small-cell lung cancer. PLoS Med **3:**e420.

34. **Shibata T, Kokubu A, Gotoh M, Ojima H, Ohta T, Yamamoto M, Hirohashi S.** 2008. Genetic alteration of Keap1 confers constitutive Nrf2 activation and resistance to chemotherapy in gallbladder cancer. Gastroenterology **135:**1358-1368, 1368 e1351-1354.

35. **Shibata T, Ohta T, Tong KI, Kokubu A, Odogawa R, Tsuta K, Asamura H, Yamamoto M, Hirohashi S.** 2008. Cancer related mutations in NRF2 impair its recognition by Keap1-Cul3 E3 ligase and promote malignancy. Proc Natl Acad Sci U S A **105:**13568-13573.

36. **Yamadori T, Ishii Y, Homma S, Morishima Y, Kurishima K, Itoh K, Yamamoto M, Minami Y, Noguchi M, Hizawa N.** 2012. Molecular mechanisms for the regulation of Nrf2-mediated cell proliferation in non-small-cell lung cancers. Oncogene **31:**4768-4777.

37. **Zhang DD, Hannink M.** 2003. Distinct cysteine residues in Keap1 are required for Keap1-dependent ubiquitination of Nrf2 and for stabilization of Nrf2 by chemopreventive agents and oxidative stress. Mol Cell Biol **23:**8137-8151.

38. **Kobayashi A, Kang MI, Okawa H, Ohtsuji M, Zenke Y, Chiba T, Igarashi K, Yamamoto M.** 2004. Oxidative stress sensor Keap1 functions as an adaptor for Cul3-based E3 ligase to regulate proteasomal degradation of Nrf2. Mol Cell Biol **24:**7130-7139.

39. **Hong F, Sekhar KR, Freeman ML, Liebler DC.** 2005. Specific patterns of electrophile adduction trigger Keap1 ubiquitination and Nrf2 activation. J Biol Chem **280:**31768-31775.

40. **Yamamoto T, Suzuki T, Kobayashi A, Wakabayashi J, Maher J, Motohashi H, Yamamoto M.** 2008. Physiological significance of reactive cysteine residues of Keap1 in determining Nrf2 activity. Mol Cell Biol **28:**2758-2770.

41. **Rachakonda G, Xiong Y, Sekhar KR, Stamer SL, Liebler DC, Freeman ML.** 2008. Covalent modification at Cys151 dissociates the electrophile sensor Keap1 from the ubiquitin ligase CUL3. Chem Res Toxicol **21:**705-710.

42. **Baird L, Dinkova-Kostova AT.** 2013. Diffusion dynamics of the Keap1-Cullin3 interaction in single live cells. Biochem Biophys Res Commun **433:**58-65.

43. **Jiang P, Mizushima N.** 2014. Autophagy and human diseases. Cell Res **24:**69-79.

44. **Klionsky DJ, Baehrecke EH, Brumell JH, Chu CT, Codogno P, Cuervo AM, Debnath J, Deretic V, Elazar Z, Eskelinen EL, Finkbeiner S, Fueyo-Margareto J, Gewirtz D, Jaattela M, Kroemer G, Levine B, Melia TJ, Mizushima N, Rubinsztein DC, Simonsen A, Thorburn A, Thumm M, Tooze SA.** 2011. A comprehensive glossary of autophagy-related molecules and processes (2nd edition). Autophagy **7:**1273-1294.

45. **Mizushima N.** 2007. Autophagy: process and function. Genes Dev **21:**2861-2873.

46. **Mizushima N.** 2010. Autophagy. FEBS Lett **584:**1279.

47. **Mizushima N, Komatsu M.** 2011. Autophagy: renovation of cells and tissues. Cell **147:**728-741.

48. **Yoshii SR, Mizushima N.** 2017. Monitoring and Measuring Autophagy. Int J Mol Sci **18**.

49. **Yin Z, Pascual C, Klionsky DJ.** 2016. Autophagy: machinery and regulation. Microb Cell **3:**588-596.

50. **Kirkin V, Lamark T, Sou YS, Bjorkoy G, Nunn JL, Bruun JA, Shvets E, McEwan DG, Clausen TH, Wild P, Bilusic I, Theurillat JP, Overvatn A, Ishii T, Elazar Z, Komatsu M, Dikic I, Johansen T.** 2009. A role for NBR1 in autophagosomal degradation of ubiquitinated substrates. Mol Cell **33:**505-516.

51. **Ichimura Y, Waguri S, Sou YS, Kageyama S, Hasegawa J, Ishimura R, Saito T, Yang Y, Kouno T, Fukutomi T, Hoshii T, Hirao A, Takagi K, Mizushima T, Motohashi H, Lee MS, Yoshimori T, Tanaka K, Yamamoto M, Komatsu M.** 2013. Phosphorylation of p62 activates the Keap1-Nrf2 pathway during selective autophagy. Mol Cell **51:**618-631.

52. **Lippai M, Low P.** 2014. The role of the selective adaptor p62 and ubiquitin-like proteins in autophagy. Biomed Res Int **2014:**832704.

53. **Yasuda D, Nakajima M, Yuasa A, Obata R, Takahashi K, Ohe T, Ichimura Y, Komatsu M, Yamamoto M, Imamura R, Kojima H, Okabe T, Nagano T, Mashino T.** 2016. Synthesis of Keap1-phosphorylated p62 and Keap1-Nrf2 protein-protein interaction inhibitors and their inhibitory activity. Bioorg Med Chem Lett **26:**5956-5959.

54. **Liu WJ, Ye L, Huang WF, Guo LJ, Xu ZG, Wu HL, Yang C, Liu HF.** 2016. p62 links the autophagy pathway and the ubiqutin-proteasome system upon ubiquitinated protein degradation. Cell Mol Biol Lett **21:**29.

55. **Moscat J, Karin M, Diaz-Meco MT.** 2016. p62 in Cancer: Signaling Adaptor Beyond Autophagy. Cell **167:**606-609.

56. **Pan JA, Sun Y, Jiang YP, Bott AJ, Jaber N, Dou Z, Yang B, Chen JS, Catanzaro JM, Du C, Ding WX, Diaz-Meco MT, Moscat J, Ozato K, Lin RZ, Zong WX.** 2016. TRIM21 Ubiquitylates SQSTM1/p62 and Suppresses Protein Sequestration to Regulate Redox Homeostasis. Mol Cell **62:**149-151.

57. **Dikic I.** 2017. Proteasomal and Autophagic Degradation Systems. Annu Rev Biochem **86:**193-224.

58. **Peng H, Yang J, Li G, You Q, Han W, Li T, Gao D, Xie X, Lee BH, Du J, Hou J, Zhang T, Rao H, Huang Y, Li Q, Zeng R, Hui L, Wang H, Xia Q, Zhang X, He Y, Komatsu M, Dikic I, Finley D, Hu R.** 2017. Ubiquitylation of p62/sequestosome1 activates its autophagy receptor function and controls selective autophagy upon ubiquitin stress. Cell Res **27:**657-674.

59. **Lee Y, Chou TF, Pittman SK, Keith AL, Razani B, Weihl CC.** 2017. Keap1/Cullin3 Modulates p62/SQSTM1 Activity via UBA Domain Ubiquitination. Cell Rep **20:**1994.

60. **Rusten TE, Stenmark H.** 2010. p62, an autophagy hero or culprit? Nat Cell Biol **12:**207-209.

61. **Fan W, Tang Z, Chen D, Moughon D, Ding X, Chen S, Zhu M, Zhong Q.** 2010. Keap1 facilitates p62-mediated ubiquitin aggregate clearance via autophagy. Autophagy **6:**614-621.

62. **Kageyama S, Sou YS, Uemura T, Kametaka S, Saito T, Ishimura R, Kouno T, Bedford L, Mayer RJ, Lee MS, Yamamoto M, Waguri S, Tanaka K, Komatsu M.** 2014. Proteasome dysfunction activates autophagy and the Keap1-Nrf2 pathway. J Biol Chem **289:**24944-24955.

63. **Suzuki T, Yamamoto M.** 2017. Stress-sensing mechanisms and the physiological roles of the Keap1-Nrf2 system during cellular stress. J Biol Chem **292:**16817-16824.

64. **Romero R, Sayin VI, Davidson SM, Bauer MR, Singh SX, LeBoeuf SE, Karakousi TR, Ellis DC, Bhutkar A, Sanchez-Rivera FJ, Subbaraj L, Martinez B, Bronson RT, Prigge JR, Schmidt EE, Thomas CJ, Goparaju C, Davies A, Dolgalev I, Heguy A, Allaj V, Poirier JT, Moreira AL, Rudin CM, Pass HI, Vander Heiden MG, Jacks T, Papagiannakopoulos T.** 2017. Keap1 loss promotes Kras-driven lung cancer and results in dependence on glutaminolysis. Nat Med doi:10.1038/nm.4407.

65. **Zhuang C, Narayanapillai S, Zhang W, Sham YY, Xing C.** 2014. Rapid identification of Keap1-Nrf2 small-molecule inhibitors through structure-based virtual screening and hit-based substructure search. J Med Chem **57:**1121-1126.

66. **Georgakopoulos ND, Frison M, Alvarez MS, Bertrand H, Wells G, Campanella M.** 2017. Reversible Keap1 inhibitors are preferential pharmacological tools to modulate cellular mitophagy. Sci Rep **7:**10303.

67. **Taguchi K, Yamamoto M.** 2017. The KEAP1-NRF2 System in Cancer. Front Oncol **7:**85.

68. **Cerami E, Gao J, Dogrusoz U, Gross BE, Sumer SO, Aksoy BA, Jacobsen A, Byrne CJ, Heuer ML, Larsson E, Antipin Y, Reva B, Goldberg AP, Sander C, Schultz N.** 2012. The cBio cancer genomics portal: an open platform for exploring multidimensional cancer genomics data. Cancer Discov **2:**401-404.

69. **Jemal A, Thun MJ, Ries LA, Howe HL, Weir HK, Center MM, Ward E, Wu XC, Eheman C, Anderson R, Ajani UA, Kohler B, Edwards BK.** 2008. Annual report to the nation on the status of cancer, 1975-2005, featuring trends in lung cancer, tobacco use, and tobacco control. J Natl Cancer Inst **100:**1672-1694.

70. **American Cancer Society.** About non-small cell lung cancer.

71. **Gao J, Aksoy BA, Dogrusoz U, Dresdner G, Gross B, Sumer SO, Sun Y, Jacobsen A, Sinha R, Larsson E, Cerami E, Sander C, Schultz N.** 2013. Integrative analysis of complex cancer genomics and clinical profiles using the cBioPortal. Sci Signal **6:**pl1.

72. **Campbell JD, Alexandrov A, Kim J, Wala J, Berger AH, Pedamallu CS, Shukla SA, Guo G, Brooks AN, Murray BA, Imielinski M, Hu X, Ling S, Akbani R, Rosenberg M, Cibulskis C, Ramachandran A, Collisson EA, Kwiatkowski DJ, Lawrence MS, Weinstein JN, Verhaak RG, Wu CJ, Hammerman PS, Cherniack AD, Getz G, Cancer Genome Atlas Research N, Artyomov MN, Schreiber R, Govindan R, Meyerson M.** 2016. Distinct patterns of somatic genome alterations in lung adenocarcinomas and squamous cell carcinomas. Nat Genet **48:**607-616.

73. **Cancer Genome Atlas Research N.** 2012. Comprehensive genomic characterization of squamous cell lung cancers. Nature **489:**519-525.

74. **Forbes SA, Beare D, Gunasekaran P, Leung K, Bindal N, Boutselakis H, Ding M, Bamford S, Cole C, Ward S, Kok CY, Jia M, De T, Teague JW, Stratton MR, McDermott U, Campbell PJ.** 2015. COSMIC: exploring the world's knowledge of somatic mutations in human cancer. Nucleic Acids Res **43:**D805-811.

75. **Gauthier NP, Reznik E, Gao J, Sumer SO, Schultz N, Sander C, Miller ML.** 2016. MutationAligner: a resource of recurrent mutation hotspots in protein domains in cancer. Nucleic Acids Res **44:**D986-991.

76. **Imielinski M, Berger AH, Hammerman PS, Hernandez B, Pugh TJ, Hodis E, Cho J, Suh J, Capelletti M, Sivachenko A, Sougnez C, Auclair D, Lawrence MS, Stojanov P, Cibulskis K, Choi K, de Waal L, Sharifnia T, Brooks A, Greulich H, Banerji S, Zander T, Seidel D, Leenders F, Ansen S, Ludwig C, Engel-Riedel W, Stoelben E, Wolf J, Goparju C, Thompson K, Winckler W, Kwiatkowski D, Johnson BE, Janne PA, Miller VA, Pao W, Travis WD, Pass HI, Gabriel SB, Lander ES, Thomas RK, Garraway LA, Getz G, Meyerson M.** 2012. Mapping the hallmarks of lung adenocarcinoma with massively parallel sequencing. Cell **150:**1107-1120.

77. **Kandoth C, McLellan MD, Vandin F, Ye K, Niu B, Lu C, Xie M, Zhang Q, McMichael JF, Wyczalkowski MA, Leiserson MDM, Miller CA, Welch JS, Walter MJ, Wendl MC, Ley TJ, Wilson RK, Raphael BJ, Ding L.** 2013. Mutational landscape and significance across 12 major cancer types. Nature **502:**333-339.

78. **Raponi M, Zhang Y, Yu J, Chen G, Lee G, Taylor JM, Macdonald J, Thomas D, Moskaluk C, Wang Y, Beer DG.** 2006. Gene expression signatures for predicting prognosis of squamous cell and adenocarcinomas of the lung. Cancer Res **66:**7466-7472.

79. **Wang XJ, Sun Z, Villeneuve NF, Zhang S, Zhao F, Li Y, Chen W, Yi X, Zheng W, Wondrak GT, Wong PK, Zhang DD.** 2008. Nrf2 enhances resistance of cancer cells to chemotherapeutic drugs, the dark side of Nrf2. Carcinogenesis **29:**1235-1243.

80. **Ohta T, Iijima K, Miyamoto M, Nakahara I, Tanaka H, Ohtsuji M, Suzuki T, Kobayashi A, Yokota J, Sakiyama T, Shibata T, Yamamoto M, Hirohashi S.** 2008. Loss of Keap1 function activates Nrf2 and provides advantages for lung cancer cell growth. Cancer Res **68:**1303-1309.

81. **Yang H, Wang W, Zhang Y, Zhao J, Lin E, Gao J, He J.** 2011. The role of NF-E2-related factor 2 in predicting chemoresistance and prognosis in advanced non-small-cell lung cancer. Clin Lung Cancer **12:**166-171.

82. **Abazeed ME, Adams DJ, Hurov KE, Tamayo P, Creighton CJ, Sonkin D, Giacomelli AO, Du C, Fries DF, Wong KK, Mesirov JP, Loeffler JS, Schreiber SL, Hammerman PS, Meyerson M.** 2013. Integrative radiogenomic profiling of squamous cell lung cancer. Cancer Res **73:**6289-6298.

83. **Barrett T, Troup DB, Wilhite SE, Ledoux P, Evangelista C, Kim IF, Tomashevsky M, Marshall KA, Phillippy KH, Sherman PM, Muertter RN, Holko M, Ayanbule O, Yefanov A, Soboleva A.** 2011. NCBI GEO: archive for functional genomics data sets--10 years on. Nucleic Acids Res **39:**D1005-1010.

84. **Cescon DW, She D, Sakashita S, Zhu CQ, Pintilie M, Shepherd FA, Tsao MS.** 2015. NRF2 Pathway Activation and Adjuvant Chemotherapy Benefit in Lung Squamous Cell Carcinoma. Clin Cancer Res **21:**2499-2505.

85. **Qian Z, Zhou T, Gurguis CI, Xu X, Wen Q, Lv J, Fang F, Hecker L, Cress AE, Natarajan V, Jacobson JR, Zhang DD, Garcia JG, Wang T.** 2015. Nuclear factor, erythroid 2-like 2-associated molecular signature predicts lung cancer survival. Sci Rep **5:**16889.

86. **Kuosmanen SM, Viitala S, Laitinen T, Perakyla M, Polonen P, Kansanen E, Leinonen H, Raju S, Wienecke-Baldacchino A, Narvanen A, Poso A, Heinaniemi M, Heikkinen S, Levonen AL.** 2016. The Effects of Sequence Variation on Genome-wide NRF2 Binding--New Target Genes and Regulatory SNPs. Nucleic Acids Res **44:**1760-1775.

87. **Bauer AK, Hill T, 3rd, Alexander CM.** 2013. The involvement of NRF2 in lung cancer. Oxid Med Cell Longev **2013:**746432.

88. **Giudice A, Arra C, Turco MC.** 2010. Review of molecular mechanisms involved in the activation of the Nrf2-ARE signaling pathway by chemopreventive agents. Methods Mol Biol **647:**37-74.

89. **Goldstein LD, Lee J, Gnad F, Klijn C, Schaub A, Reeder J, Daemen A, Bakalarski CE, Holcomb T, Shames DS, Hartmaier RJ, Chmielecki J, Seshagiri S, Gentleman R, Stokoe D.** 2016. Recurrent Loss of NFE2L2 Exon 2 Is a Mechanism for Nrf2 Pathway Activation in Human Cancers. Cell Rep **16:**2605-2617.

90. **Kansanen E, Kuosmanen SM, Leinonen H, Levonen AL.** 2013. The Keap1-Nrf2 pathway: Mechanisms of activation and dysregulation in cancer. Redox Biol **1:**45-49.

91. **Padmanabhan B, Tong KI, Ohta T, Nakamura Y, Scharlock M, Ohtsuji M, Kang MI, Kobayashi A, Yokoyama S, Yamamoto M.** 2006. Structural basis for defects of Keap1 activity provoked by its point mutations in lung cancer. Mol Cell **21:**689-700.

92. **Ritchie ME, Phipson B, Wu D, Hu Y, Law CW, Shi W, Smyth GK.** 2015. limma powers differential expression analyses for RNA-sequencing and microarray studies. Nucleic Acids Res **43:**e47.

93. **Diboun I, Wernisch L, Orengo CA, Koltzenburg M.** 2006. Microarray analysis after RNA amplification can detect pronounced differences in gene expression using limma. BMC Genomics **7:**252.

94. **Law CW, Alhamdoosh M, Su S, Smyth GK, Ritchie ME.** 2016. RNA-seq analysis is easy as 1-2-3 with limma, Glimma and edgeR. F1000Res **5:**1408.

95. **Li B, Dewey CN.** 2011. RSEM: accurate transcript quantification from RNA-Seq data with or without a reference genome. BMC Bioinformatics **12:**323.

96. **Law CW, Chen Y, Shi W, Smyth GK.** 2014. voom: Precision weights unlock linear model analysis tools for RNA-seq read counts. Genome Biol **15:**R29.

97. **Bardou P, Mariette J, Escudie F, Djemiel C, Klopp C.** 2014. jvenn: an interactive Venn diagram viewer. BMC Bioinformatics **15:**293.

98. **Dudley WN, Wickham R, Coombs N.** 2016. An Introduction to Survival Statistics: Kaplan-Meier Analysis. J Adv Pract Oncol **7:**91-100.

99. **Dazard JE, Choe M, LeBlanc M, Rao JS.** 2015. R package PRIMsrc: Bump Hunting by Patient Rule Induction Method for Survival, Regression and Classification. Proc Am Stat Assoc **2015:**650-664.

100. **Mitsuishi Y, Taguchi K, Kawatani Y, Shibata T, Nukiwa T, Aburatani H, Yamamoto M, Motohashi H.** 2012. Nrf2 redirects glucose and glutamine into anabolic pathways in metabolic reprogramming. Cancer Cell **22:**66-79.

101. **Malhotra D, Portales-Casamar E, Singh A, Srivastava S, Arenillas D, Happel C, Shyr C, Wakabayashi N, Kensler TW, Wasserman WW, Biswal S.** 2010. Global mapping of binding sites for Nrf2 identifies novel targets in cell survival response through ChIP-Seq profiling and network analysis. Nucleic Acids Res **38:**5718-5734.

102. **Namani A, Cui QQ, Wu Y, Wang H, Wang XJ, Tang X.** 2017. NRF2-regulated metabolic gene signature as a prognostic biomarker in non-small cell lung cancer. Oncotarget **8:**69847-69862.

103. **Rushmore TH, Morton MR, Pickett CB.** 1991. The antioxidant responsive element. Activation by oxidative stress and identification of the DNA consensus sequence required for functional activity. J Biol Chem **266:**11632-11639.

104. **Singh S, Vrishni S, Singh BK, Rahman I, Kakkar P.** 2010. Nrf2-ARE stress response mechanism: a control point in oxidative stress-mediated dysfunctions and chronic inflammatory diseases. Free Radic Res **44:**1267-1288.

105. **Zhao Y, Xiong X, Jia L, Sun Y.** 2012. Targeting Cullin-RING ligases by MLN4924 induces autophagy via modulating the HIF1-REDD1-TSC1-mTORC1-DEPTOR axis. Cell Death Dis **3:**e386.

106. **Luo Z, Pan Y, Jeong LS, Liu J, Jia L.** 2012. Inactivation of the Cullin (CUL)-RING E3 ligase by the NEDD8-activating enzyme inhibitor MLN4924 triggers protective autophagy in cancer cells. Autophagy **8:**1677-1679.

107. **Cleasby A, Yon J, Day PJ, Richardson C, Tickle IJ, Williams PA, Callahan JF, Carr R, Concha N, Kerns JK, Qi H, Sweitzer T, Ward P, Davies TG.** 2014. Structure of the BTB domain of Keap1 and its interaction with the triterpenoid antagonist CDDO. PLoS One **9:**e98896.

108. **Takaya K, Suzuki T, Motohashi H, Onodera K, Satomi S, Kensler TW, Yamamoto M.** 2012. Validation of the multiple sensor mechanism of the Keap1-Nrf2 system. Free Radic Biol Med **53:**817-827.

109. **Bild AH, Yao G, Chang JT, Wang Q, Potti A, Chasse D, Joshi MB, Harpole D, Lancaster JM, Berchuck A, Olson JA, Jr., Marks JR, Dressman HK, West M, Nevins JR.** 2006. Oncogenic pathway signatures in human cancers as a guide to targeted therapies. Nature **439:**353-357.

110. **Lee ES, Son DS, Kim SH, Lee J, Jo J, Han J, Kim H, Lee HJ, Choi HY, Jung Y, Park M, Lim YS, Kim K, Shim Y, Kim BC, Lee K, Huh N, Ko C, Park K, Lee JW, Choi YS, Kim J.** 2008. Prediction of recurrence-free survival in postoperative non-small cell lung cancer patients by using an integrated model of clinical information and gene expression. Clin Cancer Res **14:**7397-7404.

111. **Der SD, Sykes J, Pintilie M, Zhu CQ, Strumpf D, Liu N, Jurisica I, Shepherd FA, Tsao MS.** 2014. Validation of a histology-independent prognostic gene signature for early-stage, non-small-cell lung cancer including stage IA patients. J Thorac Oncol **9:**59-64.

112. **Botling J, Edlund K, Lohr M, Hellwig B, Holmberg L, Lambe M, Berglund A, Ekman S, Bergqvist M, Ponten F, Konig A, Fernandes O, Karlsson M, Helenius G, Karlsson C, Rahnenfuhrer J, Hengstler JG, Micke P.** 2013. Biomarker discovery in non-small cell lung cancer: integrating gene expression profiling, meta-analysis, and tissue microarray validation. Clin Cancer Res **19:**194-204.

113. **Marchetti A, Pellegrini S, Sozzi G, Bertacca G, Gaeta P, Buttitta F, Carnicelli V, Griseri P, Chella A, Angeletti CA, Pierotti M, Bevilacqua G.** 1998. Genetic analysis of lung tumours of non-smoking subjects: p53 gene mutations are constantly associated with loss of heterozygosity at the FHIT locus. Br J Cancer **78:**73-78.

114. **Pfeifer GP, Denissenko MF, Olivier M, Tretyakova N, Hecht SS, Hainaut P.** 2002. Tobacco smoke carcinogens, DNA damage and p53 mutations in smoking-associated cancers. Oncogene **21:**7435-7451.

115. **Ries LAG YJ, Keel GE, Eisner MP, Lin YD, Horner M-J (editors). .** 2007. SEER Survival Monograph: Cancer Survival Among Adults: U.S. SEER Program, Chapter 9: Cancer of the Lung, 1988-2001, Patient and Tumor Characteristics. National Cancer Institute, SEER Program, NIH Pub No 07-6215.

116. **Herbst RS, Heymach JV, Lippman SM.** 2008. Lung cancer. N Engl J Med **359:**1367-1380.

117. **Herbst RS.** 2008. Current and future strategies for antiangiogenic agents in non-small-cell lung cancer. Clin Lung Cancer **9 Suppl 2:**S50.

118. **Bar J, Herbst RS, Onn A.** 2008. Multitargeted inhibitors in lung cancer: new clinical data. Clin Lung Cancer **9 Suppl 3:**S92-99.

119. **Asomaning K, Miller DP, Liu G, Wain JC, Lynch TJ, Su L, Christiani DC.** 2008. Second hand smoke, age of exposure and lung cancer risk. Lung Cancer **61:**13-20.

120. **Chan BA, Hughes BG.** 2015. Targeted therapy for non-small cell lung cancer: current standards and the promise of the future. Transl Lung Cancer Res **4:**36-54.

121. **Liao RG, Watanabe H, Meyerson M, Hammerman PS.** 2012. Targeted therapy for squamous cell lung cancer. Lung Cancer Manag **1:**293-300.